ROBUST GMSK DEMODULATION USING DEMODULATOR DIVERSITY AND BER ESTIMATION

by
Jeffery D. Laster

Dissertation submitted to the Faculty of the
Virginia Polytechnic Institute and State University
in partial fulfillment of the requirements for the degree of

DOCTOR OF PHILOSOPHY
in
Electrical Engineering

Approved:

Jeffrey H. Reed
(Chairman)

Theodore S. Rappaport

Warren L. Stutzman

A. A. Beex

Keying Ye

March 1997
Blacksburg, Virginia

Keywords: GMSK, Interference Rejection, BER Estimation, Demodulator Diversity, Adaptive Signal Processing

Robust GMSK Demodulation Using Demodulator Diversity and BER Estimation

by
Jeffery D. Laster
Committee Chairman: Jeffrey H. Reed
Electrical Engineering

ABSTRACT

This research investigates robust demodulation of Gaussian Minimum Shift Keying (GMSK) signals, using demodulator diversity and real-time bit-error-rate (BER) estimation. GMSK is particularly important because of its use in prominent wireless standards around the world (GSM, DECT, CDPD, DCS1800, and PCS1900). The dissertation begins with a literature review of GMSK demodulation techniques (coherent and noncoherent) and includes an overview of single-channel interference rejection techniques in digital wireless communications. Various forms of GMSK demodulation are simulated, including the limiter discriminator and differential demodulator (i.e., twenty-five variations in all). Ten represent new structures and variations. The demodulator performances are evaluated in realistic wireless environments, such as additive white Gaussian noise, co-channel interference, and multipath environments modeled by COST207 and SMRCIM. Certain demodulators are superior to others for particular channel impairments, so that no demodulator is necessarily the best in every channel impairment.

This research formally introduces the concept of demodulator diversity, a new idea which consists of a bank of demodulators which simultaneously demodulate the same signal and take advantage of the redundancy in the similar signals. The dissertation also proposes practical real-time BER estimation techniques which have tremendous ramifications for communications. Using Parzen's estimator for probability density functions (pdfs) and Gram-Charlier series approximation for pdfs, BER can be estimated using short observation intervals (10 to 500 training symbols) and, in some cases, without any training sequence. We also introduce new variations of Gram-Charlier estimation using robust estimators. BER (in place of MSE) can now drive adaptive signal processing. Using a cost function and gradient for Parzen's estimator (derived in this paper), BER estimation is applied to demodulator diversity with substantial gains of 1-10 dB in carrier-to-interference ratio over individual receivers in realistic channels (with adaptive selection and weighting). With such gains, a BER-based demodulator diversity scheme can allow the employment of a frequency reuse factor of $N = 4$, instead of $N = 7$, with no degradation in performance. A lower reuse factor means more channels are available in a cell, thus increasing overall capacity. The resulting

techniques are simple and easily implemented at the mobile. BER estimation techniques can also be used in BER-based equalization and dynamic allocation of resources.

Acknowledgements

The completion of my graduate studies would have been impossible without the generous help of others. Foremost, I give credit to my Lord God, Jesus Christ, for from Him, through Him, and to Him are all things. I also appreciate my committee for their support and guidance. Dr. Reed, in particular, has been a fine advisor. I thank my parents and friends for encouraging me in the pursuit of this Ph.D. My wife, Grace, and my children deserve thanks for the sacrifices that they have made over the years. Their support has been a great source of encouragement and strength, and I dedicate this work to them.

Mike Buehrer, Nitin Mangalvedhe, Steve Nicoloso, Rong He, Paul Petrus, and Francis Dominique are among several students at the Mobile & Portable Radio Research Group (MPRG) who have helped me throughout this work by answering questions and providing a stimulating environment for research. The staff of MPRG, particularly Prab Koushik and Annie Wade, have also assisted the completion of this project.

I also thank the Harry Lynde Bradley Foundation which sponsored four-and-one-half years of my graduate studies through the Bradley Fellowship. The DuPont Fellowship also helped to provide for my family for four years of graduate school. I appreciate Dr. Stutzman and Dr. Reed for research assistance support. Finally, I give thanks to the many friends, especially Buddy and Coleen Bane, whose encouraging words and sensitive, timely giving helped us in times of need.

Contents

List of Tables

List of Figures

Chapter 1

Introduction

This research investigates robust demodulation of Gaussian Minimum Shift Keying (GMSK) signals, by the use of demodulator diversity and real-time bit-error-rate (BER) estimation. GMSK is a digital modulation scheme for sending binary information and presides as the most prominent modulation type among the wireless communications standards. The investigation focuses on GMSK demodulators used in channels typically found in wireless environments. Interference comprises one impairment which limits performance in wireless systems, and a robust demodulator is a demodulator that performs well in the presence of interference and with realistic fading channels.

1.1 Motivation

The goal of this research is to make a significant contribution to the field of communications by finding better ways to demodulate GMSK in the mobile radio environment.

1.1.1 Importance of GMSK

GMSK is particularly important because it is used in some of the most prominent standards around the world. Global Speciale Mobile (GSM), Digital European Cordless Telephone (DECT), Cellular Digital Packet Data (CDPD), DCS1800 (Digital Communications System in the 1800 MHz band) in Europe, and GSM-based PCS1900 (Personal Communications Services in the 1900 MHz band) in the U.S. all use GMSK as their modulation format. With Group Special Mobile (GSM) emerging as a dominant global standard for cellular communications, further improvements are being constantly investigated to provide optimum cellular system performance. Better GMSK demodulators can improve systems such as GSM, DECT, CDPD, and PCS with the potential of making a huge economic impact because of the enormous capital expenditure (billions of dollars) and market potential of these technologies. Because the present market and predicted volume [1], small improvements in GMSK receivers can amount to millions of dollars in savings.

[1] GSM is expected to have 52% market share worldwide by 1999.

1.1.2 Interference in Cellular

Mobile radio operators have generally adopted a cellular network structure, allowing frequency reuse. The primary driving force behind this has been the need to operate and grow almost indefinitely within the limited allocated spectrum. Cellular radio can be described as a honeycomb network set up over the required operating region, where frequencies and power levels are assigned in such a way that the same frequencies can be reused in cells some distance apart. Inherent to this configuration is the problem of co-channel interference (CCI), which limits the system performance. The rejection of CCI is also of particular interest to intelligence agencies who would like to be able to separate co-channel signals as they engage in surveillance.

In addition to CCI, the mobile radio channel is characterized by multipath propagation, where the transmitted signal travels along several paths to the receiver. At the receiver, these multiple versions of the transmitted signal with accompanying delays and frequency shifts are combined constructively and destructively. The problem of mitigating multipath interference is of particular interest to companies and government agencies who would like to implement radio access technologies such as DECT, which has also been designed to provide large cordless PBX's for business applications and public access systems, including Wireless Local Loop [165]. Improved rejection of multipath interference makes wireless technologies more viable as a cheap alternative to wired telephony.

1.1.3 Rejecting Interference By Demodulator Diversity

To combat interference inherent in cellular wireless systems, this dissertation investigates interference rejection techniques, with a focus on demodulator diversity and real-time BER estimation. Demodulator diversity (elaborated on in Chapter 6) constitutes a major contribution of the dissertation. Demodulator diversity (also denoted receiver diversity) is a new concept which has been investigated very little in the literature. A system implementing demodulator diversity consists of a bank of receivers which simultaneously demodulate the same received (corrupted) signal, and the system takes advantage of the differences in performance and redundancy in the information provided by the demodulators in different channels. This research justifies the concept of demodulator diversity by demonstrating that a demodulator diversity scheme can yield substantial gains in performance over individual receivers in typical wireless channels (e.g., 1-10 dB in signal-to-noise E_b/N_o or carrier-to-interference C/I, as shown in Chapter 10). The rejection of interference provided by this approach also facilitates increased capacity in cellular systems, which means increased revenues for wireless communications providers.

1.1.4 Rejecting Interference By BER Estimation

Another significant contribution of this dissertation is the fundamental research on real-time BER estimation. Practical real-time BER estimation techniques have tremendous ramifications for communications in general. Most adaptive systems in communications

resort to some criterion (other than BER) such as minimizing the mean squared error (MSE) to drive the adaptive process. BER, however, (not MSE) is the metric of performance that reflects QOS in most digital communications systems. Unfortunately, a reduced MSE does not always correspond to a reduced BER. In this dissertation, techniques for estimating probability density functions (pdfs) of random variables are investigated and applied to BER estimation. The results show that BER can often be estimated by use of a relatively short observation interval (10 to 500 training symbols) and, in some cases, without any training sequence at all.

This work applies BER estimation to adaptive signal processing in general, and to demodulator diversity in particular, and the approach can be extended to modulation types other than GMSK. This research demonstrates that BER can serve as the criterion for adaptive signal processing. Section 11.5.2 illustrates how a BER-based demodulator diversity scheme can potentially allow a frequency reuse factor of $N = 4$ to be employed, instead of $N = 7$, with no degradation in performance (i.e., a lower reuse factor means more channels are available in a cell, thus significantly increasing overall capacity). BER estimation techniques can also be used in equalization allowing equalization to be based on BER (not MSE) and allowing equalization to be effective after nonlinearities in receivers. BER estimation techniques can be used to perform dynamic allocation of resources. Dynamic allocation of resources includes variable coding, variable data rates, variable of allocation of spectrum or time slots, etc. This dissertation opens the door for BER-based adaptation of communications systems.

1.2 Outline of Dissertation

Pursuant to this introduction, Chapter 2 begins with an overview of GMSK and includes a literature review of GMSK research. This chapter introduces GMSK and describes the modulation format and some implementation issues, including demodulation, predetection filtering and differential encoding. Section 2.3.5 provides an introduction to Global Speciale Mobile (GSM), a prominent wireless standard which uses GMSK as its signaling structure. An overview of coherent demodulation and noncoherent demodulation follows with many references to published research. Coherent demodulation (where the reference phase is known) is commonly used (in systems such as GSM) because GMSK can be coherently demodulated in quadrature (yielding performance improvement in noise-limited channels). Coherent demodulation also facilitates linear equalization. Noncoherent demodulation is generally less expensive and less complex, when compared to coherent demodulation. Noncoherent demodulation of GMSK is implemented in systems such as DECT, where it is most desirable to have cheap mobile (cordless) phones.

As enunciated in the title, this dissertation focuses on robust GMSK demodulation, where robust means that the demodulator performs well in channel impairments such as interference. Both CCI and multipath contribute to significant performance degradations and constitute the limiting factors for the communication link. The purpose of this research is to mitigate and reject the impact of these (and other) sources of interference. Because interference (particularly co-channel interference and adjacent channel

interference in cellular systems) is a limiting factor in wireless systems, this research includes an extensive overview of single-channel adaptive interference rejection techniques for digital wireless communications, primarily since 1980. The chapter considers both spread spectrum and non-spread spectrum techniques. The material in Chapter 3 has been presented in a conference tutorial [134], published in a book chapter [135], and accepted for publication in *IEEE Signal Processing Magazine* [132]. The paper will be of broad interest to the signal processing community because it illustrates the applicability of signal processing solutions to wireless communications problems.

Chapter 4 presents a theoretical description of the receivers considered in this research. Various forms of GMSK demodulation have been simulated, which include the limiter discriminator and versions of the differential demodulator (i.e., twenty-five variations in all, incorporating features such as decision feedback and nonredundant error correction). Of the simulated demodulators, ten represent new structures and new variations on conventional demodulators. The research centers on noncoherent demodulation of GMSK, though a coherent demodulator is also included. Chapter 6 also provides a general wireless channel model for use in simulations. As an example, an analytic expression for the decision statistic of a one-bit differential demodulator is derived for the general wireless channel. The decision statistic is evaluated in more detail for an additive white Gaussian noise (AWGN) channel. An attempt is made to determine an *a priori* (deductive) analytical expression for the pdf of the decision statistic of a one-bit differential demodulator in AWGN, and it is shown that the derivation of such a pdf is exceedingly difficult. The failure to obtain a satisfactory analytical expression motivates research into *a posteriori* (inductive) techniques of determining the pdf of the decision statistic (discussed in Chapter 7).

In Chapter 5, the demodulators described in Chapter 4 are simulated, and their performances are evaluated in various wireless channel environments. Twenty-five channel impairments are simulated with various combinations of AWGN, CCI, and different types of multipath in accordance with the European COST 207 [70] propagation models, described in Appendix C (later, in Chapter 9, SMRCIM [241] software is also used to model multipath). The simulated wireless environments are realistic channel models. Chapter 5 illustrates the observation that certain demodulators are superior to other demodulators for various channel impairments, so that no one demodulator is necessarily always the best in every channel impairment. This observation motivates research into demodulator diversity schemes, which take advantage of the difference in performance and redundancy in the information provided by the demodulators in different channels. This performance evaluation of the GMSK demodulators is unique (in terms of the varied channel impairments typically encountered in the land mobile channel).

Demodulator diversity is a new concept which has not been investigated in the literature and is one of the major contributions of this research. With demodulator diversity, at the very least, we would like a combined demodulator to have a BER which tracks the BER of the best demodulator, and ideally, we would like better overall performance than that attainable by any individual demodulator. Chapter 6 provides a theoretical discussion of demodulator diversity and lays the groundwork for later simulations (in Chapter

10). This chapter includes a comparison of demodulator diversity to antenna diversity. For example, in a demodulator diversity scheme, because the bank of demodulators demodulate the same signal, the system is referred to as single-channel (i.e., the one signal can be viewed as having passed through a single channel). This contrasts with antenna diversity (or spatial diversity), which is a multi-channel scheme, where several versions of a signal are received on different antennas (separated spatially), so that the signal received on each antenna can be viewed as having passed through a different channel. Chapter 6 concludes with an analytical derivation of theoretical minimum mean squared error (MMSE) for demodulator diversity in AWGN.

Real-time BER estimation also constitutes one of the major contributions of this dissertation. Chapter 7 introduces the concept of real-time BER estimation based on estimators of the probability density function of a random variable (e.g., the decision statistic). The chapter provides a theoretical description two pdf estimators: 1) the Gram-Charlier series approximation for pdfs and 2) Parzen's pdf estimator. Parzen's estimator is very versatile and provides the basis for BER estimation in Chapters 8 and 10. Gram-Charlier pdf estimation is based on normalizing the data by the sample mean and standard deviation of the decision statistic. The performance of Gram-Charlier can be improved by substituting other robust estimators of location for the mean and other robust estimators of scale for the standard deviation, several of which are described in Section 7.5. The use of robust estimators in Gram-Charlier estimation constitutes another novel contribution of this work. In addition, Section 7.6 provides analytical justification for the use of blind Gaussian-based pdf estimation techniques (blind meaning without the use of training sequences). Blind estimation constitutes a significant contribution of this research, because it allows bits normally reserved for training to be used for other purposes which can increase quality of service or capacity.

After the theoretical introduction to BER estimation, BER estimation is applied to adaptive filtering in Chapter 8. In particular, the chapter demonstrates how BER estimation can used as the criterion to adapt a demodulator diversity scheme. Parzen's estimator is used as an example. Analytic expressions for the cost function and the gradient of Parzen's estimator are derived. The simulations of Chapter 10 make use of the gradient to perform a gradient-based search to minimize BER for weighted demodulator outputs in a demodulator diversity scheme. In Chapter 8, analytic expressions are also derived to provide theoretical justification for blind BER estimation (i.e., BER estimation without a training sequence). This form of blind BER estimation is another novel contribution of this research. The chapter concludes with an extension of BER estimation to equalization and to the combination of equalization with demodulator diversity.

Chapter 9 provides validation of BER estimation via simulations. A simple one-bit differential demodulator (DD1) is used throughout the simulations, where Gram-Charlier and Parzen BER estimation are compared to measured DD1 results. Comparisons are made for non-blind BER estimation in AWGN and CCI channels and in urban multipath (generated by SMRCIM [241]) with AWGN and CCI. The chapter also provides results

for blind BER estimation in SMRCIM urban multipath with AWGN and CCI. Gram-Charlier performs well in AWGN and requires a very short training sequence (e.g., 10 symbols). Parzen estimation performs well also in AWGN, but requires a longer training sequence (e.g., 500 symbols). Gram-Charlier estimation does not perform well in CCI, whereas Parzen estimation yields good results. Blind simulation results indicate that blind Parzen estimation performs poorly (i.e., Parzen estimation requires a training sequence), whereas blind Gram-Charlier estimation yields reliable estimates in AWGN (Gram-Charlier again performs poorly in CCI).

In Chapter 10, the concept of demodulator diversity is validated by simulations. Demodulator diversity using real-time BER estimation is a new concept which has been investigated very little in the literature. First of all, a demodulator diversity scheme using the three best noncoherent demodulators (from Chapter 5) is considered where a MSE-based criterion is used to adaptively select the best demodulator based on a given observation interval (or training sequence). In a second case, a demodulator diversity scheme using a coherent demodulator and a noncoherent demodulator is considered, where an MSE-based criterion is compared to Gram-Charlier BER-based criterion and Parzen BER-based criterion. In this second scheme, the demodulator outputs are adaptively selected and then adaptively weighted and combined by the Parzen BER-based criterion.

Section 10.4.1 of Chapter 10 provides surface plots of the Parzen-based BER cost function vs. weights for two cases of urban multipath with AWGN and CCI – (1) when the BERs of the demodulators are nearly the same and (2) when the BERs of the demodulators are different by about an order of magnitude. The plots show that many weight combinations can yield overall BERs *less* than the BER of the best individual demodulator. Section 10.4.3 of Chapter 10 demonstrates some of the performance improvements possible with a demodulator diversity scheme using Parzen-based BER estimation, by considering the cases where errors tend to occur in bursts and where errors tend to be randomly dispersed (performance gains are evident in both cases). MSE-based and BER-based selection and weighting produce results superior to that of the individual demodulators. The chapter justifies the concept of demodulator diversity by demonstrating that demodulator diversity schemes can yield substantial gains in performance over individual receivers in typical wireless channels.

The final stage of dissertation research investigates the impact of the new techniques on overall system performance, where GSM is used as an example. Little research has been published on the impact of interference rejection techniques on actual system performance, in general. System performance is evaluated by considering such performance measures as the impact on frequency reuse and the potential for increased capacity. Section 11.5 demonstrates that the gains (typically 1-10 dB) provided by a demodulator diversity scheme allow for increased capacity. A BER-based demodulator diversity scheme can potentially allow a frequency reuse factor of $N = 4$ to be employed, instead of $N = 7$, with no degradation in performance (i.e., a lower reuse factor means more channels are available in a cell, thus significantly increasing overall capacity). These techniques can serve as means of increased revenues, and thus lower system costs. The

techniques may also be used to provide better quality of service in the mobile phone.

The dissertation ends with a summary of results (also presented in Section 1.3) and an outline of areas for future research which spring from this work. Appendix A.1 provides more results for BER estimation in AWGN and in rural multipath (generated by COST 207 models [70] with AWGN using the coherent demodulator and using the one-bit DF, two-bit DF, three-bit DF differential demodulator with combined outputs (DD123DF), defined in Section 4.2. DD123DF was used with the coherent demodulator in the second demodulator diversity scheme of Chapter 10. Appendix B documents the SMRCIM software used to generate urban multipath in the simulations. Appendix C documents the COST 207 models used to generate rural multipath in the simulations.

1.3 Contribution of this Work

This section outlines the most significant contributions of this dissertation. Some of the other significant contributions of this research follow.

1.3.1 Most Important Contributions

- Formally introducing and validating the theoretical concept of demodulator diversity.
- Introducing and demonstrating the application of Parzen and Gram-Charlier pdf estimators to real-time BER estimation.
- Formulating methods of real-time BER-based adaptive signal processing, opening the door for application to equalization and dynamic allocation of resources, as well as to demodulator diversity.
- Proposing and demonstrating the use of real-time BER estimation with demodulator diversity by adaptive selection and weighting.
- Validating demodulator diversity schemes by simulation.
- Validating real-time Parzen-based and Gram-Charlier-based BER estimation by simulation.
- Extensively documenting an overview of single-channel interference rejection techniques in digital wireless communications, showing the applicability of signal processing solutions to wireless communications problems.

1.3.2 Other Significant Contributions

- Proposing ten new noncoherent GMSK demodulators, one of which (the one-bit DF, two-bit DF, three-bit DF differential demodulators with combined outputs,

DD123DF) performs better than other noncoherent demodulators examined from the literature.

- Documenting an extensive literature review of GMSK demodulation techniques (coherent and noncoherent).
- Proposing and demonstrating the use of robust estimators of scale and location in the Gram-Charlier series approximation for pdfs.
- Providing analytical justification for the use of blind Gaussian-based pdf estimation techniques for blind BER estimation, allowing bit normally reserved for training to be used to increase quality of service or capacity.
- Validating blind BER estimation by simulation.
- Investigating the performance of several GMSK demodulator structures (twenty-five) in impairments other than AWGN, such as CCI, multipath (generated according to the COST 207 models for urban, bad urban, hilly, and rural environments), and various combinations (this analysis is unique).
- Investigating the performance of coherent and noncoherent GMSK demodulator structures using SMRCIM [241] generated multipath with AWGN and CCI (this analysis is also unique).
- Demonstrating the thesis that no one GMSK demodulator is superior in all channel impairments, but particular demodulators perform better, depending on the dominant channel impairment (out of twenty-five channel environments simulated).
- Analytically deriving the gradient of Parzen's estimator.
- Applying the gradient of Parzen's estimator to BER estimation and demodulator diversity.
- Analyzing the impact on system performance of demodulator diversity and BER estimation on the GSM system, relating carrier-to-interference ratio (C/I) gains to system capacity improvements.
- Analytically showing the difficulty of determining *a priori* expressions for the pdf of a differential demodulator in typical wireless environments.
- Comparing demodulator diversity to antenna diversity (i.e., spatial diversity).
- Analytically deriving the theoretical minimum mean squared error (MMSE) of demodulator diversity in AWGN.

Chapter 2

GMSK Background

2.1 Introduction

This chapter contains some background material and technical details pertinent to Gaussian Minimum Shift Keying (GMSK). The MSK modulation format is introduced and the impact of premodulation Gaussian filtering is explained. Some implementation issues are considered which include research into the modulation and optimum intermediate frequency (IF) filtering bandwidth for GMSK and an explanation of differential encoding. Several wireless standards implement GMSK, including Global Special Mobile (GSM), the European cellular standard, which is introduced in this chapter. Throughout this chapter, references are provided where the reader can find more technical detail. A thorough survey from the literature on demodulation of GMSK (both coherent and noncoherent demodulation) concludes the chapter.

Coherent demodulation (where the reference phase is known) is commonly used (in systems such as GSM) because GMSK can be detected by coherently demodulating the in-phase and quadrature portions of the signal (yielding performance improvement in noise-limited channels). Coherent demodulation also facilitates linear equalization. Noncoherent demodulation is generally less expensive and less complex, compared to coherent demodulation. Noncoherent demodulation of GMSK is implemented in systems such as DECT, where it is most desirable to have cheap mobile (cordless) phones. Section 2.6 provides a comparison of coherent and noncoherent techniques.

2.2 Modulation Format

A modulation format is the means by which information is encoded onto a signal. Information, or data, can be carried in the amplitude, frequency, or phase of a signal. A modulation scheme can be analog (where the data is contained in a set of continuous values) or digital (where the data is contained in a set of discrete values). The information signal is called the modulating waveform. When the information is encoded on a signal, the signal is called a modulated waveform. The process of bringing the bandpass

signal down to baseband is denoted as demodulation. We distinguish detection from demodulation by denoting detection as the process of extracting the information from the baseband demodulated signal. A receiver consists of a demodulator and a detector. Noncoherent techniques (where the reference phase is unknown; discussed in Section 2.5) can often be implemented in demodulation or detection, such that the terms can be used interchangeably.

2.2.1 Minimum Shift Keying

Minimum Shift Keying (MSK) is a continuous phase (CP) Frequency Shift Keying (FSK) binary modulation format. FSK is the digital equivalent of analog frequency modulation (FM). MSK is a form of FSK, with modulation index $h = 0.5$ yielding the *minimum* frequency separation for orthogonal signaling over a signaling interval of length T, [196] (assuming coherent demodulation, where the reference phase is known as discussed in Section 2.4). MSK can also be viewed as offset (or staggered) QPSK with sinusoidal pulse-shaping. The literature contains much research on MSK. Pasupathy [187] provides a primer on MSK and can be referred to for an overview. Couch [40] also discusses the basic principles of MSK modulation.

MSK is popular in wireless communications because of its desirable characteristics. Desirable characteristics for digital modulation for land mobile radio are 1) compact output power spectrum; 2) applicability of class-C nonlinear power amplifiers; 3) high immunity to noise and interference; and 4) ease of implementation. Minimum Shift Keying (MSK) modulation satisfies the above requirements except for the first one. As discussed below, the output power spectrum of MSK can be made more compact, however, so as to satisfy the first requirement by introducing a premodulation low-pass filter (LPF).

2.2.2 Gaussian MSK

To make the MSK output power spectrum more compact, the premodulation LPF should meet the following conditions: 1) narrow bandwidth and sharp cutoff to suppress high frequency components, 2) small overshoot impulse response to prevent excess deviation of the instantaneous frequency, and 3) preservation of an integrated filter output pulse capable of accommodating a 90° phase shift to ensure coherent demodulation. A premodulation Gaussian LPF satisfying the above requirements is adopted for Gaussian Minimum Shift Keying (GMSK) modulation, where the data sequence (i.e., an information pulse train) is passed through a Gaussian LPF filter, and the output of the filter is MSK modulated. The width of the Gaussian filter is determined by the bandwidth-time product BT (e.g., $BT = 0.3$ for GSM and $BT = 0.5$ for CDPD).

Murota and Hirade [173] show that $BT = 0.28$ can be adopted as the digital modulation for conventional UHF (300-1000 MHz, IEEE designation) mobile radio communications without carrier frequency drift where the out-of-band radiation power in the adjacent channel to the total power in the desired channel must be lower than -60 dB.

The trade-off of having a more compact spectrum is that a premodulation filter spreads the signal pulse and, thus, introduces intersymbol interference (ISI) in the transmitted signal. The Gaussian premodulation filtering spreads the pulse over an interval greater than T (the bit duration, equivalent to the inverse of the bit rate R), making GMSK a partial response signal (in a full response signal, the pulse is confined to the interval T).

The impulse response of the Gaussian LPF $h(t)$ is:

$$h(t) = \frac{1}{\sqrt{2\pi}\sigma T} \exp\left(\frac{-t^2}{2\sigma^2 T^2}\right) \tag{2.1}$$

where

$$\sigma = \frac{\sqrt{\ln(2)}}{2\pi BT}, \text{ with } BT = 0.3 \text{ for GSM} \tag{2.2}$$

B is the 3 dB bandwidth of the filter. The square pulse response $g(t)$ of the Gaussian LPF is:

$$g(t) = h(t) * \text{rect}\left(\frac{t}{T}\right) \tag{2.3}$$

where the rectangular function rect(x) is defined by:

$$\text{rect}\left(\frac{t}{T}\right) = \begin{cases} 1/T, & \text{for } |t| < \frac{T}{2} \\ 0, & \text{otherwise} \end{cases} \tag{2.4}$$

The pulse response $g(t)$ can be written as

$$g(t) = \frac{1}{2T}\left[Q\left(2\pi BT \frac{t - T/2}{T\sqrt{\ln(2)}}\right) - Q\left(2\pi BT \frac{t + T/2}{T\sqrt{\ln(2)}}\right)\right] \tag{2.5}$$

where $Q(t)$ is the Q-function

$$Q(t) = \int_t^\infty \frac{1}{\sqrt{2\pi}} \exp(-\tau^2/2)\, d\tau \tag{2.6}$$

and $g(t) = 0$ for $0 \leq t \leq LT$ with L defined as the number of intervals over which the pulse is spread.

The phase of the modulated signal is:

$$\theta(t) = \sum_i m_i \pi h \int_{-\infty}^{t-iT} g(u)\, du \tag{2.7}$$

where $m_i \in \{\pm 1\}$ is the modulating Non-Return-to-Zero (NRZ) data. The modulation index $h = 0.5$ results in the maximum phase change of $\pi/2$ radians per data interval. The final GMSK signal is represented as

$$s(t) = \sqrt{2E_b T}\cos(2\pi f_c t + \theta(t) + z_o) \tag{2.8}$$

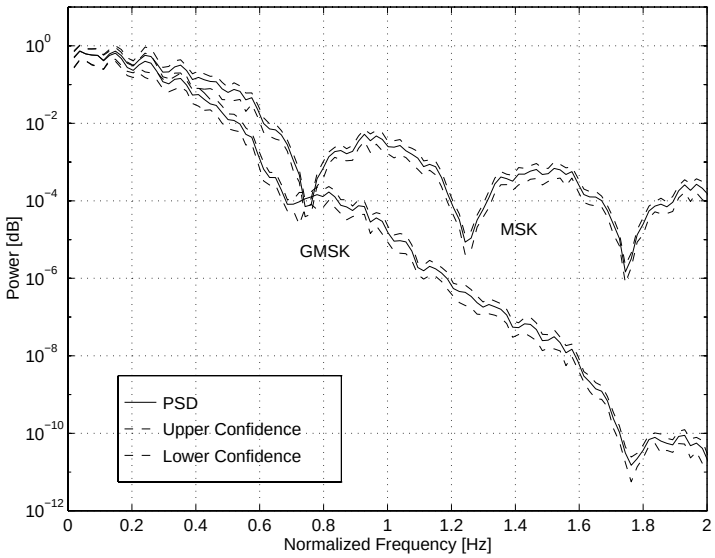

Figure 2.1: PSD of GMSK (BT=0.3) vs MSK (BT=∞)

where E_b is the signal energy per bit and z_o is a random phase constant which can be assumed to be zero ($z_o = 0$). The power spectral density (PSD) of GMSK is plotted vs. MSK in Fig. 2.1.

Kostedt, and Kemerling [126] give a broad general overview of GMSK, encompassing background, basics, performance, standards, modulation, and demodulation. They define the GMSK signal and discuss factors involved in evaluating performance. The authors point out that the modulator configuration must have a flat spectral response down to DC and that the receiver's phase response must be linear across the bandwidth occupied by the data with special attention focused on the IF filters. In his survey of Japanese research into digital modulation /demodulation techniques, Akaiwa [9] also includes a brief summary of work done on GMSK.

Daikoku, Murata, and Momma [42] outline field experiments conducted to determine the feasibility of introducing GMSK ($B_GT = 0.25$) modulation into 920 MHz mobile radio systems in Tokyo urban and Yokosuka suburban areas. Two techniques, GMSK and tamed FM (TFM), satisfy the above land mobile radio requirements, but GMSK proves to be easier to implement since it has the advantage of only requiring a Gaussian filter to manipulate the radio frequency. Three different types of demodulators are compared (coherent, one bit differential, and two bit differential - surveyed in Sections 2.4 and 2.5), in a static and in a dynamic environment, but the authors conclude that experimental results do not favor one demodulation type over the others.

2.3 Implementation Issues

This section provides an introduction to GMSK modulation and demodulation. The section includes a survey of research on the optimum intermediate frequency (IF) predetection filter. Differential encoding is described, and GSM is introduced, since it constitutes one of the most prominent wireless standards which uses GMSK.

2.3.1 Modulation

Ziemer and Ryan [271] examine methods of implementation of modulators and demodulators for MSK for high-data-rate applications. MSK (and GMSK) can be generated by modulating the frequency of a VCO directly by the use of a baseband Gaussian pulse stream, but in this simple method, it is difficult to keep the center frequency within the allowable value under the restriction of maintaining linearity and the sensitivity for the required FM modulation. Other ways to generate GMSK include the use of PLL modulator or an orthogonal modulator with digital waveform generators or a $\pi/2$-shift BPSK modulator followed by a suitable PLL phase smoother.

2.3.2 Demodulation

Because MSK is a quadrature-multiplexed modulation scheme, it can be implemented in parallel, and it can be optimally detected by coherently demodulating its in-phase and quadrature components separately (in-phase corresponds to the even bits, and quadrature corresponds to the odd bits), as illustrated in Figure 2.2. In Figure 2.2, $r(t)$ is the received signal, d is an estimate of the original data, T_b is the bit interval, and LO is a local oscillator. The quadrature channels of the modulator and demodulator must be time synchronized, amplitude balanced, and in phase quadrature to minimize overall system degradation. This becomes difficult as the data rate increases. A serial implementation avoids the balancing and timing requirements of parallel implementations, but serial implementation does require close approximation of the bandpass conversion and matched filters [271]. Implementations making use of in-phase and quadrature channel mixers to realize the conversion and matched filters as lowpass equivalents are particularly advantageous because of their compatibility with microwave integrated-circuit fabrication techniques.

MSK can also be demodulated by a variety of noncoherent demodulation techniques. Particularly, the differential demodulator (refer to Figure 4.7), the limiter discriminator (refer to Figure 4.5), and variations on these two have been used and proposed for use with GMSK signaling.

Sundberg [230] discusses various methods to improve on MSK (also referred to as Fast Frequency Shift Keying - FFSK) while maintaining a constant amplitude. The methods improve by providing a narrower power spectrum, lower spectral sidelobes, better error probability, or combinations of the above. The relationship between important system parameters such as the number of symbol levels, the smoothing pulse shape,

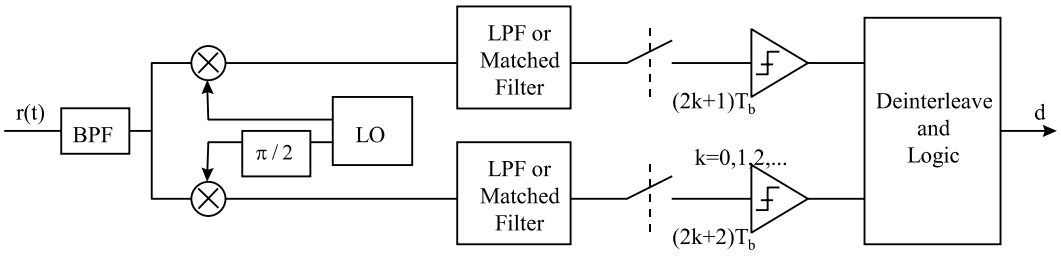

Figure 2.2: General block diagram of a coherent GMSK demodulator implemented in parallel.

and the modulation index are considered for optimum coherent reception. Some optimum and suboptimum receiver structures are studied for ideal coherent transmission. Improvements on GMSK by choosing the optimum receiver filter are also shown, with block diagrams given of both parallel and serial MSK-type receivers. Sundberg predicts that continuous phase modulation (a general modulation class which includes MSK) will become more popular as the costs of signal processing, speed, and complexity of systems are improved.

2.3.3 Optimum IF Predetection Filter

At the receiver, an IF bandpass filter (i.e., a predetection filter) is used to pass the signal, but to band-limit the noise entering the receiver (and filter out adjacent channel interference). The optimum IF filter bandwidth-time constant, $B_{IF}T$, maximizes the signal power relative to the noise power. To simplify derivations, researchers sometimes assume that the predetection IF filter contributes negligible intersymbol interference (ISI) to the signal. More accurate simulations take into account IF filter distortion. Unfortunately, the optimum $B_{IF}T$ is different for each type of demodulator. The simulations in this research assume an IF filter bandwidth of $0.9R$ (bandwidth-time product $BT = 0.9$) modeled by a 12th order Butterworth filter. Optimum IF filter $B_{IF}T$ can be found, and the following papers focus on this research problem. The differing results show that different values will be obtained, depending on the assumptions used in the derivations.

Suzuki [231] theoretically derives an optimum predetection Gaussian bandpass filter for differential demodulation of MSK. He shows that the optimum $B_{IF}T$ product is 1.21 for the bandpass filter with 4.02 dB degradation at 10^{-6} BER, where the degradation is defined as the increase in E_b/N_o relative to ideal coherent demodulation of MSK. Crozier, Mazur, and Matyas [41] find that a 4-pole Butterworth predetection bandpass filter provides the least E_b/N_o degradation. Murota and Hirade [173] use a predetection Gaussian BPF with $BT = 0.63$ which they show is nearly optimum for GMSK with premodulation $BT = 0.25$.

Ogose [181] derives the optimum predemodulation Gaussian bandpass filter for MSK with 2-bit differential demodulation. The optimum $B_{IF}T$ product for 10^{-3} and 10^{-4}

BER is $B_{IF}T = 1.0$ and 1.2 with 3.2 dB and 3.8 dB E_b/N_o degradation, respectively, from the ideal coherent transmission system. Ogose also shows that the BER performance of 2-bit differential demodulation is better than that of 1-bit differential demodulation for values of $B_{IF}T \leq 1.5$. Kishi, Sasase, and Mori [121] make use of Stein's formula to calculate the optimum $B_{IF}T$ at 0.52 for 2-bit differential demodulation.

Simon and Wang [224] maintain (via simulation results) that the optimum receiver bandwidths of 1-bit and 2-bit differential demodulators are a function of transmitter bandwidth and BER. They find that the average optimum receiver bandwidth for a GMSK signal with $BT = 0.3$ is $BT = 1.2$ for 1-bit differential demodulation and $BT = 0.9$ for 2-bit differential demodulation.

Yongacoglu, Makrakis, and Feher [267] find that a 4th-order Butterworth ($BT = 1.0$) predetection filter performs better than a Gaussian predetection filter for two-bit differential demodulation. Horikoshi and Shimura [106] obtain $B_{IF}T = 0.9$ as the preferable receiving bandpass filter bandwidth two-bit differential demodulation.

2.3.4 Differential Encoding

Differentially encoded data offers the advantage that information is carried in the phase changes, rather than in the phase itself. Under certain conditions, a phase ambiguity of $\pm 180^\circ$ ($\pm\pi$) can arise in the demodulation and detection process. For example, certain synchronization and carrier recovery techniques result in a phase ambiguity. Differential encoding overcomes this ambiguity since the information is carried in the phase differences. Knowing the absolute phase becomes unnecessary. Differential encoding inserts memory into the signal, since each data bit sent is encoded with respect to the previous data bit. The cost of overcoming phase ambiguity is increase BER (potentially doubled), because each bit error will result in an error in the adjacent bit. The actual bit error probability P_b (after differential decoding) is related to the probability of error before decoding P_e by the relation $P_b = 2P_e(1 - P_e)$.

If the input data is a binary unipolar sequence ($d_i \in \{0, 1\}$), the encoding sequence e_i (also binary unipolar) is defined as

$$e_i = d_i \oplus e_{i-1} \tag{2.9}$$

where i is the bit index. The decoding sequence is defined as:

$$d_i = e_i \oplus e_{i-1} \tag{2.10}$$

If the input data is a NRZ or bipolar ($d_i \in \{\pm 1\}$) data sequence, the encoding sequence (also bipolar) is defined as

$$e_i = -d_i e_{i-1} \tag{2.11}$$

The decoding sequence is defined as

$$d_i = -e_i e_{i-1} \tag{2.12}$$

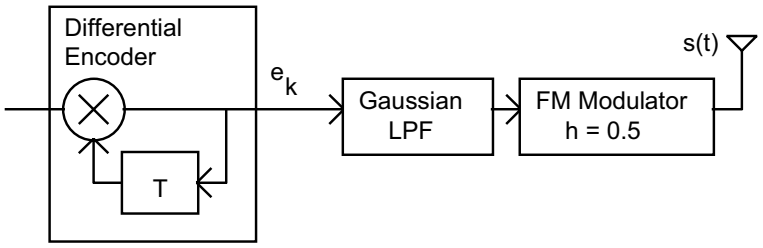

Figure 2.3: Generation of a GMSK Signal

Unipolar data $d_{unipolar}$ is converted to bipolar data $d_{bipolar}$ by the relation

$$d_{bipolar} = 2d_{unipolar} - 1 \tag{2.13}$$

If the data is differentially encoded (as in the case of GSM, explained below), the generation of the transmitted signal can be generally depicted as in Fig. 2.3, where e_k is the differentially encoded data and $s(t)$ is the signal sent (or transmitted).

2.3.5 Implementation of GMSK in GSM

GMSK is used in many important wireless standards. GMSK (with $BT = 0.3$) is the modulation format in Groupe Spécial Mobile, or GSM (also known as the Global System for Mobile Communications) which is the European digital cellular standard in the 900 MHz band. GSM is one of the fastest-growing cellular standards, in use around the world. Digital European Cordless Telephony (DECT) is the standard for cordless telephones in Europe and also uses a GMSK format similar to GSM. Cellular Digital Packet Data (CDPD), implemented on top of the analog AMPS standard in the U.S. cellular band to allow data transfer, uses GMSK (with $BT = 0.5$). In addition, many third generation wireless standards - such as DCS1800 (Digital Communications System in the 1800 MHz band) in Europe and PCS1900 (Personal Communications System in the 1900 MHz band) in the U.S. - will likely be GSM-based and will thus implement GMSK.

This paper will focus on GSM because of its popularity and because it is foundational to several other standards. An introduction to GSM follows. GSM uses GMSK modulation (thus is a digital system) where the data is differentially encoded, passed through a Gaussian filter with $B_G T = 0.3$, and then MSK modulated with a modulating bit rate of 1625/6 kbps (270.833 kbps) [71]. GSM is a TDMA system where 200 kHz channels are divided among 8 simultaneous users in 8 time slots. The European Telecommunications Standard Institute (ETSI) has published voluminous reports on the technical details of GSM. More succinct summaries of GSM can be found by Redl, Weber, and Oliphant [204] and by Mouly and Pautet [169].

D'Aria, Muratore, and Palestini [43] present a performance evaluation (by computer simulation) of the GSM radio transmission system, which includes GMSK together with

concatenated block and convolutional coding, Viterbi adaptive equalization, and soft-decision Viterbi decoding to cope with the severe time- and frequency- selective distortions caused by propagation phenomena. They show that a soft-decision Viterbi algorithm allows the performance of some GSM traffic and control channels to be considerably improved with respect to hard decisions. Improvement can be achieved with a not too heavy increase of hardware complexity.

Linear equalization is required in GSM to mitigate the ISI introduced by the premodulation filtering, multipath, and predetection bandpass filtering. GSM specifications require that equalizers should be able to compensate for delay spreads up to $16\mu s$. Adaptive linear equalization facilitates the mitigation of ISI introduced by the channel (e.g., by dynamic multipath), as well as ISI due to filtering.

GSM traditionally uses coherent demodulation of GMSK (as opposed to noncoherent demodulation, where the reference phase in unknown) (1) because of the performance gain of demodulating the in-phase and quadrature signals separately (decisions are made over $2T$ rather than over T) and (2) to preserve linearity in the receiver prior to linear equalization. As will be discussed later, coherent demodulation has its own problems in terms of expense, complexity, and inability to perform well in certain channel impairments.

2.4 Coherent Demodulation

Coherent demodulation is common in GMSK-based systems. GSM, for example, employs coherent demodulation at the base station and mobile. Coherent demodulation requires knowledge of the reference phase or exact phase recovery, meaning local oscillators, phase-lock loops, and carrier recovery circuits may be required, adding to complexity and expense.

As mentioned earlier, MSK can be represented as a form of QPSK, where the even-numbered binary valued symbols of the information sequence are transmitted via the cosine of the carrier (in-phase), while the odd-numbered symbols are transmitted via the sine of the carrier (quadrature). The transmission rate on the two orthogonal carrier components is $1/2T$ bits per second so that the combined transmission rate is $1/T$ bits/s, with decisions made over $2T$ seconds for even and odd bits. The bit transitions are staggered or offset in time by T seconds (OQPSK). Coherent demodulation of MSK as two orthogonal binary channels provides a 3-dB E_b/N_o advantage over coherent detection of orthogonal FSK for matched-filter demodulation in the presence of AWGN [228].

Coherent demodulation is also required to facilitate linear equalization, which is necessary in GSM to compensate for ISI resulting from delay spreads due to multipath and from premodulation and predetection filtering. Coherent demodulation degrades in fading environments due to imperfect tracking of the received signal phase which results in irreducible error rates.

Murota and Hirade [173] propose the use of GMSK with coherent demodulation as an effective digital modulation for mobile radio services. The authors show how various properties such as output power spectrum and the BER performance are calculated and

used to evaluate performance. They show the relationship between normalized bandwidth and fractional power of the GMSK signal at various BT values. The theoretical degradation of GMSK ($BT = 0.3$) from MSK is about 0.5 dB in terms of E_b/N_o. Block diagrams are given of analog and digital versions of an orthogonal coherent demodulator. Performance is evaluated in static and dynamic environments, and theoretical BER formulas are given, except for the fast Rayleigh fading case where tracking performance of the carrier recovery circuit cannot be analyzed.

Ishizuka and Yasuda [114] propose the use of analog addition detection to improve upon conventional GMSK coherent demodulation. The proposed deviated-frequency-locking scheme from coherent detection takes advantage of the fact that the degradation effect from intersymbol interference (ISI) due to the premodulation filtering is smaller at the center of the time slot than at the edge of the time slot. In this method, the signal is sampled at the center of the time slot, and two consecutive sampled data are then combined for the purpose of decision by utilizing a restriction of the possible phase transitions. The detection scheme is numerically tested based of worst-case signal patterns and shown to offer 0.55 dB improvement (for $B_GT = 0.3$) over conventional coherent demodulation.

Lee, Chung, and Kim [139] analyze coherent demodulation of a GMSK signal, using a MSK-type receiver. Use of a simple MSK-type receiver to detect GMSK results in a degradation of about 0.3 dB at BER = 10^{-5} when compared to MSK (that is, filters matched to MSK result in negligible degradation when used with GMSK). BER and eye patterns of GMSK and MSK are compared for various channel conditions, including nonfading, Rayleigh fading, AWGN with CCI, Rayleigh fading with CCI, AWGN with ACI, and Rayleigh fading with ACI. Channel separation is set at $f = 1.5$ (approximately 400 kHz channels at $R = 270.833$ kbps), which makes CCI more significant than ACI. In AWGN, $C/I = 20$ dB is required to provide negligible CCI performance, while $C/I = 0$ dB is enough for negligible ACI performance. In slow Rayleigh fading, $C/I = 30$ dB gives no degradation in CCI, and $C/I = 10$ dB is required to provide no degradation in ACI.

Leung and Feher [141] propose a scheme to insert a carrier pilot to a GMSK signal using binary block coding and a high pass filter at baseband. This allows the signal to be coherently demodulated even in a fast Rayleigh fading environment, resolving the problem of the carrier recovery loop hanging up and losing synchronization. The scheme was applied to a 16 kbps GMSK signal. The irreducible error rate (or error floor) of the proposed coherent demodulator was found to be an order of magnitude better than that of noncoherent differential demodulation in a fast Rayleigh fading environment.

Turkmani and Carter [240] study the impact of CCI on GMSK ($BT = 0.3$) in a Rayleigh fading environment using an MSK-type receiver. They found that the irreducible error rate decreases with the fading rate values as would be encountered in GSM. When considering total signal-to-interference ratios (S/I), the error rate is independent of the number of interferers.

2.5 Non-Coherent Demodulation

Noncoherent demodulation techniques do not require knowledge of the reference phase, eliminating the need for phase-lock loops, local oscillators, and carrier recovery circuits. Noncoherent techniques are generally less expensive and easier to build than coherent techniques (since coherent reference signals do not have to be generated), and are often preferable, though they can degrade performance under certain channel conditions. Several types of noncoherent demodulation exist, including the differential demodulator and the limiter discriminator (and variations on these two). A brief introduction to the direct conversion receiver is also included.

2.5.1 Differential Demodulation

Simon and Wang [223] compare the error probability performance of differential demodulation of narrow-band FM to that of limiter discriminator demodulation in AWGN and in partial-band noise jamming. In AWGN, the two demodulators performed almost identically for modulation index $h \leq 0.5$, but for $h > 0.5$, the performance of the limiter discriminator demodulator outperforms that of the differential demodulator. In a partial-band jamming environment, the performance of the two demodulators was found to be almost identical. It is concluded that differential demodulation offers no theoretical performance advantage over the limiter discriminator receiver with integrate and dump postdetection filtering in an AWGN and partial-band jamming environment, where a Gaussian filter has B_GT between 1 and 3 and the modulation index $h < 1$.

Simon and Wang [224] then compare 1-bit and 2-bit differential demodulation for GMSK transmission and give a comprehensive analytical treatment of performance, emphasizing the trade-offs among the various system design parameters such as transmit and receive filter bandwidths and detection threshold level. The authors provide complicated theoretical formulas for each demodulator performance in AWGN and in Rician fading. In terms of the average probability of bit error, the 2-bit differential demodulation offers superior performance over 1-bit differential demodulation in the presence of AWGN and Rician fading environments. The advantage stems from the asymmetry of the eye pattern produced at the 2-bit demodulator output (1-bit demodulation has a symmetrical eye pattern with a smaller eye opening), thus enabling one to bias the detection threshold in the direction of the larger opening of the eye. They find that the optimum threshold (calculated to minimize each E_b/N_o) is virtually insensitive to the fading level.

Elnoubi [65] analyzes theoretically the effect of ISI on GMSK 1-bit differential demodulation in a fast Rayleigh fading environment. A closed-form expression is derived for the probability of error as a function of the fading rate, IF filter bandwidth, SNR, and ISI. Plots of the probability of error of GMSK and of MSK with differential demodulation versus SNR are given. Elnoubi [67] also derives a closed form expression for the probability of error of 2-bit differential demodulation of GMSK in fast Rayleigh fading. He assumes that only adjacent bits contribute to ISI and that the IF filter has negligible

effect on ISI. In both analyses, he assumes an adjusted modulation index (i.e., widening the frequency separation between signals) to improve the performance of the decision statistic.

Leung and Feher [142] extend Elnoubi's analysis of 1-bit differential demodulation in fast Rayleigh fading to include the effect of the Gaussian IF bandpass filter and of frequency-selective fading. They also investigate the modem performance's sensitivity to the offset in the time delay element and the 90° phase shifter in the receiver.

Mason [155] presents a method for determining the error probability of a receiver using differential demodulation in the presence of Gaussian noise and fast Rician fading. He includes the effect of IF filter distortion. His method can be modified to apply to spectrally-shaped MSK, such as GMSK.

Ariyavisitakul, Yoshida, Ikegami, and Takeuchi [17] propose the use of fractional-bit differential demodulation of MSK to improve performance of the receiver in a frequency-selective fading environment. The purpose of this demodulation scheme is to reduce the timing fluctuations of eye patterns, which are caused by multipath-induced envelope delay distortion. When the bit delay of a differential demodulation scheme is reduced to less than one bit, there is a major improvement in the measured average BER, indicating that a fractional-bit differential demodulation scheme can significantly improve performance with MSK demodulation.

Ohno and Adachi [183] investigate a half-bit offset decision frequency demodulator for GMSK. The demodulation scheme requires differential encoding. The demodulator is compared with conventional 2-bit differential demodulation and multilevel decision frequency detection, in Rayleigh fading and in no fading. It is found that the half-bit offset decision frequency demodulator can significantly improve BER performance.

Yongacoglu, Makrakis, and Feher [267] investigate 1-bit, 2-bit, and 3-bit differential demodulators with and without decision feedback (DF), for various bandwidth-time (B_GT) products. They also give the performance of combination receivers (1-bit + 2-bit with DF, and 2-bit + 3-bit with DF). Block diagrams, eye diagrams, and phase state diagrams of each receiver are given along with helpful tables. DF allows the use of lower B_GT values, because DF facilitates the removal of ISI (DF, as used here, is form of nonlinear equalization). The BER of each differential demodulation technique is brought closer to that of coherent demodulation (without the carrier recovery problems). It is shown that the combined 2-bit and 3-bit differential demodulator with decision feedback offers the best performance among the differential demodulators, performing only 3 dB worse than the coherent receiver (in the absence of the carrier recovery problem).

Masamura, et al., [154, 153] present theoretical analysis and experimental validation for differential demodulation of MSK with nonredundant error correction (i.e., error correction without the addition of redundant bits to the transmitted data). Placing a 1-bit demodulator in parallel with a 2-bit demodulator (and/or a 3-bit demodulator), the proposed technique utilizes the output detected from the difference in phase over two or three time slot intervals (which can be interpreted as the parity check sum of two or three successive transmitted data elements) of the 2-bit and 3-bit demodulators, respectively, to correct the 1-bit demodulator output. It is shown that a single error (among the

demodulators) can be corrected using two differential demodulators, and that a double error (among the demodulators) can be corrected using three demodulators. Compared to coherent demodulation, differential demodulation was 2.2 dB worse without error correction, 1.2 dB worse with single error correction, and only 0.7 dB worse with double error correction in the presence of ISI. Samejima, et al., [213] derive a general form for nonredundant error correction for m-phase DPSK.

Korn [123] derives a formula for the error probability of partial-response continuous-phase modulation - PRCPM (which comprises GMSK as a special case) - with 1-bit and 2-bit differential phase demodulation (with and without DF) for the satellite mobile channel (which contains as special cases the Gaussian and Rayleigh channels). He claims that DF is more effective for GMSK for premodulation normalized filter bandwidths of $B_GT < 0.5$. The 2-bit demodulator is shown to be superior to the 1-bit demodulator for low Doppler frequencies and SNRs, and vice versa for large Doppler frequencies and SNRs. Elnoubi [69] corrects Korn's conclusion that DF gives a lower error probability only for smaller values for the normalized B_GT, higher values of the ratio of powers in the direct and diffuse signal components K, and a lower range of signal-to-noise ratio. Elnoubi shows that DF reduces the error probability for all values of B_GT and SNR ratios. Here, Elnoubi's BER formula for one-bit differential detection assumes no adjustment to the modulation index.

Korn [125] derives a formula for error probability of PRCPM with differential demodulation and limiter discriminator demodulation in a multipath Rayleigh fading channel, taking into account frequency-selective fading, cochannel interference, Doppler frequency shift, and AWGN. Numerical results are presented for GMSK with $B_GT = 0.25$. Under mild channel conditions and low energy-to-noise ratios, the best demodulator is an optimized (threshold) 2-bit differential demodulator. Overall, with these minor exceptions, Korn concludes that the best system is GMSK with limiter discriminator demodulation.

Horikoshi and Shimura [106] investigate the error performance of GMSK with 2-bit differential demodulation in a frequency-selective mobile radio channel. Two-bit differential detection is focused on because its performance is superior to that of coherent detection in a fast Rayleigh fading channel [120]. The authors derive a BER formula for the 2-ray Rayleigh fading channel model (typical of the frequency-selective mobile channel). BER degradation with relation to the sample-timing offset and delay time-difference are numerically computed. Their analytical method maintains high accuracy when the maximum Doppler frequency is very small compared to the symbol transmission rate.

Kwon, Miller and Lee [130] analyze the error probability achieved by a differential demodulator with a bandpass limiter preceding the receiver for a slow-frequency-hopped CPFSK diversity waveform transmitted over a partial-band noise jamming channel. Each bit is repeated on L different hops and for the FH/CPFSK system analyzed, these repetitions are combined to yield a soft decision. A diversity gain for error rate improvement in worst-case partial-band jamming is realized for the differential demodulator preceded by the limiter.

Chung, Han, and Song [39] compare differential MSK and GMSK using k-th order

differential demodulators. They derive mathematical results for the output of k-th order demodulators in noiseless environments. A generalized receiver is proposed which consists of parallel combinations of k-th order differential demodulators utilizing DF, where the DF is used to effectively decode the outputs of the differential demodulators. The error rate performance of differential MSK and GMSK (with $B_GT = 0.3$ and 0.5) in AWGN are plotted. The higher bit delay demodulators show higher performance gains.

Shin and Mathiopoulos [222] evaluate the performance of differential demodulators with and without DF for GMSK signals in CCI and AWGN. They find that a 2-bit differential demodulation with DF can outperform a conventional 2-bit differential demodulation scheme by as much as 14 dB in static CCI, with lesser improvement in faded (or dynamic) CCI. The BER of conventional and DF differential demodulation are plotted for static CCI, fading, and faded CCI. They conclude that 2-bit differential demodulation outperforms 1-bit differential demodulation in a static, AWGN or Rician-fading environment, but that 1-bit differential demodulation outperforms 2-bit differential demodulation in a Rayleigh faded CCI channel. They also note that DF provides the most improvement in a static environment such as static CCI and AWGN, and only slight improvement in a fading environment.

Varshney, Salt, and Kumar [244] examine the effects of frequency-selective fading, Rayleigh fading, Doppler shift, AWGN, ISI (from prefiltering of the data and band-limiting by the IF filter), and CCI on the BER performance in a mobile channel using GMSK 1-bit differential demodulation. A useful table lists authors who have contributed to BER analysis of GMSK. The optimum IF filter bandwidth was found to be $B_{IF}T = 1$ for all types of channels when the CIR and/or the CDR (carrier power to delayed signal power ratio) is much greater than the CNR (carrier to noise ratio). However, when the CNR is much greater than the CIR and/or the CDR, the errors are mainly produced by CCI, Doppler spread, and delay spread. In this case, there is no optimum IF filter bandwidth for all types of channels.

Abrardo, Benelli, and Cau [6] consider a new differential demodulation algorithm using multiple-symbol observation interval of a GMSK signal. In [7], a multiple differential detection (MDD) sequence estimator is described which uses decision feedback for the demodulation of a GMSK signal. This technique is based on a maximum-likelihood sequence estimation (MLSE) of the transmitted phases rather than symbol-by-symbol detection. Upper and lower bounds on the bit error probability are derived for AWGN and a two-ray Rayleigh fading channel. Performance of multiple-symbol differential demodulation approaches the optimum coherent demodulator using the Viterbi algorithm as the observation interval becomes high.

Abrardo, Genelli, Bini, and Garzelli [5] analyze the performance of a diversity receiver which is on the classical MLSE Viterbi algorithm and which uses a new distance combination technique. The BER performance of the system is given in rural, hilly, and urban settings. It is shown that the BER can be significantly reduced with only a slight increase in receiver complexity.

Smith and Wittke [226] investigate the symbol error probability of GMSK using differential demodulation in a Rician fast fading environment. With the effect of the

infinite sequence of ISI considered, the conditional and average probability of error is formulated and compared for filter bandwidth and average SNR, with and without fading. It is shown that, for $B_GT = 0.6$, GMSK has an equivalent error performance comparable to MSK.

Yao and Reed [265] investigate 1-bit, 2-bit, 1-bit DF, and 2-bit DF differential demodulation techniques for various B_GT values of a GMSK signal in the presence of channel impairments such as AWGN, static Rician multipath, multipath, and CCI. Their results show that DF provides interference resistance capability. They show that 2-bit differential demodulation with DF generally has the best performance in all channels. In strong interference environments, however, 1-bit differential demodulation outperforms 2-bit differential demodulation.

Safavi, et al., [165] introduce a simple noncoherent equalizer receiver for DECT, as a means to obtain robust performance in outdoor and large indoor applications. This structure renders the receiver insensitive to dispersion; it can extend the operating range to delay spreads of 530 ns (standard DECT receivers can cope with 90-100 ns of delay spread). A 12-bit subsequence of the DECT synchronization field (S-field) can be used for correlative channel estimation. The receiver cannot, however, substitute for antenna diversity in flat fading channels, so the authors combine the equalizer with an antenna diversity scheme in order to obtain robust overall performance.

2.5.2 Limiter Discriminator

The limiter discriminator consists of a limiter (to restore the constant envelope property to the corrupted received signal) and a discriminator (to convert the phase modulation to amplitude modulation for envelope detection). The discriminator is often followed by a LPF, such as an integrate-and-dump filter, after which a decision is made.

Hirono, Miki, and Murota [101] propose a multilevel decision method for band-limited digital FM with limiter-discriminator demodulation. Particularly, they propose a two-level (and also a four-level) method which follows the limiter-discriminator and integrate-and-dump filter. In the two-level method, the decisions level is chosen based on the previously detected bit. The four-level method chooses one of four decision levels based on the two previous bits. Both methods can be modeled as Markov processes. Theoretical BER analysis and experimental results indicate more than 10 dB improvement of the required E_b/N_o can be obtained with two-level decision method, when compared to that of the conventional zero-threshold decision method for GMSK. In addition, the four-level decision method has about 1 dB improvement over the two-level method at a BER of 10^{-3}. The authors also find that a predetection bandpass filter with $B_{IF}T = 0.6$ minimizes the BER.

Carney and Dennis [30] investigate the BER performance of 18 kbps GMSK ($B_GT = 0.2$) using limiter discriminator demodulation. They find that a 10-pole IF filter is superior to an 8-pole IF filter in a static channel.

Assuming an ideal IF filter, Elnoubi [66] presents a simple analysis of GMSK with discriminator demodulation and derives closed form expressions for the probability of

error in fast Rayleigh fading environments. In a subsequent paper, Elnoubi [68] takes into account the IF filter bandwidth and outlines an approach for determining the probability error numerically. The optimum IF filter bandwidth is the one corresponding to the minimum probability of error for specified E_b/N_o and fading rate.

El-Tanany, Stern, and Mahmoud [64] investigate BER performance of a limiter discriminator with 1-bit or 2-bit integrate-and-dump for various B_GT and modulation index h combinations. They conclude that a phase-equalized Butterworth filter is the best practical IF filter for the noncoherent GMSK receiver, and a filter order of 6 or 8 poles is sufficient for noise rejection. Timing recovery jitter (due to pattern noise, zero crossing jitter, and thermal noise) is also reduced if IF filter $B_{IF}T$ is raised to 1.1, and they claim that the increased bandwidth does not significantly impact demodulator performance.

Ohno and Adachi [182] investigate the applicability of maximum likelihood sequential estimation (MLSE) to limiter discriminator GMSK demodulation. Experimental results show that BER performance with MLSE approaches that of MSK, with a loss of about 2-5 dB in the E_b/N_o and about 3-5 dB in the S/I (signal to interferer ratio).

Ohno and Adachi [184] consider various decision schemes which can follow a limiter-discriminator. The decision schemes considered include 1-bit and 2-bit DF equalizer decision, three-level eye decision, and maximum-likelihood sequence estimate (MLSE) decision. A BER performance experiment is setup to compare the four decision schemes against each other in AWGN with no fading, a CCI limited channel with no fading, AWGN with Rayleigh fading, and a CCI limited channel with Rayleigh fading. It is concluded that in AWGN, a 2-bit DF equalizer has the best BER performance, while MLSE has the best BER performance of CCI limited channels. In regard to block error rate performance, three level eye decision (a bit-by-bit decision) has superior performance because there is no error propagation, but in fading environments its superior performance is diminished because of bursty errors due to deep fades. If interleaving is used to randomize bursty errors, however, the DFE and MLSE decision schemes provide better performance than the three-level eye decision scheme.

Korn [124] derives a formula for the error probability of partial response FSK with limiter discriminator demodulation with and without DF for the satellite mobile channel. The error probability formula is applied to GMSK and computed as a function of energy to noise ratio, Doppler frequency, maximum Doppler frequency, bandwidth of the Gaussian filter, ratios of power in the direct and diffuse signal components, and time delay between direct and diffuse components. For Rayleigh fading in the land mobile channel, DF is found to have no effect on the system performance.

Varshney and Kumar [243] analyze discriminator demodulation of GMSK in a cellular mobile communication channel, where the channel is modeled as a frequency selective fast Rayleigh fading channel corrupted by AWGN and CCI. Simulations are conducted for frequency-selective/flat (with and without dispersion), fast/slow (with and without Doppler effects) Rayleigh fading. Varied parameters include ratio of Doppler spread to the data rate, ratio of relative delay between the two paths to the symbol duration, average carrier power to additive Gaussian noise power ratio (CNR), ratio of average carrier power to the interfering signal power (CIR), and the ratio of average carrier power

to the delayed path signal power (CDR). A closed form expression for the probability of error is also derived. It is shown that GMSK gives slightly better performance over $\pi/4$-QPSK.

Djen, Dang, and Feher [46] demonstrate the robustness of using a 4th order premodulation Gaussian LPF (GLPF) paired with a 4th order post-discriminator Butterworth LPF to improve BER performance in GMSK systems. A DC-offset compensation technique based on decision detection is investigated and found to compensate for 40propose the use of a Pseudo Error monitor for DC-offset compensation caused by frequency drift of the VCO and IC type mismatch during noncoherent demodulation (with an FM discriminator, the frequency drift will only be translated into DC-offset at the receiver). A B_GT of 1.0 for the Butterworth LPF can solve the phase nonlinearity problem of the GLPF.

Asano and Pasupathy [18] propose simple, robust processing strategy called Fading Magnitude - Integrate, Sample, and Dump (FM-ISD) processor, for use with Limiter Discriminator (LD) detection of continuous phase modulation (CPM) signals in Rayleigh, fast fading channels. The envelope of the received signal is multiplied by the output of the LD and then passed through an integrate, sample, and dump. This technique only yields small improvement for GMSK.

2.5.3 Direct Conversion

Schultes, Scholtz, Bonek, and Beith [217] propose a low-cost incoherent homodyne receiver for mobile communications systems and discuss its advantages and disadvantages. The advantages include fewer RF circuits, signal processing transferred to baseband, no mirror frequency problems, no expense associated with carrier or modulation tracking, AC-coupled baseband signal processing allowed, insensitivity against carrier to local oscillator (LO) frequency offset and drift, and applicability to nearly all two or four level modulation techniques. The main disadvantage is an approximate 3 dB loss of sensitivity against synchronous coherent demodulation. Wu, Wang, and Yao [258] also investigate quadrature demodulation from a direct conversion receiver.

2.6 Coherent versus Noncoherent

Advantages and disadvantages exist with both coherent and noncoherent techniques. Coherent demodulation leads to a better BER when in the presence of AWGN, but fast Rayleigh fading can cause cycle-slipping and hang-up in the phase-lock loop of the carrier recovery circuit, making coherent demodulation difficult, and resulting in an irreducible error rate. A lower irreducible error rate is encountered with differential detection and is caused by random FM noise that partially destroys the carrier phase coherency in adjacent symbol time. In fast Rayleigh fading, noncoherent demodulation can become preferable.

MSK is called Minimum Shift Keying (a form of CPFSK) because $h = 1/2$ yields the minimum frequency separation $\Delta f = f_1 - f_2 = 1/2T$ that is necessary to ensure

orthogonality of signals over a signaling interval of length T. This minimum separation assumes coherent demodulation. If noncoherent demodulation is used (such as envelope or square-law detection of FSK signals), the minimum frequency separation required for orthogonality of the signals is $f = 1/T$ in the presence of AWGN. This separation is twice as large as that required for coherent detection. This accounts for performance degradation when noncoherent demodulation is used instead of coherent demodulation. For example, at a BER of 10^{-4}, coherent FSK is 1 dB better than noncoherent FSK in terms of E_b/N_o.

In AWGN, the optimum receiver for MSK (i.e., using correlation demodulation or matched-filter demodulation) yields a BER for coherent MSK which is the same as the BER for coherent FSK

$$P_e = Q\left(\sqrt{2\left(\frac{E_b}{N_o}\right)}\right), \qquad \text{for coherent MSK demodulation} \tag{2.14}$$

where P_e is the probability of bit error and Q function defined as

$$Q(z) \equiv \frac{1}{\sqrt{2\pi}} \int_z^\infty \exp(-\lambda^2/2)\, d\lambda \tag{2.15}$$

In AWGN, the optimum receiver for MSK yields a BER for noncoherent MSK which is the same as the BER for noncoherent FSK (assuming that, for example, the matched bandpass filter introduces no ISI)

$$P_e = \frac{1}{2} \exp\left(-\frac{1}{2}\frac{E_b}{N_o}\right), \qquad \text{for noncoherent MSK demodulation} \tag{2.16}$$

For GMSK, the BERs of coherent and noncoherent demodulation will be degraded from these optimum values because of the ISI introduced by the premodulation Gaussian filtering.

For digital FM, Hirade, Ishizuka, Adachi, and Ohtani [100] compare differential demodulation with discriminator and coherent demodulation. They derive analytical BER formulas for differential demodulation in the presence of AWGN and CCI in a fast (and also slow) Rayleigh fading environment. The authors conclude that discriminator demodulation is superior to differential demodulation in a random FM noise environment, but differential demodulation is slightly superior to discriminator demodulation when co-channel interference (CCI) is present.

Kinoshita, Hata, and Nagabuchi [120] experimentally compare GMSK ($B_G T = 0.25$) coherent demodulation with differentially encoded 1-bit and 2-bit differential demodulation and with discriminator demodulation methods. For static thermal noise performance in a nonfading environment, coherent demodulation is superior to the other schemes. Coherent demodulation and discriminator demodulation exhibit small degradation due to carrier drift, while in differential demodulation, degradation due to carrier drift is proportional to the carrier frequency drift. Discriminator demodulation is shown to be preferable to other demodulation schemes in a fast Rayleigh fading environment

(where the maximum Doppler frequency, or fading rate, f_d is 40 Hz), since its irreducible BER is about one-fourth that of 2-bit differential demodulation and one-tenth that of coherent demodulation. Coherent demodulation can achieve good static BER performance, but degradation due to random FM noise is larger than that of other schemes. Therefore, it is suitable for systems operating in slow fading environments. Differential demodulation is unsuitable for a system which has large carrier drift, because of its sensitivity to the carrier drift. The authors conclude that discriminator demodulation is most practically suited for mobile radio, since it has the advantage that degradations due to carrier drift and random FM noise are small.

Saulnier, Puckette, Gaus, Dunki-Jacobs, and Thiel [215] propose an all-digital demodulator/detector suitable for both analog FM and digital phase/frequency modulation. Two demodulators are used simultaneously to provide both noncoherent and differentially coherent demodulation, as well as automatic gain control (AGC) and automatic frequency control (AFC). Since the two demodulators in this demodulator/detector scheme are operating simultaneously, one demodulator can be used for signal detection while the other is used for AGC and AFC. Advantages of an all digital system include security, increased system capacity, and better handling of data-intensive applications.

Feher [73] examines the performance and implementation complexity of coherent and noncoherent QPSK and GMSK modulation/demodulation. A comparison of various performance advantages and disadvantages of coherent and noncoherent GMSK and Feher-QPSK (F-QPSK) is given in tabular form. For large f_dT_b products where f_d is the Doppler shift and T_b is the bit duration, noncoherent systems (such as discriminator demodulation and differential demodulation) have a lower BER floor than their coherent counterparts. For significant delay spreads (e.g., $\tau_{rms} > 0.4T_b$) and low C/I, coherent systems outperform noncoherent systems, but coherent systems require longer synchronization time than noncoherent systems. Feher claims a 7 dB E_b/N_o advantage of his coherent filtered QPSK (F-QPSK) over noncoherent GMSK (filtered with $BT = 0.5$). He also provides a plot of ACI versus normalized channel spacing (WT) for GMSK with a 4th order Gaussian BPF ($B_iT = 0.6$); ACI= -12 dB for $WT = 0.74$ (i.e., 200 kHz in GSM).

2.7 Summary

Overall, Chapter 2 comprises a literature review of GMSK research. The chapter introduces GMSK and describes the modulation format and some implementation issues, including demodulation, predetection filtering, and differential encoding. Section 2.3.5 provides an introduction to GSM, a prominent wireless standard which uses GMSK. An overview of coherent demodulation and noncoherent demodulation (including the differential demodulator and limiter discriminator) follows with many references to published research. Section 2.6 provides a comparison of coherent and noncoherent techniques.

Chapter 3

Single-Channel Adaptive Interference Rejection

This chapter comprises an extensive overview of single-channel interference rejection, primarily since 1980. The material in this chapter was presented in a conference tutorial [134], published in a book chapter [135], and accepted for publication in *IEEE Signal Processing Magazine* [132].

3.1 Abstract of Chapter

The growth in wireless communications necessitates more efficient utilization of spectrum. The increased sharing of spectrum translates into a higher likelihood of users interfering with one another. Interference rejection techniques allow a higher capacity of users within available spectrum. Interference rejection is important in increasing cellular capacity, because cellular systems are inherently interference limited, particularly by co-channel interference and adjacent channel interference. Interference rejection is also important in helping to facilitate compatibility during transitions between old and new communication technologies that share the same spectrum.

This chapter surveys significant advances in interference rejection in recent years and seeks to summarize and place in perspective the many proposed techniques. This overview focuses on single-channel adaptive filtering techniques for interference rejection (that is, techniques employing one antenna) as opposed to multi-channel techniques (which employ multiple antennas, such as arrays or cross-polarized antennas). The chapter divides interference rejection techniques for digital modulation into spread spectrum techniques and non-spread spectrum techniques. Implementation papers are de-emphasized in this overview since techniques constitute the main interest.

Spread spectrum categories include narrowband and wideband interference in direct sequence (DS), and frequency hopping (FH). Narrowband interference DS techniques include adaptive notch filters, decision feedback filters, adaptive A/D conversion, and nonlinear techniques. Wideband interference rejection for DS is divided into single-user and multiuser techniques (with emphasis on code division multiple access - CDMA).

FH techniques apply adaptive notch filters and make use of the transient nature of the hopping signal. Non-spread spectrum techniques include those based on adaptive equalization, the constant modulus algorithm, neural networks, nonlinear filters, and time-varying filters that use spectral correlation properties. The chapter concludes with a discussion of the future direction of interference rejection.

3.2 Introduction

The growth in wireless communications necessitates more efficient utilization of spectrum. The increased sharing of spectrum translates into a higher likelihood of users interfering with one another. Interference rejection techniques allow a higher capacity of users within available spectrum. This overview comprises a literature review of published papers pertaining to single-channel adaptive interference rejection in digital wireless dating primarily from 1980 to the present. Though previous overviews are referenced and summarized, the focus is on advances not covered by previous overviews (consequently, some papers are included which predate 1980 and are not covered by previous overviews).

The organizational chart shown in Figure 3.1 outlines the types of techniques covered by this chapter. For the benefit of the non-specialist, tutorial material begins most sections to introduce each category. Following the tutorial material, each section contains a summary of recent advances and contributions to the particular area. For cursory reading, one can focus on the first few paragraphs to gain insight into the general technique and skip the subsequent summary of particular contributions. To assist in the reading of the material, Table 3.1 furnishes a list of abbreviations used throughout this chapter.

3.2.1 Importance of Interference Rejection

Interference rejection is important for several reasons. Cellular capacity is inherently interference limited, particularly by co-channel interference (CCI) and adjacent channel interference (ACI). One solution to combat CCI and ACI is to split cells and decrease power, but cell-splitting is expensive. Interference rejection techniques often represent a less expensive alternative to cell-splitting.

In addition, as newer communication technologies supersede older technologies, interference rejection techniques are important in helping to facilitate compatibility during transitions between the old and new technologies. Several examples illustrate the need for compatibility: co-utilization of the existing cellular band with new narrowband code division multiple access (CDMA) and time division multiple access (TDMA) digital cellular signals, broadband CDMA overlaying Advanced Mobile Phone System (AMPS) signals in the cellular bands, co-utilization of the new personal communication system band (1.8 - 2.2 GHz) with existing microwave systems, the addition of a vast number of new low-earth-orbiting (LEO) satellites with overlapping footprints with older satellites, and accommodation of high definition television (HDTV) transmissions within the current TV band.

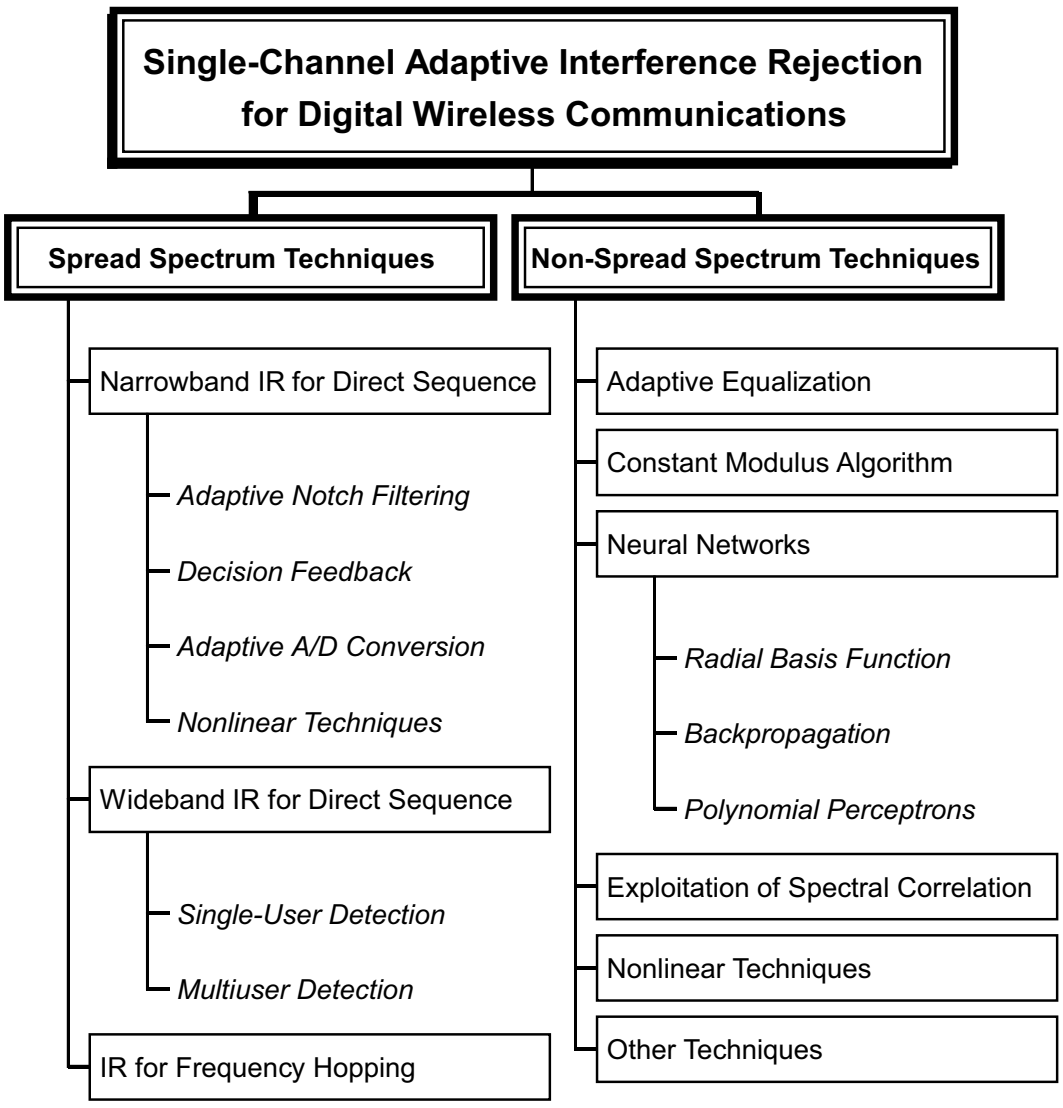

Figure 3.1: Organizational chart of single-channel adaptive interference rejection (IR) techniques for wireless digital communications.

Table 3.1: Abbreviations used throughout this chapter.

A/D..... Analog to digital
ACI..... Adjacent channel interference
ADC..... Analog to digital converter
ADF..... Adaptive digital filter
AEQ..... Adaptive linear equalizer
AIC..... Adaptive interference canceler
AJ..... Anti-jam
ALE..... Adaptive line enhancer
AMPS..... Advanced Mobile Phone System
ANC..... Adaptive nonlinear converter
ANLE..... Adaptive nonlinear equalizer
AR..... Autoregressive
ATF..... Adaptive time-frequency
AWGN..... Additive white Gaussian noise
B-CDMA..... Broadband CDMA
BER..... Bit error rate
CCI..... Cochannel interference
CDMA..... Code Division Multiple Access
CMA..... Constant modulus algorithm
CNNDFF..... Complex neural network-based adaptive DF filter
COF..... Code-orthogonalizing filter
CPM..... Continuous Phase Modulation
CW..... Continuous wave
DEDS..... Discrete event dynamic system
DF..... Decision feedback
DPSK..... Differential phase shift keying
DS..... Direct sequence
DSSS..... DS spread spectrum
FDM..... Frequency division multiplexing
FDMA..... Frequency division multiple access
FH..... Frequency hopped
FFH..... Fast frequency hopped
FIMM..... Fast interacting multiple model
FIR..... Finite impulse response
FSBLP..... Fractionally-spaced bilinear perceptron
FSDFMLP..... Fractionally-spaced DF multilayer perceptron
FSRPP..... Fractionally-spaced recursive polynomial perceptron
GFC..... Gradient-search fast converging
GLRT..... Generalized likelihood-ratio test
GPS..... Global Positioning System
HDTV..... High definition television
HOS..... Higher order statistics
ICE..... Interference canceling equalizer
IMM..... Interacting multiple model
IPA..... Infinitesimal perturbation analysis
IR..... Interference rejection
ISI..... Intersymbol interference
LCCM..... Linearly constrained constant modulus
LEO..... Low-earth orbiting
LFSE..... Linear fractionally-spaced equalizer
LMS..... Least mean square
LO..... Locally optimal
LPF..... Low pass filter
LS..... Least squares
LTE..... Linear transversal equalizer
MAI..... Multiple access interference
MF..... Misadjustment filter
MIMO..... Multiple input multiple output
ML..... Maximum likelihood
MLSE..... Maximum likelihood sequence estimation
MMF..... Modified median filter
MMSE..... Minimum mean squared error
NBI..... Narrowband interference
OTDR..... Optimal time-dependent receiver
PCS..... Personal communications systems
PN..... Pseudonoise
QPRS..... Quadrature partial response signaling
RBF..... Radial basis function
RLS..... Recursive least squares
SDR..... Symmetric dimension reduction
SIR..... Signal to interference ratio
SINR..... Signal to interference noise ratio
SOI..... Signal-of-interest
SNOI..... Signal-not-of-interest
SPREIS..... SPectral Redundancy Exploiting Interference Suppressor
SSMA..... Spread spectrum multiple access
SSMF..... Spread spectrum matched filter
TDL..... Tapped delay line
TDMA..... Time Division Multiple Access
TFD..... Time-frequency distributions
THE..... Threshold excision
VSIE..... Vector space interference excision
WF..... Wiener filter
WHT..... Walsh-Hadamard transform

The CDMA overlay or coexistence with AMPS results in interference - the key problem in making viable this new digital cellular format. Schilling, Lomp, and Garodnick [216] present a broadband CDMA (B-CDMA) scheme that will overlay the existing cellular telephone spectrum (824-894 MHz). The overlay will provide additional capacity to the network while allowing high quality voice and high speed data services to coexist with the existing cellular services (AMPS and IS-54). The absence of mutual interference to and from the B-CDMA overlay will be accomplished by using an adaptive filter. CDMA based on IS-95 must also contend with AMPS interference from other cells, even though it is not an overlay system.

In satellite-based personal communications systems, geostationary satellites can interfere with each other, as well as with LEO satellites, limiting capacity. This issue is especially relevant because of the large number of LEO satellites proposed for worldwide cellular and information networks. An informative overview of satellite interference is found in the work of Kennedy and Koh [119]. Their paper discusses the background and relevance of the problem of frequency-reuse interference in TDMA/QPSK satellite systems and suggests techniques to alleviate interference effects.

Global Positioning System (GPS) applications potentially will experience a mixture of both narrowband and wideband interferences. For example, commercial aircraft are susceptible to having their GPS receivers jammed (intentionally or unintentionally). Sources of unintentional interference range from RF transmitters onboard the aircraft or on nearby aircraft to other RF transmitters, such as TV and FM stations and personal communications systems (PCS) using mobile satellite services. Onboard RF transmitters (e.g., VHF radio and satellite communications equipment) comprise the most immediate and highest degree of threat to GPS receivers [45].

The military applications of interference rejection are numerous. The most obvious application is in mitigating the effects of intentional jamming. A not so obvious application is the mitigation of self-jamming from harmonics produced by operating transmitters and receivers in close proximity to each other [236]. In addition, in reconnaissance applications, a stand-off receiver covering a wide geographical region is subject to interference from non-intelligence bearing signals operating in the same band.

3.2.2 Adaptive Interference Rejection

Interference rejection techniques often need to be adaptive because of the dynamic or changing nature of interference and the channel. In this chapter, methods of interference rejection are viewed as adaptive filtering techniques. The term filter is often used to describe a device (in the form of software or hardware) that is applied to a set of noisy data in order to extract information about a prescribed quantity of interest. The design of an optimum filter requires *a priori* information about the statistics of the data to be processed. Where complete knowledge of the relevant signal characteristics is not available, an adaptive filter is needed, meaning that the filter is a self-designing device which relies on a recursive algorithm to converge to the optimum solution in some statistical sense. A useful approach to the filter-optimization problem is to minimize

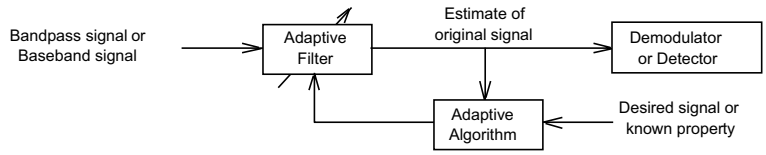

Figure 3.2: A typical adaptive filter applied to the communications problem.

the mean-square value of the error signal that is defined as the difference between some desired response and the actual filter output [93]. A general block diagram of an adaptive filter applied to the communications problem is given in Figure 3.2.

3.2.3 Single-channel versus Multi-channel

This overview chapter focuses on single-channel adaptive filtering techniques for interference rejection (that is, techniques employing one antenna) as opposed to multi-channel techniques (which employ multiple antennas, such as arrays or cross-polarized antennas). Multiple antennas allow multi-channel reception, where each channel carries a different version of the transmitted signal. The differences in the received versions of the signal at each antenna can be used to enhance and detect the desired signal. With single-channel reception, only one version of the transmitted signal is received, usually by only one antenna or sensor.

The military has always been interested in single channel techniques because they have been generally cheaper, less complex, smaller in size, and more suited to rugged military applications than multi-channel techniques. Along the same lines, the commercial wireless community will likely favor interference rejection techniques which are inexpensive and simple to implement.

3.2.4 Spread Spectrum versus Non-Spread Spectrum

As shown in Figure 3.1, this chapter divides interference rejection techniques for digital modulation into spread spectrum techniques and non-spread spectrum techniques (loosely, techniques for wideband signals and techniques for narrowband signals). This categorization is made for several reasons relating to the nature of the interference to be rejected or mitigated. For example, the case of narrowband interference on a spread spectrum signal leads to a class of different techniques which would not be applicable to the case of narrowband interference co-channeled with a narrowband signal. In spread spectrum systems employing Code Division Multiple Access (CDMA), the users share the same frequency and, at the same time, interfere with each other by design (users are separated by code). Though high levels of interference exist, the interfering users have similar statistics, leading to another class of techniques. One can also take advantage of unique spread spectrum properties such as code repetition to reject interference and

increase the number of users that can be supported in a given band.

3.3 Spread Spectrum Techniques

Spread spectrum (SS), by its very nature, is an interference tolerant modulation. However, there are situations where the processing gain is inadequate and interference rejection techniques must be employed. This is especially true for direct sequence spread spectrum (DS-SS) which suffers from the near-far problem. For this chapter, SS categories include direct sequence (DS), CDMA, and frequency hopping (FH).

Several tutorial papers have been published on interference rejection in SS, of which Milstein's paper [161] is of particular interest. Milstein discusses in depth two classes of rejection schemes (both of which implement an adaptive notch filter): 1) those based upon least mean square (LMS) estimation techniques, and 2) those based upon transform domain processing structures. The improvement achieved by these techniques is subject to the constraint that the interference be relatively narrowband with respect to the DS waveform. The present overview focuses on advances in interference rejection not covered by the 1988 Milstein paper. Kohno [122] provides another overview of classic solutions and promising techniques being studied in Japan and, in particular, describes a temporal domain approach where an adaptive digital filter (ADF) is employed to adaptively identify the time-varying response of the CCI in a DS-SS multiple access (MA) system without excessive noise enhancement.

Poor and Rusch [195, 211] give an overview of narrowband interference suppression in SS CDMA. They categorize CDMA interference suppression by linear techniques, nonlinear estimation techniques, and multiuser detection techniques. Using Milstein's 1988 paper, they describe linear techniques which include estimator/subtractor methods that perform time-domain notch filtering and transform-domain methods that operate to block (or suppress) narrowband energy in the frequency domain. In addition, Poor [194] reviews the adaptive filtering techniques for mitigation of multiple-access and narrowband interferences that arise in multiple access communications applications.

With particular application to CDMA, Duel-Hallen, Holtzman and Zvonar [58] provide a very useful overview of multiuser detection to mitigate multiple access interference (MAI) (refer to Section 3.3.2). They describe the concept of multiuser detection and typical techniques which are used, considering both coherent and noncoherent detection. Verdú [246] also gives a survey of various techniques proposed for adaptive multiuser detection.

3.3.1 Narrowband Interference Rejection for Direct Sequence

Interference rejection techniques for DS-SS systems are numerous. In particular, much literature exists on the adaptive notch filter as it relates to rejecting narrowband interference (NBI) on a wideband DS-SS signal. Decision-directed adaptive filtering is another well established technique for interference rejection. Other techniques for narrowband

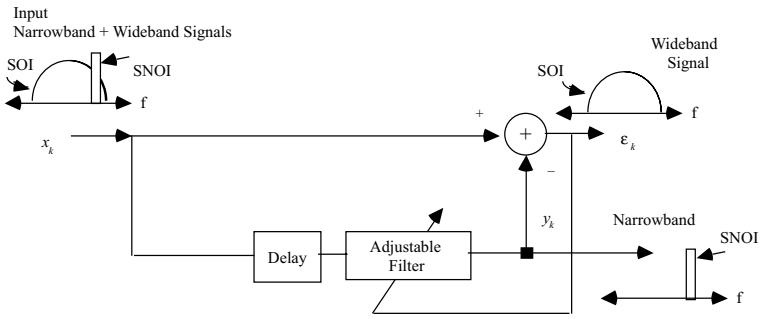

Figure 3.3: An adaptive notch filter or whitening filter.

DS-SS include adaptive analog-to-digital (A/D) conversion and nonlinear adaptive filtering. The following discussion focuses on innovative techniques developed since the 1988 tutorial paper by Milstein [161].

Adaptive Notch Filtering

The basic idea in employing an adaptive notch filter is to notch out the spectrum of the interference. SS tends to have a flat and wide spectrum and is affected little by this process, while NBI is characterized by spikes in the spectrum. The adaptive notch filter places notches at the location of the NBI to bring the interference level down to the level of the SS signal. At least two main approaches exist for creating an adaptive notch filter - 1) rejection schemes based on estimation-type filters (using adaptive techniques such as least mean square) and 2) rejection schemes based on transform domain processing structures.

Prediction/estimation-type filters Estimation-type filters (sometimes called prediction-type filters or whitening filters) can be viewed as performing a whitening (i.e., making the output samples uncorrelated) of the entire received signal. Usually the whitening process is implemented by an adaptive filter configured as a predictor of the narrowband signal. A tapped delay line can implement either a one-sided prediction filter (Wiener filter) or a two-sided filter (which is based on future values, as well as past values) to estimate the present. For a DS signal corrupted by noise and narrowband interference, future values tend to be uncorrelated with past values for DS and noise since they are wideband processes. Other the other hand, the interference, being a narrowband process, exhibits correlation between the past values and future values. The interference can therefore be predicted from past values and subtracted from the input signal. The wideband SS signal would then appear at the error output of the adaptive filter. An example of this type of adaptive notch filtering is shown in Figure 3.3 and is sometimes referred to an adaptive line enhancer (ALE).

The filter weights are updated with some adaptive algorithm such as least mean

square (LMS) estimation techniques. The LMS algorithm (complex) can be expressed in the form of three basic relations [255, 93]

1. The filter output:
$$y_k = \mathbf{w}_k^H \mathbf{x}_k \tag{3.1}$$
2. The adaptation error:
$$\varepsilon_k = d_k - y_k \tag{3.2}$$
3. The tap weight adaptation
$$\mathbf{w}_{k+1} = \mathbf{w}_k + \mu \mathbf{x}_k \varepsilon_k^* \tag{3.3}$$

where k denotes the discrete time, y_k is the filter output, $\mathbf{w}_k$ is the tap-weight vector, $\mathbf{x}_k$ is the tap-input vector, H indicates Hermitian transposition (i.e., conjugate transposition), ε_k is the estimation error, d_k is the desired response, μ is the step-size parameter, and * denotes conjugation.

Doherty [48, 50] presents an enhancement of the whitening filter technique which adds constraints based on the known characteristics of the pseudo-noise (PN) SS sequence to enhance the detection capabilities diminished by interference excision. Operating without training bits, the constrained updating of the filter coefficients retains the interference rejection properties of the excision filter while decreasing the variance of the decision variable. The standard least-squares rejection filter adds distortion to the decision variable at the output of the despreading operation. Doherty [49, 52] describes a constrained least-squares technique that utilizes a constrained optimality criterion to enhance the detection capabilities of DS-SS systems. Two transversal tapped delay lines (TDLs) are operated simultaneously, one containing the received data and the other containing the constraint data, as one set of adaptive weights operates on both TDLs with the LMS algorithm as the update technique. The filter weights are updated with respect to both minimizing the mean-square output error and minimizing the constraint error, with two types of constraint conditions: a correlation-matching condition (which induces the filter to pass the chip sequence undistorted) and a minimum-filter-energy condition. Doherty [51] incorporates vector space projection techniques to arrive at constraint surfaces used to suppress correlated interference.

Davis and Milstein [44] investigate the narrowband interference rejection capability of the fractionally-spaced equalizer and describe an adaptive tapped delay line equalizer which operates in a DS-CDMA receiver, where the taps are adapted to minimize the MSE of each chip. The overall effect of such equalization is to whiten the noise (in this case, MAI). This structure can be applied to reject NBI, and with sufficiently small tap spacing, it can reject NBI before the jammer is aliased at the chip rate. The technique is also compared to previously published methods of NBI rejection.

Krieger [127] proposes a constrained optimization criterion to drive an adaptive algorithm that operates on the output of a DS-SS demodulator. Based on maximum SINR, the adaptive algorithm estimates the generalized smallest and largest eigenvalues and their corresponding eigenvectors for positive definite matrices. Haimovich and Vadhri [92] state that while the energy of the SS signal is distributed across all the eigenvalues

of the data correlation matrix, the energy of the interference is concentrated in a few large eigenvalues. The corresponding eigenvectors span the same signal subspace as the interference. Their method of rejecting NBI in PN SS systems derives an error prediction filter with the additional constraint of orthogonality to these eigenvectors.

Stojanovic, Dukic, and Stojanovic [227] use linear mean-square (LMS) estimation to determine the tap weights of two-sided adaptive transversal filters so as to minimize the receiver output mean-square error caused by the presence of NBI and additive white Gaussian noise (AWGN). The results obtained show a significant reduction of the error rate in comparison to previously published results. Theodoridis, et al., [235] propose a block least-squares (LS) order-recursive algorithm for FIR filters with linear phase to design an FIR whitening filter for narrow-band interference rejection in PN SS systems. Simulations show 4-5 dB improvement in the output SNR over previously proposed schemes.

Several researchers have analyzed the impact of adaptive algorithms on performance. Bershad [23] investigates the effects of the LMS ALE weight misadjustment errors on the BER for a DS-SS binary communication system in the presence of strong NBI. The converged ALE weights are modeled as the parallel connection of a deterministic FIR (finite impulse response) filter and a random FIR filter. The statistics of the random filter are derived, assuming the output of the random filter to be primarily due to the jammer convolved with random filter weights, yielding a non-Gaussian output which causes significant error rate degradation in comparison to a Gaussian model.

Lee and Lee [138] suggest a gradient-search fast converging algorithm (GFC). For the case of a sudden parameter jump or new interference, the transient behavior of the receiver using a GFC adaptive filter is investigated and compared with that of receivers using a LMS or a lattice adaptive filter. They maintain that the GFC is superior for suppressing irregular hostile jamming in DS-SS. For better stability, He, Lei, Das, and Saulnier [97] discuss the modified LMS algorithm for transversal filter structures and lattice filter structures, comparing their bit error rate (BER) performance and convergence characteristics.

Mammela [151] simulates the performance of optimal and adaptive interference suppression filters for DS-SS systems. The simulations include the linear M-step prediction and interpolation filters and some of the best-known iterative and time-recursive algorithms (LMS, Burg, and Kalman algorithms). Mammela demonstrates that linear filters work well if the interference bandwidth is a small fraction of the signal bandwidth, and he shows that linear interpolation filters work better than prediction filters.

Iltis [113] proposes a receiver based on the generalized likelihood-ratio test (GLRT) where the interferer is modeled as an Nth order circular Gaussian autoregressive (AR) process and the multipath channel is represented by a tapped-delay line. He derives the maximum-likelihood (ML) joint estimator for the channel coefficients and interferer AR parameters. The GLRT receiver outperforms the transversal equalizer-based receiver by 2-3 dB.

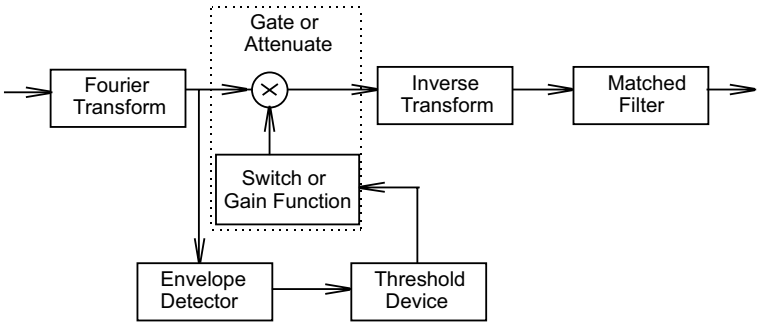

Figure 3.4: Block diagram of adaptive transform domain processing receiver.

Transform domain processing structures Performing notch filtering in a manner quite different from estimation-type filters, transform domain processing structures utilize, as a basic building block, a device which performs a real-time Fourier transform. An example of this technique is given in Figure 3.4, based on [161]. The lower branch envelope detects the Fourier transformed output, and the output of the envelope detector is fed into a switch (or an attenuator) controlled by a threshold device. The upper branch passes the Fourier transformed input directly to the multiplier. To implement the adaptive notch filter, the switch in the lower branch is forced to zero (or the attenuator is turned on) whenever the output of the envelope detector exceeds a predetermined level [161].

To suppress powerful narrowband interference in a pseudonoise (PN) SS system, Guertin [90] develops vector space interference excision (VSIE) methods which suppress the sidelobes of a sine wave interferer, in addition to the central lobe, while removing little signal power. VSIE methods are compared to frequency-domain methods, such as threshold excision (THE), which are complicated by the distribution of some of the power in a narrow band in sidelobes lying outside the original bandwidth. Guertin finds that SNR after VSIE is as much as 8 dB better than the SNR after THE.

Dominique and Petrus [53] excise NBI from a DS-SS signal by making use of the spectral redundancy between the sidebands of the PN-BPSK signal. The SPectral Redundancy Exploiting Interference Suppressor (SPREIS) uses this redundancy to obtain a better estimate of the spectral energy of the signal-of-interest (SOI), by replacing corrupted spectral estimates with uncorrupted and correlated estimates. They show improved performance over the THE with small increase in computational complexity.

Gevargiz, Das, and Milstein [80] demonstrate the advantage of an intercept receiver which uses a transform-domain-processing filter and detects DS BPSK SS signals in the presence of NBI by employing adaptive NBI rejection techniques. The receiver uses one of two transform-domain-processing techniques. In the first technique, the NBI is detected and excised in the transform domain by using an adaptive notch filter. In the second technique, the interference is suppressed using soft-limiting in the transform domain.

Since transversal filter techniques achieve a better performance when the reference signal is error-free, Lee and Essman [136] propose a scheme which utilizes a reference signal generating loop (to generate a reference signal) and which makes use of a scalar Wiener filtering technique in the Walsh-Hadamard transform (WHT) domain. The WHT is easy to implement since it requires only addition and subtraction. The scheme is not based on time-averaging methods, as in the lowpass filter or chip decision filter, so that a burst of errors due to the time-delayed reference signal is nearly absent and so that the chip error probability is significantly reduced. The WHT scalar filter prevents the weights from oscillating in steady state when the additional reference signal is employed in interference suppression.

Ruth and Wickert [212] examine the performance of a DS-SS receiver with a transform domain prefilter, as a function of noise power and jammer power. This time-varying interference rejection filter introduces intersymbol interference (ISI) which must be then addressed. Ruth and Wickert also explore digital design tradeoff issues such as the transform domain excision filter bandwidth and window functions. Medley, Saulnier, and Das [157] extend transform domain processing to include wavelets as the basis functions, in order to excise jamming signals from SS.

Tazebay and Akansu [234] propose a smart Adaptive Time-Frequency (ATF) exciser which intelligently decides the domain of the excision by evaluating both the time and frequency domain properties of time-varying signals. The input signal is processed in the domain where the interference is more localized. For frequency domain excision, adaptive subband transforms are utilized to track the spectral variations of the incoming signal. The ATF exciser performs well in narrowband interference and time-localized wideband Gaussian interference, and it is very robust to variations of the input signal when compared to conventional techniques (such as transform-domain filtering).

Amin, Venkatesan, and Tyler [10] exploit the capability of time-frequency distributions (TFDs) to excise interference in spread spectrum. TFDs can properly represent single as well as multiple component signals in time and frequency. The instantaneous frequency from the TFD is used to construct a finite impulse response filter which substantially reduces the interference power with a minimum possible distortion of the desired signal.

With a CDMA overlay in mind, Kanterakis' [117] technique for narrowband /broadband frequency selective limiting relies on setting the magnitude response of the received signal Fourier transform to a predetermined function while leaving the phase response unchanged. When the Fourier transform magnitude response of the signal is made constant over the entire signal spectrum, this nonlinear processor will operate as a whitening filter.

Wei, Zeidler, and Ku [253] examine the SS overlay problem assuming a realistic scenario that interferers are likely to occupy a significant portion of the CDMA bandwidth and have center frequencies which are offset from the carrier frequency of the CDMA signal. They derive an optimum suppression filter and demonstrate SNR improvement when compared to the optimal Wiener filter. For suppression filters for CDMA overlay, Wang and Milstein [250, 162, 251] evaluate the average BER and investigate how the

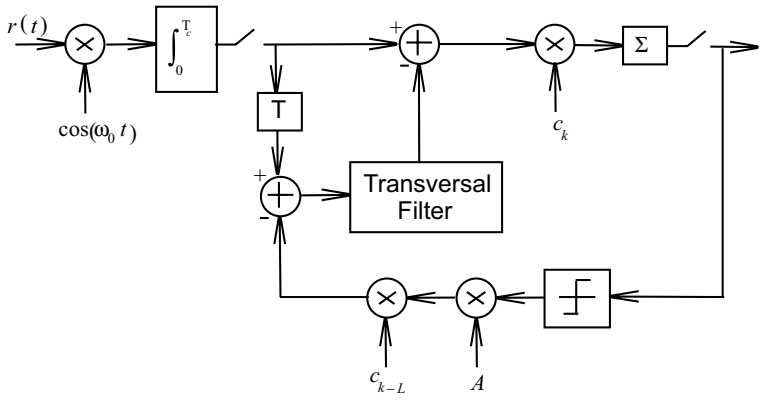

Figure 3.5: Decision feedback receiver.

performance is influenced by parameters such as the number of taps of the suppression filter, the number of multiple access users, the ratio of NBI bandwidth to SS bandwidth, the interference power-to-signal power ratio, and so forth.

Decision Feedback

An alternative to a transversal filter is a decision feedback (DF) filter. Decision feedback, or decision-directed, techniques use an adaptive filter to notch interference. Decisions (or "best guesses" of the signal state) are made at the output of the filter and then fed back to train the adaptive filter and/or be included in the filtering process. Variations of this technique exist where either the incoming signal is filtered and/or the estimation error is filtered. One version of such a filter is analyzed in [233] and shown in Figure 3.5. In Figure 3.5, $r(t)$ is the received signal which is coherently demodulated (ω_o is the carrier frequency) and then integrated over the symbol interval (T_c) and sampled. T is the delay, c_k is the kth chip of the PN sequence, and A is the amplitude of the received signal.

The rationale for using DF is to whiten just the noise and interference, necessitating some means of removing the desired signal. Since the output of the receiver is an estimate of the desired DS signal, this estimate can be used to generate a replica of the transmitted waveform, which can, in turn, be subtracted from the received signal. The possibility of error propagation exists but this effect appears negligible in certain applications [161].

Detection in DS-SS systems is often performed by correlating the received signal with the transmitter's spreading sequence. Pateros and Saulnier [189, 190] analyze the BER performance of an adaptive correlator, having the same structure as a DF filter, that detects the incoming data and compensates for the channel. The adaptive correlator, using DF, is shown to be capable of removing relatively wideband interference in the transmission bandwidth. The method implements a linear minimum mean square

estimator of the transmitted data based on the received samples. The receiver structure (which requires a training sequence but does not require the spreading sequence) is capable of removing single tone interference, and its performance in multipath is shown to be comparable and even superior to that of a Rake receiver in some instances.

Ogawa, Sasase, and Mori [179] examine suppression of CW interference and colored noise in a QPSK system using DF filters. They also [180] examine the performance of a differential phase-shift-keying (DPSK) DS-SS receiver using DF filters in the presence of NBI and multipath. They find that the two-sided DF filter is superior for suppressing both interference and multipath in the SS system. Miyagi, Ogawa, Sasase, and Mori [164] analyze the performance of three types of quadrature partial response signaling (QPRS) systems using complex one-sided and two-sided transversal filters, with additional DF taps, in the presence of single continuous wave (CW) interference and AWGN. They find that both DF filters suppressed CW interference and also suppressed noise. They also show that the duobinary system has the best performance of the three types of QPRS systems when the frequency of CW interference is low.

Dukic, Stojanovic, and Stojanovic [61, 62, 59, 60] combine two-sided transversal filters along with DF to combat NBI. Their receiver is made up of two branches: the conventional demodulator followed by a DF filter and, in an auxiliary branch, a demodulator with the carrier in quadrature followed by a two-sided adaptive transversal filter. The results show significant NBI rejection, with little dependence on the difference in frequencies of the desired and interfering carriers or on the interfering carrier level. The receiver is also robust to impulsive interference. Dobrosavljevic, Dukic, et al., [47] improve the receiver with two-stage DF filter techniques.

Shah and Saulnier [218] conclude that LMS adaptive filtering improves the probability-of-error performance of a DS-SS system operating in the presence of stationary single-tone jammers. They also claim that, when compared with the no feedback case, LMS adaptive systems with DF do not degrade probability of error performance; however, DF does not always appreciably improve system error rates either. Error rates for the systems with DF approach error rates for the no feedback case as the processing gain increases.

Other sections in this overview contain examples of DF for interference rejection, such as DF used in CDMA adaptive multiuser detection (Section 3.3.2), in adaptive equalization (Section 3.4.1), in backpropagation neural networks (Section 3.4.3), with radial basis functions (Section 3.4.3), in spectral correlation (Section 3.4.4), and in novel techniques (Section 3.4.6).

Adaptive A/D Conversion

Milstein's 1988 tutorial gives brief mention to another technique proposed by Amoroso [11, 14] and Pergal [192] for making the DS receiver more robust with respect to interference. Adaptive A/D conversion is a scheme using an A/D converter, in conjunction with a variable threshold, to retain those chips of the spreading sequence which, when added to a strong interfering signal, are still received with their correct polarity. The idea

behind adaptive A/D conversion is that the bias introduced by a high-power narrowband interferer can be tracked and compensated for before entering the A/D converter. Equivalently, thresholds of the A/D converter can be changed to minimize the impact of the interference. Adaptive threshold A/D techniques exploit the statistical behavior of constant envelope, angle modulated, sinusoidal jammers to enhance the effective processing gain of a PN receiver. For proper operation, it is necessary for this system to have both a large jammer/signal (J/S) ratio and a large ratio of interference power-to-noise power.

The A/D converter is distinguished from various forms of notch filtering in that the A/D converter performs well against CW even if the interference is frequency or phase modulated, as long as the amplitude of the CW mixed with the signal remains fairly constant. Pergal points out that A/D conversion gain depends only on the statistical distribution of the interfering signal (as opposed to notch filtering which is spectrally dependent). Bricker [27] derives a closed form expression for the output SNR of the A/D as a function of the input SNR and the A/D parameter settings.

Amoroso [12] extends previous analyses to give the performance of the adaptive two-bit A/D converter for combined CW and Gaussian interference. The converter yields substantial conversion gain even when the DS-SS is much weaker than the Gaussian component of interference. The upper bound on conversion gain depends primarily on the relative strengths of the Gaussian and CW components of interference. Cai [29] discusses the optimization of the two-bit A/D converter.

Goiser and Sust [85, 86] consider digital matched filters for DS-SS communications and find that minimum complexity is obtained if hard-limiting analog-to-digital converters (ADCs) are used. This structure, however, while yielding good performance in AWGN, experiences intolerable degradation for non-Gaussian interference. They propose a hard-limited two-bit ADC (with adaptive thresholds) noncoherent receiver and examine its performance in AWGN, CW, and combined CW/AWGN interference. When compared to just hardlimiting, slightly better performance in AWGN with the ADC is overshadowed by increased complexity. On the other hand, results show dramatic improvements in the presence of CW interference for little increase in complexity.

Amoroso and Bricker [15] extend the theory of A/D conversion in the case of noncoherent reception of DS PN signals and find that the A/D converter performs well in both CW and Gaussian interference. Amoroso [13] applies adaptive A/D conversion to suppress co-channel constant envelope interference in mobile digital links. He proposes a polar adaptive A/D converter, operating in a noncoherent detection setting, which exhibits performance superior to previous Cartesian A/D converters (even when Cartesian converters are allowed to operate in a coherent detection mode).

Nonlinear Techniques

For prediction of a narrowband interferer in the presence of non-Gaussian noise (such as the SS signal itself), linear methods are no longer optimal and nonlinear methods can yield better performance. Narrowband interference can be mitigated in SS systems

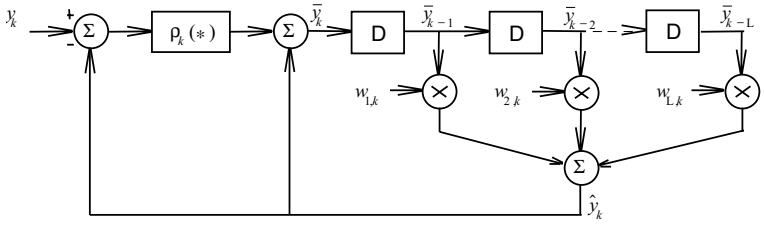

Figure 3.6: Nonlinear adaptive predictor.

(such as CDMA) by techniques based on nonlinear filtering, where, for example, the CDMA signal is modeled as non-Gaussian noise in the interference suppression process. The narrowband signal is modeled as an autoregressive (AR) process (i.e., as the output of an all-pole linear filter driven by additive white Gaussian noise). When the statistics of this AR process are unknown to the receiver, the parameters can be estimated by an adaptive nonlinear filter which uses a standard LMS adaptation algorithm to predict the interferer by incorporating a nonlinearity which takes the form of a soft decision feedback of an estimate of the spread spectrum signal [195]. As in previous sections, the narrowband prediction is subtracted from the observation, leaving the SS signal plus AWGN.

An example of a nonlinear adaptive predictor is given in Figure 3.6, based on [211], where the nonlinearity involves a soft decision feedback via the tanh function [211]. The LMS algorithm is employed in this filter where

$$\varepsilon_k = y_k - \hat{y}_k \tag{3.4}$$

$$\rho(\varepsilon_k) = \varepsilon_k - \tanh\left(\frac{\varepsilon_k}{\sigma_k^2}\right) \tag{3.5}$$

$$\bar{y}_k = y_k - \tanh\left(\frac{\varepsilon_k}{\sigma_k^2}\right) = \hat{y}_k + \rho(\varepsilon_k) \tag{3.6}$$

where y_k is the input signal, $\rho(\varepsilon_k)$ is a nonlinear function (the output of this transformation represents the residual less the soft decision on the SS signal - ideally noise), $\hat{y}_k$ is the estimate of the interference, $\bar{y}_k$ is the observation less the soft decision on the SS signal, the residual ε_k represents observation less the interference estimate, $w_{L,k}$ are the tap-weights, D is the delay, and L is the number of taps.

Several papers serve as background to the previous illustration. Garth, Vijayan, and Poor [78] generalize the nonlinear filter derived by Vijayan and Poor [247] and show that for channels corrupted by impulsive noise, the binary nature of the DS signals can be exploited to obtain better performance by using nonlinear filters. Garth and Poor [79] develop DS-SS suppression algorithms which are based on nonlinear filters that produce predictions of the interfering signals that are then subtracted from the received signal to suppress the interference. Overall, the interference rejection capability provided by

the nonlinear filter (compared to the linear filter) for impulsive noise background is substantial.

Higbie [99] describes a nonlinear signal processing technique designed to suppress interference in DS-SS receiving systems. The basic idea is to optimize the detection process dynamically, in the presence of interference, by estimating the statistics of the interference and then by using this information to derive a nonlinear transform to apply to the corrupted signal. This adaptation is open-loop, thus avoiding convergence problems and yields large improvements (tens of dB).

Kasparis, Georgiopoulos, and Payne [118] propose the use of a conditional nonlinear median filter operating in the transform domain, for the detection and suppression of narrowband signals of sufficient power, without regard to their center frequency, bandwidth, or peak power. Nelson and Kasparis [175] extend this work by confronting problems incurred in Rayleigh distributed fading channels. Their solution is a normalized adaptive median filter, which considers each received bit independently and uses a normalization metric to compensate for fading.

Jacklin, Grimm, and Ucci [115] present the performance results of a two-dimensional DS-SS communications system employing Locally Optimal (LO) Maximum Likelihood detection. The LO receiver is robust in the sense that no *a priori* interference statistics are assumed. Instead, the required LO memoryless nonlinear transform is estimated directly from the statistics of the received data. The LO nonlinear processor provides a performance improvement over traditional demodulation methods when the SS system is subjected to a CW jammer, and it is shown to depend on the number of chips per information bit and the ratio of the jammer frequency to the transmitted signal's carrier frequency.

Krinsky, Haddad, and Lee [128] propose a system to adaptively mitigate burst type interference, where the interference is modeled as a combination of an autoregressive process and a Markov process. The optimal receiver is shown to have a computational complexity which increases exponentially with the system's processing gain. They present two suboptimal receivers, one based on the interacting multiple model (IMM) and one based on the simpler fast IMM (FIMM). Since the P_e performance of these receivers is comparable, the substantial complexity reduction offered by the FIMM-based receiver makes it the better choice. The FIMM-based receiver may be viewed as a time-varying nonlinearity. This nonlinearity is a function of the current model probabilities and interference estimates, and thus is a nonlinear function of past observations. The nonlinearity can resemble a linear filter, a soft limiter, or a noise blanker depending on the current state of the system.

3.3.2 Wideband Interference Rejection for Direct Sequence

Whereas the previous section focused on narrowband interference in DS-SS, this section considers ways to mitigate wideband interference in DS spread spectrum systems. A primary example of the wideband interference problem is found in CDMA systems, where all users (each with his own spread spectrum signal) share the same band and interfere

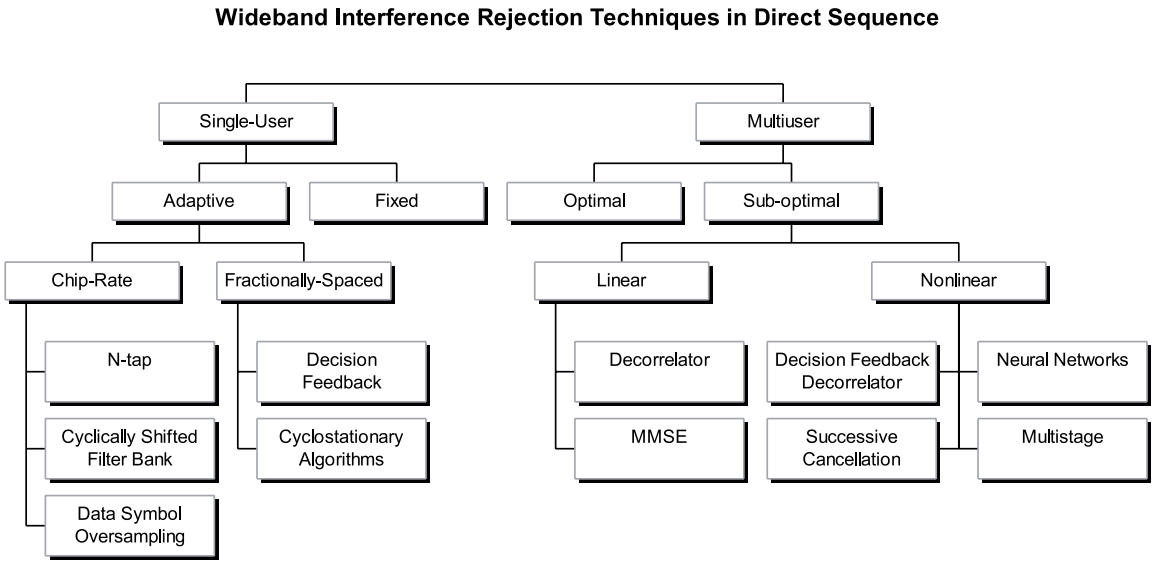

Figure 3.7: Organizational chart for wideband interference rejection in direct sequence spread spectrum (e.g., CDMA).

with each other. Interference rejection is important to facilitate increased capacity in the licensed bands which deploy CDMA. Wideband interference rejection is also important in other applications, such as the unlicensed ISM bands (902-928 MHz and 2.4-2.835 GHz) where spread spectrum is often the best system. The commercial implications of this subject has spawned a great volume of papers in this area in recent years.

We divide this section into single-user detection and by multiuser detection. CDMA interference rejection is accomplished by both techniques. Techniques to mitigate non-CDMA wideband interference (e.g., as encountered in the unlicensed ISM bands) fall under the category of single-user detection. By single-user detection, we mean that only one user's spreading code and delay is known and utilized at the receiver. With multiuser detection, several (if not all) of the users' spreading codes and delays are known and used at the receiver. Some authors categorize single-user detection (in a multiuser environment such as CDMA) under the heading of multiuser detection, but we distinguish single-user and multiuser detection as defined above. As mentioned, Verd [246] and Duel-Hallen, et al., [58] provide surveys, wider in scope than that presented here, of various techniques proposed to mitigate MAI. An organizational chart of wideband interference rejection for DS CDMA receiver is given in Figure 3.7, which represents a combination of charts proposed by [28] and [150] for CDMA interference rejection.

The current generation of CDMA systems employs single stage correlation receivers that correlate the received signal with a synchronized copy of the desired signal's spreading code. The receiver consists of a bank of matched filters, each of which is matched to a particular user's spreading code. Conventional receivers treat MAI, which is inherent in

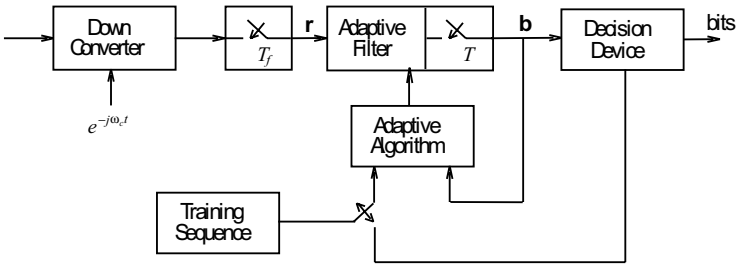

Figure 3.8: Block diagram of an adaptive single-user receiver in CDMA.

CDMA, as if it were additive noise. However, in asynchronous systems, MAI is generally correlated with the desired signal and thus causes degradation. Synchronous systems (which allow the use of codes which make the MAI uncorrelated) can be implemented on the downlink, but not on the uplink.

In a single cell environment, CDMA systems employing simple correlation receivers cannot approach the spectral efficiency of orthogonal multiplexing schemes such as TDMA or FDMA [197]. Furthermore, correlation receivers are particularly susceptible to the near-far problem when multiple access signals are received with different signal powers. Even if sophisticated power control is employed, the near-far effect can still result in significant performance degradation. Greater channel capacity for CDMA can be achieved by using interference rejection techniques to mitigate MAI.

Single-User Detection

By single-user detection, we mean that only one user's spreading code and delay are known at the receiver. The structure (such as spreading codes, delays, and powers) of the multiple access interferers are assumed to be unknown. The complexity in single-user detection is generally much smaller than that of multiuser detection.. Single-user schemes can be adaptive or fixed. We focus on adaptive techniques, which can be categorized as chip rate structures or fractionally-spaced structures. An general block diagram of fractionally-spaced adaptive single-user receiver based on [200] is given in Figure 3.8 for CDMA. T_f represents fractionally-spaced sampling, T is the symbol interval, r is the sampled received signal, b is the decision statistic, and c is the carrier frequency.

Chip rate Using the MMSE criterion, Madhow and Honig [148, 147, 149] consider interference suppression schemes for DS-SS CDMA systems. They look at N-tap chip rate filters, the cyclically shifted filter bank, and data symbol oversampling. These schemes have the virtue of being amenable to adaptation and simple implementation (in comparison to multiuser detectors), while, at the same time, alleviating the near-far problem to a large extent. The channel output is first passed through a filter matched to the chip waveform and then sampled at the chip rate. Because of the complexity

and coefficient noise associated with such an adaptive filter when spreading gain N is large, simpler structures with fewer adaptive components are proposed. In each case the multiple samples per symbol are combined via a tapped delay line, where the taps are selected to minimize the mean square error.

Honig, Madhow, and Verd [104] propose an interesting and simple blind multiuser linear detector which requires only knowledge of the desired user's signature sequence (and associated timing). The received amplitudes need not be known or estimated, and the signature waveforms of the interferers need not be known. The technique is blind because training sequences are not required for any user. The detector converges always to an optimally near-far resistant solution. The strategy is to minimize the output error, which is equivalent to minimizing the mean square error (but without the requirement of training sequences). The authors give an overview of blind multiuser detection in [105]. Honig [103] also proposes a blind algorithm using the orthogonal Sato cost criterion, which leads to a stochastic gradient algorithm that has advantages relative to the minimum variance algorithms.

Tahernezhad and Zhu [232] evaluate the BER performance of two adaptive schemes in asynchronous CDMA - the N-tap filter and the D-tap cyclical shifted filter bank filter. LMS and predictive LMS are employed for the adaptation of the tap weights.

Ström and Miller [229] present a common mathematical framework for comparing simpler structures in terms of their probability of bit error, deriving the form of the optimum complexity (dimension) reduction. They propose a simple scheme called symmetric dimension reduction (SDR), which is shown to outperform the cyclically shifted filter bank structure [148] (another complexity reduction scheme). Miller [160] proposes an adaptive receiver that uses a chip matched filter followed by an adaptive equalizer to perform the despreading operation. The receiver is shown to be immune to the near-far problem.

Lee [137] presents rapidly converging adaptive equalization algorithms for interference suppression in DS/CDMA. The algorithms, based on an orthogonal transformation, do not require *a priori* knowledge of interfering signal parameters, such as spreading code sequences and relative signal power levels. The convergence rate of these algorithms is independent of the eigenvalue spread of the input data correlation matrix. Lee's proposed adaptation algorithm is shown to be superior to LMS and RLS.

Fractionally-spaced (*Decision Feedback*) In the context of DS-SS CDMA, Abdulrahman, Falconer, and Sheikh [2, 3, 4] present work on a receiver consisting of a spread sequence matched filter (SSMF), matched to a desired user's spreading code, followed by a fractionally-spaced decision feedback equalizer (DFE) MMSE filter. This technique does not need the assumption that the spreading sequences of all users are known at the receiver; the receiver only uses information about the desired user's spreading code and a training sequence. The authors document performance in slow fading and how a fractionally-spaced DFE can be used as a CDMA demodulator. In an implementation that does not require knowledge of any user's spreading code, the authors replace the SSMF with a lowpass filter (LPF) having a bandwidth equal to the spread signal

bandwidth. Simulation of both receivers yields better MMSE performance by the SSMF receiver.

Rapajic and Vucetic [201] describe a fully asynchronous single user receiver in a CDMA system where the receiver is trained by a known training sequence prior to data transmission and continuously adjusted by an adaptive algorithm during data transmission. An adaptive, fractionally-spaced LMS filter, instead of a matched filter with constant coefficients, is employed for each user separately. Experimental results show that a considerable improvement in BER is achieved with respect to the conventional single-user receiver. In [199], Rapajic and Vucetic consider additional adaptive linear and decision feedback structures for coherent demodulation in asynchronous CDMA. In [200], they also investigate the use of adaptive transmitters and receivers, where it is assumed that there is no knowledge of the signature waveforms and timing of other users. The transmitter adapts based on feedback information from the receiver, which is used to calculate the optimum transmitter signature. The signatures are adaptively adjusted according to the MSE criterion during the training period as well as during data transmission. CDMA systems employing the adaptive transmitters in the presence of MAI achieve the matched filter bound with no interference.

Fractionally-spaced (*Cyclostationarity Algorithms*) Many signals exhibit cyclostationarity; that is, the statistics of the signal are periodic, with resulting spectral correlation. A complete analysis of cyclostationarity in DS-SS signals was presented by [33]. Fundamental statistical periodicities exist at the chip rate, data rate, and code repetition rate, with denoting the cycle frequencies associated with these periodicities. Cyclostationarity exploiting algorithms which, in many instances, resemble fractionally-spaced equalizers (FSEs) [20, 19], represent another class of techniques for combatting MAI. Although essentially equivalent to the MMSE structures presented earlier, the framework of the analysis is different and provides additional insight to the problem. A complete analysis by Agee [8] shows that the stability and efficiency of near-far power management strategies used in CDMA are greatly enhanced by exploiting the spectral diversity of CDMA networks. Specifically, spectral diversity is easily exploited in CDMA networks employing modulation-on-symbol DS-SS modulation formats where the direct-sequence code repeats once per message signal.

Holley and Reed [102] and also Aue and Reed [20, 19] show how spectral correlation properties can be exploited by a time dependent adaptive filter (TDAF). This technique provides increased capacity for CDMA close to that of FDMA or TDMA using frequency-domain and time-domain filtering structures. CDMA capacity plots shown in [102] are typical of those found in FDMA and TDMA. The idea is to view the spreading process as replicating the data sequence on multiple carriers spaced at multiples of the code repeat rate. The adaptive filter combines this replicated spectrally correlated data using a time-varying filter. A frequency domain implementation is shown in Figure 3.9 [102], where $x(k)$ is the received signal, α is the code repetition rate cycle frequency, $y(k)$ is the desired signal, and $\hat{y}(k)$ is the estimate of the desired signal.

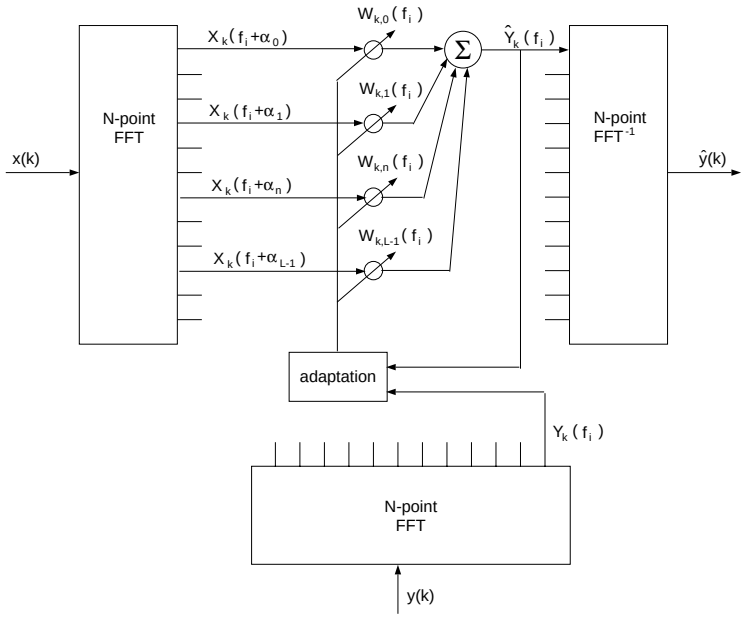

Figure 3.9: FFT time-dependent adaptive filter structure (frequency domain implementation) showing estimation of one output bin.

Monogioudis, Tafazolli, and Evans [167, 168] employ a technique based on adaptive linear fractionally-spaced equalization (LFSE) to adaptively cancel MAI in CDMA systems. Simulation results indicate that the LFSE offers significant gains over the conventional detector, eliminating the near-far problem without explicit knowledge of the interfering spreading sequences. The E_b/N_o degradation due to multipath propagation is insignificant, so that the LFSE is also able to combine optimally the multipath rays and act as an adaptive Rake combiner-canceller.

Yoshida, Ushirokawa, Yanagi, and Furuya [268] propose an adaptive interference canceller (AIC) consisting of a fractionally chip-spaced code-orthogonalizing filter (COF) and a differential detector. Using only the desired spreading code, the COF adaptively makes its tap coefficients orthogonal to all other users' spreading codes by minimizing the MSE between the detected and decision signal. The COF is a linear adaptive filter used to cancel MAI. After the MAI cancellation, the differential detector removes fast phase variation in the desired carrier due to fading. Placed separately from the COF, the differential detector determines the tracking ability for fast fading. A DS/CDMA system using the proposed AIC is able to accommodate an increased number of multiple-access users when compared with the case of using the conventional matched filter receiver.

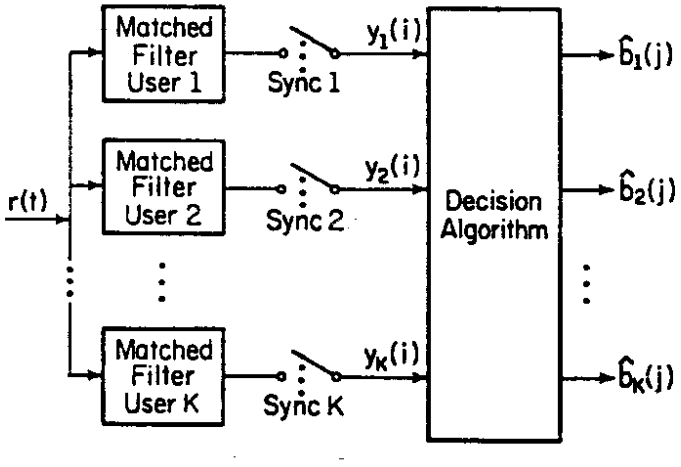

Figure 3.10: Optimum K-user detector for asynchronous multiple-access Gaussian channels.

Multiuser Detection

Much of the motivation for designing better multiuser detectors results from the theoretical capacity work of Verd [245] for optimal CDMA receivers. Multiuser detectors require that all CDMA users' spreading codes and delays are known at the receiver. Verd shows that the near-far problem is not an inherent flaw of CDMA, but results from the inability of the conventional receiver to exploit the structure of the MAI. Because, however, the optimal receiver is hopelessly complex, several suboptimal receivers have been proposed to approximate it, resulting in a large number of published papers. These detection schemes are considered adaptive because they adapt to the changing channels of the users to track delays and often power levels.

Optimal A block diagram for an optimum k-user detector for an asynchronous multiple-access Gaussian channel is given in Figure 3.10 [245]. The received signal $r(t)$ is a corrupted composite of the K CDMA users with s_k the unit-energy signature waveforms . The received signal passes through a bank of matched filters, where each filter is matched to a particular user's spreading code. The outputs of the matched filters are sampled, with knowledge of each user's delay (i.e., sync), yielding $y_K(i)$ which are passed through a decision algorithm to produce the estimates $\hat{b}_K(j)$ of the desired signals.

Generally, the optimum receiver processes the received waveform with a bank of matched filters, which produce a vector of observables:

$$\mathbf{y} = \mathbf{RAb} + \mathbf{n} \tag{3.7}$$

where $\mathbf{A}$=diag$A_1, \ldots, A_k$, A_k is the received amplitude of the kth user, $\mathbf{b}$=$b_1, \ldots, b_k{}^{\mathrm{T}}$, $b_k \in \{-1, +1\}$ is the data stream modulated by the kth user, $\mathbf{n}$ is a zero mean Gaussian

vector, and $\mathbf{R}$ is the crosscorrelation of s_k the unit-energy signature waveforms of the kth users [246].

Linear Sub-optimal An example of a suboptimal receiver is the decorrelating detector [146] which multiplies the matched filter outputs in (3) by the inverse crosscorrelation matrix $\mathbf{R^{-1}}$, i.e., it takes the sign of the vector

$$\mathbf{R^{-1}y} = \mathbf{Ab} + \mathbf{R^{-1}n} \tag{3.8}$$

For frequency-nonselective Rayleigh fading asynchronous CDMA channels, Zvonar and Brady [272] focus on two low-complexity sub-optimal multiuser receivers with diversity reception, namely a coherent decorrelating and a differentially coherent decorrelating detector. They also analyze an adaptive coherent multiuser receiver utilizing decision-directed carrier recovery and maximal ratio combining. They bound its error probability showing the impact of imperfect channel estimates and MAI. The comparison of two receiver structures indicates that the coherent decorrelating detector with diversity reception is preferable in nonselective fading CDMA channels with memory.

A linear MMSE multiuser detector can outperform a decorrelating detector when all the interferers are very weak. The linear MMSE detector replaces the inverse crosscorrelation matrix $\mathbf{R^{-1}}$ by the matrix

$$\mathbf{R^{-1}} = [\mathbf{R} + \sigma^{\mathbf{2}}\mathbf{A^{-2}}]^{\mathbf{-1}} \tag{3.9}$$

where σ^2 is the background noise power spectral density.

Mandayam and Aazhang [152] consider a DS-CDMA system from the framework of a discrete event dynamic system (DEDS) and develop infinitesimal perturbation analysis (IPA) for estimating the sensitivity of the average probability of bit-error in such systems. The estimates are shown to be unbiased, and this technique is then further incorporated into a stochastic gradient algorithm for achieving adaptive multiuser interference rejection. They develop an algorithm for an adaptive linear detector with the average probability of error being the minimization criterion. The algorithm is shown to converge, and the resulting detector performs better than the MMSE detector.

Monk, Davis, Milstein, and Helstrom [166] approximate multiple access noise by a Gaussian process of the same power spectral density, leading to the criterion of maximizing SNR. They propose and analyze receivers that maximize SNR under various constraints, without requiring locking and despreading multiple arriving CDMA signals.

Nonlinear Sub-optimal (*Decision Feedback Decorrelator*) Duel-Hallen [57] proposes a decorrelating decision feedback (DF) detector for synchronous CDMA which utilizes decisions of the strongest users when forming decisions for the weaker ones. The complexity of the DF is linear in the number of users, and it requires only one decision per user. Performance gains with respect to the linear decorrelating detector are more significant for relatively weak users, and the error probability of the weakest user approaches the single-user bound as interferers grow stronger. The error rate of DF is compared to those of the decorrelator and the two-stage detector.

Nonlinear Sub-optimal (*Neural Networks*) Neural networks are receiving increased interest for spread spectrum applications. These advanced algorithms simultaneously account for nonlinearity, nonstationarity, and non-Gaussianity. Haykin provides a good introduction into how neural networks expand the horizons of signal processing [94]. Mulgrew [172] also provides an overview into how radial basis function neural networks (see Section 3.4.3) can be applied in spread spectrum systems.

Multiuser detection using a backpropagation neural net is proposed by Aazhang, Paris, and Orsak [1] to approximate the highly complex optimal receiver. Mitra and Poor [163] also investigate neural network techniques to adaptively determine unknown system parameters. They show that the optimal multiuser receiver for synchronous detection of DS spread spectrum multiple access (SSMA) signals can be implemented with a radial basis function (RBF) network. The authors consider how to find the optimal weights and the use of clustering methods to determine the centers of the RBF neurons. Simulations show that the RBF network has the desirable properties of moderate weight convergence rate and near-optimal performance in realistic communication environments.

Nonlinear Sub-optimal (*Successive interference cancellation*) Under the category of tentative-decision based multiuser detection, Verd [246] discusses successive cancellation and DF. The idea is to estimate and cancel each user successively. For example, one would detect the data of the strongest user with a conventional detector and then subtract the signal due to that user from the received signal. This process assumes extremely accurate estimation and ordering of received user amplitudes. Viterbi first proposed the use of successive cancellation for CDMA [248], yet in a more recent paper [249] Viterbi states that, at best, this type of interference cancellation would have a similar effect to having same-cell-user orthogonality, and at worst, successive cancellation may lack robustness and consequently may make matters worse. Viterbi concludes that the processing complexity and possible processing delay make the application of successive cancellation questionable. Nevertheless, research continues in this area because of the large capacity gains that have been demonstrated theoretically [188].

Nonlinear Sub-optimal (*Multistage techniques*) Multistage techniques also involve making estimates and cancelling, where the number of stages represents the number of times that estimates of all the users are made. Successive cancellation (discussed in the previous section) could be the first stage of a multistage receiver. We do not cover these multistage techniques in depth; nevertheless, they represent a useful class of techniques for rejecting MAI.

A few examples illustrate multistage detection. Grant, Mowbray, and Pringle [88] model the subscriber interference through channel measurement to permit adaptive cancellation of co-channel CDMA interference. Using a conventional first stage, the authors [171, 170] show a theoretical upper bound on the spectral efficiency approaching 130% or 1.3 normalized channels per hertz for successive cascaded cancellation stages, but their simulations only approach about 80%. Better results might be obtained by using a more accurate first stage. Proposing an adaptive version of a multistage detector, Bar-Ness,

Siveski, and Chen [22, 225] present a bootstrapped decorrelating algorithm for adaptive interference cancellation in synchronous CDMA. A combination of a correlation detector and a multiuser adaptive interference canceller uses weight control criterion based on minimizing the correlation between the signals at the outputs of the canceller. Its performance is compared to that obtained with the minimum power criterion. In [270], Zhu, Ansari, and Siveski investigate this adaptive synchronous CDMA receiver in more depth.

3.3.3 Interference Rejection for Frequency Hopping

Interference rejection for frequency hopping is not as well developed as interference rejection for DS or for CDMA. Typically, frequency hopping interference rejection techniques often employ a whitening stage to reject narrowband and wideband interference. In some instances, they also use the transient property of the hopper to distinguish it from persistent background interference.

Kurita, Sasase, and Mori [129] examine the performance of a hard-limited combining receiver using fractional tap spacing transversal filters in fast frequency hopping (FFH) BPSK systems in the presence of stationary NBI. A block diagram of their receiver is given in Figure 3.11 [129]. The fractional tap spacing filter uses a tap spacing of $T_h/4L$, where T_h is the duration of each hop and L is the total number of hops. The output of the transversal filter is demodulated to FFH-BPSK signals which are low-pass filtered and envelope detected. After each chip is decided MARK (1) or SPACE (0), the bit is decided by the majority. The tap coefficients a_k are updated by an adaptive algorithm. The BER performance of the proposed receiver does not have an error floor and is superior to that of a hard-limited combining receiver without the transversal filters (which is shown to have a lower bound in BER with interferers in two frequency slots).

Unlike DS signals, FH signals are instantaneously narrowband, but when observed over a time span encompassing multiple hops, the FH signal becomes wideband. Exploiting this property, Iltis [112] shows how prewhitening filters designed using linear least-squares estimation techniques can be applied to improve the detection performance of FH signals. Iltis presents two interference suppression filters. One filter - with taps spaced at the hop duration T_h - can reject interference with a bandwidth of up to π/T_h radians/sec. A second filter uses fractionally-spaced taps at intervals of T_h/L (where L is the number of hops) and rejects interference with a bandwidth of up to $L\pi/T_h$ radians/sec, providing improved detection performance when the FH signal is linearly combined over L hops.

Iltis, Ritcey, and Milstein [111] describe a fast frequency-hopped (FFH) receiver which employs a prewhitening filter to reject NBI. By using an appropriate fractional tap spacing, it is shown that the interference can be estimated independently of the desired signal. This least-squares interference rejection technique is shown to compare favorably with maximal-ratio combiner technique.

Reed and Agee [205] extend and improve on the idea of whitening by using a time

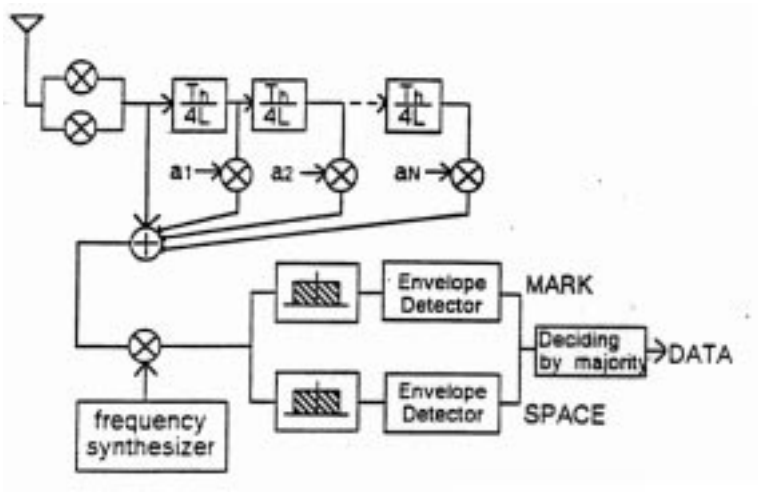

Figure 3.11: Hard-limited combining receiver using a transversal filter.

dependent filter structure to estimate and remove interference, based on the interference spectral correlation properties. The detection of FH SS in the presence of spectrally correlated interference is nearly independent of the SIR. The process can be viewed as a time-dependent whitening process with suppression of signals that exhibit a particular spectral correlation. The technique is developed from the maximum-likelihood estimate of the spectral frequency of a frequency agile signal received in complex Gaussian interference with unknown spectral correlation. The resulting algorithm uses the correlation between spectrally separated interference components to reduce the interference content in each spectral bin prior to the whitening/detection operation.

Glisic and Pajkovic [83, 84, 82] analyze the performance of a DS QPSK SS receiver using adaptive filtering to reject a FH multiple access signal. Considering the adaptive prediction error filter with two-sided taps, they show graphically the conditions and number of FH multiple access signals that can be efficiently suppressed using adaptive filtering in a DS-SS receiver.

Bishop and Leahy [26] present a technique for enhancing a wideband signal of narrow instantaneous bandwidth, such as a FH signal, from wideband and narrowband interference. The central concept is that statistical estimation inherently involves a time average with an accompanying convergence time, and this property can be used to separate signals. A device, such as an ALE, that separates wideband and narrowband waveforms can use this property to distinguish the SOI from the interference.

Gulliver [91] proposes a concatenation of order statistics (OS) and normalized envelope detection (NED) to combat noise and multi-tone jamming. He shows that the OS-NED method significantly improves the performance of NED alone in multi-tone jamming, with only slight degradation in noise jamming.

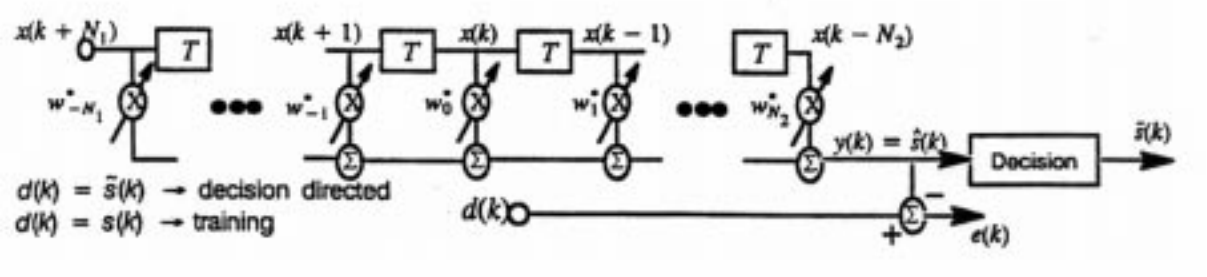

Figure 3.12: A two-sided T-spaced adaptive linear equalizer.

3.4 Non-Spread Spectrum Techniques

A number of techniques exist for rejecting interference for non-SS signals. Many of these techniques, such as the constant modulus algorithm and decision-directed adaptive filtering, are well-known adaptive equalization techniques. In addition, some emerging interference rejection techniques which are based on neural nets, time-dependent filtering (which exploits spectral correlation), and nonlinear filtering show great promise.

3.4.1 Adaptive Equalization

Some techniques for interference rejection find their roots in adaptive equalization research, which primarily focuses on mitigating ISI. Much research on adaptive equalization has been documented in the literature. Proakis devotes an entire chapter to adaptive equalization in his thorough textbook on digital communications [196]. Because this overview focuses on channel interference and not ISI, only adaptive equalization work that is combined with interference rejection is surveyed. The following papers illustrate the application of adaptive equalization to interference rejection. An example of an adaptive linear equalizer is given in Figure 3.12 [178], where T is the symbol duration. The ideal equalizer will extract the transmitted signal, $s(k)$ from the received data at each time instant.

North, Axford, and Zeidler [178] analyze the effects of interference on the steady-state performance of several adaptive equalization algorithms and show that the built-in capability to reject NBI deteriorates in performance as the bandwidth of the interference increases. The existence of a time-varying misadjustment component in the adaptive equalizer weight vector is shown to affect the interference cancellation properties. By decomposing the output of the adaptive linear equalizer (AEQ) into a Wiener filter (WF) term and a misadjustment filter (MF) term, the authors interpret the AEQ as a device which rejects interference by creating a notch in the frequency response of the WF, but that the time-varying MF under certain conditions fills the notch (i.e., compensates for WF generated ISI), thereby improving performance over that of the WF alone.

Niger and Vandamme [177] show that synchronous decision-feedback equalizers are

powerful countermeasure devices for radio channels affected by both selective fading and sinusoidal interferers. They demonstrate that both $T/2$-spaced linear and nonlinear equalizers can provide a significant improvement of the adjacent channel interference margin, especially in the case of multi-carrier interleaved frequency arrangements.

Considering narrowband TDMA, Lo, Falconer, and Sheikh [145, 144] investigate the performance of an adaptive fractionally-spaced decision-feedback equalizer (DFE) in the presence of CCI, ACI, and additive Gaussian noise for a frequency-selective quasi-static channel environment. A directly adapted recursive least squares (RLS) DFE performs better than a computed MMSE DFE, which employs estimates of the channel impulse response and the autocorrelation of interference plus noise. The use of a wide receiver bandwidth yields a performance improvement for channel spacings which allow for sufficient spectral overlap of ACI with the desired signal bandwidth. Thus, a reduction in channel spacing increases the radio capacity while maintaining a desired average BER or outage performance.

Yoshino, Fukawa, and Suzuki [269] propose an adaptive Interference Canceling Equalizer (ICE) which uses RLS Maximum-Likelihood-Sequence-Estimation (RLS-MLSE) to cancel CCI in the received signal in Rayleigh fading environments. Fukawa and Suzuki [74] discuss in detail a blind ICE which can operate well without training signals for the interference.

Petersen and Falconer [193] describe the ability of a linear equalizer/combiner or decision feedback equalizer to suppress all received ACI, CCI, and ISI. They found that with one antenna and a linear equalizer, arbitrarily large receiver bandwidths allow for marginal improvements in spectral efficiency through decreased carrier spacing, because the carrier spacing cannot be reduced to a value below the symbol rate without incurring insuppressible interference. Their results demonstrate how equalizers are able to extract the SOI and to provide interference suppression even under condition of considerable mutual overlap of all signals. Greater interference suppression is possible using equalizers with larger receiver bandwidths.

Other parts of this overview contain examples of adaptive equalization as applied to interference rejection, including the section dealing with CDMA interference rejection (found in Section 3.3.2). The mechanism for equalizer operation non-spread spectrum tends to be different from that in spread spectrum. For example, equalization in spread spectrum tends to operate by exploiting the code repetition feature. Several non-SS techniques also utilize adaptive equalization, including those employing the constant modulus algorithm (Section 3.4.2), neural networks (Section 3.4.3), spectral correlation (Section 3.4.4), and nonlinear techniques (Section 3.4.5).

3.4.2 Constant Modulus Algorithm

Interference and channel distortion will alter the envelope of a constant modulus (envelope) signal, such as FM or QPSK. For constant modulus signals (e.g., FM, FSK, and PSK), the constant modulus algorithm (CMA) works by adapting a filter to restore the constant envelope, thereby rejecting interference and suppressing channel distortion.

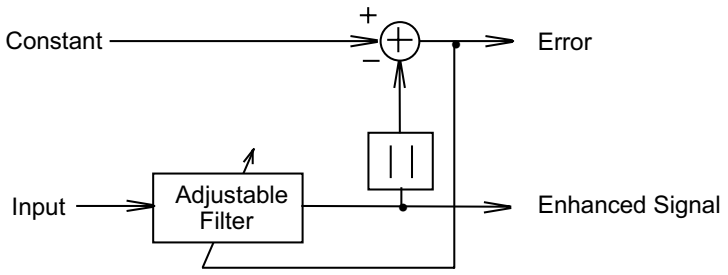

Figure 3.13: Implementation of the constant modulus algorithm.

Treichler and Agee [238] originally formulated CMA where, by sensing the received envelope variations, the complex coefficients of an FIR filter can be adapted to remove the variations and, in the process, remove interference components from the received signal. Much of the literature on CMA focuses on its equalization capability. Here, literature is addressed which investigates CMA's interference rejection capability. An example of CMA is given in Figure 3.13. The error which drives the adaptive (adjustable) filter is derived from the difference between a constant and the magnitude of the output of the filter.

A real input, real coefficient version of CMA is formulated by Treichler and Larimore [239], and the algorithm is extended for the enhancement of signals having nonconstant but known envelope, as might arise in data signals with pulse shaping. Treichler and Larimore [237] also survey developments in applying CMA.

Ferrara [63] presents a method for adaptively canceling interference from a constant envelope target signal, even when some of the interfering signals also have constant envelopes. The adaptive algorithm distinguishes between target signal and interference on the basis of signal amplitude and envelope shape, given that the amplitude of the target signal is approximately known or measurable.

Gooch and Daellenbach [87] describe a technique for preventing interference capture by using a spectral whitening algorithm to initialize the filter weights prior to switching to the CMA. The method requires no knowledge of the received interference scenario, and it allows notching of one or more interferers. Satorius, et al., [214] compare the interference rejection performance of the CMA to linear prediction or whitening techniques.

Rude and Griffiths [210] develop a fractionally-spaced adaptive equalizer based on the linearly constrained constant-modulus (LCCM) algorithm. The LCCM algorithm exploits prior knowledge of synchronization, sampling strategy, and pulse shape to prevent capture of the CMA by narrowband constant envelope interferers. LCCM uses *a priori* knowledge of only the SOI. Simulations show that this approach greatly reduces the vulnerability of CMA to strong constant envelope interferers and yields a set of tap values that can be successfully used as initial conditions for follow-on DF adaptation.

Kwon, Un, and Lee [131] investigate the convergence properties of CMA when applied to interference rejection, by analyzing the convergence behavior of the squared output

modulus and the MSE of the modulus. They find that the convergence behavior can be modeled by a recursive equation with a varying convergence factor.

White [254] addresses the problem of blind equalization of constant modulus signals which are degraded by frequency selective multipath propagation and additive white noise. An adaptive observer is used to update the weights of an FIR equalizer in order to restore the signal's constant modulus property. The observer gain is selected using fake algebraic Riccati methods in order to guarantee local stability. When compared to the constant modulus algorithm for simulated FM-FDM signals, the performance of this method exhibits significantly better convergence properties, particularly for heavy-tailed noise.

3.4.3 Neural Networks

Howitt, Reed, Vemuri, and Hsia [109] survey recent developments in applying neural networks (nets) to equalization and interference rejection. Haykin [94] also provides an introduction to the use of neural networks in signal processing. Advantages of neural nets over conventional linear filtering and equalization include: (1) better rejection of non-Gaussian interference, (2) superior rejection of noise, (3) availability of additional blind equalization algorithms, (4) more robust startup, (5) capability of rejecting CDMA interference, (6) better equalization of non-minimal phase channels, and (7) better compensation of nonlinear distortion. On the negative side, with present neural net equalization techniques, there is no guarantee of reaching an optimal solution, and the convergence rate is very slow (and therefore not as viable for dynamic channels).

The ability of neural networks to reject interference can be viewed using different perspectives; that is, a) neural nets can create nonlinear decision boundaries between signal states, b) neural nets provide a means of implementing nonlinear filters for rejecting non-Gaussian interference, and c) neural nets can be used to identify specific error patterns. Three types of neural nets stand out - 1) feed-forward neural nets (trained using a variant of the backpropagation algorithm, 2) those based on the polynomial perceptron, and 3) those utilizing radial basis functions. Neural networks using a self-organizing feature map (SOM) are also used for adaptive equalization and interference rejection, but are only referenced here [198, 191, 54]. Applications of neural nets to interference rejection for spread spectrum can be found in Section 3.3.2.

Radial Basis Function

The most promising work to date for interference rejection is with the use of radial basis functions (RBFs). A general example of a RBF two-layer neural net is given in Figure 3.14, where the input data x_m are passed through some nonlinear function (such as a Gaussian function) before being weighted and summed, and m is the dimension of the input space. The first layer, the hidden layer, takes the input vector $\mathbf{x}$ and produces a nonlinear mapping based on the nonlinear elements. The second layer is a linear mapping from the output of the hidden layer to the output of the network (i.e., a weighted sum of the hidden layer output). RBF networks exploit the premise that a

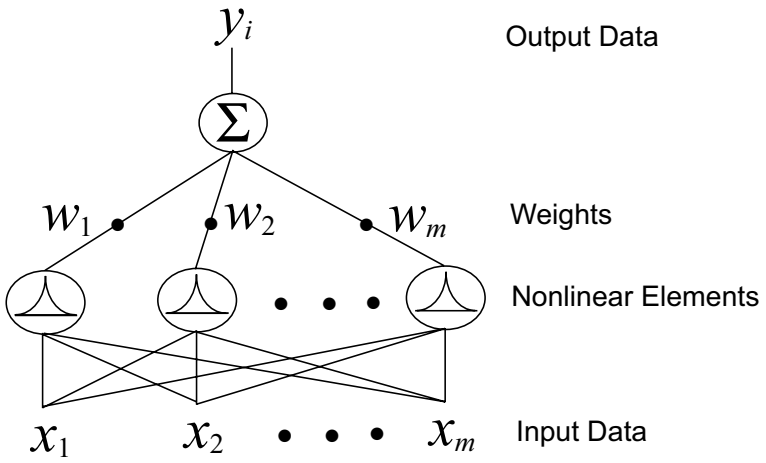

Figure 3.14: An example of a radial basis function neural net.

classification problem transformed into a higher dimension through a nonlinear mapping is more likely to be solved, than if the solution to the problem is attempted in its original space [109].

Cha and Kassam [31] give an overview of adaptive interference cancellation with radial basis function networks. They investigate the applicability of the RBF network in adaptive interference cancellation problems. An extended structure that combines a linear canceller with an RBF network is shown to be more robust than a structure using an RBF network only. In [32], they study RBF networks from the perspective of optimal signal estimation. Optimum interference cancellation usually requires nonlinear processing of signals. Since RBF networks can approximate nonlinear functions, they can be expected to implement or approximate the operation of optimum interference cancellation with appropriate network configuration and training. Cha and Kassam examine a number of different RBF structures as well as training algorithms, showing that RBF networks can be very useful for interference cancellation problems in which traditional linear cancellers may fail badly.

Chen and Mulgrew [38, 37] show the results of using an adaptive radial basis function neural net for interference rejection and equalization. They state that an adaptive RBF neural net equalizer can implement the optimal Bayesian symbol-decision equalizer using a two-stage learning algorithm. The first stage is a supervised or decision-directed clustering algorithm which learns the centers of the desired signal states, and the second stage is a variation of an unsupervised k-means clustering algorithm for modeling the effect of the interference. In one example, the neural net provides an effective reduction in SINR of 7 dB over the transversal equalizer for a BER of 10^{-4}. The algorithm converges remarkably fast when compared to traditional equalization algorithms. Chen, McLaughlin, and Mulgrew [35] apply the results to digital communications channel equalization and incorporate co-channel interference compensation [36].

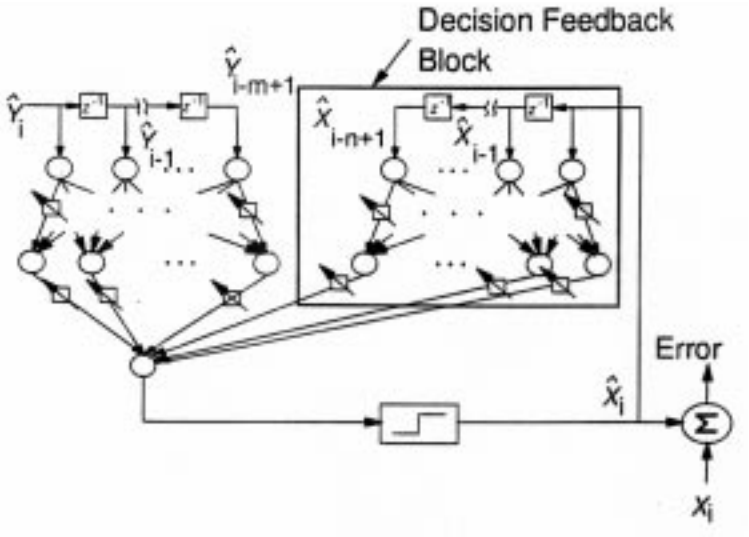

Figure 3.15: Feed forward NN adaptive equalizer with optional decision feedback.

A means for growing the RBF network in interference rejection applications is addressed by Howitt, et al., [108]. Howitt points out that direct correspondence can be obtained between RBF networks and the symbol-by-symbol maximum likelihood receiver structure for equalization in an interference environment and also for continuous phase modulation (CPM) receivers [110].

Feed Forward Networks with Backpropagation

Nonlinear adaptive equalizers have been implemented using a feed forward neural net with backpropagation. This structure can also reject interference. The general implementation scheme is a straightforward extension of the linear transversal equalizer (LTE) as shown in Figure 3.15 [109], where $\hat{y}_i$ is the input, $\hat{x}_i$ is the output, and x_i is a desired signal. Figure 3.15 includes a decision feedback extension to the basic transversal equalizer.

Bijjani and Das [25] present a multilayer backpropagation perceptron model as a means of detecting a wideband signal in the presence of narrowband jammers and additive white noise. The nonlinear neural network filter is demonstrated to offer a faster convergence rate and an overall better performance over the LMS adaptive transversal filter.

Zengjun and Guangguo [260] describe a fractionally-spaced DF multilayer perceptron (FSDFMLP) for adaptive multilevel QAM digital mobile radio reception that can reject CCI and AWGN simultaneously. The FSDFMLP is trained by a fast adaptive learning algorithm called the mixed gradient-based fast learning algorithm with variable learning gain and selective updates (based on a combination of the steepest descent

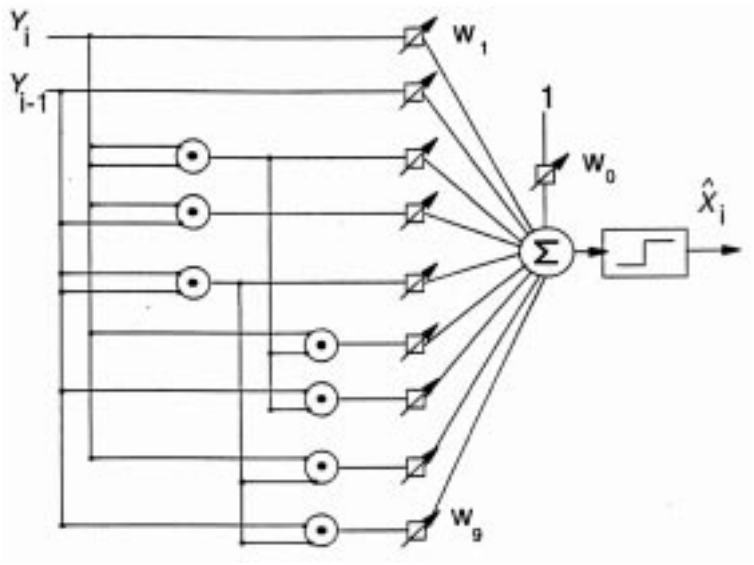

Figure 3.16: Polynomial perceptron structure.

and the conjugate gradient methods). FSDFMLP can perform more efficiently than the conventional LMS based DF filter in the presence of multipath fading of channels with non-Gaussian interferences. Similarly, Zengjun and Guangguo [259] describe the complex neural-network-based adaptive DF filter (CNNDFF) for M-QAM digital communication reception systems. Experimental results indicate that the CNNDFF can simultaneously overcome the performance degradations due to multipath fading of channels and reject the non-Gaussian co-channel interferences efficiently. The convergence rate of the CNNDFF is significantly better than that of the standard backpropagation network.

Polynomial Perceptrons

Another adaptive non-linear equalizer approach is the polynomial perceptron. The idea behind this approach is to approximate the decision function based on the Volterra series polynomial expansion. Figure 3.16 [107] illustrates the polynomial perceptron for a two-input third-order structure, where $\hat{y}_i$ is the input, $\hat{x}_i$ is the output, and w_i are the weights. The complexity is greater than that of the LTE but less than that of the feed forward network (assuming the order of the network is moderately low).

Zengjun and Guangguo [261] present methods of joint adaptive channel equalization and interference suppression by neural networks in digital communications systems with high spectrum efficiency and high bit rate. They propose a lattice polynomial perceptron (LPP) and a fast learning algorithm (FLA) to train the LPP. Their simulations show improvement of the LPP over the multilayer perceptron and backpropagation algorithm.

Zengjun and Guangguo [262, 263] extend their previous work by investigating the behaviors of polynomial perceptrons (PP). They show that a PP with degree $L(\geq 4)$

satisfies the Stone-Weierstrass theorem and can approximate any continuous function to within a specified accuracy. They also introduce a fractionally-spaced recursive polynomial perceptron (FSRPP) with low complexity and fast convergence rate. The FSRPP is a structure of PP that requires a smaller number of coefficients. A fractionally-spaced bilinear perceptron (FSBLP) is a simple FSRPP. Simulation results show the performance of the FSBLP is superior to that of previously investigated structures, including the conventional DFE due to the use of the sigmoid function and the cross terms.

3.4.4 Exploitation of Spectral Correlation

An adaptive filter is a time-varying filter, where the filter coefficients change with time, minimizing some error criterion function. If the signal statistics change rapidly, a conventional adaptive filter is incapable of converging to the optimum solution, as is often the case in applications when an adaptive filter is used for filtering digitally modulated signals. When these signals exhibit periodic statistics, they are generally referred to as cyclostationary signals, possessing the property of spectral correlation. Reed and Hsia [206] present the basic theory of the time-dependent adaptive filter (TDAF) which allows for the cyclostationary nature of communications signals by periodically changing the filter and adaptation parameters. By exploiting spectral correlation, the TDAF achieves improved interference rejection capability over that of conventional time-independent filters.

Analog and digital carrier modulated signals, such as AM, digital QAM, PSK and FSK, exhibit correlation among spectral components separated by multiples of the keying rate and separated by the doubled carrier frequency plus multiples of the keying rate. Gardner and Venkataraman [77] observe that this spectral redundancy can be exploited to facilitate rejection of CCI, while maintaining minimal signal distortion. Gardner and Brown [75] show how spectral redundancy can be exploited by multichannel frequency shift filtering of the corrupted data and by adding the results to implement a time-dependent filter.

Gardner [76] develops some of the theoretical concepts underlying this type of filtering and summarizes the theory of optimal FREquency SHift (FRESH) filtering - a generalization of Wiener filtering, termed cyclic Wiener filtering. The idea is to jointly filter frequency shifted, but correlated versions of the signal as shown in Figure 3.17, where the input signal $x(t)$ is shifted in the frequency domain at multiples of the cyclic frequency α and then the shifted outputs are adaptively filtered and summed. This "spectral diversity" can greatly improve interference rejection. Gardner also shows how the performance depends on the signal's excess bandwidth. A FRESH DF equalizer is a DFE where the forward filter is replaced by a bank of filters whose inputs are frequency-shifted. By exploiting the spectral redundancy of modulated signals, this technique improves the DFE performance in a cyclostationary environment. Hendessi, Hafez, and Sheikh [98] show that the performance of the FRESH-DFE is superior to that of a conventional DFE.

The process of time-dependent filtering is illustrated in Figure 3.18, which shows

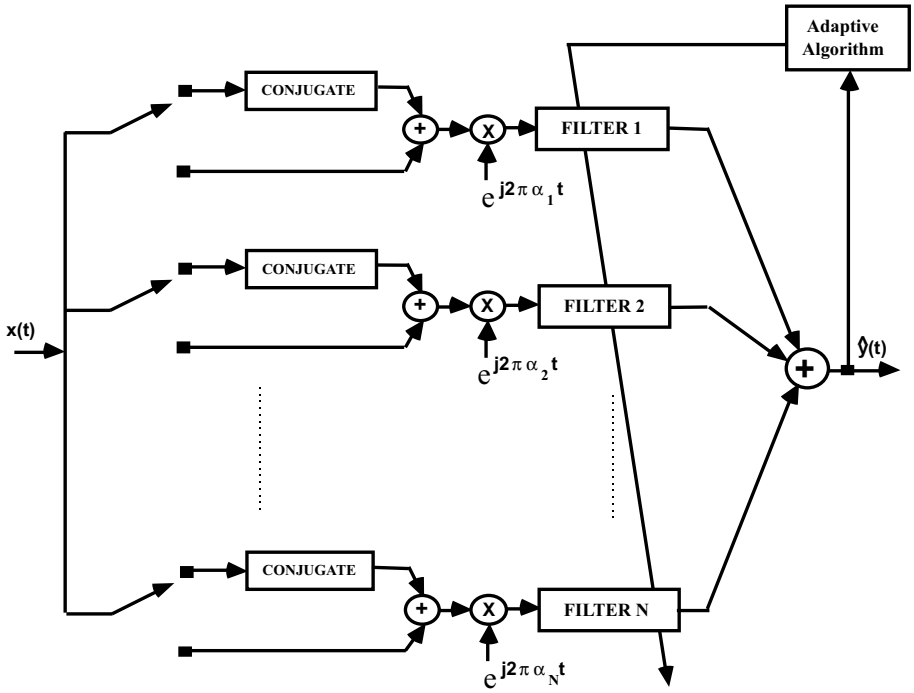

Figure 3.17: Optimal FREquency SHift (FRESH) filtering.

the spectrum of a SOI and that of a signal-not-of-interest (SNOI). Signals frequency-shifted by the baud rate of the SOI use the opposite sidebands of the SOI to improve the contribution of the SOI in the estimated signal. The signal spectrum is shifted by the baud rate of the SOI so that the opposite sidebands line up. Redundant information in the sideband is used to improve the signal. In addition, signals frequency-shifted by the baud rate of the SNOI are used to reduce the contribution of the SNOI in the estimated signal.

Greene, Reed, Yuen, and Hsia [89, 207] present the optimal time-dependent receiver (OTDR) and show it to be superior to the conventional matched filter receiver when cyclostationary interference is present, because the OTDR exploits the statistical periodicities of the interference. The matched filter is periodic at the baud rate of the SOI; while the OTDR is periodic at the baud rate of the SOI and any other statistical periodicity of the received signal (including that of the interfering signal).

Mendoza, Reed, Hsia, and Agee [158] present two new blind adaptive filtering algorithms for interference rejection using time-dependent filtering structures that exploit cyclostationary signals. They show that the blind (i.e., operating without the use of an external training signal) time-dependent filtering algorithms can provide MSE and BER that are significantly lower than the MSE and BER provided by conventional time-independent adaptive filters (which are non-blind and training-sequence directed).

Nicolas and Lim [176] address the problem of transmitting digital HDTV signals in

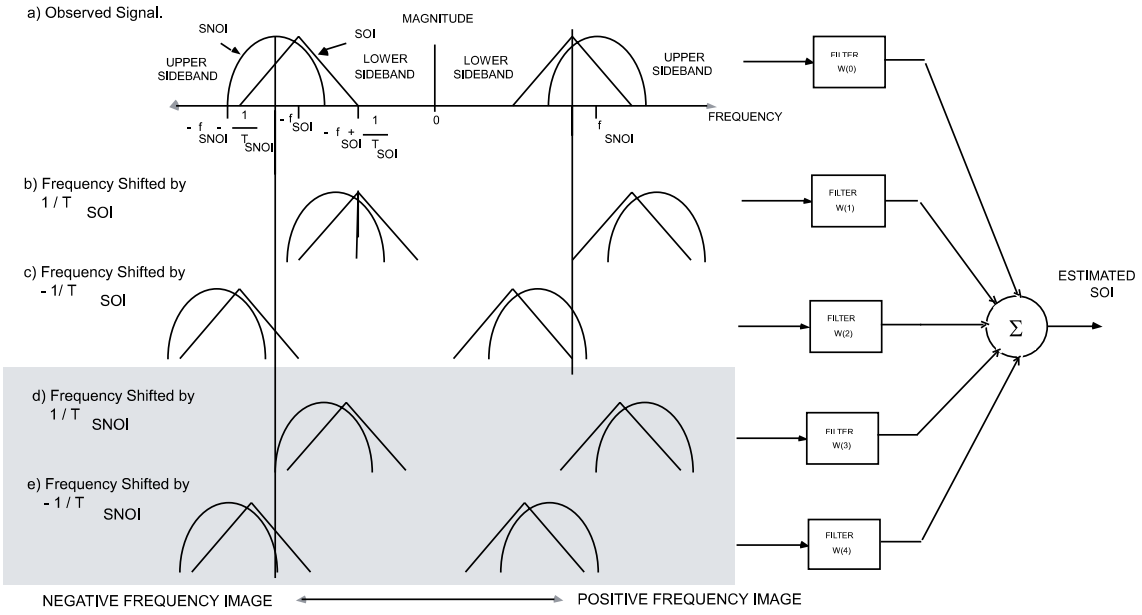

Figure 3.18: The process of time-dependent filtering.

a CCI limited environment. They describe a new signal processing technique aimed at rejecting CCI from adjacent analog transmitters. The proposed scheme uses a form of joint DFE/trellis coded modulation to combat the interference. DFE can be used in the application by exploiting the cyclostationary properties of the interference. The technique has several advantages over methods previously proposed: 1) processing is constrained to the receiver, 2) the scheme is able to make use of powerful coding schemes, 3) the scheme is adaptive and 4) reception on conventional NTSC (National Television System Committee) receivers is not affected by this scheme.

3.4.5 Nonlinear Techniques

Nonlinear interference rejection techniques have been applied to non-spread spectrum signals as well as spread spectrum signals (see Section 3.3.1). The capabilities of a nonlinear filter are illustrated using the nonlinear canceller shown in Figure 3.19, based on [174]. Given

$$\text{a desired wave:} \qquad a \sin 2\pi f_1 t \qquad (a \ll 1) \tag{3.10}$$

$$\text{a large undesired wave:} \qquad \sin 2\pi f_2 t \tag{3.11}$$

assuming no noise, the input $x(t)$ becomes

$$x(t) = a \sin 2\pi f_1 t + \sin 2\pi f_2 t \tag{3.12}$$

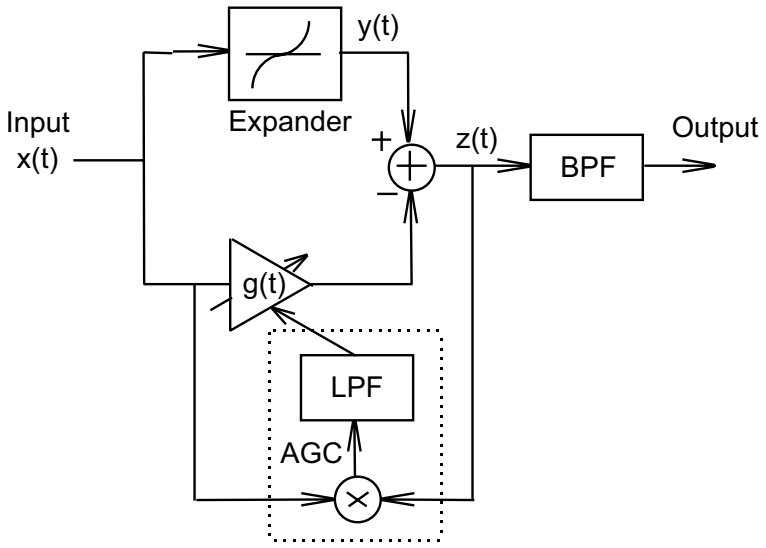

Figure 3.19: Configuration and spectrum of a nonlinear canceller.

and only small signals are amplified by the expander (with cubed elements here) to become

$$y(t) = x^3(t) \approx 2a \sin 2\pi f_1 t + \sin 2\pi f_2 t + a \sin 2\pi(2f_2 - f_1)t \tag{3.13}$$

If ideal amplifier gain control (AGC) is assumed, the output of the canceller becomes

$$z(t) = y(t) - x(t) = a \sin 2\pi f_1 t + a \sin 2\pi(2f_2 - f_1)t \tag{3.14}$$

and the desired is extracted. In real conditions, however, the AGC will sometimes eliminate the desired signal.

To overcome the deficiencies of the AGC, Nagayasu and Sampei [174] propose an adaptive nonlinear equalizer (ANLE) containing the conventional ALE and a nonlinear canceller, which eliminates ACI by nonlinear processing. The intermodulated wave occurring inside the nonlinear canceller is eliminated by the bandpass filter (BPF). The results show that the ANLE can effectively eliminate an interfering wave component whose spectrum has become overlapped with a desired wave, thus giving it better interfering wave-eliminating characteristics than the ALE or the nonlinear canceller by themselves.

Maulhardt, Davis, and May [156] present techniques for designing frequency-domain nonlinear adaptive filters. These techniques make use of hierarchical memory structures that are trained to learn the appropriate transfer functions for a given signal and interference environment. Valeev and Yazovskii [242] consider a method for construction of an adaptive nonlinear converter (ANC) as a preprocessor to a correlation receiver for improving immunity to non-Gaussian interference. The authors show how to construct the nonlinearity to maximize output SNR.

By viewing noise cancellation as an input/output identification problem, Giannakis and Dandawate [81] develop designs using third-order statistics which are insensitive to corruption of the reference signal by additive Gaussian noise of unknown covariance. As a by-product of designing linear noise cancellers, a parametric time-delay estimate is readily available, and higher-order statistics can be employed to design nonlinear cancellers of the discrete Volterra-type which maximize the output SNR.

3.4.6 Other Techniques

Bar-Ness and Bunin [21] improve on a method for CCI suppression and signal separation which uses the amplitude variation of the composite signal to estimate the parasitic phase modulation impinged on the strong desired signal by the weak interference signal. This estimate is then used to cancel out the distortion of the composite signal, revealing the desired signal. In the cancellation process, initial amplitude estimates for both signals are obtained from measurements. An adaptive method is proposed which improves these estimates and, hence, results in a better cancellation of interference. In comparison with non-adaptive methods, the adaptive approach exhibits an additional 21 dB of interference suppression.

Libing, Guangguo, and Boxiu [143] examine the suppression of FM interference in QAM systems using adaptive decision-feedback filters. They provide analytic expressions and plots of symbol error probability.

Shin and Nikias [220, 221] introduce a new higher-order statistics-based adaptive interference canceller to eliminate additive narrowband and wideband interferences in environments where the interference is non-Gaussian and where a reference signal, which is highly correlated with the interference, is available. The scheme uses higher-order statistics (HOS) of the primary and reference inputs and employs a gradient-type algorithm for updating the filter coefficients. The authors demonstrate that the HOS-based adaptive algorithm performs more effectively than the second-order statistics-based adaptive algorithm not only for single and multiple NBI with/without Gaussian uncorrelated noise sources but also for wideband (AM and FM) interferences. Exploiting higher order statistics can lead to new blind adaptive filtering techniques for interference rejection. This is a promising approach that could lead to new blind algorithms for interference rejection.

3.5 Conclusion

Because interference (particularly co-channel interference and adjacent channel interference in cellular systems) is a limiting factor in wireless systems, this chapter comprises an extensive overview of single-channel adaptive interference rejection techniques for digital wireless communications, primarily since 1980, considering both spread spectrum and non-spread spectrum techniques.

Though finding their roots in military anti-jam research, interference rejection techniques are of increasing interest to industry because of their applicability to commercial

wireless communications. The prediction filter is one of the earliest and simplest forms of adaptive interference rejection and has been supplemented by many new interference rejection techniques capable of rejecting interference with less distortion and under a wider variety of signal conditions.

Among spread spectrum techniques, we have surveyed advances in narrowband interference rejection for direct sequence systems (including adaptive notch filtering, decision feedback, adaptive A/D conversion, and nonlinear techniques), wideband interference rejection for direct sequence (dividing into single-user and multiuser techniques, with particular focus on CDMA interference rejection), and interference rejection for frequency hopping. Among the non-spread spectrum techniques, we have surveyed advances in interference rejection based on adaptive equalization, the constant modulus algorithm, neural networks (including the self-organizing feature map, feedforward networks with backpropagation, polynomial perceptrons, and the radial basis function), spectral correlation, nonlinear techniques, and some miscellaneous techniques.

Many of the techniques show promise of mitigating interference in digital wireless communications. There remains much work, however, in determining the relative merits and practicality of the newer techniques.

In regard to the future direction of interference rejection, work will now focus more on commercial signals, such as IS-95 and IEEE 802.11 WLAN spread spectrum systems, or IS-54, GSM, DECT, PACS, or IS-136 TDMA systems, where techniques will be directly applied. Research will center on specific standards, as opposed to generic spread spectrum and other generic digitally modulated signal formats. Having fixed standards will also encourage research into hardware implementations of techniques that are applicable to widely acknowledged digital modulation standards (e.g., Gaussian Minimum Shift Keying - GMSK).

Undoubtedly, many of the MAI CDMA interference rejection techniques will end up in hardware because of the tremendous gains in spectral capacity provided - doubling or even tripling channel capacity. The inherent spectral inefficiency of single cell spread spectrum systems can be overcome by interference rejection techniques, approaching and exceeding spectral capacities provided by TDMA or FDMA.

The performance of traditional notch filtering (or prediction based filtering) approaches is being exceeded by the use of non-linear filtering techniques (such as the radial basis function (RBF) neural network) and time-varying filtering (such as the FRESH filter).

There is generally a lack of good blind algorithms, though decision directed training techniques and the constant modulus algorithm still serve as basic, practical blind algorithms. Training techniques derived by using self training neural networks, higher order statistic characterization, and cyclostationary exploitation algorithms are promising, but these techniques tend to require a heavy computational load and are susceptible to degradation in dynamic channels because of the long time-bandwidth products necessary to obtain consistent statistical estimates. So far, most of the work in these promising interference rejection techniques tends to be applied to channels that are not realistic for wireless systems. The sophistication of channel models is increasing and providing

more accurate performance predictions via simulations of real world performance.

The analysis for the interference rejection techniques is beginning to be more complete, providing theoretical BER or frame error rate (FER) estimates, instead of MSE (which may or may not be reflective of BER or FER). Furthermore, the analysis of the interference rejection techniques will need to include (and demonstrate) the impact on overall system capacity in order to be fully appreciated.

Chapter 4

Receiver Theory for GMSK

4.1 Motivation

One of the main goals of this research involves the investigation of demodulator diversity schemes (discussed in Chapter 6) to improve GMSK demodulation performance, particularly by mitigating interference (such as CCI). Demodulator diversity involves the use of a bank of receivers, rather than one individual receiver. Before demodulator diversity can be addressed, however, we need to examine the individual receivers that might compose a demodulator diversity scheme. In Chapter 2, various GMSK receivers (i.e., demodulators) were discussed from the perspective of the technical literature.

In this chapter, those individual demodulators, along with others, are examined in more detail. The research centers on noncoherent demodulation of GMSK (1) because coherent demodulation is well-documented in the literature, (2) because noncoherent techniques are generally less expensive than coherent techniques, and (3) because coherent demodulation performs worse than noncoherent demodulation in certain wireless channel impairments (e.g., severe multipath fading). Block diagrams and signal space constellations of three of the better performing noncoherent demodulators are included. The goal is to find a demodulator (or demodulators) which is (or are) simple and easily implemented, particularly at the mobile.

This chapter also includes a general analytical examination of differential demodulation (a noncoherent technique). The analytical expressions derived are also applicable to differential detection (refer to Section 2.2). We define a general wireless channel model which includes noise (AWGN), co-channel interference (CCI), and flat Rayleigh fading. Analytical expressions for the output of a one-bit differential demodulator (DD1) are derived using the general wireless channel model. The derivation then focuses on the case of AWGN, and an attempt is made to derive an analytic expression for pdf of the DD1 decision statistic in AWGN. This exercise shows that *a priori* (deductive) methods of determining expressions for the pdf in this simple case are very difficult. The failure to obtain a satisfactory analytical expression motivates research into *a posteriori* (inductive) techniques of determining the pdf of the decision statistic (discussed in Chapter 7).

4.2 Receivers Used in Research

Various forms of GMSK demodulation have been simulated, which include limiter discriminator and differential demodulators (i.e., twenty-three variations, incorporating features such as decision feedback and nonredundant error correction, and including some novel structures). Several new structures have been proposed which make use of decision feedback and nonredundant error correction. The coherent demodulator has also been simulated, since it is commonly used for GMSK. Dissertation research, however, has focused on noncoherent demodulation techniques.

4.2.1 Description of Demodulators

Twenty-seven demodulators simulated and evaluated are listed in Table 4.1 (where DD stands for differential demodulator and DF stands for decision feedback). These include the coherent demodulator and noncoherent demodulators such as the limiter discriminator and variations on the differential demodulator. In a separate technical report [34], block diagrams have been drawn and signal space constellations (phase state diagrams) and eye diagrams have been plotted for each demodulator. Examples of three of the better performing noncoherent demodulators (in terms of BER) are included here:

- 2-bit differential demodulator with decision feedback
- 1-bit DF, 2-bit DF, & 3-bit DF differential demodulators with combined outputs
- limiter discriminator demodulator

The block diagrams and signal space constellations for each of these three demodulators are given in Figures 4.1 - 4.6, where $s(t)$ is the received signal, T is the bit interval, b_k is the hard decision on the data, and e_k is a differentially encoded version of b_k. In Figure 4.3, λ and ψ represent phase shifts determined by the logic circuits. Eye diagrams of the signals are also available [34].

4.2.2 New Demodulator Variations and Structures

Of the twenty-seven demodulators, ten of them (listed in Table 4.2) are new variations of demodulators discussed in the literature.

4.3 Differential Demodulation in the Wireless Channel

This section contains an general analysis of differential demodulation (a noncoherent technique). The expressions are also applicable to differential detection (refer to Section 2.2). First, we consider a general wireless channel model which includes noise (AWGN),

Table 4.1: Twenty-seven demodulators simulated and evaluated.

1)	1-bit differential demodulator (DD)
2)	2-bit DD
3)	3-bit DD
4)	1-bit with decision feedback (DF) DD
5)	2-bit DF DD
6)	3-bit DF DD
7)	1-bit DD with 2-bit DD used for error correction
8)	1-bit DD with 2-bit & 3-bit DDs used for error correction
9)	1-bit and 2-bit DDs with combined outputs
10)	1-bit and 3-bit DDs with combined outputs
11)	2-bit and 3-bit DDs with combined outputs
12)	1-bit, 2-bit, and 3-bit DDs with combined outputs
13)	1-bit DF and 2-bit DF DDs with combined outputs
14)	1-bit DF and 3-bit DF DDs with combined outputs
15)	2-bit DF and 3-bit DF DDs with combined outputs
16)	1-bit DF, 2-bit DF, and 3-bit DF DDs with combined outputs
17)	1-bit DD with improved DF logic scheme
18)	1-bit DF DD with 2-bit DF DD used for error correction
19)	1-bit DF DD with 2-bit DF & 3-bit DF DDs used for error correction
20)	1-bit and 2-bit DDs with combined outputs with 2-bit & 3-bit DDs used for error correction
21)	1-bit DF and 2-bit DF DDs with combined outputs with 2-bit DF & 3-bit DF DDs used for error correction
22)	1-bit, 2-bit, and 3-bit DDs with combined outputs with 2-bit & 3-bit DDs used for error correction
23)	1-bit DF, 2-bit DF, and 3-bit DF DDs with combined outputs with 2-bit DF & 3-bit DF DDs used for error correction
24)	Limiter discriminator demodulator
25)	Limiter discriminator demodulator with integrate-&-dump
26)	Coherent demodulator
27)	Coherent demodulator with integrate-&-dump

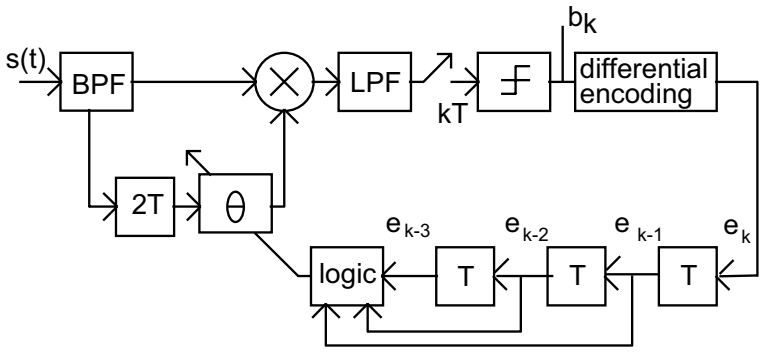

Figure 4.1: Block diagram of a 2-bit differential demodulator with decision feedback.

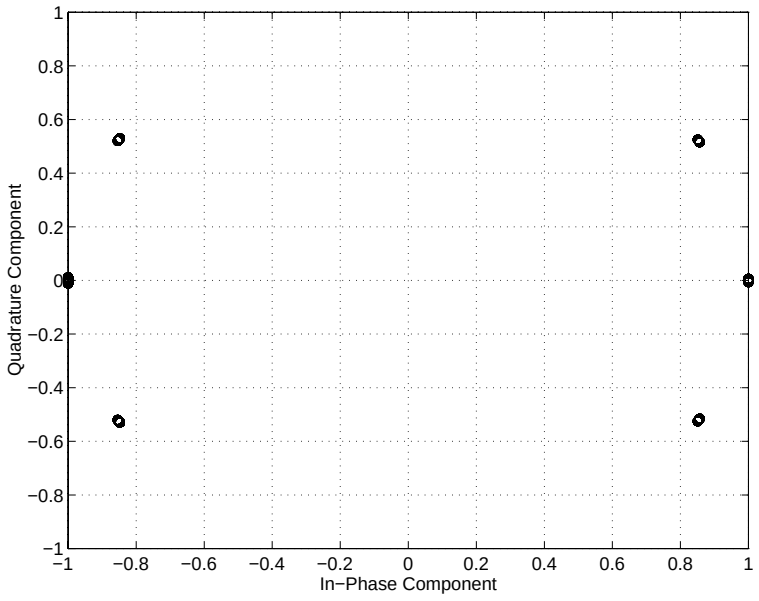

Figure 4.2: Phase state diagram for 2-bit differential demodulator with decision feedback.

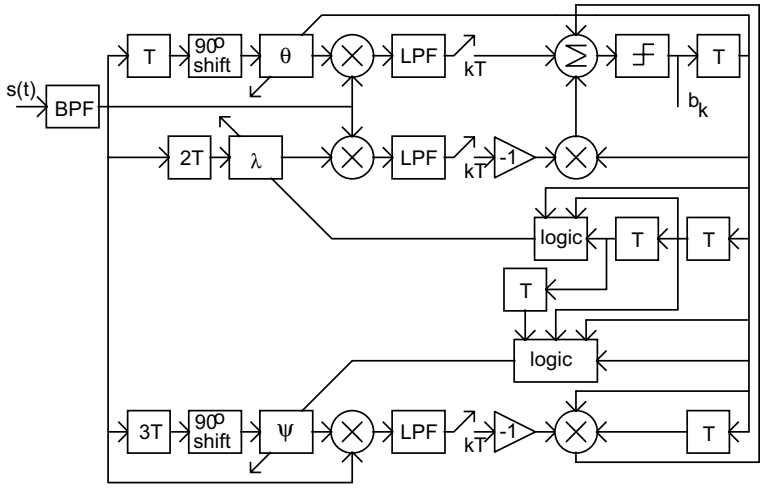

Figure 4.3: Block diagram of a 1-bit, 2-bit, and 3-bit differential demodulator combination with decision feedback.

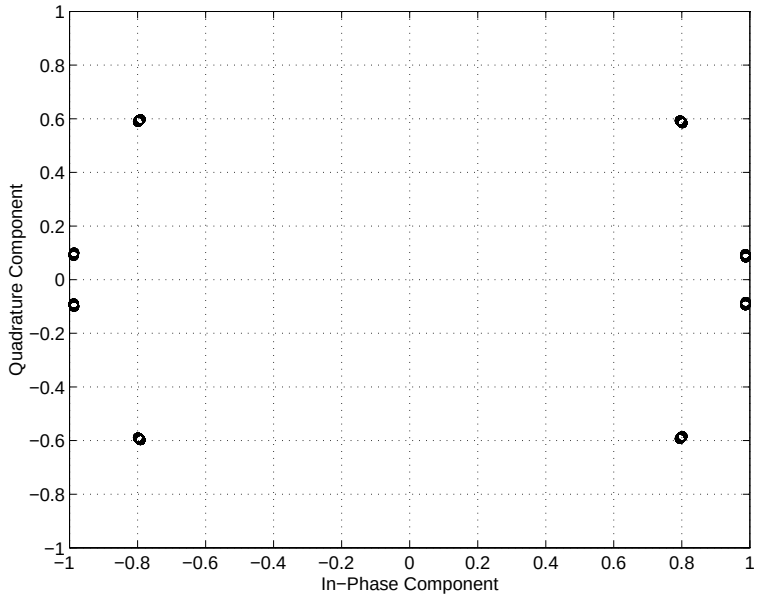

Figure 4.4: Phase state diagram for 1-bit, 2-bit, and 3-bit differential demodulator combination with decision feedback.

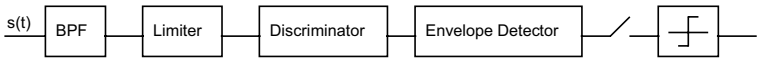

Figure 4.5: Block diagram of a limiter discriminator demodulator.

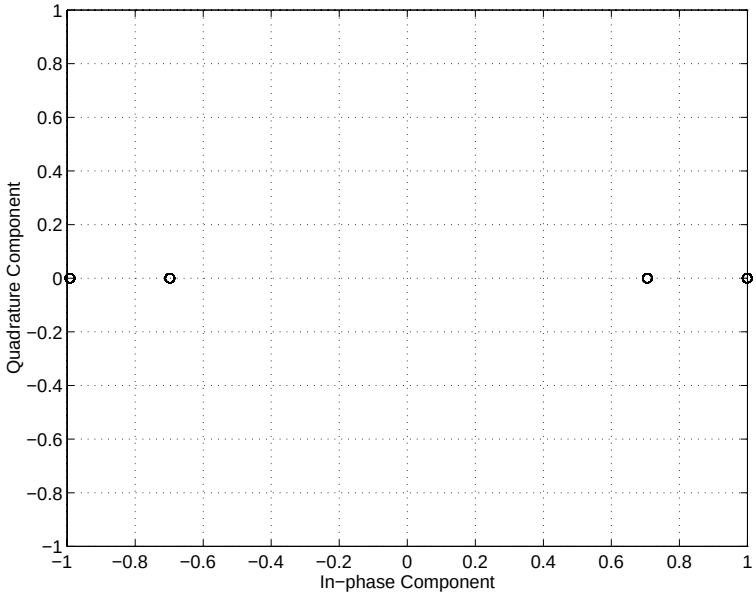

Figure 4.6: Phase state diagram for limiter discriminator demodulator.

Table 4.2: Ten new variations on differential demodulation.

1)	1-bit DF and 2-bit DF DDs with combined outputs
2)	1-bit DF and 3-bit DF DDs with combined outputs
3)	2-bit DF and 3-bit DF DDs with combined outputs
4)	1-bit DF, 2-bit DF, and 3-bit DF DDs with combined outputs
5)	1-bit DF DD with 2-bit DF DD used for error correction
6)	1-bit DF DD with 2-bit DF & 3-bit DF DDs used for error correction
7)	1-bit and 2-bit DDs with combined outputs w/ 2-bit & 3-bit DDs used for error correction
8)	1-bit DF and 2-bit DF DDs with combined outputs w/ 2-bit DF & 3-bit DF DDs used for error correction
9)	1-bit, 2-bit, and 3-bit DDs with combined outputs w/ 2-bit & 3-bit DDs used for error correction
10)	1-bit DF, 2-bit DF, and 3-bit DF DDs with combined outputs w/ 2-bit DF & 3-bit DF DDs used for error correction

co-channel interference (CCI), and flat Rayleigh fading (one path). Analytical expressions for the output of a one-bit differential demodulator (DD1) are derived using the general wireless channel model. The derivation then focuses on the case of AWGN, and an attempt is made to derive an analytic expression for pdf of the DD1 decision statistic in AWGN. This exercise shows that *a priori* methods of determining expressions for the pdf in this simple case is very difficult. The failure to obtain a satisfactory analytical expression motivates research into *a posteriori* techniques of determining the pdf of the decision statistic.

4.3.1 A General Wireless Channel Model

The transmitted GMSK signal $s(t)$ is represented as

$$s(t) = \cos(\omega_c t + \phi_s(t)) \tag{4.1}$$

In the fading mobile radio environment, $s(t)$ becomes corrupted by multipath and can be represented by the faded signal $\tilde{s}(t)$

$$\tilde{s}(t) = x_s(t)\cos(\omega_c t + \phi_s(t)) - y_s(t)\cos(\omega_c t + \phi_s(t)) \tag{4.2}$$

where $x_s(t)$ and $y_s(t)$ are independent zero-mean Gaussian baseband random processes.

After bandpass filtering and before demodulation (i.e., at the predetection bandpass filter output), the signal-of-interest (SOI) $\tilde{s}(t)$ can be represented as

$$\tilde{s}(t) = \mathrm{Re}\left[z_s(t)\exp\left[j\left(\omega_c t + \phi_s(t)\right)\right]\right], \qquad \text{where } z_s(t) = x_s(t) + jy_s(t) \tag{4.3}$$

Undesired co-channel interference (CCI) can be represented in a similar way. The CCI is the signal-not-of-interest (SNOI) $i(t)$

$$i(t) = \mathrm{Re}\left[z_i(t)\exp\left[j\left(\omega_c t + \phi_i(t)\right)\right]\right], \qquad \text{where } z_i(t) = x_i(t) + jy_i(t) \tag{4.4}$$

For the case of additive white Gaussian noise (AWGN) at the receiver, the received signal $r(t)$ is simply the transmitted signal plus a bandpass Gaussian noise process

$$r(t) = s(t) + n(t) \tag{4.5}$$

where $n(t)$ is a Gaussian random process with power spectral density

$$S_n(f) = \begin{cases} \frac{N_o}{2}, & |f - f_c| < \frac{B}{2} \\ 0, & else \end{cases} \tag{4.6}$$

The AWGN $n(t)$ can be represented as

$$n(t) = \mathrm{Re}\left[z_n(t)\exp\left[j\omega_c t\right]\right], \qquad \text{where } z_n(t) = x_n(t) + jy_n(t) \tag{4.7}$$

The received signal $r(t)$ can also be modeled as a combination of the faded signal, CCI, and AWGN

$$\begin{aligned} r(t) &= \tilde{s}(t) + i(t) + n(t) \\ r(t) &= \mathrm{Re}\left[z(t)\exp\left[j\omega_c t\right]\right] \end{aligned} \tag{4.8}$$

The complex baseband representation of $r(t)$ is given by $z(t)$

$$z(t) = z_s(t)\exp\left(j\phi_s(t)\right) - z_i(t)\exp\left(j\phi_i(t)\right) + z_n(t) \tag{4.9}$$

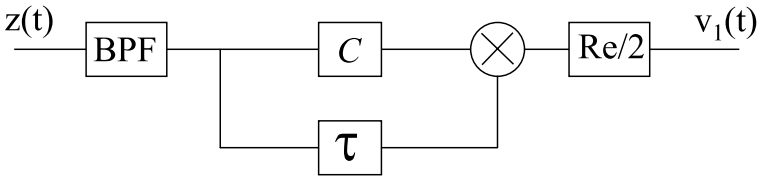

Figure 4.7: General block diagram of a differential demodulator (Re/2 is a complex representation equivalent to the lowpass filtering).

4.3.2 Modeling Differential Demodulation

From Figure 4.7, the output $v_1(t)$ of a differential demodulator can be represented as

$$v_1(t) = \frac{1}{2}\mathrm{Re}\left[Cz(t)z(t-\tau)^*\right] \tag{4.10}$$

where τ is some arbitrary delay (usually a multiple of the bit interval T), C is some complex constant dependent on the delay τ and * represents conjugation. For one-bit differential demodulation, $\tau = T = 1$ bit interval and $C = -j$,

$$v_1(t) = \frac{1}{2}\mathrm{Re}\left[-jz(t)z(t-T)^*\right]. \tag{4.11}$$

We subsequently examine one-bit differential demodulation.

In the absence of fading, $x_s(t) = 1$ and $y_s(t) = 0$ (that is, there is no envelope degradation on the signal). In the absence of CCI, $x_i(t) = 0$ and $y_i(t) = 0$. In the absence of AWGN, $x_n(t) = 0$ and $y_n(t) = 0$. Ideally (with no fading, CCI, or AWGN),

$$v_1(t) = \sin(\Delta\phi_s) \tag{4.12}$$

where $\Delta\phi_s$ is the change in ϕ_s over one bit interval (T) and where the scalar $1/2$ has been dropped without loss of generality. For the case of ideal MSK (no ISI), $\Delta\phi_s = \pm\pi/2$. For GMSK, however, ISI is introduced so that

$$\Delta\phi_s = \pi h \sum_{i=-L/2}^{L/2} m_i \int_{-T/2}^{T/2} g(\tau - iT)\, d\tau \tag{4.13}$$

where $g(t)$ is defined in Eqn. 2.5, $m_i = \pm 1$ is the binary sequence, h is the modulation index, and L is the number of bit intervals over which the pulse is spread (L is a measure of ISI). The change in phase $\Delta\phi_s$ can be expressed as

$$\begin{aligned} \Delta\phi_s &= \sum_{i=-L/2}^{L/2} m_i p_i \\ &= m_0 p_0 + (m_1 + m_{-1})p_1 + (m_2 + m_{-2})p_2 \end{aligned} \tag{4.14}$$

taking the pulse spread to be significant over five bit intervals, where

$$p_i = \pi h \int_{-\frac{T}{2}-iT}^{\frac{T}{2}-iT} g(\tau)\, d\tau \tag{4.15}$$

For $BT = 0.3$ (as in GSM), $p_0 = 1.023$ radians, $p_1 = p_{-1} = 0.271$ radians, and $p_2 = p_{-2} = 0.003$ radians. Thus, for $BT = 0.3$, most (99.6%) of the pulse (and therefore, the information) is contained within three bit intervals.

One-bit differential demodulation with decision feedback (DF) is similar, with

$$\Delta\phi_s = m_0 p_0 + m_1 p_1 + m_2 p_2 \tag{4.16}$$

assuming reliable decisions are fed back (usually a valid assumption at low BER).

The output $v_2(t)$ of a two-bit differential demodulator is

$$v_2(t) = \frac{1}{2}\mathrm{Re}\left[z(t)z(t-2T)^*\right] \tag{4.17}$$

Ideally (with no fading, CCI, or AWGN),

$$v_2(t) = \cos(\Delta\phi_s) \tag{4.18}$$

The phase change $\Delta\phi_s$ is the change in ϕ_s over two bit intervals ($2T$) and can be expressed as

$$\Delta\phi_s = (e_{-1} + e_0)p_0 + (e_1 + e_{-2})p_1 + (e_2 + e_{-3})p_2 \tag{4.19}$$

where e_i is a differentially encoded version of the binary data sequence as in Eqn. 2.12

$$e_i = -m_i m_{i-1} \tag{4.20}$$

If the data is differentially encoded before transmission as in Eqn. 2.11, then the two-bit differential demodulator yields differentially decoded data (i.e., the original unencoded data). For BT=0.3 (as in GSM), $p_0 = p_1 = 1.294$ radians, $p_2 = p_{-1} = 0.274$ radians, and $p_3 = p_{-2} = 0.003$ radians.

Two-bit differential demodulation with decision feedback (DF) is similar, with

$$\Delta\phi_s = e_0 p_0 + e_1 p_1 + e_2 p_2 \tag{4.21}$$

assuming reliable decisions are fed back (i.e., low BER).

4.3.3 DD1 Decision Statistic in the Wireless Channel

Let the signal samples in a one-bit differential demodulator be denoted $z_1 = z(kT)$ and $z_2 = z(kT - T)$ as in Eqn. 4.11, then the decision statistic v_k of a one-bit differential demodulator is

$$v_k = \mathrm{Re}\left[-jz_1 z_2^*\right] \tag{4.22}$$

where the scalar 1/2 has been dropped without loss of generality. The output of a differential demodulator consists of

$$\begin{aligned} z_1 z_2^* &= z_{s1} z_{s2}^* e^{j(\phi_{s1}-\phi_{s2})} + z_{s1} z_{i2}^* e^{j(\phi_{s1}-\phi_{i2})} + z_{s1} z_{n2}^* e^{j\phi_{s1}} \\ &\quad + z_{i1} z_{i2}^* e^{j(\phi_{i1}-\phi_{i2})} + z_{i1} z_{s2}^* e^{j(\phi_{i1}-\phi_{s2})} + z_{i1} z_{n2}^* e^{j\phi_{i1}} \\ &\quad + z_{n1} z_{s2}^* e^{-j\phi_{s2}} + z_{n1} z_{i2}^* e^{j\phi_{i2}} + z_{n1} z_{n2}^* \end{aligned} \tag{4.23}$$

such that

$$v_k = \mathrm{Re}\left[-j z_1 z_2^*\right] = \mathrm{Im}\left[z_1 z_2^*\right] \tag{4.24}$$

$$\begin{aligned} v_k &= (x_{s1}x_{s2} + y_{s1}y_{s2})\sin(\phi_{s1}-\phi_{s2}) + (y_{s1}x_{s2} - x_{s1}y_{s2})\cos(\phi_{s1}-\phi_{s2}) \\ &\quad + (x_{i1}x_{i2} + y_{i1}y_{i2})\sin(\phi_{i1}-\phi_{i2}) + (y_{i1}x_{i2} - x_{i1}y_{i2})\cos(\phi_{i1}-\phi_{i2}) \\ &\quad + (x_{s1}x_{i2} + y_{s1}y_{i2})\sin(\phi_{s1}-\phi_{i2}) + (y_{s1}x_{i2} - x_{s1}y_{i2})\cos(\phi_{s1}-\phi_{i2}) \\ &\quad + (x_{i1}x_{s2} + y_{i1}y_{s2})\sin(\phi_{i1}-\phi_{s2}) + (y_{i1}x_{s2} - x_{i1}y_{s2})\cos(\phi_{i1}-\phi_{s2}) \\ &\quad + (x_{s1}x_{n2} + y_{s1}y_{n2})\sin(\phi_{s1}) + (y_{s1}x_{n2} - x_{s1}y_{n2})\cos(\phi_{s1}) \\ &\quad + (x_{i1}x_{n2} + y_{i1}y_{n2})\sin(\phi_{i1}) + (y_{i1}x_{n2} - x_{i1}y_{n2})\cos(\phi_{i1}) \\ &\quad - (x_{n1}x_{s2} + y_{n1}y_{s2})\sin(\phi_{s2}) + (y_{n1}x_{s2} - x_{n1}y_{s2})\cos(\phi_{s2}) \\ &\quad - (x_{n1}x_{i2} + y_{n1}y_{i2})\sin(\phi_{i2}) + (y_{n1}x_{i2} - x_{n1}y_{i2})\cos(\phi_{i2}) \\ &\quad + (y_{n1}x_{n2} - x_{n1}y_{n2}) \end{aligned} \tag{4.25}$$

4.3.4 DD1 Decision Statistic in AWGN

In AWGN ($x_s = 1$, $y_s = 0$, $x_i = 0$ and $y_i = 0$ so that $z_s = 1$ and $z_i = 0$),

$$\begin{aligned} v_k &= \sin(\phi_{s1}-\phi_{s2}) + x_{n2}\sin\phi_{s1} - y_{n2}\cos\phi_{s1} \\ &\quad - x_{n1}\sin\phi_{s2} + y_{n1}\cos\phi_{s2} + y_{n1}x_{n2} - x_{n1}y_{n2} \qquad (4.26) \\ &= s_k + \eta_k \qquad (4.27) \end{aligned}$$

where $s_k = \sin(\phi_{s1} - \phi_{s2}) = \sin\Delta\phi_s$ is the SOI and the rest of the terms η_k represent the noise.

$$\eta_k = x_{n2}\sin\phi_{s1} - y_{n2}\cos\phi_{s1} - x_{n1}\sin\phi_{s2} + y_{n1}\cos\phi_{s2} + y_{n1}x_{n2} - x_{n1}y_{n2} \tag{4.28}$$

Again, in ideal conditions, $v_k = \sin\Delta\phi_s$.

The impact of the bandpass filter(s) on the analytical expressions remains to be investigated (refer to Section 2.3.3). Some GMSK researchers [65, 68, 100] try to take into account the bandpass filtering in the analytical expressions). For the above mathematical analysis to remain valid, the complex random variables (z_s, z_i, and z_n) would have to be assumed Gaussian after bandpass filtering. If the filtering is more realistically modeled, then a transformation of variables would have to be performed to model the impact of the filtering. It is unlikely that the transformed variables (of z_s, z_i, and z_n) would be Gaussian. The signal component would also be filtered.

This outlines a general approach to deriving the decision statistic at the output of a differential demodulator, using a one-bit differential demodulator as an example. An analytic solution for the decision statistic, however, is complicated for all but the most simple channels. Here, the derivation is for an AWGN channel. The decision statistic in fading and CCI is much more complicated and is omitted here.

4.3.5 DD1 Decision Statistic PDF in AWGN

For BER estimation (discussed in Chapter 7), one would like know the pdf of the decision statistic. This section shows how the pdf of the decision statistic might be determined analytically. It is shown that the pdf of the decision statistic is very difficult, if not impossible, to obtain, in the simple case of one-bit differential demodulation in AWGN with ideal filtering and amplification. If other operations on the signal (such as RF, IF, and baseband filtering and amplification) are included, then the derivation becomes even more complicated. Taking into account other channel impairments and practical receiver operations will be even more difficult.

This section outlines a general approach to deriving the decision statistic at the output of a differential demodulator, using a one-bit differential demodulator as an example. The appendix also shows how the pdf of the decision statistic might be determined analytically. An analytic solution for the decision statistic, however, is complicated for all but the most simple channels. Here, the derivation is for an AWGN channel. It is shown that the pdf of the decision statistic is very difficult, if not impossible, to obtain, in the simple case of one-bit differential demodulation in AWGN with ideal filtering and amplification. If other operations on the signal (such as RF, IF, and baseband filtering and amplification) are included, then the derivation becomes even more complicated. Taking into account other channel impairments and practical receiver operations will be even more difficult.

Now, from the power spectral density given in (4.6), if the system uses a sampling rate which an integer of the bandwidth, noise samples will be uncorrelated, i.e.

$$\mathrm{E}\left[n(t)n(s)\right] = \begin{cases} \sigma_n^2\delta(t-s) & t = s \end{cases} \tag{4.29}$$

where σ_n^2 is the total noise power.

Let the signal samples in a one-bit differential demodulator be denoted $z_1 = z(kT)$ and $z_2 = z(kT-T)$ as in Eqn. 4.11, then the decision statistic v_k of a one-bit differential demodulator is

$$v_k = \mathrm{Re}\left[-jz_1z_2^*\right] \tag{4.30}$$

where the scalar $1/2$ has been dropped without loss of generality. From Eqn. 4.26, the output of a one-bit differential demodulator in AWGN ($x_s = 1$, $y_s = 0$, $x_i = 0$ and $y_i = 0$, so that $z_s = 1$ and $z_i = 0$) consists of

$$\begin{aligned} v_k &= \sin(\phi_{s1} - \phi_{s2}) + x_{n2}\sin\phi_{s1} - y_{n2}\cos\phi_{s1} \\ &\quad -x_{n1}\sin\phi_{s2} + y_{n1}\cos\phi_{s2} + y_{n1}x_{n2} - x_{n1}y_{n2} \qquad (4.31) \\ &= s_k + \eta_k \qquad (4.32) \end{aligned}$$

where $s_k = \sin(\phi_{s1} - \phi_{s2}) = \sin \Delta\phi_s$ is the SOI and the rest of the terms η_k represent the noise.

$$\eta_k = x_{n2} \sin \phi_{s1} - y_{n2} \cos \phi_{s1} - x_{n1} \sin \phi_{s2} + y_{n1} \cos \phi_{s2} + y_{n1} x_{n2} - x_{n1} y_{n2} \tag{4.33}$$

Again, in ideal conditions, $v_k = \sin \Delta\phi_s$.

The expected value of SOI s_k is related to the BT value of the premodulation filtering, which induces ISI. E[s_k]=0 for the entire signal for symmetric signal constellations. For +1 data or -1 data, E[s_k] will be some constant with magnitude ≤ 1, respectively, depending on BT. The expected value of the noise term η_k of the DD1 decision statistic v_k (using Eqn. 4.26) is

$$\begin{aligned} \mathrm{E}[\eta_k] &= \mathrm{E}[x_{n2}]\mathrm{E}[\sin \phi_{s1}] - \mathrm{E}[y_{n2}]\mathrm{E}[\cos \phi_{s1}] \\ &\quad -\mathrm{E}[x_{n1}]\mathrm{E}[\sin \phi_{s2}] + \mathrm{E}[y_{n1}]\mathrm{E}[\cos \phi_{s2}] \\ &\quad +\mathrm{E}[y_{n1}]\mathrm{E}[x_{n2}] - \mathrm{E}[x_{n1}]\mathrm{E}[y_{n2}] \\ \mathrm{E}[\eta_k] &= 0 \end{aligned} \tag{4.34}$$

because x_{ni} and y_{ni} are independent zero-mean Gaussian random processes and the noise is independent of the signal.

The variance of the noise after differential demodulation η_k is

$$\begin{aligned} \mathrm{var}[\eta_k] &= \mathrm{E}[\eta_k^2] \\ &= \mathrm{E}[x_{n2}^2]\mathrm{E}[\sin \phi_{s1}^2] - \mathrm{E}[y_{n2}^2]\mathrm{E}[\cos \phi_{s1}^2] \\ &\quad -\mathrm{E}[x_{n1}^2]\mathrm{E}[\sin \phi_{s2}^2] + \mathrm{E}[y_{n1}^2]\mathrm{E}[\cos \phi_{s2}^2] \\ &\quad +\mathrm{E}[y_{n1}^2]\mathrm{E}[x_{n2}^2] - \mathrm{E}[x_{n1}^2]\mathrm{E}[y_{n2}^2] \\ \mathrm{var}[\eta_k] &= \sigma_n^2 + \frac{\sigma_n^4}{2} \end{aligned} \tag{4.35}$$

where the other cross-products are zero (as follows from Eqn. 4.29) because x_{ni} and y_{ni} are independent, uncorrelated, and zero-mean so that

$$\begin{aligned} \mathrm{E}[x_{ni} y_{ni}] &= \mathrm{E}[x_{ni}]\mathrm{E}[y_{ni}] = 0 \\ \mathrm{E}[x_{ni} x_{nj}] &= \mathrm{E}[x_{ni}]\mathrm{E}[x_{nj}] = 0, \qquad i \neq j \\ \mathrm{E}[y_{ni} y_{nj}] &= \mathrm{E}[y_{ni}]\mathrm{E}[y_{nj}] = 0, \qquad i \neq j \end{aligned} \tag{4.36}$$

and

$$\mathrm{E}[x_{ni}^2] = \mathrm{E}[y_{ni}^2] = \sigma_n^2/2 \tag{4.37}$$

There is some loss of signal energy during the differential demodulation operation. In other words, differential demodulation lowers the S/N ratio, as evidenced by the mixing of signal energy with noise energy in the cross-terms.

The decision statistic in fading and CCI is much more complicated and is omitted here. The derivation of decision statistics for other type of differential demodulation (such as two-bit differential demodulation) follows in a similar way.

The incorporation of decision feedback (DF) changes the derivation by changing the relationship between $\Delta\phi_s$ and the original binary data sequence. The output of a two-bit differential demodulator is a two-bit encoded version of the data sequence, the output of a three-bit differential demodulator is a three-bit encoded version of the data sequence, etc.

4.3.6 Analysis of DD1 PDF in AWGN

The following derivations illustrate how one might approach finding analytically expressions for the pdf of the decision statistic at the output of a one-bit differential demodulator. The general approach is to find the pdfs of the individual terms of the DD1 decision statistic in AWGN v_k, as given in Eqn. 4.31, and then determine if the pdfs can be combined in some way to provide an overall all pdf for the decision statistic.

PDF of $Z = XY$

The derivation of the pdf of $Z = XY$ is of interest because of the terms $y_{n1}x_{n2}$ and $x_{n1}y_{n2}$ found in Eqn. 4.31. In these terms, x and y are N[0,1] (Gaussian random variables with zero-mean and unit-variance).

In general, given two RVs X and Y and two functions $g(x, y)$ and $h(x, y)$, we want to determine the joint density of the RVs

$$Z = g(X, Y) \qquad W = h(X, Y) \tag{4.38}$$

in terms of the joint density of X and Y [185]. To find the joint density $f_{zw}(z, w)$, we solve the system

$$g(x, y) = z \qquad h(x, y) = w \tag{4.39}$$

Denoting by (x_n, y_n) its real roots

$$g(x_n, y_n) = z \qquad h(x_n, y_n) = w \tag{4.40}$$

it is a fundamental theorem that

$$f_{zw}(z, w) = \frac{f_{xy}(x_1, y_1)}{|J(x_1, y_1)|} + \cdots + \frac{f_{xy}(x_n, y_n)}{|J(x_n, y_n)|} + \cdots \tag{4.41}$$

where

$$J(x, y) = \begin{vmatrix} \frac{\partial z}{\partial x} & \frac{\partial z}{\partial y} \\ \frac{\partial w}{\partial x} & \frac{\partial w}{\partial y} \end{vmatrix} = \begin{vmatrix} \frac{\partial x}{\partial z} & \frac{\partial x}{\partial w} \\ \frac{\partial y}{\partial z} & \frac{\partial y}{\partial w} \end{vmatrix}^{-1} \tag{4.42}$$

is the *jacobian* of the transformation in Eqn. 4.39.

The density of one function $Z = g(X, Y)$ of two RVs can be determined from Eqn. 4.41 where W is a conveniently chosen auxiliary variable, for example $W = X$ or $W = Y$. The density of Z is then found by integrating the function $f_{zw}(z, w)$ so obtained.

For example, let X and Y be i.i.d. (independent, identically distributed) RVs with normal distribution (zero-mean, unit variance) N(0,1). Define Z to be a function of two

random variable X and Y such that $Z = XY$, and let $W = X$. The system $xy = z$, $x = w$ has a single solution: $x = w$, $y = z/w$. The jacobian of the transformation

$$J = (x_1, y_1) = \begin{vmatrix} y & x \\ 1 & 0 \end{vmatrix} = -x = -w \tag{4.43}$$

so that

$$f_{zw}(z, w) = \frac{1}{|w|} f_{xy}(w, z/w) \tag{4.44}$$

and

$$f_z(z) = \int_{-\infty}^{\infty} \frac{1}{|w|} f_{xy}(w, z/w)\, dw \tag{4.45}$$

But X and Y are independent and N(0,1), so $f_{xy}(w, z/w) = f_x(w) f_y(z/w)$, therefore

$$\begin{aligned} f_z(z) &= \int_{-\infty}^{\infty} \frac{1}{|w|} f_x(w) f_y(z/w)\, dw \\ &= \frac{1}{2\pi} \int_{-\infty}^{\infty} \frac{1}{|w|} e^{-w^2/2} e^{-(z/w)^2/2}\, dw \\ &= \frac{1}{2\pi} \int_{-\infty}^{\infty} \frac{1}{|w|} e^{-\frac{w^2}{2} - \frac{z^2}{2w^2}}\, dw \\ f_z(z) &= \frac{1}{\pi} \int_0^{\infty} \frac{1}{w} e^{-\frac{1}{2}\left(w^2 + \frac{z^2}{w^2}\right)}\, dw \end{aligned} \tag{4.46}$$

Monte Carlo simulations confirm the validity of this analytical result.

PDF of $Z = aX + bY$

The derivation of the pdf of $Z = aX + bY$ is of interest because of the terms $x_{n2} \sin \phi_{s1}$, $y_{n2} \cos \phi_{s1}$, $x_{n1} \sin \phi_{s2}$, and $y_{n1} \cos \phi_{s2}$ found in Eqn. 4.31. In these terms, x and y are i.i.d. (independent, identically distributed) Gaussian random variables N[0,1] (zero-mean with unit-variance), which are scaled by some scalar value a or b.

In general, because x and y are independent (and scaled versions ax and $by$are also independent), the density of their sum equals the convolution of their densities (see Section 4.3.6). Let $x' = ax$ and $y' = by$, such that $z = x' + y'$. Therefore,

$$\begin{aligned} f_z(z) &= f_{x'}(x') * f_{y'}(y') \\ &= \int_{-\infty}^{\infty} f_{x'}(z - x') f_{y'}(y') \end{aligned} \tag{4.47}$$

It is well-known that the sum of two Gaussian RVs is a Gaussian RV. Particularly, given two normally (Gaussian) distributed RVs $N(\mu_1, \sigma_1^2)$ and $N(\mu_2, \sigma_2^2)$ with means μ_1 and μ_2, respectively and variances σ_1^2 and σ_2^2, the result of summing these RVs can be derived as

$$N(\mu_1, \sigma_1^2) + N(\mu_2, \sigma_2^2) = N(\mu_1 + \mu_2, (\sigma_1 + \sigma_2)^2) \tag{4.48}$$

$$N(\mu_1, \sigma_1^2) - N(\mu_2, \sigma_2^2) = N(\mu_1 - \mu_2, (\sigma_1 - \sigma_2)^2) \tag{4.49}$$

Therefore, applying Eqn. 4.47, for x and y N[0,1], the pdf of z becomes

$$f_z(z) = \frac{1}{\sqrt{2\pi}(a+b)} \exp(-\frac{z^2}{2(a+b)^2}) \qquad \text{for } z = ax + by \tag{4.50}$$

$$f_z(z) = \frac{1}{\sqrt{2\pi}(a-b)} \exp(-\frac{z^2}{2(a-b)^2}) \qquad \text{for } z = ax - by \tag{4.51}$$

PDF of $Z = XY - UV$

The derivation of the pdf of $Z = XY - UV$ is of interest because of the term $y_{n1}x_{n2} - x_{n1}y_{n2}$ found in Eqn. 4.31. In this term, x and y are Gaussian random variables (zero-mean with unit-variance).

Let X, Y, U, V be i.i.d. random variables with normal distribution (zero-mean, unit variance) N(0,1). Define Z to be a function of four random variable X, Y, U, V such that

$$Z = XY - UV \tag{4.52}$$

The moment generating function of Z is [266]

$$M_Z(t) = \mathrm{E}\left[e^{t(XY-UV)}\right] = \mathrm{E}\left[e^{tXY}\right] \mathrm{E}\left[e^{-tUV}\right] \tag{4.53}$$

Since

$$\begin{aligned} \mathrm{E}\left[e^{tXY}\right] &= \frac{1}{2\pi} \int_{-\infty}^{\infty} \int_{-\infty}^{\infty} e^{tXY} e^{-\frac{1}{2}(x^2+y^2)}\, dx\, dy \\ &= \frac{1}{2\pi} \int_{-\infty}^{\infty} \int_{-\infty}^{\infty} e^{-\frac{1}{2}[(x-ty)^2+y^2-t^2y^2]}\, dx\, dy \\ &= \frac{1}{\sqrt{1-t^2}}, \qquad \text{for} \qquad |t| < 1 \end{aligned} \tag{4.54}$$

So,

$$M_Z(t) = \frac{1}{\sqrt{1-t^2}} \frac{1}{\sqrt{1-(-t)^2}} = \frac{1}{1-t^2} \tag{4.55}$$

However, for a double exponential distribution $f(x) = \frac{1}{2}\exp(-|x|)$, $-\infty < x < \infty$, its moment generating function is also $1/(1-t^2)$. Therefore, $Z = XY - UV$ has a double exponential distribution (consequently, a double exponential density). That is,

$$f_Z(z) = \frac{1}{2} \exp(-|z|) \tag{4.56}$$

Overall PDF by Combining the Terms

The linear combination $Z = X + Y$ yields a pdf $f_z(z)$

$$f_z(z) = \int_{-\infty}^{\infty} f(z-y, y)\, dy \tag{4.57}$$

If the RVs X and Y are independent, then $f(x,y) = f_x(x)f_y(y)$. Inserting into Eqn. 4.57, we obtain

$$f_z(z) = \int_{-\infty}^{\infty} f_x(z-y)f_y(y)\,dy \tag{4.58}$$

which is the convolution of the functions $f_x(x)$ and $f_y(y)$, leading to the fundamental conclusion:

> *If two RVs are independent, then the density of their sum equals the convolution of their densities.*

We have derived analytical expressions for the pdf each of the RV terms of v_k of Eqn. 4.26. If these terms are independent, then an overall analytic expression for the pdf of v_k can be obtained by convolving the individual pdfs of the individual terms of v_k. Unfortunately, some of the terms are not independent, making the derivation of an overall pdf very difficult for even this simple case of a basic one-bit differential demodulator in AWGN with ideal receiver processing.

This exercise serves to show the difficulties involved with *a priori* methods of pdf estimation (and consequently, BER estimation). The attempt to derive an closed form analytical expressions for the pdf of the decision statistic at the output of a one-bit differential demodulator is abandoned at this point. We look to *a posteriori* methods to yield more practical solutions to the problem of pdf and BER estimation. Fortunately, *a posteriori* pdf estimation methods exist and are discussed in Section 7.4.

4.4 Summary

In this chapter, individual coherent and noncoherent demodulators (introduced in Chapter 2) are examined in more detail. Examples of three of the better performing noncoherent demodulators (the 2-bit differential demodulator with decision feedback; the 1-bit DF, 2-bit DF, & 3-bit DF differential demodulators with combined outputs; and the limiter discriminator demodulator) are included, along with block diagrams and signal space constellations.

This chapter also includes a general analytical examination of differential demodulation (a noncoherent technique). The analytical expressions derived are also applicable to differential detection (refer to Section 2.2). Section 4.3.1 defines a general wireless channel model which includes noise (AWGN), co-channel interference (CCI), and flat Rayleigh fading. Analytical expressions for the output of a one-bit differential demodulator (DD1) are then derived using the general wireless channel model. The derivation focuses on the case of AWGN, and an attempt is made to derive an analytic expression for pdf of the DD1 decision statistic in AWGN. This exercise shows that *a priori* (deductive) methods of determining expressions for the pdf in this simple case are very difficult. The failure to obtain a satisfactory analytical expression motivates research into *a posteriori* (inductive) techniques of determining the pdf of the decision statistic (discussed in Chapter 7).

Chapter 5

Performance of Individual Receivers

5.1 Motivation

In this chapter, the demodulators described in Chapter 4 are simulated, and their performance is evaluated in various wireless channel environments. Twenty-five channel impairments are simulated with various combinations of additive white Gaussian noise (AWGN), CCI, and different types of multipath in accordance with the European COST 207 [70] propagation models (see also Appendix C). Results indicate that there is no one technique which is superior in all channel impairments, but particular techniques show promise of improving GMSK demodulation, depending on the dominant channel impairment. This extensive performance evaluation of GMSK demodulators is a unique contribution of this research.

This chapter illustrates the thesis that individual demodulators can be superior to other demodulators in differing channel impairments, so that no one demodulator is necessarily always the best in every channel impairment. This thesis motivates research into demodulator diversity schemes, which can maximize the information extracted from several demodulators in a changing channel to take advantage of the respective strengths of the individual demodulators.

5.2 Simulated Channel Impairments

The simulations throughout this research utilize a complex baseband bandpass signal representation. This general signal is given by

$$s(t) = \mathrm{Re}\left[g(t) \exp j\theta(t)\right], \tag{5.1}$$

where $g(t)$ is the complex envelope of the bandpass signal, $\theta(t)$ is the phase of the bandpass signal, and Re[$\cdot$] denotes the real part. For more details on the GMSK signal generated in simulations, refer to Section 2.2.2.

The performance of each demodulator listed in Table 4.1 was evaluated in terms of BER in twenty-five channel impairments with various combinations of Additive White Gaussian Noise (AWGN), Co-Channel Interference (CCI), and different types of multipath in accordance with the European COST 207 propagation models (refer to Appendix C for more details). COST 207 propagation models are used in this chapter, Section 10.2, and Appendices A.1 and A.2. SMRCIM [241] is used to simulate multipath in Chapter 9 and Sections 10.3, 10.4, and 11.5.2 (refer to Appendix C for more details). The research initially used COST 207 multipath models because they are GSM standards. Later research included SMRCIM multipath models because SMRCIM incorporates real measurements into the models.

The channel impairments simulated are listed in Table 5.1, where AWGN is Additive white Gaussian noise (E_b/N_o varied from 0 to 30 dB), CCI is co-channel interference (C/I varied from 0 to 30 dB), C/I is the carrier-to-interference ratio. E_b/N_o calculations assume a predetection filter bandwidth of $0.75R$. This is the first-null bandwidth for GMSK (and MSK). It is also approximately equal to the channel bandwidth of a GSM channel, where 200 kHz channel $\approx 0.75 \cdot 270.833$ kbps bit rate ($= 0.7384R$). This bandwidth limits the noise power added to the signal in computer simulations. When there is no CCI, E_b/N_o is varied.

The channel is assumed to be co-channel interference-limited (not noise-limited, where $E_b/N_o = 12$ dB when AWGN is included with CCI). One interferer is assumed to be dominant (typical in real systems). When CCI is presence, C/I varied. The demodulators are also evaluated when the CCI has a 200 Hz carrier offset which represents a worst-case scenario of frequency drift in the transceivers.

The fading environment typical in a mobile radio channel was simulated using European COST 207 propagation models [70] where Rayleigh fading conditions are based on four typical environments (refer to Appendix C for more details). A sampling rate of $M = 18$ samples per bit was chosen to simulate typical multipath delays of about 2 μs, as modeled by COST 207. For the GSM data rate, the simulated sampling interval $T_{sample} = T_b/M = 270,833/18 = 0.205\mu s$.

5.3 The Best Demodulator for Each Channel Impairment

The three best demodulators were chosen based on the results from Table 5.2. If two structures have equivalent performance, the simplest structure is chosen. If BERs for two demodulators cross, the best demodulator at the lower values of E_b/N_o and C/I is chosen.

The best three demodulators chosen are

- 2-bit differential demodulator with decision feedback
- 1-bit DF, 2-bit DF, & 3-bit DF differential demodulators with combined outputs

Table 5.1: Simulated channel impairments and abbreviations.

	Channel Impairment	Abbrev.
1)	AWGN	A
2)	CCI	C
3)	CCI with 200 Hz offset	C2
4)	AWGN & CCI	CA
5)	AWGN & CCI with 200 Hz offset	CA2
6)	AWGN & Hilly (bad) urban Rayleigh fading	ARb
7)	AWGN & Urban Rayleigh fading	ARu
8)	AWGN & Hilly rural Rayleigh fading	ARh
9)	AWGN & Rural Rayleigh fading	ARr
10)	CCI & Hilly (bad) urban Rayleigh fading	CRb
11)	CCI & Urban Rayleigh fading	CRu
12)	CCI & Hilly rural Rayleigh fading	CRh
13)	CCI & Rural Rayleigh fading	CRr
14)	CCI with 200 Hz offset & Hilly (bad) urban Rayleigh fading	CRb2
15)	CCI with 200 Hz offset & Urban Rayleigh fading	CRu2
16)	CCI with 200 Hz offset & Hilly rural Rayleigh fading	CRh2
17)	CCI with 200 Hz offset & Rural Rayleigh fading	CRr2
18)	AWGN, CCI, & Hilly (bad) urban Rayleigh fading	CARb
19)	AWGN, CCI, & Urban Rayleigh fading	CARu
20)	AWGN, CCI, & Hilly rural Rayleigh fading	CARh
21)	AWGN, CCI, & Rural Rayleigh fading	CARr
22)	AWGN, CCI with 200 Hz offset, & Hilly (bad) urban Rayleigh fading	CARb2
23)	AWGN, CCI with 200 Hz offset, & Urban Rayleigh fading	CARu2
24)	AWGN, CCI with 200 Hz offset, & Hilly rural Rayleigh fading	CARh2
25)	AWGN, CCI with 200 Hz offset, & Rural Rayleigh fading	CARr2

Table 5.2: The best demodulator for each channel impairment (abbreviations defined in Table 5.1).

	Channel Impairment	Best Demodulator (in terms of BER)	Comments
1)	A	1-2-3 DF DD	coherent demodulation is superior
2)	C	1-2-3 DF DD	coherent demodulation is superior
3)	C2	1-2-3 DF DD	coherent demodulation is superior
4)	CA	1-2-3 DF DD	coherent demodulation is superior
5)	CA2	1-2-3 DF DD	coherent demodulation is superior
6)	ARb	2 DF DD	
7)	ARu	1-2-3 DF DD	
8)	ARh	1-2-3 DF DD	
9)	ARr	2 DF DD	
10)	CRb	1-2 DF DD	only slightly better than 1-2-3 DF DD
11)	CRu	Limiter Discriminator	
12)	CRh	1-2-3 DF DD	
13)	CRr	2 DF DD	
14)	CRb2	1-2 DF DD	only slightly better than 1-2-3 DF DD
15)	CRu2	1-2-3 DF DD	
16)	CRh2	1-2-3 DF DD	
17)	CRr2	2 DF DD	
18)	CARb	2 DF DD	
19)	CARu	1-2-3 DF DD	
20)	CARh	1-2-3 DF DD	
21)	CARr	1-2-3 DF DD	
22)	CARb2	2 DF DD	
23)	CARu2	1-2-3 DF DD	
24)	CARh2	1-2-3 DD	only slightly better than 1-2-3 DF DD
25)	CARr2	1-2-3 DF DD	

- limiter discriminator demodulator

The limiter discriminator demodulator yields better results only for CRu (CCI and urban Rayleigh fading) environments. The 2-bit differential demodulator with decision feedback yields better results only for ARr (AWGN and rural Rayleigh fading), CARb (AWGN, CCI, & hilly urban Rayleigh fading), and CRr (CCI & rural Rayleigh fading). The 1-bit DF, 2-bit DF, and 3-bit DF differential demodulators with combined outputs (DD123DF) performs the best in the other channel impairments. The 200 Hz frequency offset (with CCI) generally resulted in a degradation in performance.

5.4 Sample Histograms in Multipath and CCI

Because the outputs of the demodulators have different probability density functions (pdfs), a data fusion problem exists when trying to combine (or fuse) the outputs (addressed in Chapter 10). The data at the output of the demodulatorsThe pdfs are illustrated by the histograms of the demodulator outputs as given in Figures 5.1 - 5.3. The histograms (200 bin) are based on the transmitted +1 and -1 bits, where the signal is corrupted by rural Rayleigh fading and CCI with $C/I = 8$ dB. Figure 5.1 is the histogram for the 2-bit DF DD, Figure 5.2 is the histogram for the 1-bit, 2-bit, 3-bit DF DD, and Figure 5.3 is the histogram for the limiter discriminator.

5.5 Analysis of Performance

In the midst of simulating differential demodulation, we found that 1-bit differential demodulation could be improved by a new decision logic in the feedback (i.e., 1-bit DD with improved DF logic scheme). The new decision logic is easily implemented and requires only minor changes in conventional 1-bit DF DD. This is a new result, but the improvement is not enough to compete with the performance offered by 2-bit differential demodulation with decision feedback.

Though nonredundant error correction circuits yield improvements in performance when applied as outlined in Table 4.1, the gain is one of diminishing return. The improvement (particularly in the case of the 1-bit DF, 2-bit DF, and 3-bit DF DDs with combined outputs) is not statistically significant to warrant the added complexity introduced by error correction circuits.

The other new variations listed in Table 4.2 perform well, but the best among the new structures is the 1-bit DF, 2-bit DF, and 3-bit DF differential demodulators with combined outputs (DD123DF). This new structure yields superior performance over the others in many channel impairments. Preliminary results indicate, however, that there is no one technique which is superior in all channel impairments, but particular techniques show promise of improving GMSK demodulation, depending on the dominant channel impairment.

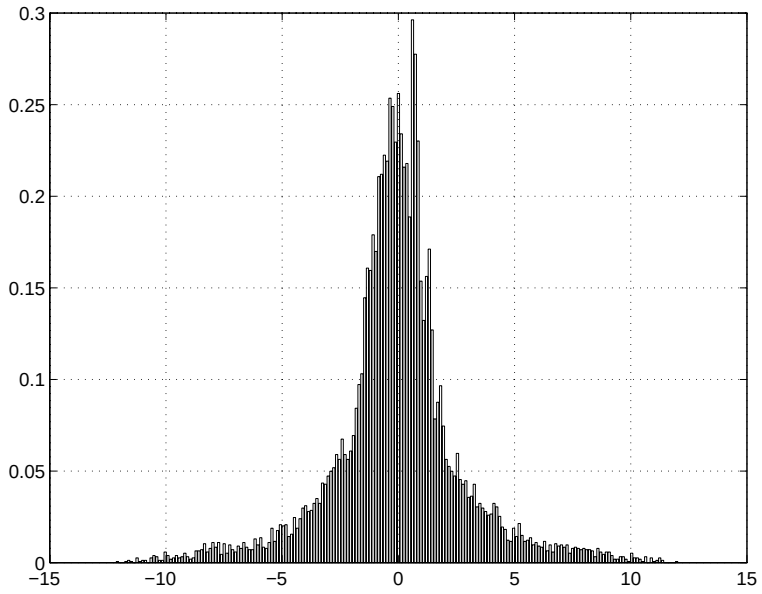

Figure 5.1: Histogram of 2-bit DF DD output in rural Rayleigh fading and CCI with $C/I = 8$ dB.

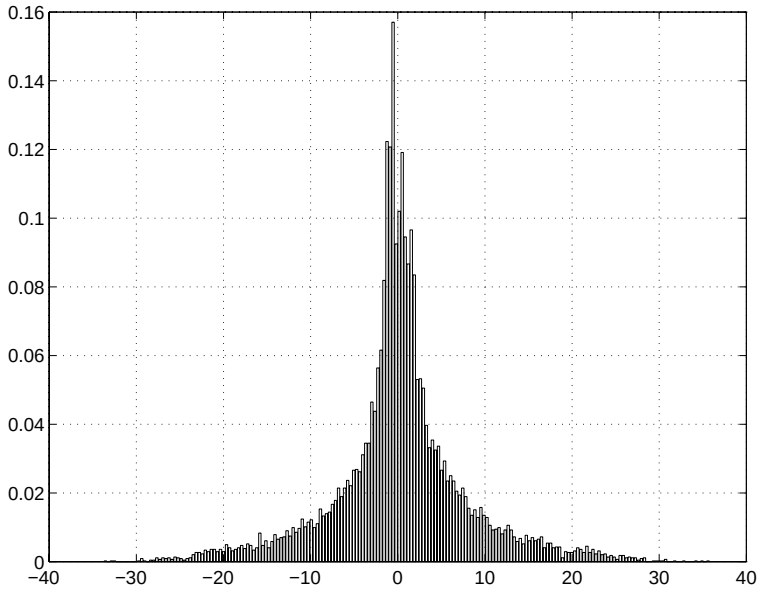

Figure 5.2: Histogram of 1-bit, 2-bit, 3-bit DF DD with combined outputs in rural Rayleigh fading and CCI with $C/I = 8$ dB.

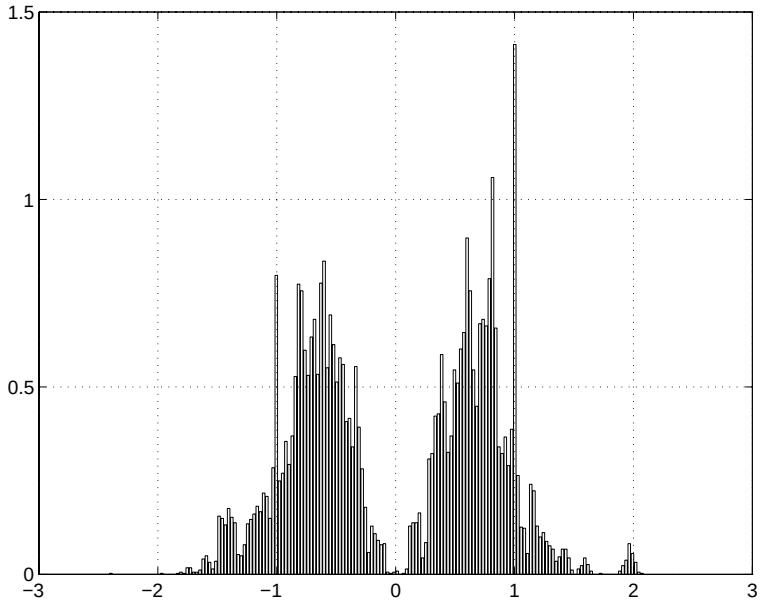

Figure 5.3: Histogram of limiter discriminator demodulator output in rural Rayleigh fading and CCI with $C/I = 8$ dB.

5.6 Summary

This chapter simulates the demodulators described in Chapter 4 and evaluates their performance in various wireless channel environments. Twenty-five channel impairments are simulated with various combinations of additive white Gaussian noise (AWGN), CCI, and different types of multipath in accordance with the European COST 207 [70] propagation models. The coherent demodulator, of course, performs best in AWGN. The best three noncoherent demodulators chosen were found to be the 2-bit differential demodulator with decision feedback; the 1-bit DF, 2-bit DF, & 3-bit DF differential demodulators with combined outputs (a new structure); and the limiter discriminator demodulator. This performance evaluation of the noncoherent demodulators is unique (in terms of the varied channel impairments typically encountered in the land mobile channel).

Chapter 5 illustrates the thesis that individual demodulators can be superior to other demodulators in differing channel impairments, so that no one demodulator is necessarily always the best in every channel impairment. This thesis motivates research into demodulator diversity schemes, which can maximize the information extracted from several receivers in a changing channel to take advantage of the respective strengths.

Chapter 6

Demodulator Diversity Theory

6.1 Motivation

This chapter provides theoretical (and analytical) support for the concept of demodulator diversity. By demodulator diversity, we mean receiver diversity, where the outputs of a bank of demodulators are combined in some way so as to take advantage of their diverse merits in a changing channel. Chapter 5 demonstrated that individual demodulators can be superior to other demodulators in differing channel impairments, so that no one demodulator is necessarily always the best in every channel impairment. This result motivates research into demodulator diversity schemes, which can maximize the information extracted from several demodulators in a changing channel to take advantage of the respective strengths.

With demodulator diversity, at the very least, we would like a combined demodulator to have a BER which tracks the BER of the best demodulator for given channel impairment. Ideally, we would like demodulator diversity to provide better overall performance than that attainable by any individual demodulator. As discussed in Section 6.2, an analogy can be drawn between demodulator diversity and spatial diversity (e.g., smart antennas) which helps to motivate this research. In Section 6.3, we derive the theoretical minimum mean squared error (MMSE) for a demodulator diversity scheme in AWGN.

6.2 Demodulator Diversity vs. Antenna Diversity

Diversity means a state of difference or variety. Diversity is (1) the fact or quality of being distinct or (2) a point or respect in which things differ [252]. In the reception of a signal in wireless communications, diversity can increase the amount of information available to accurately detect the transmitted signal in the presence of channel impairments. In a communications application, diversity means that there are different versions of a signal or signals. A communications system takes advantage of these differences to extract the desired information.

Several types of diversity are proposed in wireless communications, such as time diversity, frequency diversity, polarization diversity, and spatial diversity. Time, frequency, and polarization diversity schemes usually involve the transmission of redundant information in time, by frequency, or by polarization, respectively. Spatial diversity, also referred to as antenna diversity, focuses on the reception of different versions of a transmitted signal using multiple sensors or antennas (e.g., channel distortions such as multipath can produce multiple versions of a transmitted signal - delayed and attenuated - at the receiver).

Demodulator diversity, sometimes referred to as receiver diversity, is another type of diversity which has received little attention in the literature. Demodulator diversity also focuses on reception, but the diversity does not stem from redundant transmission or reception of multiple versions of a signal, but involves multiple demodulators (e.g., a bank of demodulators) with each demodulating the signal received by one sensor. Demodulator diversity compares and contrasts with antenna diversity in several ways.

With antenna diversity, antennas (or sensors) are separated in space (spatially) and receive versions of a signal which are similar, yet different because spatial separation of antennas which results in the signal traveling different paths to each antenna. Multiple antennas or sensors allow multi-channel reception, when each antenna detects a different version of the transmitted signal. The differences in the received versions of the signal at each antenna can be used to enhance and detect the signal [116]. For example, the fading that commonly occurs on a signal passing through the land mobile channel is often dependent on the channel path. With antenna diversity, one antenna may receive a version of the signal that is deeply faded while the another antenna may receive a stronger version of the signal. This diversity provided by multiple antennas can be exploited by utilizing the following approaches [55]:

switching: The received signal strength is monitored at each antenna and the receiver switches to that antenna for a set period of time. Only one antenna output is demodulated.

selection: All antenna outputs are demodulated, and the best one is selected so as to maximize signal detection or enhancement.

equal gain combining: Each branch of antenna output is weighted equally and are combined before detection.

maximal ratio combining: Each branch of antenna output is weighted according to the relative strength (power) of each output and are then combined before detection.

adaptive combining: MSE (means square error) or MLSE (maximum likelihood sequence estimation) criterion - the antenna outputs are adaptively combined.

Demodulator diversity, by contrast, involves only one version of the transmitted signal. Usually only one antenna or sensor is employed, resulting in single-channel

reception (i.e., the one signal can be viewed as having passed through a single channel, since there is only one version of the transmitted signal received. Demodulator diversity relies on the fact that the received signal is transformed in a different (usually nonlinear) way by each demodulator, providing similar but different information that depends on the channel conditions. Demodulator diversity also relies on the assumption that each demodulator is superior to the others in some type of channel impairment (illustrated in Sections 5.3 and 10.3). As the channel changes, the outputs of the demodulators can be adaptively selected or combined to equal or improve the performance of that of the best demodulator for the particular channel impairment. This contrasts with antenna diversity (or spatial diversity), which is a multi-channel scheme, where several versions of a signal are received on different antennas (separated spatially), so that the signal received on each antenna can be viewed as having passed through a different channel. With an antenna array (under the narrowband assumption, i.e., antenna elements are closely spaced), the received versions of the signal are linear transformations of each other. For antenna diversity schemes where the antennas are not closely spaced (e.g., ten wavelengths apart), the received versions of the signal are not necessarily linear transformations of each other.

Distinct tradeoffs exist in overall performance between antenna diversity and demodulator diversity, depending on the channel characteristics. Antenna diversity works much better than single channel techniques if the information signals are well separated and the antenna array is not overloaded (i.e., an array is generally overloaded is there are more received signals than sensors). Single-channel techniques often only work well under very restrictive assumptions about the environment. For example, Viterbi-based detection methods require baud and carrier sync on all signals. Also, demodulation/remodulation methods make assumptions about relative power levels. Single-channel techniques are generally more limited in the amount of interference that can be rejected compared to schemes employing antenna diversity [24]. Sometimes, however, an antenna array (or beamformer) cannot resolve received incoming signals (e.g., when the signals arrive from the same direction), whereas single-channel techniques may still be able to resolve the signals.

The advantages of antenna diversity compared to demodulator diversity differ depending on the channel conditions (e.g., fading performance is distinct from the performance in interference). In Chapter 5, the bit error rate (BER) performance of a bank of Gaussian Minimum Shift Keying (GMSK) noncoherent demodulators has been quantified in twenty-five channel impairments [133]. Simulations indicate that simple selection of the best demodulator output (determined by minimum MSE using a training sequence) can improve the overall performance as the channel changes.

Antenna array methods are expensive because of receiver requirements, since multiple antennas and receivers are necessary. In addition, arrays often require high quality components and very high dynamic range. In addition, increased receiver components adds to the power requirements, particularly at the mobile, which is limited by the battery life. Demodulator diversity schemes will also have additional receiver requirements, but the goal of these demodulator diversity schemes is to use inexpensive, noncoherent

demodulators, and thus decrease costs relative to performance. The real-time processing (e.g., weighting and summing) required for antenna arrays is usually not that intensive. Single-channel methods, on the other hand, are sometimes expensive because of more demanding processing requirements.

6.3 Theoretical MMSE for Demodulator Diversity in AWGN

The problem exists that a noisy version of a signal is observed (e.g., in the first demodulator diversity scheme detailed in Section 10.2.1, observed by three demodulators). It is desirable to estimate the "true" value of the signal. This is often viewed as the problem of separating the signal from the noise [219] (though we are also interested in other channel impairments encountered in the land mobile channel, such as cochannel interference and multipath fading, these impairments can be incorporated into the noise term). In the standard (or classical) approach, theory is presented in terms of minimizing the expected squared error (or mean squared error - MSE) between the estimator and the true (but unknown) signal. This estimation problem has been historically viewed as filtering the narrowband signal from wideband noise, and the process is termed linear mimimum mean squared error filtering. If the channel adds noise $N(t)$ (i.e., AWGN) to the signal $S(t)$, then the received signal (or observation) $X(t)$ can be expressed as $X(t) = S(t) + N(t)$. $X(t)$ is used to produce an estimator $\hat{S}(t)$ of $S(t)$.

In the mean square error (MSE) criterion, the error ε_k is defined as

$$\varepsilon_k = S_k - \hat{S}_k \tag{6.1}$$

where S_k is the information symbol transmitted in the kth signaling interval (for example, a known training sequence) and $\hat{S}(t)$ is the estimate of that symbol at the output of the demodulator where symbols are corrupted by some channel impairment. When the information symbols S_k are complex-valued, the performance index for the MSE criterion, denoted by J, is defined as [196]

$$J = \mathrm{E}\left[|\varepsilon|^2\right] = \mathrm{E}\left[|S_k - \hat{S}_k|^2\right] \tag{6.2}$$

On the other hand, when the information symbols are real-valued, the performance index is simply the square of the real part of ε_k . For example, the receiver input is complex-valued because of baseband complex representation, but the demodulator outputs for 2DD DF, 123DD DF, and Limiter Discriminator are real-valued because of the decision feedback and envelope detection, respectively. In the case of Gaussian Minimum Shift Keying (GMSK), S_k not only takes the values of ± 1 for binary signaling, but also values with magnitude less than 1 because of the intersymbol interference due to premodulation filtering. For exact values of S_k, refer to the signal space constellations (i.e., phase state diagrams) for the demodulators of interest in the preliminary report (Figures 4.2, 4.4, and 4.6).

For multivariable linear minimum MSE estimation, we assume that the values of the random sequence $X_1, \ldots, X_n$ are observed (e.g., where X_n are the outputs of n demodulators, consisting of the desired signal corrupted by channel impairments) and that the value of the desired signal S is to be estimated with a linear estimator of the form

$$\hat{S} = h_o + \sum_{i=1}^{n} h_i X_i \tag{6.3}$$

such that $E\{(S - \hat{S})^2\}$ is minimized by the choice of the weights h_i, $i = 1, \ldots, n$ (that is, the MSE is minimized by adapting some weight vector, which is represented here by h_i). To obtain the coefficients h_i, we differentiate $E\{(S - \hat{S})^2\}$ with respect to each h_j, $j = 0, 1, \ldots, n$, resulting in

$$\mathrm{E}\left[S - h_o - \sum_{i=1}^{n} h_i X_i\right] = 0, \qquad j = 0 \tag{6.4}$$

$$\mathrm{E}\left[\left(S - h_o - \sum_{i=1}^{n} h_i X_i\right) X_j\right] = 0, \qquad j = 1, \ldots, n \tag{6.5}$$

Eqn. 6.4 can be viewed as stating that the error is orthogonal to a constant, and Eqn. 6.5 can be visualized as stating that the error is orthogonal to each observation. These two equations are called the orthogonality conditions.

Eqn. 6.4 can be converted to

$$h_o = \mu_S - \sum_{i=1} n h_i \mu_{X_i} \tag{6.6}$$

where

$$\mu_S = \mathrm{E}[S]$$
$$\mu_{X_i} = \mathrm{E}[X_i]$$

and using this in the n equations represented by Eqn. 6.5 produces

$$\sum_{i=1}^{n} h_i C_{XX}(i,j) = \sigma_{SX(j)}, \qquad j = 1, 2, \ldots, n \tag{6.7}$$

where

$$\sigma_{SX(j)} = \mathrm{E}[(S - \mu_S)(X_j - \mu_{X_j})] \tag{6.8}$$

and

$$C_{XX}(i,j) = \mathrm{E}[(X_i - \mu_{X_i})(X_j - \mu_{X_j})] \tag{6.9}$$

Eqn. 6.6 and 6.7 can be shown to result in a minimum (not just a saddle point). The n equations of Eqn. 6.7 can be written in matrix form. Defining

$$\begin{aligned} \mathbf{X^T} &= [X_1, X_2, \ldots, X_n] \\ \mathbf{h^T} &= [h_1, h_2, \ldots, h_n] \\ \mathbf{\Sigma_{XX}} &= [C_{XX}(i,j)] \\ \mathbf{\Sigma_{SX}^T} &= [\sigma_{SX}(1), \sigma_{SX}(2), \ldots, \sigma_{SX}(n)] \end{aligned} \tag{6.10}$$

then Eqn. 6.7 can be written as

$$\mathbf{\Sigma_{XX}h} = \mathbf{\Sigma_{SX}} \tag{6.11}$$

If the covariance matrix $\mathbf{\Sigma_{XX}}$ has an inverse, the solution to Eqn. 6.7 is

$$\mathbf{h} = \mathbf{\Sigma_{XX}^{-1}\Sigma_{SX}} \tag{6.12}$$

If the variable S and X_n are zero-mean processes, then Eqn. 6.7 becomes

$$\sum_{i=1}^{n} h_i R_{XX}(i,j) = R_{SX}(j) \tag{6.13}$$

where $R_{XX}(i,j)$ is an autocorrelation function and $R_{SX}(j)$ is a cross-correlation function. If the $X(n)$ are assumed to be jointly stationary, then $R_{XX}(i,j) = R_{XX}(i-j)$, thus

$$\begin{bmatrix} R_{XX}(0) & R_{XX}(1) & R_{XX}(2) & \cdots & R_{XX}(n-1) \\ R_{XX}(1) & R_{XX}(0) & R_{XX}(1) & \cdots & R_{XX}(n-2) \\ R_{XX}(2) & R_{XX}(1) & R_{XX}(0) & \cdots & R_{XX}(n-3) \\ \vdots & \vdots & \vdots & \ddots & \vdots \\ R_{XX}(n-1) & R_{XX}(1) & R_{XX}(2) & \cdots & R_{XX}(0) \end{bmatrix} \begin{bmatrix} h_1 \\ h_2 \\ h_3 \\ \vdots \\ h_n \end{bmatrix} = \begin{bmatrix} R_{SX}(1) \\ R_{SX}(2) \\ R_{SX}(3) \\ \vdots \\ R_{SX}(n) \end{bmatrix} \tag{6.14}$$

The variable X_i can be the result of a nonlinear operation on the input S (e.g., $X_1 = \cos S$ or $X_2 = S^2$), while the estimator is still linear in the h_i's and thus is within the theory developed. This is particularly important in the evaluation of the bank of demodulators under consideration, since the demodulator output variables (e.g., X_i) will tend to be nonlinear functions of the desired signal S.

This theory can be applied to the bank of noncoherent demodulators forming a demodulator diversity scheme in Section 10.2.1. We can denote

X_1 = output of the 2 bit differential detector with decision feedback (DF)
X_2 = output of 1-bit, 2-bit, and 3-bit differential detector with DF
X_3 = output of limiter discriminator

Figure 10.3 provides a block diagram of this demodulator diversity scheme.

We weight each of the three outputs (or branches) of the demodulators and then coherently combine the weighted outputs. The estimator of S is then

$$\hat{S} = h_1 X_2 + h_2 X_2 + h_3 X_3 \tag{6.15}$$

Using Eqn. 6.7 through 6.11, the weight vector $\mathbf{h}$ minimizes the MSE as the solution to the relation

$$\begin{bmatrix} R_{XX}(0) & R_{XX}(1) & R_{XX}(2) \\ R_{XX}(1) & R_{XX}(0) & R_{XX}(1) \\ R_{XX}(2) & R_{XX}(1) & R_{XX}(0) \end{bmatrix} \begin{bmatrix} h_1 \\ h_2 \\ h_3 \end{bmatrix} \begin{bmatrix} R_{SX}(1) \\ R_{SX}(2) \\ R_{SX}(3) \end{bmatrix} \tag{6.16}$$

These expressions can be readily evaluated numerically for given data sequences of S and X_i. X_i are the decision statistics of each demodulator. S is the sum of the ideal outputs (i.e., ideal decision statistics) of each demodulator. Ideal analytic expressions for the outputs of a bank of demodulators are involved (because of the nonlinear operations such as differential detection and decision feedback are often employed). Analytical expressions for X_i which take in account AWGN and other channel impairments (typically encountered in wireless environments) are much more complex and difficult to obtain. Only the most basic cases are tractable, and that by means of simplifying assumptions.

Section 4.3 provides a general approach for deriving analytical expressions for the decision statistic of various type of differential demodulation, where the one-bit differential demodulator is used as an example. As another example, the output (i.e., decisions statistic) of the 2-bit differential demodulator (before hard decision) in AWGN can be expressed as [267]

$$X_1(kT) = \begin{cases} r(kT)r(kT-2T)\cos(\Delta V_k)\exp(2\hat{b}_{k-2}V_2) + n_2(kT), & \text{if } \hat{b}_{k-1} \neq \hat{b}_{k-2} \\ r(kT)r(kT-2T)\cos(\Delta V_k) + n_2(kT), & \text{if } \hat{b}_{k-1} = \hat{b}_{k-2} \end{cases} \tag{6.17}$$

where $\Delta V_k = b_{k+2}V_{-2} + b_{k+1}V_{-1} + b_kV_0 + b_{k-1}V_1 + b_{k-2}V_2 + b_{k-3}V_3$ with T the bit interval, b_k the original binary data, $r(t)$ the received signal, $n_2(kT)$ representing all the noise terms. V_k are values determined by the intersymbol interference inherent in GMSK and are $V_{-2} = V_3 = 0.2°$, $V_{-1} = V_2 = 16.2°$, and $V_0 = V_1 = 73.6°$ for $BT = 0.3$ (as in Global Speciale Mobile - GSM).

In practice, however, the dynamic nature of the wireless channel renders the tractable derivations of little practical value. Analytical *a priori* expressions based on simplistic channel models will rarely accurately model real wireless channels. Real-time estimation of the pdfs of decision statistics (of the demodulator outputs) is much more practical, since *a priori* assumptions about the channel are not needed. The *a posteriori* pdf estimators described in Section 7.4 allow estimation of the decision statistic pdfs and form the basis for *a posteriori* BER estimation, so that *a priori* approaches are not needed.

The 1-bit, 2-bit, 3-bit differential demodulator is a new structure, but a formula for its output decision statistic (a random variable) can be derived from expressions given in [267, 39]. An expression for the output of the limiter discriminator can be found in [124]. These expressions are primarily for the case of a signal corrupted by noise (AWGN). The reader is referred to Chapter 2 for other literature references which deal with other channel impairments.

Even more difficult is the derivation of closed form expressions for $C_{XX}(i,j)$ and $\sigma_{SX}(j)$. Calculations of the moments contained in these expressions are complex and involve probability density functions (pdfs), which (as stated above) can be very difficult, if not impossible, to derive, in the absence of very simplistic assumptions. Examples of histograms (which approximate the pdfs) of the demodulators of interest are given in Figures 5.1 - 5.3. In Section 4.3.3, an attempt is made to derive useful analytical expressions for X_i for the simple case of a one-bit differential demodulator.

Values for the weight vectors yielding MMSE can be determined numerically for each simulated channel impairment (see Table 5.1). One set of weights will be associated with each static channel environments (e.g., there will be one weight vector for each E_b/N_o, energy per bit to noise power spectral density ratio, and one weight vector for each C/I, carrier-to-interference ratio). Such analyses involve intense computational complexity and are consequently, not pursued in this research. Instead, we focus in Section 10.2.1 on MSE-based selection of demodulator outputs which tends to track the lower bit error rate (BER) of the individual demodulators as shown in Figures 10.4 through 10.7. In addition, in Sections 10.3 and 10.4, demodulator diversity schemes based on BER criterion are evaluated.

6.4 Summary

This chapter provides theoretical (and analytical) support for the concept of demodulator diversity, where one seeks to maximize the information extracted from several receivers in a changing channel to take advantage of the respective strengths. With demodulation diversity, at the very least, we would like a combined demodulator to have a BER which tracks the BER of the best demodulator for given channel impairment. Ideally, we would like receiver diversity to provide better overall performance than that attainable by any individual demodulator. Section 6.2 compares and contrasts demodulator diversity and spatial (or antenna) diversity (e.g., smart antennas) which helps to motivate this research. Section 6.3 derives the theoretical minimum mean squared error (MMSE) for a receiver diversity scheme in AWGN. The resulting MMSE expression is primarily of theoretical interest because of its complexity and necessarily simplified assumptions. These problems, inherent in the implementaton of ideal MMSE, motivate investigation of the use of pdf estimation techniques for exploiting demodulator diversity.

Chapter 7

Real-Time BER Estimation Theory

7.1 Motivation

In digital communications systems, transmitter, channel and receiver imperfections corrupt an ideal digital communications signal so that the digital information is corrupted. Bit error rate (BER) provides a fundamental measure of system performance in digital communications systems. For ideal assessment of system performance, it is desirable to estimate BER in real-time. If accurate BER estimation can be done in real-time, various techniques can be employed to combat the sources of bit errors and thus minimize the BER. This, of course, translates into benefits such as better quality of service (QOS), greater capacity, and/or less power requirements. This chapter outlines techniques for performing real-time BER estimation.

System providers need techniques to approximate real-time BER estimation, without having to resort to brute-force counting methods. Because of the dynamic, often unpredictable, nature of the wireless channel, *a priori* (deductive) techniques (e.g., where the channel is assumed **before** demodulation) are not very useful and are unreliable (as illustrated in Section 4.3.6). *A posteriori* (inductive) estimation techniques (e.g., where knowledge of signal impairments is acquired **after** the signal is demodulated) are preferable because they assume no prior knowledge of the channel.

Section 7.4 describes two *a posteriori* techniques which yield reliable BER estimates over relatively small observation intervals in various channel conditions – the Gram-Charlier series approximation for pdfs and Parzen's pdf estimator. The use of these pdf estimators for BER estimation is validated in Chapter 9. Parzen's estimator is very versatile and provides the basis for BER estimation in Chapters 8 and 10. Gram-Charlier pdf estimation is based on normalizing the data by the sample mean and standard deviation of the decision statistic. The performance of Gram-Charlier can be improved by substituting other robust estimators of location for the mean and other robust estimators of scale for the standard deviation, several of which are described in Section 7.5. The use of robust estimators in Gram-Charlier estimation constitutes another novel contribution of this work.

We initially assume a training sequence to obtain bit error estimates for the BER

estimators. If the training sequence can be circumvented, however, then data rates or capacity can be increased and system flexibility is improved. Blind estimation means that a training sequence is not required for the performance of BER estimation. Section 7.6 provides analytical justification for the use of blind Gaussian-based pdf estimation techniques, such as the Gram-Charlier series approximation for pdfs.

7.2 BER Measurement

BER can be measured by counting the number of errors that occur within a given sequence of bits. This method becomes impractical for small BERs of interest. For example, one would have to transmit a known training sequence of 10,000 bits and receive one error out of that known sequence to calculate a very crude BER=10^{-4} (and the variance of the estimator would still be quite high). BERs on the order of 10^{-6} or 10^{-7} require training sequences of 1,000,000 or 10,000,000 bits, respectively.

Measured BER based on one error is unreliable, since BER is a random variable with some probability density function (pdf). For more accurate BER estimates, the BER pdf should be taken into account. Even for known data, received communications signals are random processes (since the channel conditions are random), and thus, BER is a random variable. In a binary system, the decision statistic is that quantity (usually a sample) by which a decision is made at the receiver as to whether a +1 or a -1 (i.e., zero) was sent.

7.3 BER and the Decision Statistic PDF

A close relationship exists between BER and the decision statistic. BER, in fact, can be estimated from the pdf of the decision random variable, also denoted the decision statistic.

Consider a binary communications system, where the decision statistic is to interpret a +1 sent for positive samples and -1 sent for negative samples (such a system is unbiased, in that the optimum decision threshold is zero). The decision statistic samples will have a pdf comparable to that of the example given in Fig. 7.1. If a training sequence is available, the decision statistic samples corresponding to +1 transmitted bits have a pdf which can be isolated as shown in the example of Fig. 7.2.

In addition, if the pdf of the -1 transmitted symbol is symmetric with the pdf of the +1 transmitted samples (which is the case for antipodal signaling with additive zero-mean random processes like AWGN), the -1 samples can be included in the determination of the +1 pdf (i.e., the -1 samples are simply multiplied by -1 to change their sign). The BER of the positive symbol is then the area under the left tail of the pdf from $-\infty$ to 0 (the decision threshold). This area to the left of the threshold represents the percentage of bits that are in error (i.e., a +1 detected when a -1 was sent, or vice versa). This can also be interpreted as the cumulative distribution function (cdf) of the +1 decision

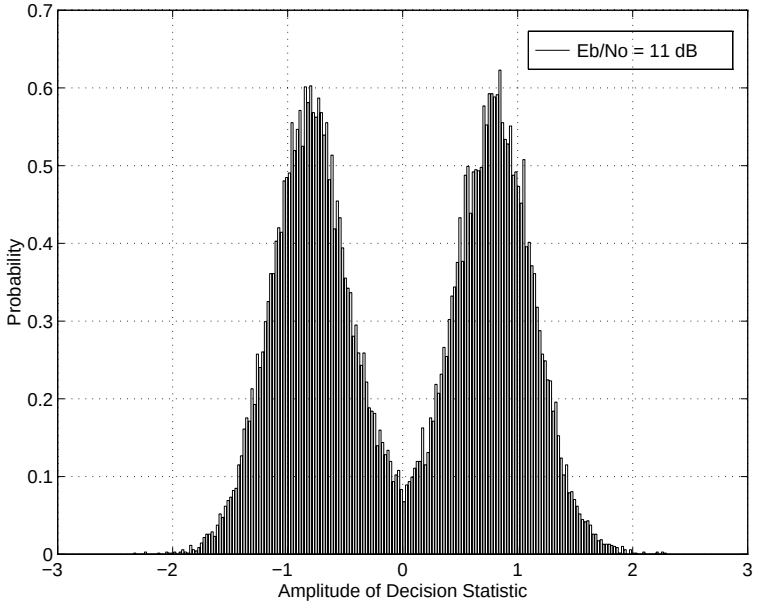

Figure 7.1: Histogram of one-bit differential demodulator output in AWGN (± 1 bits out of 10,000 random bits sent)

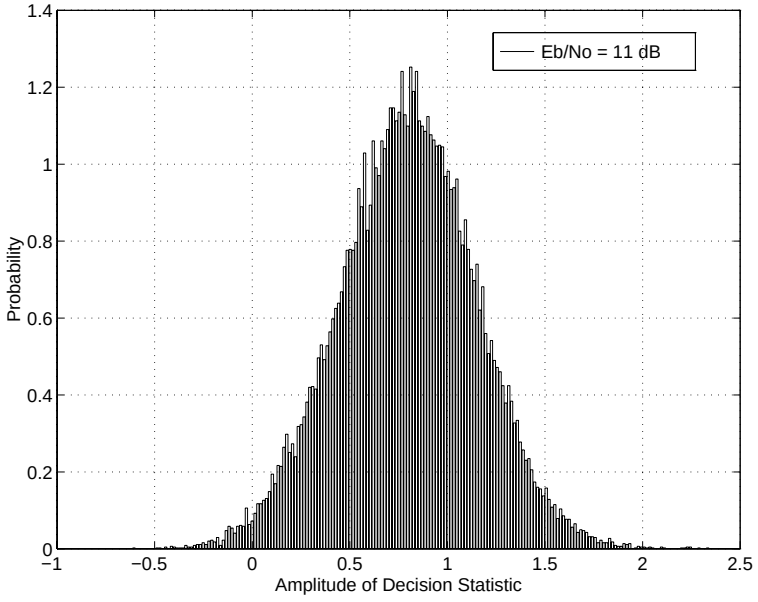

Figure 7.2: Histogram of one-bit differential demodulator $+1$ output in AWGN ($+1$ bits out of 10,000 random bits sent)

statistic evaluated at the threshold (e.g., 0). Throughout this dissertation, the BER pdf is found directly from the decision statistic pdf.

In typical wireless environments, however, the pdf of the decision statistic is very difficult (if not impossible) to determine analytically (refer to Section 4.3). Where channels are known to be static, BER will also assume some static function of the known channel impairments (e.g., a function of E_b/N_o in an additive white Gaussian noise channel). However, if the channel is dynamic (changing), BER is a dynamic function of the channel impairments. The problem of deriving theoretical expressions for the decision statistic and BER is exacerbated, not only by dynamic channel conditions, but also by nonlinearities which are often (if not always) present in real-world systems (which are being modeled). Noncoherent demodulation (or detection) is but one example of nonlinearity in a receiver.

Required knowledge of the BER pdf can be avoided if one assumes that a fixed number of errors yields an acceptable BER estimate. For many systems, about thirty errors is considered to yield a reliable estimate. For measured BER, however, this would require an observation interval (e.g., training sequence) of 30/BER bits (e.g., 30,000,000 bits for a BER of 10^{-6}). This is very impractical in most applications. The expense of resources (such as spectrum) prohibits the use of such resources for this "brute-force" method of BER estimation. In addition, the length of the required observation interval renders the estimate of little use because channel conditions, especially wireless environments, will likely change over that observation interval. In other words, the BER estimate for one observation interval will not necessarily be reliable for the bits surrounding the observation interval (where a training sequence is not used).

7.4 PDF Estimators

System providers need techniques to approximate real-time BER estimation, without having to resort to brute-force counting methods. *A priori* estimation means that knowledge of signal impairments is assumed **prior** the signal being sent. *A posteriori* estimation means that knowledge of signal impairments is acquired **after** the signal is sent (e.g., after demodulator processing). Because of the dynamic, often unpredictable, nature of the wireless channel, *a priori* techniques are not very useful and are unreliable. Some type of *a posteriori* BER estimation is needed. In course of this research, two *a posteriori* techniques have been found to yield reliable BER estimates over relatively small observation intervals in various channel conditions. The Gram-Charlier series approximation for pdfs and Parzen's pdf estimator [219] yield very good approximations to the decision statistic pdfs. These techniques perform pdf estimation of the decision random variable (i.e., statistic), from which BER can be estimated by integrating the pdf to the left of the threshold (i.e., evaluating the cdf at the threshold value).

7.4.1 Gram-Charlier Series Approximation

Nonlinear transformations of random variable often make it impossible to calculate the pdf of the random variable in closed form. However, it is easier to estimate the expected values (i.e., moments). Gram-Charlier is a method of approximating the unknown pdf $f_Y(y)$ of a random variable Y whose moments $\mathrm{E}[Y^k]$ are known. To simplify the algebra, we assume that $\mathrm{E}[Y] = 0$ and $\sigma_Y^2 = 1$.

The pdf can be expanded into a series using orthogonal basis functions. The Gram-Charlier series is a commonly used and mathematically tractable series approximation, which has the form [219]:

$$f_Y(y) = h(y) \sum_{j=0}^{\infty} C_j H_j(y) \tag{7.1}$$

where

$$h(y) = \frac{1}{\sqrt{2\pi}} \exp(-y^2/2) \tag{7.2}$$

and the basis functions of the expansion, $H_j(y)$, are the Tchebycheff-Hermite $(T-H)$ polynomials. These polynomials are formed by the kth derivative of $\exp(-y^2/2)$ such that

$$H_k(y) = \frac{[\exp(-x^2/2)]^{(k)}}{exp(-y^2/2)}(-1)^k \tag{7.3}$$

The first ten $T-H$ polynomials are

$$\begin{aligned}
H_0(y) &= 1 \\
H_1(y) &= y \\
H_2(y) &= y^2 - 1 \\
H_3(y) &= y^3 - 3y \\
H_4(y) &= y^4 - 6y^2 + 3 \\
H_5(y) &= y^5 - 10y^3 + 15y \\
H_6(y) &= y^6 - 15y^4 + 45y^2 - 15 \\
H_7(y) &= y^7 - 21y^5 + 105y^3 - 105y \\
H_8(y) &= y^8 - 28y^6 + 210y^4 - 420y^2 + 105 \\
H_9(y) &= y^9 - 36y^7 + 378y^5 - 1260y^3 + 945y \\
H_{10}(y) &= y^{10} - 45y^8 + 630y^6 - 3150y^4 + 4725y^2 - 945
\end{aligned} \tag{7.4}$$

and they have the following properties:

$$\begin{aligned}
&1. \quad H_k(y)h(y) = -\frac{d(H_{k-1}(y)h(y))}{dy}, \qquad k \geq 1 \\
&2. \quad H_k(y) - yH_{k-1}(y) + (k-1)H_{k-2}(y) = 0, \qquad k \geq 2 \\
&3. \quad \int_{-\infty}^{\infty} H_m(y)H_n(y)h(y)\,dy = 0, \qquad m \neq n \\
&\qquad \int_{-\infty}^{\infty} H_m(y)H_n(y)h(y)\,dy = n! \qquad m \neq n
\end{aligned} \tag{7.5}$$

The coefficients of series expansion are evaluated by multiplying both sides of Eqn. 7.1 by $H_k(y)$ and integrating from $-\infty$ to ∞. Because of the orthogonality property given in Eqn. 7.5, the coefficients can be expressed as

$$\begin{aligned} C_k &= \frac{1}{k!}\int_{-\infty}^{\infty} H_k(y) f_Y(y)\, dy \\ &= \frac{1}{k!}\left[\mu_k - \frac{k^{[2]}}{(2)1!}\mu_{k-2} + \frac{k^{[4]}}{2^2 2!}\mu_{k-4} - \cdots\right] \end{aligned} \tag{7.6}$$

where

$$\mu_m = \mathrm{E}[Y^m]$$

and

$$k^{[m]} = \frac{k!}{(k-m)!} = k(k-1)\cdots[k-(m-1)], \qquad k \geq m$$

The first ten coefficients follow directly from Eqn. 7.5 and 7.6 and are given as

$$\begin{aligned} C_0 &= 1 \\ C_1 &= \mu_1 \\ C_2 &= \frac{1}{2}(\mu_2 - 1) \\ C_3 &= \frac{1}{6}(\mu_3 - 3\mu_2) \\ C_4 &= \frac{1}{24}(\mu_4 - 6\mu_2 + 3) \\ C_5 &= \frac{1}{120}(\mu_5 - 10\mu_3 + 15\mu_1) \\ C_6 &= \frac{1}{720}(\mu_6 - 15\mu_4 + 45\mu_2 - 15) \\ C_7 &= \frac{1}{5040}(\mu_7 - 21\mu_5 + 105\mu_3 - 105\mu_1) \\ C_8 &= \frac{1}{40320}(\mu_8 - 28\mu_6 + 210\mu_4 - 420\mu_2 + 105) \\ C_9 &= \frac{1}{362880}(mu_9 - 36\mu_7 + 378\mu_5 - 1260\mu_3 + 945\mu_1) \\ C_{10} &= \frac{1}{3628800}(\mu_{10} - 45\mu_8 + 630\mu_6 - 3150\mu_4 + 4725\mu_2 - 945) \end{aligned} \tag{7.7}$$

Substituting Eqn. 7.6 into Eqn. 7.1, the series expansion for the pdf of a random variable is obtained in terms of the moments of the random variable and the $T-H$ polynomials. The Gram-Charlier series expansion for the pdf of a random variable X with mean μ'_X and variance σ_X^2 has the form:

$$f_X(x) = \frac{1}{\sqrt{2\pi}\sigma_X}\exp\left[-\frac{(x-\mu'_X)^2}{2\sigma_X^2}\right]\sum_{j=0}^{\infty} C_j H_j\left(\frac{x-\mu'_X}{\sigma_X}\right) \tag{7.8}$$

where the coefficients C_j are given by Eqn. 7.6 and

$$\mu_k = \mathrm{E}\left[\left(\frac{X - \mu'_k}{\sigma_X}\right)^k\right]. \tag{7.9}$$

Eqn. 7.8 is a series approximation to the pdf of a random variable X whose moments are known. If only the two moments are known or significant, the series reduces to

$$f_X(x) = \frac{1}{\sqrt{2\pi}\sigma_X} \exp[-(x - \mu'_X)^2/2\sigma_X^2] \tag{7.10}$$

which is the Gaussian pdf (e.g., normal distribution). As higher terms are added, the pdf will take a more proper shape.

The Gram-Charlier series approximation is useful only if it converges rapidly and the terms can be easily calculated. In wireless applications, the moment terms can be easily calculated with digital signal processing (DSP), making Gram-Charlier a feasible option. With Gram-Charlier estimation, however, rapid convergence only occurs when the underlying pdf is nearly Gaussian (e.g., when the random variable X is the sum of many independent components, such that Gaussianity is approached by the Central Limit Theorem). Nearly Gaussian means that the pdf generally has some bell shape (though possibly skewed); it excludes multi-modal distributions (e.g., pdfs characterized by multiple Gaussian distributions, sometimes termed Gaussian mixtures).

In addition, the Gram-Charlier series approximation is not a true pdf. Gram-Charlier results can have negative values in the tails of the distribution, whereas true pdfs always have positive values. To illustrate how Gram-Charlier results can have negative values, Figure 7.3 shows the tail of 10th order Gram-Charlier pdf approximation of the decision statistic of a coherent demodulator ($E_b/N_o = 5$ dB). Since BER estimation depends on the tails of the pdf estimate, a poor pdf tail estimate (e.g., negative values) will result in a poor BER estimate. This accounts for some of the poor performance of Gram-Charlier estimation when the decision statistic pdfs are not nearly Gaussian (such as in cases of multipath and CCI).

Despite its drawback, the Gram-Charlier series (it is shown later) yields excellent results in some wireless channel conditions and poor results in others, as demonstrated in Chapter 9. For example, BER estimation based on Gram-Charlier give very good results with a very short observation interval for the AWGN channel, including channels with multipath. In some cases, blind Gram-Charlier estimation can yield good results (that is, without the use of a training sequence). Gram-Charlier based estimation in co-channel interference (CCI), however, is poor, due primarily to the fact that CCI tends to cause the decision statistic pdf to look like a Gaussian mixture. Unfortunately, the Gram-Charlier series is not uniformly convergent; thus, adding more terms does not guarantee increased accuracy. Usually, however, four to six terms are enough for many applications.

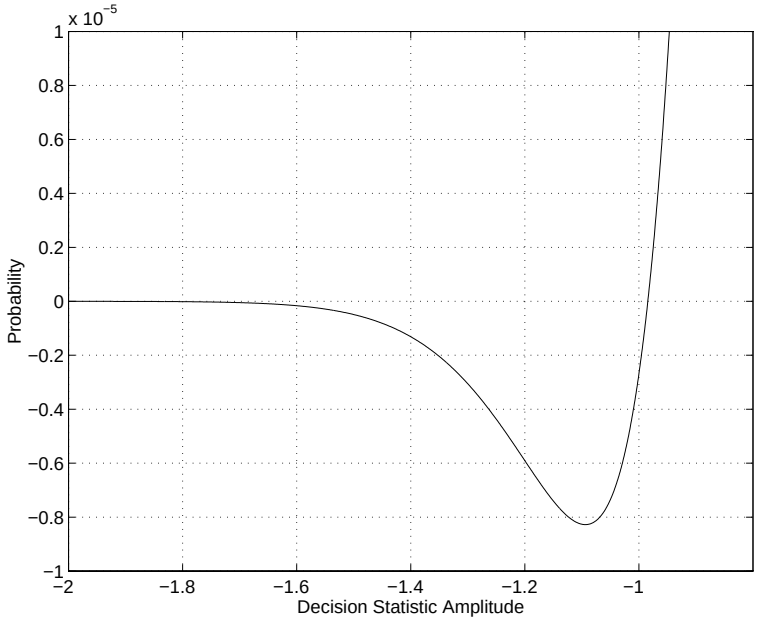

Figure 7.3: Negative values of a Gram-Charlier pdf estimate of coherent output in AWGN ($E_b/N_o = 5$ dB)

7.4.2 Parzen's Estimator

While Gram-Charlier yields only a series approximation, Parzen [186] provides a smoothed estimator of a pdf in analytical form as

$$\hat{f}_X(x) = \hat{f}_{X|X_1,\ldots,X_n}(x|x_1,\ldots,x_n) \triangleq \frac{1}{nh(n)} \sum_{i=1}^{n} g\left(\frac{x - x_i}{h(n)}\right) \tag{7.11}$$

In Eqn. 7.11, n is the sample size, $g(\cdot)$ is a weighting function, and $h(n)$ is a smoothing factor. In order for $\hat{f}_X(x)$ to be a valid pdf, $g(y)$ and $h(n)$ must satisfy

$$\begin{aligned} &h(n) > 0 \\ &g(y) \geq 0 \\ &\int_{-\infty}^{\infty} g(y)\, dy = 1 \end{aligned} \tag{7.12}$$

While the choice of $h(n)$ and $g(y)$ are somewhat arbitrary, they do influence the accuracy of the estimator. If additional constraints are added to those of Eqn. 7.12, namely

$$\begin{aligned} &|yg(y)| \longrightarrow 0, \qquad as \qquad |y| \longrightarrow \infty \\ &\int_{-\infty}^{\infty} y^2 g^2(y)\, dy < \infty \end{aligned} \tag{7.13}$$

then the bias and variance of Parzen's estimator in Eqn. 7.11 are [186]

$$\begin{aligned}\text{Bias}[\hat{f}_X(x)] &= -f_X''(x)\frac{h^2(n)}{2}\int_{-\infty}^{\infty} y^2 g^2(y)\,dy \\ \text{Variance}[\hat{f}_X(x)] &= \frac{f_X(x)}{nh(n)}\int_{-\infty}^{\infty} g^2(y)\,dy\end{aligned} \tag{7.14}$$

for large values of n, where $f_X(x)$ is the true pdf. If $h(n)$ is chosen such that

$$\begin{aligned}h(n) &\longrightarrow 0, \qquad \text{as} \qquad n \longrightarrow \infty \\ nh(n) &\longrightarrow \infty, \qquad \text{as} \qquad n \longrightarrow \infty\end{aligned} \tag{7.15}$$

then the estimator is asymptotically unbiased and the variance of the estimator approaches zero [186].

Reasonable choices for the weighting function and smoothing factor are

$$\begin{aligned}g(y) &= \frac{1}{\sqrt{2\pi}}\exp\left(\frac{-y^2}{2}\right) \\ h(n) &= \frac{1}{\sqrt{n}}\end{aligned} \tag{7.16}$$

which are used throughout this research.

7.5 Gram-Charlier and Robust Estimators

Gram-Charlier is based on normalizing the data by its mean and standard deviation (as one would normalize data with a Gaussian pdf). The expected moments of the normalized data are then calculated to determine the coefficients of the series approximation. The *sample mean* can be thought of as an estimator of location (i.e., it give some indication of the location of the pdf of the data). The mean can also be viewed as the center of gravity of the pdf. The *sample standard deviation* can be thought of as an estimator of scale (i.e., it give some indication of the scale of the pdf of the data). For the standard deviation, the scale is the root of the variance for zero-mean processes.

7.5.1 Robust Estimation

As estimators of location and scale, the mean and standard deviation tend not to be robust. Robust estimation is a field of study which proposes robust alternative estimators of location and scale. Robust, in this context, refers to the characteristic that the estimator is resistant to spurious data points (e.g., outliers - data points which fall outside the main body of data). Robust estimators yield consistent estimates even when the number of outliers increase. A good introduction to robust estimation is given by Rousseeuw [208].

Robust Estimators of Location

The median can be viewed as the center of probability of the pdf.

$$\int_{-\infty}^{\text{med}} f(z)\,dz = \int_{\text{med}}^{\infty} f(z)\,dz = \frac{1}{2} \tag{7.17}$$

Although many robust estimators of location exist, the *sample median* is the most widely known. If $\{x_1, \ldots, x_n\}$ is a batch of number, its sample median is denoted by

$$\text{med}_i x_i \tag{7.18}$$

which is simply the middle order statistic when n is odd. Order statistics consist of the data ordered by amplitude. When n is even, we use the average of the order statistics with ranks $(n/2)$ and $(n/2)+1$. The median has a breakdown point of 50% (which is the highest possible), because the estimate remains bounded when fewer than 50% of the data points are replaced by arbitrary numbers.

The mode is the most probable point of the pdf; it is the value that maximizes the pdf $f(z)$ (i.e., the mode corresponds to the peak value of the pdf). Robust estimators of location include estimators of the mode, such as the *shorth* and *midshort*. Estimators of the mode are based on the *shortest half*. A *half* is a subsample containing ν successive ordered data points

$$\text{half}_i = x_{\nu+i-1} - x_i \tag{7.19}$$

where $\nu = \lfloor \frac{m}{2} \rfloor + 1$ and m is the number of data points.[1] The shortest half is the half having the shortest length. The midshort is the midpoint of the shortest half. The mean of the shortest half is known as the *shorth*. Both the midshort and shorth are robust estimators of the mode (i.e., they are estimators of location).

Robust Estimators of Scale

Robust estimation of scale has gained somewhat less acceptance among general users of statistical methods [209]. The only robust scale estimator to be found in most statistical packages is the *interquartile range*, which has a breakdown point of 25% (that is, up to 25% of the data can be outliers or spurious before the estimator breaks down or becomes unreliable). Some people erroneously consider the *average deviation*

$$\text{ave}_i |x_i - \text{ave}_j x_j| \tag{7.20}$$

(where ave stands for "average") to be a robust estimator, although its breakdown point is 0. If one of the averages in Eqn. 7.20 is replaced by the median, we obtain the "median deviation about the average" and the "average deviation about the median," both of which suffer from a breakdown point of 0 as well.

A very robust scale estimator is the *median absolute deviation about the median* (MAD), given by

$$\text{MAD}_n = b\,\text{med}_i |x_i - \text{med}_j x_j|. \tag{7.21}$$

[1] $\lfloor \cdot \rfloor$ is the floor function, which rounds the result toward zero to nearest integer

The MAD has the best possible breakdown point of 50%. The constant b in Eqn. 7.21 is needed to make the estimator consistent for the parameter of interest. To be consistent with the usual parameter σ (standard deviation) at Gaussian distributions, we need to set $b = 1.4826$.

The sample median and the MAD are simple and easy to compute, and also very useful. Their extreme sturdiness makes them ideal for screening the data for outliers in a quick way, by computing

$$\frac{|x_i - \text{med}_j x_j|}{\text{MAD}_n} \tag{7.22}$$

for each x_i and flagging those x_i as spurious for which this statistic exceeds a certain cutoff (say, 2.5 or 3.0).

In spite of its advantages, the MAD also has some drawbacks. For example, the MAD takes a symmetric view on dispersion, because one first estimates a central value (the median) and then attaches equal importance to positive and negative deviations from it. The MAD corresponds to finding the symmetric interval (around the median) that contains 50% of the data (or 50% of the probability), which does not seem to be a natural approach for asymmetric distributions. Though the MAD can be used with highly skewed distributions, it may be inefficient and artificial to do so.

In wireless channels, particularly with nonlinear operations on the signal (e.g., at the receiver), the distributions tend often to be asymmetric. We need estimators of scale which are more suited to asymmetric distributions.

Rousseeuw and Croux [209] propose alternatives to the MAD which are more efficient and applicable to asymmetric distributions. The scale estimator S_n is superior to MAD and is defined as

$$S_n = c\,\text{med}_i\{\text{med}_j|x_i - x_j|\} \tag{7.23}$$

and should be read as follows. For each i we compute the median of $\{|x_i - x_j|; j = 1, \ldots, n\}$. The yields n numbers, the median of which gives our final estimate S_n. The factor c is again for consistency, with a default value of 1.1926. Unfortunately, S_n is computationally intensive, so we do not consider it useful for real-time BER estimation.

Another robust scale estimator which is efficient and applicable to asymmetric distributions is a version of the shortest half h_s [159]

$$h_s = b\,\frac{\min_i\{\text{half}_i\}}{2} \tag{7.24}$$

where $b = 1.4826$ makes the estimator consistent at Gaussian distributions.

7.5.2 Robust Estimators Used in Gram-Charlier

Robust estimators (such as the median and the MAD) are often used as initial values for the computation of more efficient robust estimators. It was confirmed by simulation [16] that it is very important to have robust starting values for the computation of more efficient robust estimators. Simply starting from the mean (average) and standard deviation is often inadequate. This beneficent characteristic of robust estimators motivates

the substitution of robust estimators of location and scale for the mean and standard deviation used in Gram-Charlier series approximations for pdfs (defined in Section 7.4.1 and illustrated in Sections 9.2 and 9.3 and in Appendix A.1.1).

7.6 Blind BER Estimation

Previous simulations made use of training sequence to isolate the decisions in error (which have crossed the threshold). If the training sequence can be neglected, then data rates or capacity can be increased and system flexibility improved. Instead of multiplying the data by a training sequence (to form a one-sided +1 pdf), a straight-forward blind technique simply takes the absolute value of all the data. Those bits in error (which have crossed the decision threshold) will cause the estimate to degrade, but, as we shall see in some cases, the degradation is often minor. Here, we first derive the pdf resulting from the transformation of the data to absolute data. We show that, under certain conditions, the transformed pdf can be used to obtain BER estimates with an accuracy approaching the BER estimation of the original pdf.

7.6.1 PDF Derivation of $y = |x|$

In this section, a formula is derived to determine the pdf of the absolute value of a random variable given the pdf of the random variable. Let x be a random variable (RV) and $y = |x|$ be the transformed RV. For a function of one random variable, a fundamental theorem [185] states that to find $f_y(y)$ for a specific y, we solve the equation $y = g(x)$. Denoting its real roots by x_n,

$$y = g(x_1) = \cdots = g(x_n) = \cdots \tag{7.25}$$

the resulting pdf is

$$f_y(y) = \frac{f_x(x_1)}{|g'(x_1)|} + \cdots + \frac{f_x(x_n)}{|g'(x_n)|} + \cdots \tag{7.26}$$

where $g'(x)$ is the derivative of $g(x)$. A generalized form of this theorem is given in Eqn. 4.41.

In the case under consideration, $|x| = y$ has two solutions $x = \pm y$ for $y > 0$ and no real solution for $y < 0$, and $g'(x)$ is given by

$$g'(x) = \begin{cases} +1 & x > 0 \\ -1 & x < 0 \end{cases} \tag{7.27}$$

The resulting pdf $f_y(y)$ is

$$f_y(y) = f_x(y) + f_x(-y) \tag{7.28}$$

Because the pdf $f_y(y)$ has two terms, the law of superposition (based on linearity) allows the expected value of y to be derived in part. The expected value of y is

$$\begin{aligned} \mathrm{E}[y] &= \mathrm{E}[y_1] + \mathrm{E}[y_2] \\ &= \int_0^\infty y f_x(y)\, dy + \int_0^\infty y f_x(-y)\, dy \end{aligned} \tag{7.29}$$

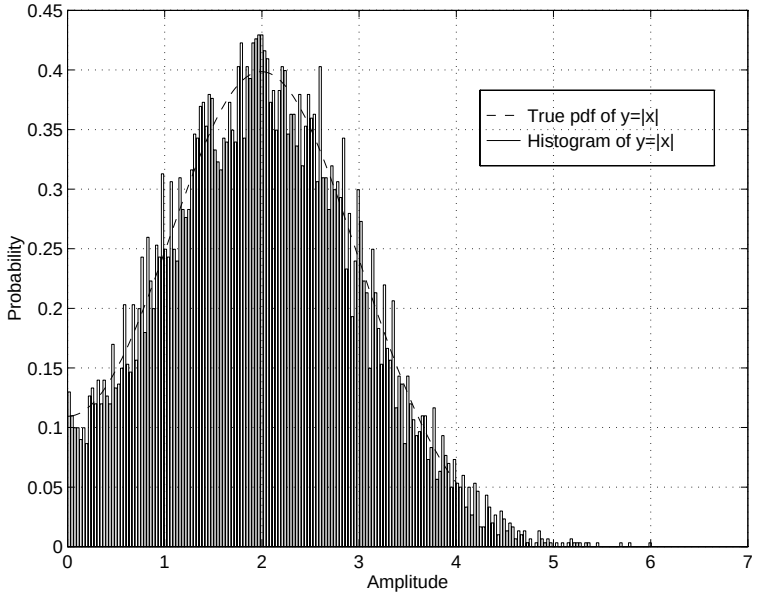

Figure 7.4: Analytic pdf and histogram of the random variable $y = |x|$, where x=N[2,1]

where y_1 is the RV y corresponding to the first term of the pdf $f_y(y)$ and y_2 is the RV y corresponding to the second term of the pdf $f_y(y)$.

If $f_x(x)$ is Gaussian,

$$f_x(x) = \frac{1}{\sqrt{2\pi}\sigma_x} \exp\left(\frac{-(x-\mu_x)^2}{2\sigma_x^2}\right) \tag{7.30}$$

then, using Eqns. 7.27 and 7.28, Eqn. 7.26 becomes

$$f_y(y) = \begin{cases} \frac{1}{\sqrt{2\pi}\sigma_x} \exp\left(\frac{-(y-\mu_x)^2}{2\sigma_x^2}\right) + \frac{1}{\sqrt{2\pi}\sigma_x} \exp\left(\frac{-(-y-\mu_x)^2}{2\sigma_x^2}\right) & y \geq 0 \\ 0 & y < 0 \end{cases} \tag{7.31}$$

In Fig. 7.4, the analytic pdf of Eqn. 7.31 is plotted against a histogram of the simulated random variable $y = |x|$ (where x is Gaussian with $\mu_x = 2$ and $\sigma_x^2 = 1$). This plot supports Eqn. 7.31 as the correct pdf for $y = |x|$.

7.6.2 Analytical Mean of $y = |x|$ for Gaussian x

The expected value (or first moment) of the Gaussian pdf $f_x(x)$ is μ_x (also denoted E[x]). The expected value (first moment) of y_1 (E[y_1]) using the first term of $f_y(y)$ is

$$\mathrm{E}[y_1] = \int_0^\infty \frac{1}{\sqrt{2\pi}\sigma_x} y \exp\left(\frac{-(y-\mu_x)^2}{2\sigma_x^2}\right)$$

$$
\begin{aligned}
&= \frac{\sigma_x^2}{\sqrt{2\pi}\sigma_x}\left[\int_0^\infty \frac{y-\mu_x}{\sigma_x^2}\exp\left(\frac{-(y-\mu_x)^2}{2\sigma_x^2}\right)dy + \int_0^\infty \frac{\mu_x}{\sigma_x^2}\exp\left(\frac{-(y-\mu_x)^2}{2\sigma_x^2}\right)dy\right] \\
&= \frac{\sigma_x}{\sqrt{2\pi}}\left[\exp\left(\frac{-\mu_x^2}{2\sigma_x^2}\right) + \int_{\mu_x}^\infty \frac{\mu_x}{\sigma_x^2}\exp\left(\frac{-t^2}{2\sigma_x^2}\right)dt\right] \\
&= \frac{\sigma_x}{\sqrt{2\pi}}\left[\exp\left(\frac{-\mu_x^2}{2\sigma_x^2}\right) + \frac{\mu_x}{2\sigma_x^2}\sqrt{2\pi\sigma_x^2}\,\mathrm{erfc}\left(\frac{\mu_x}{\sqrt{2\sigma_x^2}}\right)\right] \\
&= \frac{\sigma_x}{\sqrt{2\pi}}\exp\left(\frac{-\mu_x^2}{2\sigma_x^2}\right) - \frac{\mu_x}{2\sigma_x}\sqrt{2\pi\sigma_x^2}\mathrm{erfc}\left(\frac{\mu_x}{\sqrt{2\sigma_x^2}}\right) \\
&= \frac{\sigma_x}{\sqrt{2\pi}}\exp\left(\frac{-\mu_x^2}{2\sigma_x^2}\right) - \frac{\mu_x}{2}\,\mathrm{erfc}\left(\frac{\mu_x}{\sqrt{2}\sigma_x}\right) \qquad (7.32)
\end{aligned}
$$

where $\mathrm{erfc}(\cdot)$ is the complementary error function defined as

$$\mathrm{erfc}(y) \triangleq \int_y^\infty \exp(-z^2)\,dz \qquad (7.33)$$

where $\mathrm{erfc}(y) \to 2$ as $y \to -\infty$ and $\mathrm{erfc}(y) \to 0$ as $y \to \infty$.

The second term of $f_y(y)$ can similarly be written as

$$
\begin{aligned}
\mathrm{E}[y_2] &= \int_0^\infty \frac{1}{\sqrt{2\pi}\sigma_x} y \exp\left(\frac{-(y+\mu_x)^2}{2\sigma_x^2}\right) \\
&= \frac{\sigma_x}{\sqrt{2\pi}}\exp\left(\frac{-\mu_x^2}{2\sigma_x^2}\right) + \frac{\mu_x}{2}\mathrm{erfc}\left(\frac{-\mu_x}{\sqrt{2}\sigma_x}\right) \qquad (7.34)
\end{aligned}
$$

Combining the two expectations, we arrive at the expected value of y

$$
\begin{aligned}
\mathrm{E}[y] &= \mathrm{E}[y_1] + \mathrm{E}[y_2] \\
&= \frac{2\sigma_x}{\sqrt{2\pi}}\exp\left(-\frac{\mu_x^2}{2\sigma_x^2}\right) - \frac{\mu_x}{2}\,\mathrm{erfc}\left(\frac{\mu_x}{\sqrt{2}\sigma_x}\right) + \frac{\mu_x}{2}\,\mathrm{erfc}\left(\frac{-\mu_x}{\sqrt{2}\sigma_x}\right) \qquad (7.35)
\end{aligned}
$$

Rearranging Eqn. 7.35,

$$\mathrm{E}[y] = \mu_x\left[\frac{\sigma_x}{\mu_x}\sqrt{\frac{2}{\pi}}\exp\left(-\frac{1}{2}\left(\frac{\mu_x}{\sigma_x}\right)^2\right) - \frac{1}{2}\,\mathrm{erfc}\left(\frac{1}{\sqrt{2}}\frac{\mu_x}{\sigma_x}\right) + \frac{1}{2}\,\mathrm{erfc}\left(-\frac{1}{\sqrt{2}}\frac{\mu_x}{\sigma_x}\right)\right] \qquad (7.36)$$

As μ_x/σ_x becomes large (e.g., $\mu_x/\sigma_x > 1$), the first and second terms (within the brackets) go to zero, and the third term goes to one, resulting in $\mathrm{E}[y]$ approximating μ_x ($\mathrm{E}[y]$ can also be denoted μ_y). That is,

$$\mathrm{E}[y] = \mu_y \to \mu_x \qquad \text{for } \frac{\mu_x}{\sigma_x} > 1 \qquad (7.37)$$

The convergence of the bracketed terms ($\mathrm{E}[y]/\mu_x = \mu_y/\mu_x$), to one is shown in Fig. 7.5 where μ_y/μ_x is plotted against μ_x/σ_x.

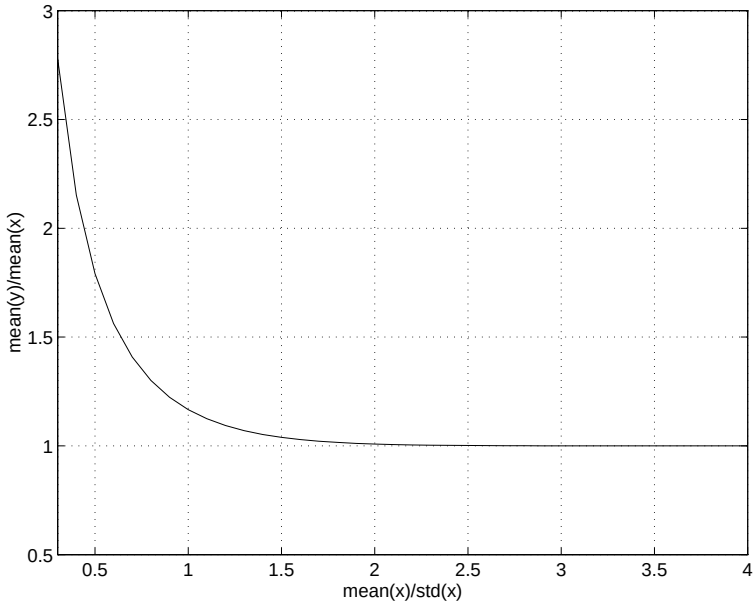

Figure 7.5: Convergence of μ_y to μ_x, μ_y/μ_x versus μ_x/σ_x

7.6.3 Analytical Variance of $y = |x|$ for Gaussian x

The variance of y, σ_y^2, can be derived in similar fashion, using

$$\sigma_y^2 = \mathrm{E}\left[y^2\right] - \left(\mathrm{E}\left[y\right]\right)^2 \tag{7.38}$$

where the second moment of y is denoted $\mathrm{E}\left[y^2\right]$. Because the pdf $f_y(y)$ has two terms, the law of superposition allows the second moment of y (expected value of y^2) to be derived in parts. The expected value of y^2 is

$$\begin{aligned} \mathrm{E}\left[y^2\right] &= \mathrm{E}\left[y_1^2\right] + \mathrm{E}\left[y_2^2\right] \\ &= \int_0^\infty y^2 f_x(y)\, dy + \int_0^\infty y^2 f_x(-y)\, dy \end{aligned} \tag{7.39}$$

The second moment of the Gaussian random variable y using the first term of $f_y(y)$ is

$$\mathrm{E}\left[y_1^2\right] = \int_0^\infty \frac{1}{\sqrt{2\pi}\sigma_x} y^2 \exp\left(-\frac{(y-\mu_x)^2}{2\sigma_x^2}\right) dy \tag{7.40}$$

which, with a change of variables becomes

$$\begin{aligned} \mathrm{E}\left[y_1^2\right] &= \frac{\sigma_x^2}{\sqrt{2\pi}\sigma_x} \int_{-\mu_x}^\infty \left(t^2 + 2t\mu_x + \mu_x^2\right) \exp\left(-\frac{t^2}{2\sigma_x^2}\right) dt \\ &= \frac{\sigma_x \mu_x}{\sqrt{2\pi}} \exp\left(\frac{-\mu_x^2}{2\sigma_x^2}\right) + \left(\frac{\sigma_x^2}{2} + \frac{\mu_x^2}{2}\right) \mathrm{erfc}\left(-\frac{\mu_x}{\sqrt{2\sigma_x^2}}\right) \end{aligned} \tag{7.41}$$

The second term of E$[y^2]$ can similarly be written as

$$\begin{aligned} \mathrm{E}\left[y_2^2\right] &= \int_0^\infty \frac{1}{\sqrt{2\pi}\sigma_x} y^2 \exp\left(-\frac{(y+\mu_x)^2}{2\sigma_x^2}\right) dy \\ &= -\frac{\sigma_x \mu_x}{\sqrt{2\pi}} \exp\left(\frac{-\mu_x^2}{2\sigma_x^2}\right) + \left(\frac{\sigma_x^2}{2} + \frac{\mu_x^2}{2}\right) \mathrm{erfc}\left(\frac{\mu_x}{\sqrt{2\sigma_x^2}}\right) \end{aligned} \tag{7.42}$$

Combining the two expections, we arrive at the second moment of y

$$\begin{aligned} \mathrm{E}\left[y^2\right] &= \mathrm{E}\left[y_1^2\right] + \mathrm{E}\left[y_2^2\right] \\ &= \left(\frac{\sigma_x^2}{2} + \frac{\mu_x^2}{2}\right) \left[\mathrm{erfc}\left(\frac{1}{\sqrt{2}}\frac{\mu_x}{\sigma_x}\right) + \mathrm{erfc}\left(-\frac{1}{\sqrt{2}}\frac{\mu_x}{\sigma_x}\right)\right] \end{aligned} \tag{7.43}$$

Rearranging Eqn. 7.43,

$$\mathrm{E}\left[y^2\right] = \sigma_x^2 \left[\left(\frac{1}{2} + \frac{1}{2}\frac{\mu_x^2}{\sigma_x^2}\right) \mathrm{erfc}\left(\frac{1}{\sqrt{2}}\frac{\mu_x}{\sigma_x}\right) + \left(\frac{1}{2} + \frac{1}{2}\frac{\mu_x^2}{\sigma_x^2}\right) \mathrm{erfc}\left(-\frac{1}{\sqrt{2}}\frac{\mu_x}{\sigma_x}\right)\right] \tag{7.44}$$

As μ_x/σ_x becomes large (e.g., $\mu_x/\sigma_x > 1$), the first term (within the brackets) goes to zero, and the second term goes to $1 + \mu_x^2/\sigma_x^2$, so that the second moment of y approaches the second moment of x. That is,

$$\mathrm{E}\left[y^2\right] \to \sigma_x^2 + \mu_x^2 = \mathrm{E}\left[x^2\right] \qquad \text{for } \frac{\mu_x}{\sigma_x} > 1 \tag{7.45}$$

From Eqn. 7.37, $\mu_y \approx \mu_x$ for large μ_x/σ_x. The variance of y also then approaches the variance of x for $\mu_x > \sigma_x$

$$\sigma_y^2 \to \mathrm{E}\left[x^2\right] - \mu_y^2 \approx \mathrm{E}\left[x^2\right] - \mu_x^2 = \sigma_x^2 \qquad \text{for } \frac{\mu_x}{\sigma_x} > 1 \tag{7.46}$$

The variance of y also approaches the variance of x for large μ_x/σ_x. The convergence of σ_y^2/σ_x^2 to one is shown in Fig. 7.6 where σ_y^2/σ_x^2 is plotted against μ_x/σ_x.

This result provides additional analytical justification for the use of blind Gaussian-based pdf estimation techniques, such as the Gram-Charlier series approximation for pdfs. For nearly Gaussian distributions, taking the absolute value of the random variable transforms the pdf such that methods like Gram-Charlier can still yield good pdf estimates, provided that the standard deviation of the original data σ_x is less than the mean of the data μ_x. This is an important result because it justifies not relying on a training sequence to obtain a good BER estimate.

7.7 Summary

Real-time BER estimation also constitutes one of the major contributions of this dissertation. If accurate BER estimation can be done in real-time, various techniques can

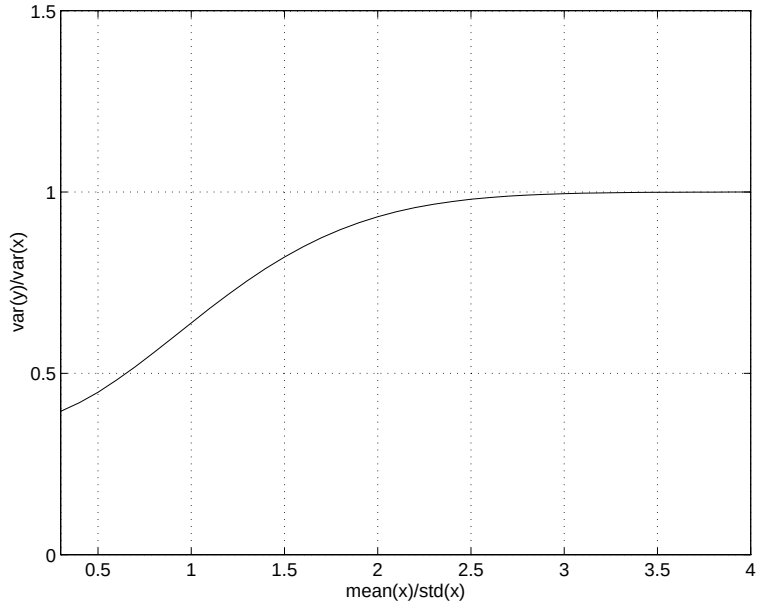

Figure 7.6: Convergence of σ_y^2 to σ_x^2, σ_y^2/σ_x^2 versus μ_x/σ_x

be employed to combat the sources of bit errors and thus minimize the BER. This, of course, translates into benefits such as better quality of service (QOS), greater capacity, more revenue, and/or less power requirements. This chapter introduces the concept of real-time BER estimation based on estimators of the probability density function of a random variable (e.g., the decision statistic).

Chapter 7 provides a theoretical description two pdf estimators – 1) the Gram-Charlier series approximation for pdfs and 2) Parzen's pdf estimator. Section 7.5 describes the use of robust estimators of location and scale to improve the performance of Gram-Charlier estimation, resulting in another novel contribution of this work. Section 7.6 provides analytical justification for the use of blind Gaussian-based pdf estimation techniques (blind meaning without the use of training sequences). Blind estimation constitutes a significant contribution of this research, because it allows bits normally reserved for training to be used for other purposes which can increase quality of service or capacity.

Chapter 8

BER Estimation Applied to Adaptive Filtering

8.1 Motivation

In this chapter, we apply the real-time BER estimation techniques of Chapter 7 to adaptive filtering (as discussed in Section 3.2.2). We take adaptive filtering in a general sense and consider it to be synonymous with adaptive signal processing. There are many potential applications of BER estimation to adaptive signal processing, some of which are outlined in Section 12.2 on areas for future work. Here, we focus on demodulator diversity and briefly generalize demodulator diversity to incorporate equalization. Demodulator diversity and real-time BER estimation constitute two of the major contributions of this dissertation, and this chapter combines the two concepts. This research makes fundamental contributions to the communications field by defining and validating these ideas.

Chapter 8 is organized in the following way. Section 8.2 analyzes the use of BER estimators in demodulator diversity schemes (introduced in Chapter 6). In a simple demodulator diversity scheme, the adaptation operates on a weight vector for combined demodulator outputs. In Section 8.3, Parzen's estimator is used in an example of a BER-based demodulator diversity technique, where analytical expressions for the cost function and the gradient of Parzen's estimator are derived. The chapter concludes with an extension of BER estimation to equalization and to the combination of equalization with demodulator diversity.

8.2 BER Estimators and Demodulator Diversity

Either Gram-Charlier or Parzen's can be used to estimate the pdf of the decision statistic in a conventional receiver. Let x denote the decision statistic. Given the decision rule as an analytic expression for a received symbol, that analytic expression can be used into the Gram-Charlier or Parzen estimator to derive an equation for the pdf estimate of the

decision statistic. Theoretical expressions for the decision statistic x (e.g., the output of the differential demodulator) given in Section 4.3 can be inserted into the general wireless channel model.

As discussed in Section 7.3, given an estimate of the pdf of a decision statistic (and assuming a training sequence), the area under the +1 pdf to the left of the decision threshold is an estimate of the BER for the positive symbols (and, assuming symmetry, also for the negative symbols). This use of pdf estimation to estimate BER can be applied to a host of demodulators. For example, in Sections 9.3.1 and 9.3.2, the two pdf estimators (Gram-Charlier and Parzen's) have been applied to a conventional one-bit differential demodulator, and the performance results are plotted.

8.3 Parzen's Estimator and Demodulator Diversity

In this section, we focus on theoretical derivation of the Parzen's pdf estimator as it applies to receiver diversity. Section 8.3.1 discusses the expected value of Parzen's estimator as used in these simulation. The demodulator diversity scheme is described in Section 8.3.2. Sections 8.3.3 and 8.3.4 develop additional algorithms for BER minimization by providing derivations of the cost function and gradient, used by gradient-based methods for unconstrained optimization. Though Parzen's estimator generally requires a longer training sequence, we focus on it because it is more robust in and more widely applicable to wireless channel conditions, than is Gram-Charlier estimation, especially for interference environments.

8.3.1 Expected Value of Parzen's PDF Estimator

Using the weighting function and smoothing factor of Eqn. 7.16, Parzen's pdf estimator becomes

$$\hat{f}_x(x) = \frac{1}{\sqrt{2\pi n}} \sum_{i=1}^{n} \exp\left(-\frac{n(x-x_i)^2}{2}\right) \tag{8.1}$$

where n is the number of samples and x_i represents the individual samples.

The expected value of the Parzen estimator $\hat{f}_x(x)$ is the bias of Eqn. 7.14. For large sample sizes, the estimator is asymptotically unbiased; that is, the expected value of the estimator approaches the true value $f_x(x)$ [186],

$$\mathrm{E}\left[\hat{f}_x(x)\right] = \mathrm{E}\left[\frac{1}{\sqrt{2\pi n}} \sum_{i=1}^{n} \exp\left(-\frac{n(x-x_i)^2}{2}\right)\right] \rightarrow f_x(x), \qquad \text{for large } n \tag{8.2}$$

Eqn. 8.2 is the expected value (or bias) of Parzen's estimator using the weighting function and smoothing factor of Eqn. 7.16.

8.3.2 Demodulator Diversity Scheme

A generalized block diagram of a BER-based demodulator diversity scheme is given in Fig. 8.1. For a demodulator diversity scheme with K weighted demodulator decision

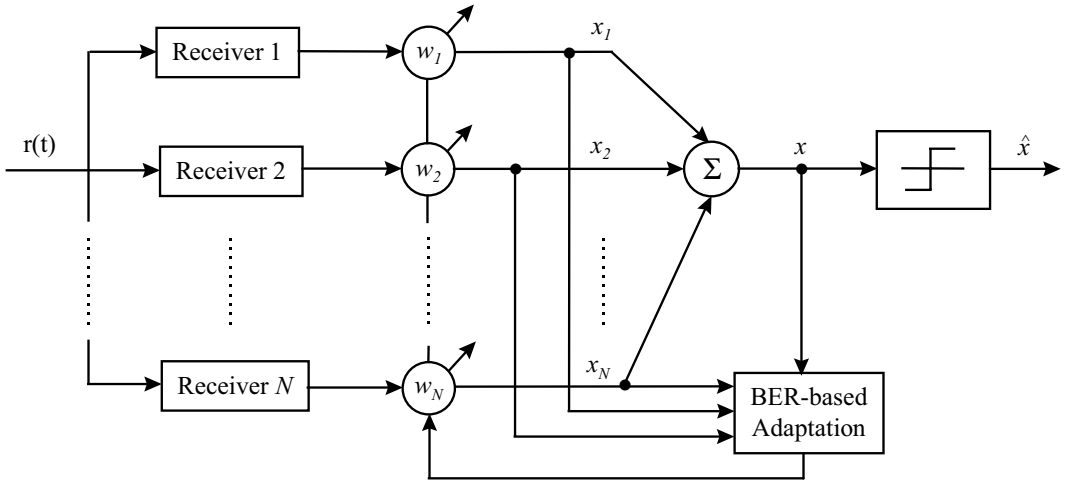

Figure 8.1: Generalized block diagram of a BER-based demodulator diversity scheme

statistics, the combination (of the weighted decision statistics) x_i is

$$x_i = \sum_{k=1}^{K} w_k x_{ki} \tag{8.3}$$

where w_k are the weights and x_{ki} are the ith sampled decision statistics multiplied by the original data (known by the training sequence). For a demodulator diversity scheme of two weighted demodulator outputs (which is the example used in subsequent simulations), the combined weighted output x_i is

$$\begin{aligned} x_i &= \text{real}\,(w_1 x_{1i} + w_2 x_{2i}) \\ x_i &= \frac{1}{2}\left((w_1 x_{1i} + w_2 x_{2i}) + (w_1 x_{1i} + w_2 x_{2i})^*\right) \\ x_i &= \frac{1}{2}\left(w_1 x_{1i} + w_2 x_{2i} + w_1^* x_{1i}^* + w_2^* x_{2i}^*\right) \end{aligned} \tag{8.4}$$

where * denotes complex conjugation. The decision statistics can be real or complex. The weights, as well, can be real or complex. Because in many communication systems of interest, the decision statistics are real, we will focus on the case of real decision statistics and real weights.

8.3.3 Cost Function of Parzen BER Estimator

Assuming a large enough sample size such that the Parzen BER estimator is effectively unbiased, the expected value of the BER estimate is then

$$\text{E[BER]} = \text{BER}$$

$$
\begin{aligned}
&= \int_{-\infty}^{0} \hat{f}_x(x)\, dx \\
&= \frac{1}{\sqrt{2\pi n}} \sum_{i=1}^{n} \left[\int_{-\infty}^{0} \exp\left(-\frac{n}{2}(x - x_i)^2 \right) dx \right] \\
&= \frac{1}{\sqrt{2\pi n}} \frac{1}{\sqrt{n}} \sum_{i=1}^{n} \left[\int_{-\infty}^{-x_i\sqrt{n}} \exp\left(-\tau^2/2 \right) d\tau \right] \\
&= \frac{1}{n} \sum_{i=1}^{n} \left[\frac{1}{\sqrt{2\pi}} \int_{-\infty}^{-x_i\sqrt{n}} \exp\left(-\tau^2/2 \right) d\tau \right] \\
&= \frac{1}{n} \sum_{i=1}^{n} Q(x_i\sqrt{n}) \qquad (8.5)
\end{aligned}
$$

where Q(t) is the Q-function defined in Eqn. 2.6 and x_i is a function of w_k as given in Eqn. 8.3 and Eqn. 8.4. Eqn. 8.5 is the cost function that defines the error performance surface which we would like to minimize. The weights w_k that minimize Eqn. 8.5 minimize the expected BER for the combined output.

8.3.4 Gradient of Parzen BER Estimator

In this section, the gradient is derived for the Parzen BER estimator used in these simulations. An analytic expression for the gradient allows the use of gradient-based algorithms (such as the Method of Steepest Descent) to more efficiently perform the adaptive signal processing. Assuming a large enough sample size to ensure that the estimator is effectively unbiased, the elements of the gradient vector of the error performance surface (i.e., of the expected value of the BER with respect to the weights) are given by

$$
\begin{aligned}
\nabla_k \mathrm{E[BER]} &= \frac{\partial}{\partial w_k} \mathrm{E[BER]} = \frac{\partial}{\partial w_k} \mathrm{BER} \\
\nabla_k \mathrm{E[BER]} &= \frac{\partial}{\partial w_k} \frac{1}{n} \sum_{i=1}^{n} Q(x_i\sqrt{n}) \qquad (8.6)
\end{aligned}
$$

such that the gradient vector consists of

$$
\begin{aligned}
\nabla \mathrm{E[BER]} &= \left[\frac{\partial}{\partial w_1} \mathrm{E[BER]} \quad \cdots \quad \frac{\partial}{\partial w_k} \mathrm{E[BER]} \right] \\
&= \left[\frac{\partial}{\partial w_1} \frac{1}{n} \sum_{i=1}^{n} Q(x_i\sqrt{n}) \quad \cdots \quad \frac{\partial}{\partial w_k} \frac{1}{n} \sum_{i=1}^{n} Q(x_i\sqrt{n}) \right] \qquad (8.7)
\end{aligned}
$$

where Q(t) is the Q-function defined in Eqn. 2.6 and x_i is a function of w_k as given in Eqn. 8.3 and Eqn. 8.4. The gradient vector is *normal* to the error performance surface.

In [93], expressions are given for partial complex derivatives in terms of real derivatives. The chain rule of changes of variables must be obeyed. Letting $w_k = a_k + jb_k$, the

complex partial derivative can be expressed as

$$\frac{\partial}{\partial w_k} = \frac{1}{2}\left(\frac{\partial}{\partial a_k} - j\frac{\partial}{\partial b_k}\right) \tag{8.8}$$

with

$$\frac{\partial w_k}{\partial w_k^*} = \frac{\partial w_k^*}{\partial w_k} = 0 \qquad \frac{\partial w_k}{\partial w_k} = 1 \tag{8.9}$$

In the example used in our derivation, we encounter the derivative of the expression real($w_k x_{ki}$). The partial derivative of real($w_k x_{ki}$) with respect to w_k is different depending on the whether w_k is real or complex. In particular,

$$\begin{aligned} \frac{\partial \text{real}(w_k x_{ki})}{\partial w_k} &= \frac{1}{2}x_{ki}, & \text{for } w_k \text{ complex} \\ \frac{\partial \text{real}(w_k x_{ki})}{\partial w_k} &= \text{real}(x_{ki}), & \text{for } w_k \text{ real} \end{aligned} \tag{8.10}$$

Exchanging the linear operations of differentiation and integration, we obtain

$$\nabla_k \,\text{E[BER]} = \frac{1}{\sqrt{2\pi n}} \sum_{i=1}^{n} \text{real}(x_{ki}) \exp\left(-\frac{n}{2}x_i^2\right) \quad \text{for } w_k \text{ real} \tag{8.11}$$

$$\nabla_k \,\text{E[BER]} = \frac{1}{2\sqrt{2\pi n}} \sum_{i=1}^{n} x_{ki} \exp\left(-\frac{n}{2}x_i^2\right) \quad \text{for } w_k \text{ complex} \tag{8.12}$$

Eqn. 8.11 (with real weights) is used in the BER-based receiver diversity simulations of Sections 10.3 and 10.4.

Eqn. 8.7 is the gradient of the cost function to be minimized. The gradient vector will be zero at minima of the cost function (i.e., weights w_k that minimize Eqn. 8.5 produce a zero gradient). The gradient vector can be used in a recursive fashion according to Method of Steepest Descent to find minima of the cost function. Unfortunately, the error surface of the cost function in Eqn. 8.5 does not always have one minimum (i.e., it can have local minima), as shown in Section 10.4.1. We desire to find the global minimum in order to attain to the lowest BER. This can be achieved by carefully choosing the initial conditions of some optimization technique related to the Method of Steepest Descent.

In Sections 10.3 and 10.4, the weights are not updated every symbol, but a batch of symbol data (corresponding to the length of the training sequence) is processed to provided the Parzen-based BER estimate. That BER estimate is then used to update the weights. In other words, the weights are not continuously updated with each new symbol, but are updated at the end of each training sequence. Algorithms can be derived to update the Parzen-based weights continuously, but this is area for further research.

8.3.5 Gradient Methods for Unconstrained Optimization

The method of steepest descent is a well-known technique in optimization [93]. The method is gradient-based and is recursive in the sense that starting from initial (arbitrary) values for the weight vector, it tends to improve as the increased number of

interations increases. Let $\nabla \mathrm{E}[\mathrm{BER}(n)]$ denote the gradient vector at time n. Let $\mathbf{w}(n)$ denote the value of the weight vector at time n. According to the method of steepest descent, the updated value of the weight vector at time $n+1$ is computed by using the simple recursive relation

$$\mathbf{w}(n+1) = \mathbf{w}(n) + \mu\left[-\nabla \mathrm{E}[\mathrm{BER}(n)]\right] \tag{8.13}$$

where μ is a positive real-valued constant.

The method of steepest descent is very inefficient when the function minimized has long narrow valleys, but it is very simple to implement. Other methods which use gradient information are the quasi-Newton methods utilizing Hessian updating methods (using a line search, quadratic interpolation, or cubic interpolation) [257].

8.4 BER Estimators and Equalization

BER estimation can also be extended to equalization and then further generalized to a demodulator diversity scheme with equalization. Equalization based on BER rather than MSE of greater interest, because digital systems are ultimately concerned about BER. Unfortunately, minimizing MSE does not always correspond to minimizing BER (e.g., when certain nonlinearities are present before equalization). This section extends BER-based adaptive signal processing to equalization and to the general case of adaptation operating on a weight matrix, such as might be done in the case of demodulator diversity combined with equalization. Using Eqn. 8.1, the only parameter which is changed is the expression for the decision statistic x_i.

In the case of coherent demodulation, adaptive equalization is added to mitigate ISI caused by factors such channel multipath and filtering (i.e., premodulation and predetection). Effective equalization usually requires linearity in the receiver, so the channel impairment remains linear after the demodulation process. In addition, conventional adaptive equalization is usually based on a MSE criterion, which does not guarantee a minimum BER. Nonlinearities tend to reduce the usefulness of MMSE approaches to adaptive equalization (e.g., receiver nonlinearities, such as differential demodulation or detection, diminish the effectiveness of equalization since linear equalization cannot perfectly remove nonlinear distortion). With the BER estimation techniques discussed in this chapter, it is expected that effective adaptive equalization can possibly be performed even if nonlinearities are present, because the adaptation criterion is no longer MSE-based but is now BER-based (this prediction has yet to be validated). Consequently, these BER estimation techniques allow equalization after noncoherent demodulation or detection (such as with the limiter discriminator or differential demodulator).

For equalization for an individual demodulator, x_i is a sum of weighted taps of a tapped delay line (or transversal filter), where the weighted are adapted by a BER-based estimation technique (such as Parzen's in the case under consideration). Then, x_i is

$$x_i = \sum_{l=1}^{L} w_l x_{li} \tag{8.14}$$

where w_l form a weight vector of length L (indexed by lower case l) and x_{li} are the ith sampled decision statistics multiplied by the original data (i.e., a training sequence) with L taps on the delay line (indexed by lower case l). As in the simple demodulator diversity scheme, x_i is a scalar and x_{li} is a vector of same length L as the weight vector.

For a demodulator diversity scheme with equalization, the decision statistic x_i is still a scalar (as in the simple demodulator diversity scheme), but the weights w_k form a matrix instead of a vector and x_{ki} is a matrix instead of a vector. Denote the matrices as $w_{k,l}$ and $x_{ki,l}$, where lower case k is the index for K demodulators and lower case l is the index for L equalization taps, then

$$x_i = \sum_{l=1}^{L} \sum_{k=1}^{K} w_{k,l} x_{ki,l} \tag{8.15}$$

where $w_{k,l}$ are the weights of a (K x L) matrix and $x_{ki,l}$ are the ith sampled decision statistics of a (K x L) matrix multiplied by the original data (i.e., a training sequence). The Parzen cost functions and gradients (found throughout Section 8.3) remain unchanged, other than the substitution for x_i.

8.5 Summary

This chapter applies the real-time BER estimation techniques of Chapter 7 to adaptive filtering (i.e., adaptive signal processing). Here, we focus on combining the concepts of demodulator diversity and real-time BER estimation, which constitute two of the major contributions of this dissertation. This research makes seminal contributions to the communications field by defining and validating these ideas.

Section 8.2 analyzes the use of BER estimators in demodulator diversity schemes (introduced in Chapter 6), where the adaptation operates on a weight vector for combined demodulator outputs. Section 8.2 derives analytical expressions for the cost function and the gradient of Parzen's estimator, which is used as an example. These techniques are inexpensive and can be easily implemented at the mobile with the use of a Q-function look-up table. The chapter concludes with an extension of BER estimation to equalization and to the combination of equalization with demodulator diversity.

Chapter 9

Validation of BER Estimation by Simulation

9.1 Motivation

In this chapter, we validate via simulations the BER estimation techniques analyzed in Chapters 7 and 8. Simulations are important because most of the receiver decision statistics are exceedingly difficult to analyze theoretically in channel environments of interest. Simulations also provide a stepping stone between theory and real-world implementation. This chapter justifies the concept of real-time BER estimation, which has tremendous ramifications for communications in general and for wireless communications in particular.

Chapter 9 documents results of non-blind and blind BER estimation using the Gram-Charlier series approximation for pdfs and using Parzen's pdf estimator. The performances of Gram-Charlier BER estimation and Parzen BER estimation are compared to measured BER. Blind techniques do not require a training sequence.

A simple one-bit differential demodulator (DD1) is used in these simulations, where the channel is modeled as AWGN (noise-limited) and CCI (interference-limited) with and without a 100 Hz carrier offset and also where the wireless channel is modeled as urban multipath (generated by SMRCIM [241]) with AWGN and CCI.

Gram-Charlier performs well in AWGN and requires a very short training sequence. Parzen estimation performs well also in AWGN, but requires a longer training sequence. Gram-Charlier estimation does not perform well in CCI, whereas Parzen estimation yields good results. Blind simulation results indicate that blind Parzen estimation performs poorly (i.e., Parzen's requires a training sequence), whereas blind Gram-Charlier yields reliable estimates in AWGN.

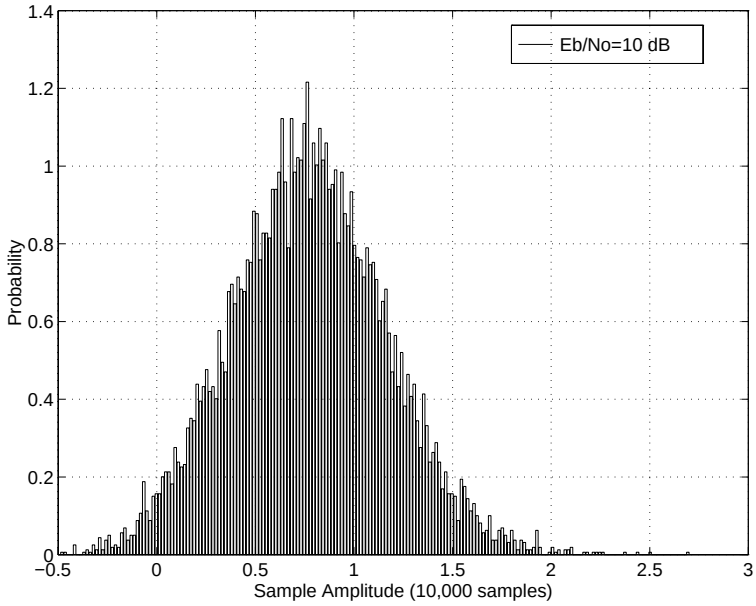

Figure 9.1: Histogram of a DD1 decision statistic x in AWGN ($E_b/N_o = 10$ dB)

9.2 Non-Blind BER Estimation in AWGN and CCI

This section provides examples of non-blind Gram-Charlier and Parzen BER estimation in AWGN and CCI using a one-bit differential demodulator (DD1). Here, a training sequence is used, where it is assumed that the channel does not change appreciably between observation intervals (i.e., between training sequences). The received symbols have been multiplied by a training sequence yielding positive symbol histograms (approximating the pdfs). For reference, Fig. 9.1 shows a histogram of DD1 output in AWGN where $E_b/N_o = 10$ dB and Fig. 9.2 shows a histogram of DD1 output in CCI where C/I=7 dB (with AWGN $E_b/N_o = 20$ dB added). These figures provide an indication of how AWGN and CCI affect the pdf of a simple differential demodulator.

9.2.1 Non-Blind Gram-Charlier in AWGN

The results in this section (and subsequent sections) follow from simulations where the received symbols have been multiplied by a training sequence yielding positive symbols (with the exception of errors which cross the decision threshold). Gram-Charlier pdf estimation is performed on the resulting decision statistic (random variable) over some observation interval (equal to the length of the training sequence; indicated on the abscissa label). One hundred trials are conducted where, in each trial, 30,000 bits are simulated with a sample frequency $f_s = 19$ samples/bit. For the measured results, the BER is taken as out of 30,000 bits, so that a BER=10^{-3} corresponds to thirty errors (BER=$10^{-3} = 30/30,000$). The visible data points ('x' for measured results and 'o'

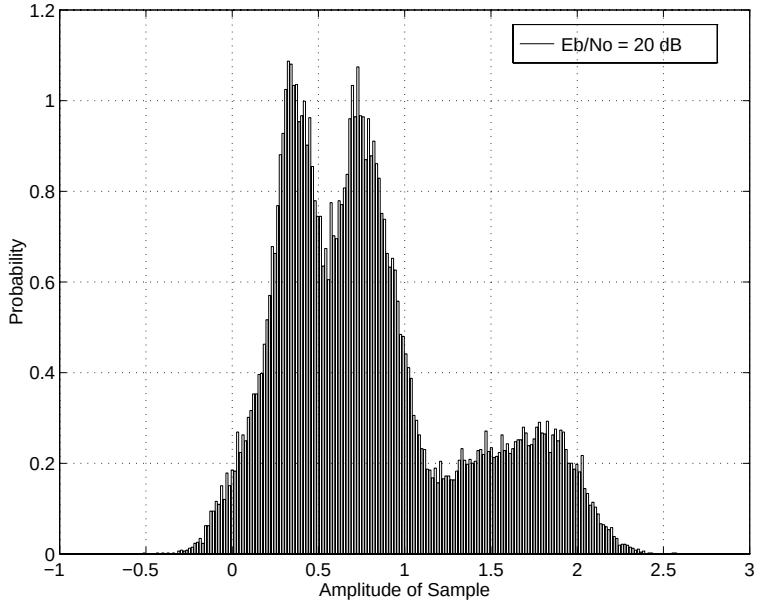

Figure 9.2: Histogram of a DD1 decision statistic x in CCI ($C/I = 7$ dB)

for Gram-Charlier results) are plotted. The spread in the plots represents ± 1 standard deviation (std) from the mean of the results.

Fig. 9.3 illustrates that 7th-order Gram-Charlier, denoted GC-7, provides a very good estimate of measured BER in AWGN with as few as 1000 symbols, compared to measurements based on 30,000 symbols. Note that the width (2 std) of the BER estimation spans only 0.5 dB. In this case, the robust h_s of Eqn. 7.24 is used as an estimator of scale along with the mean as the estimator of location, and these are indicated in the parentheses in the caption (the sample mean and standard deviation are used unless indicated otherwise). Other combinations of robust estimators of location and scale (discussed in Section 7.5) also perform well in Gram-Charlier BER estimation in AWGN.

9.2.2 Non-Blind Parzen in AWGN

The results in this section (and subsequent sections) follow from simulations where the received symbols have been multiplied by a training sequence yielding positive symbols (with the exception of errors which cross the decision threshold). Parzen pdf estimation is performed on the resulting decision statistic (random variable) over some observation interval (equal to the length of the training sequence; indicated on the abscissa label). One hundred trials are conducted where, in each trial, 30,000 bits are simulated with a sample frequency $f_s = 19$ samples/bit. For the measured results, the BER is taken

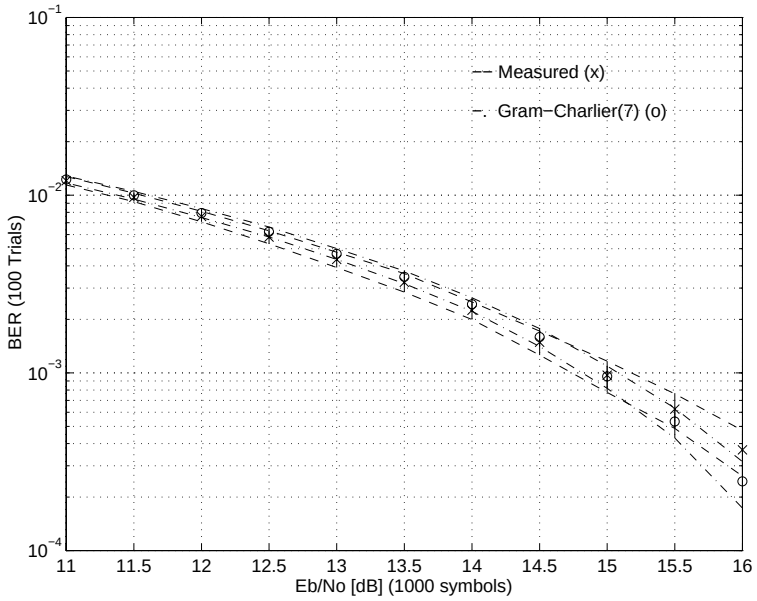

Figure 9.3: Measured and GC-7 BER (mean ± 1 std) vs. E_b/N_o in AWGN (using mean and h_s)

as out of 30,000 bits, so that a BER=10^{-3} corresponds to thirty errors (BER=$10^{-3} = 30/30,000$). The visible data points ('x' for measured results and 'o' for Parzen results) represent the mean for measured and Parzen results, respectively. The spread in the plots represents ± 1 standard deviation from the mean of the results. Fig. 9.4 illustrates that Parzen-based BER estimation yields good results with as few as 1050 symbols.

In Fig. 9.5, Parzen BER is plotted versus the number of symbols for the Parzen's estimate. Parzen pdf estimation is performed on the positive decision statistic for the observation interval (i.e., training sequence or sample size length) indicated on the abscissa. The Parzen estimate is compared to measured results, taken from 30,000 bits, where, at $E_b/N_o = 11$ dB, measured BER is about 1% (10^{-2}), representing about 300 errors. One hundred trials are conducted where, in each trial, 30,000 bits are simulated with a sample frequency $f_s = 19$ samples/bit. The visible data points ('x' for measured results and 'o' for Parzen results) represent the mean for measured and Parzen results, respectively. The spread in the plots represents ± 1 standard deviation from the mean of the results and is indicated by the vertical lines. Fig. 9.5 demonstrates that Parzen-based BER estimation provides a very good estimate with a sample size on the order of a few hundred symbols (i.e., the Parzen estimate converges quickly to the measured results as a function of sample size).

In Fig. 9.6, Parzen BER is plotted versus the number of symbols for the Parzen's estimate and compared to measured results, where, for $E_b/N_o = 15$ dB, measured BER is about 0.1% (10^{-3}), representing about 30 errors. As shown in Fig. 9.6, Parzen's

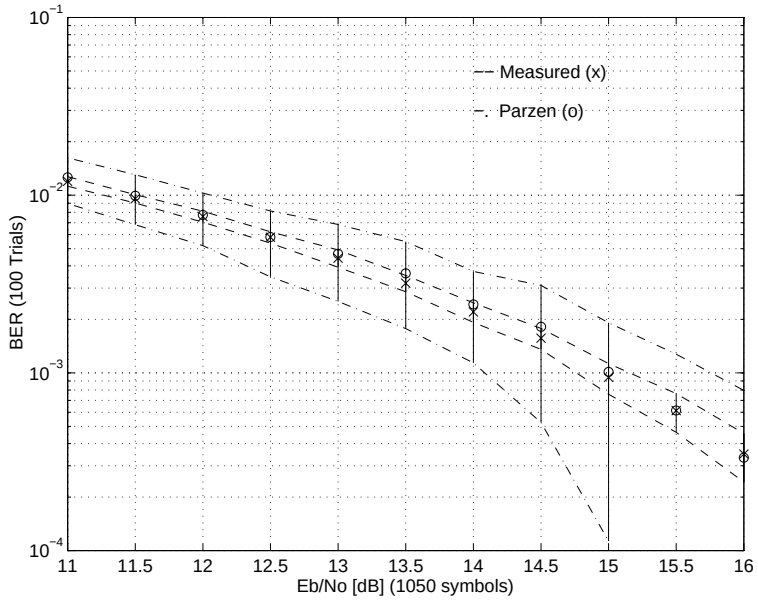

Figure 9.4: Measured and Parzen BER (mean ± 1 std) vs. E_b/N_o in AWGN

again provides a very good estimate with a sample size on the order of a few thousand symbols. Note that the width (2 std) of the BER estimation spans about 1.5 dB. The difference between Fig. 9.5 and Fig. 9.6 can be attributed to the number of errors used to estimate the BER.

9.2.3 Non-Blind Gram-Charlier in CCI

Fig. 9.7 illustrates the poor performance of Gram-Charlier estimation in CCI. This stems from pdf of the DD1 output decision statistic tending to be multi-modal (or looking like a Gaussian mixture) as shown by the DD1 histogram in CCI in Fig. 9.2. The Gram-Charlier series approximation for pdfs does not model this type of density very well.

9.2.4 Non-Blind Parzen in CCI

Fig. 9.8 illustrates that Parzen-based BER estimation yields good results in CCI with a 100 Hz carrier offset with as few as 1050 symbols. In Fig. 9.9, measured and Parzen BER are plotted versus the number of symbols for the Parzen's estimate (measured BER is about 0.2% at $C/I = 11.5$ dB; representing about 60 errors). Parzen's provides a very good estimate with a sample size on the order of a few hundred symbols.

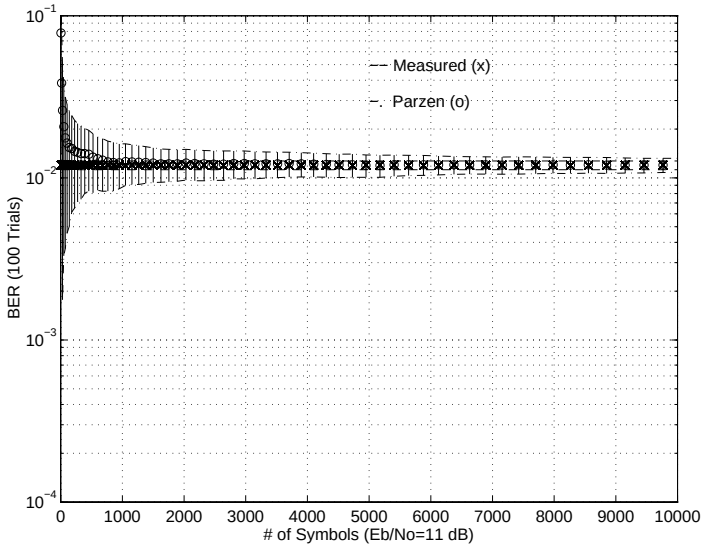

Figure 9.5: Measured and Parzen BER (mean ± 1 std) vs. # of Symbols $E_b/N_o = 11$ dB

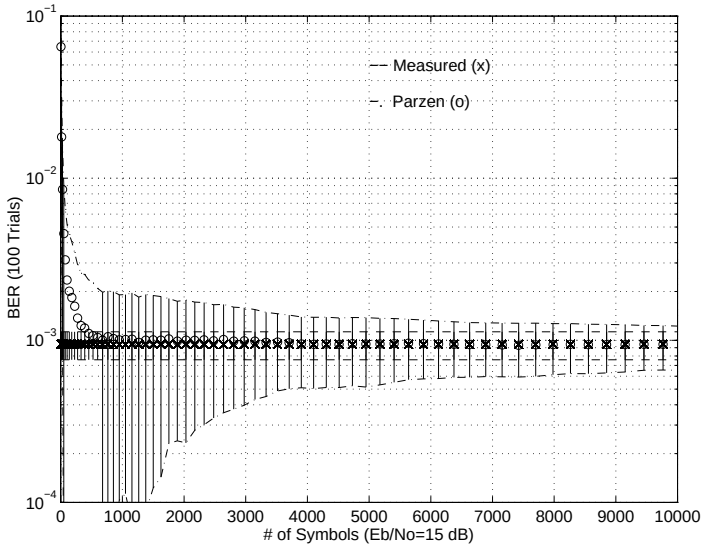

Figure 9.6: Measured and Parzen BER (mean ± 1 std) vs. # of Symbols $E_b/N_o = 15$ dB

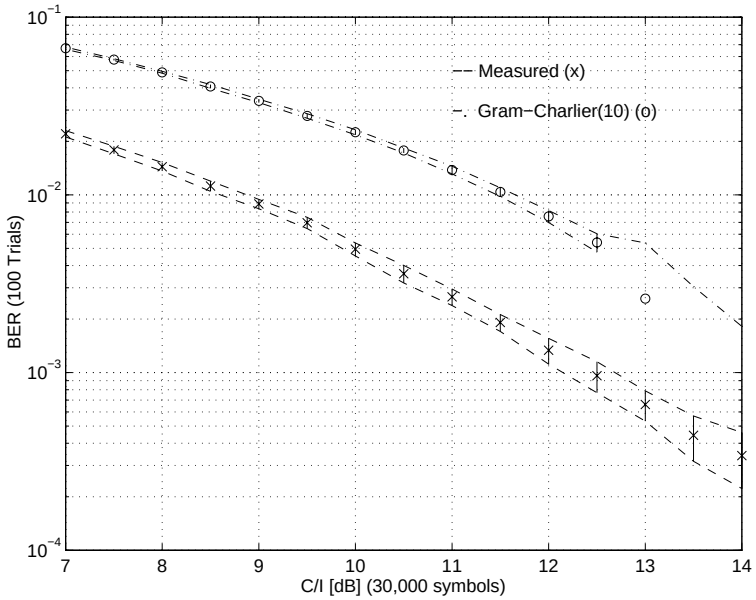

Figure 9.7: Measured and GC-10 BER (mean ± 1 std) vs. C/I in CCI (1 interferer)

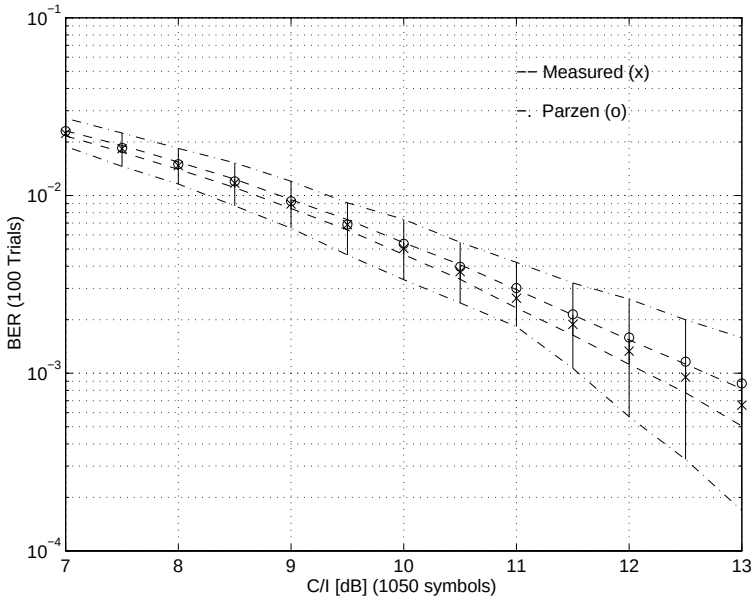

Figure 9.8: Measured and Parzen BER (mean ± 1 std) vs. C/I in CCI (1 interferer)

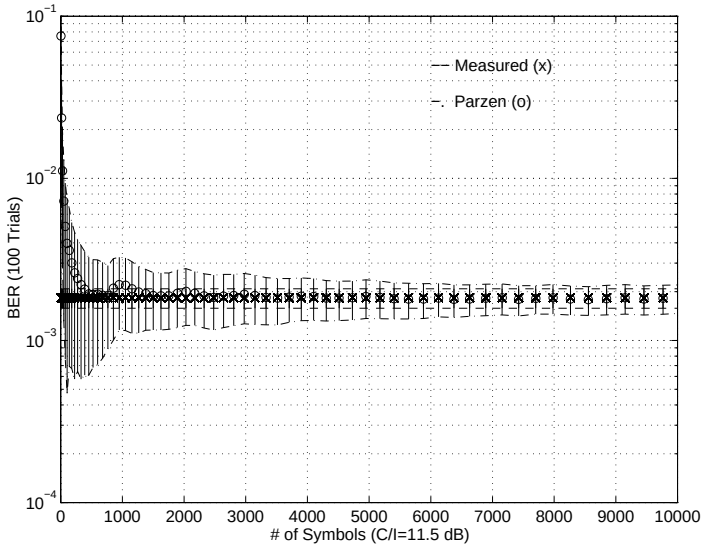

Figure 9.9: Measured and Parzen BER (mean ± 1 std) vs. # of Symbols $C/I = 11.5$ dB

9.2.5 Non-Blind Parzen in CCI (100 Hz Carrier Offset)

Fig. 9.10 illustrates that Parzen-based BER estimation yields good results in CCI with a 100 Hz carrier offset with as few as 1050 symbols. In Fig. 9.11, measured and Parzen BER are plotted versus the number of symbols for the Parzen's estimate (measured BER is about 0.1% at $C/I = 12.5$ dB; representing about 30 errors). Parzen's provides a very good estimate with a sample size on the order of a few hundred symbols. These simulations also show that a 100 Hz carrier offset in CCI results in negligible degradation of Parzen-based BER estimation.

9.3 Non-Blind BER Estimation in Urban Multipath

The following sections provide examples of Gram-Charlier and Parzen BER estimation for urban multipath channels (modeled by SMRCIM software [241] in AWGN and CCI using a one-bit differential demodulator (DD1). Section 9.2 provides examples of the performance of Gram-Charlier BER estimation and Parzen BER estimation in AWGN and CCI. Fig. 9.12 is a sample histogram of DD1 output in urban multipath and AWGN. Fig. 9.13 shows a histogram of DD1 output in urban multipath and CCI.

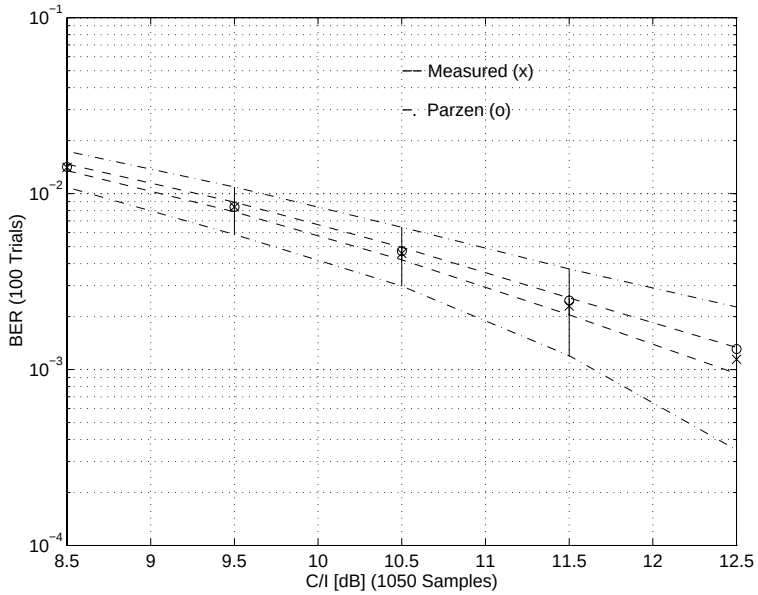

Figure 9.10: Measured and Parzen BER (mean ± 1 std) vs. C/I in CCI (100 Hz carrier offset)

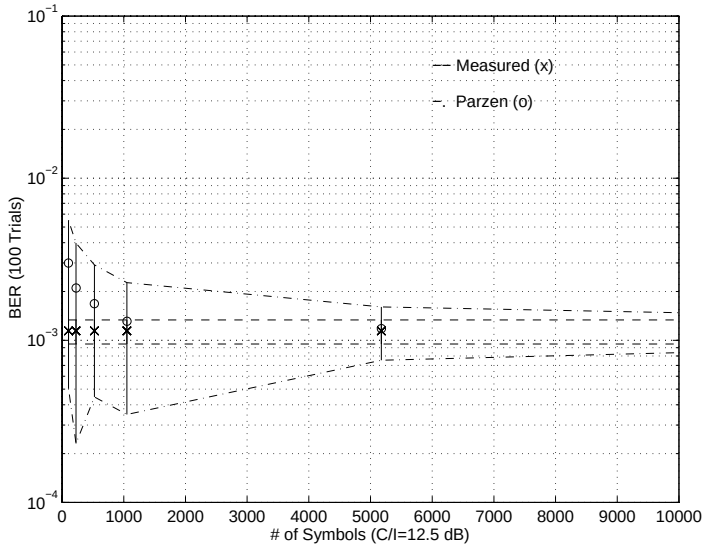

Figure 9.11: Measured and Parzen BER (mean ± 1 std) vs. # of Symbols $C/I = 12.5$ dB (100 Hz carrier offset)

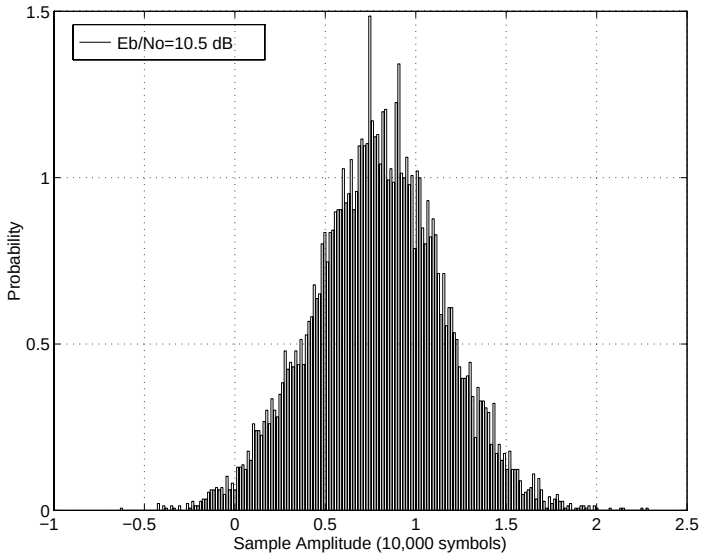

Figure 9.12: Histogram of a DD1 decision statistic x in urban multipath and AWGN ($E_b/N_o = 10.5$ dB)

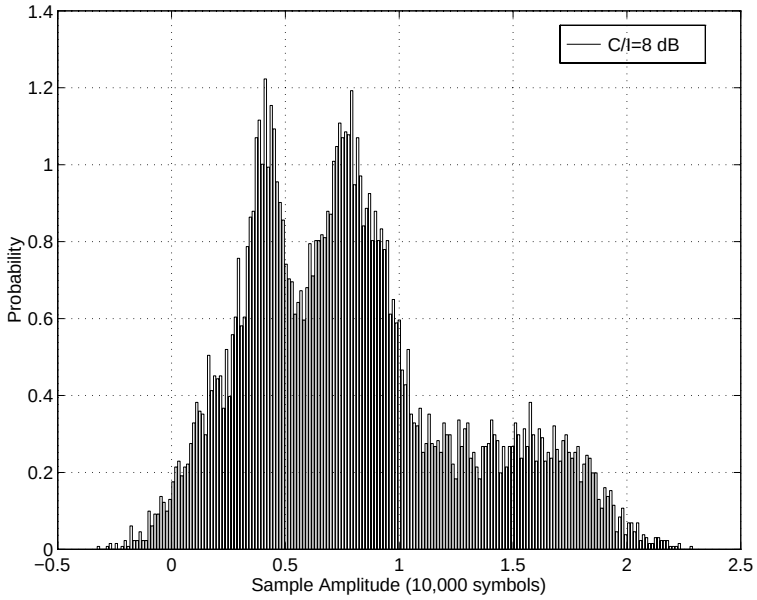

Figure 9.13: Histogram of a DD1 decision statistic x in urban multipath and CCI ($C/I = 8$ dB)

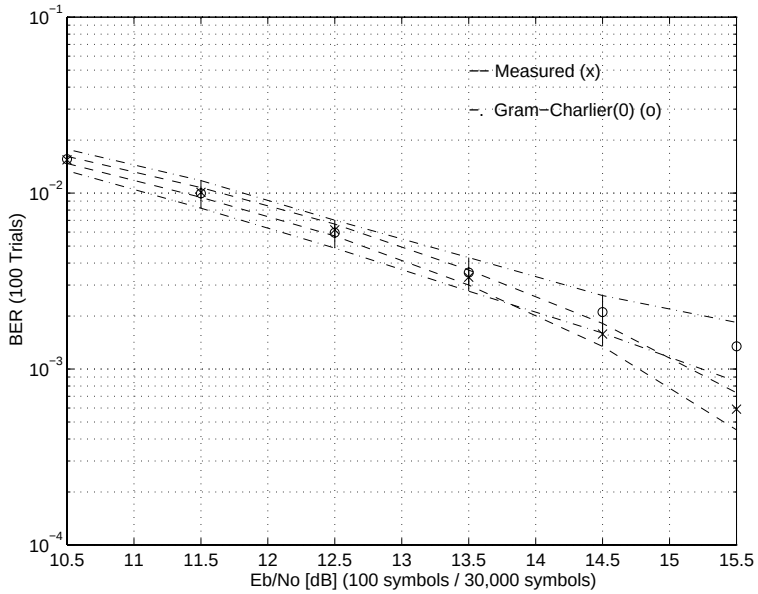

Figure 9.14: DD1 Measured and GC-0 BER (mean ± 1 std) in urban multipath and AWGN (using sample mean and standard deviation)

9.3.1 Non-Blind Gram-Charlier in Urban Multipath and AWGN

In this section, we compare measured BER to BER estimated with the Gram-Charlier series approximation for pdfs. Robust estimators of scale and location (substituted for the mean and standard deviation used in conventional Gram-Charlier estimation) are shown to yield superior performance over that of conventional Gram-Charlier estimation.

Fig. 9.14 shows that a conventional (using mean and standard deviation) 0th order Gram-Charlier, denoted GC-0, yields a very good approximation to measured BER in urban multipath with AWGN. A 0th order Gram-Charlier is equivalent to a Gaussian distribution. As shown, a good estimate can be achieved with a 100 bit training sequence (i.e., observation interval).

To illustrate the performance improvements possible with robust estimators used in Gram-Charlier, we include several plots of different combinations of robust estimators. Fig. 9.15 shows that a substitution of the midshort for the mean and of h_s for the standard deviation (std) into a 2nd order Gram-Charlier, denoted GC-2, also yields a very good approximation to measured BER in urban multipath with AWGN. Fig. 9.16 illustrates the use of the midshort and the MAD. Fig. 9.17 illustrates the use of the shorth (for the mean) and h_s (for the std). Fig. 9.18 illustrates the use of the shorth and the MAD. Again, for each of these, only a 100 bit training sequence is needed. Figs. 9.15 through 9.18 all yield comparable performances.

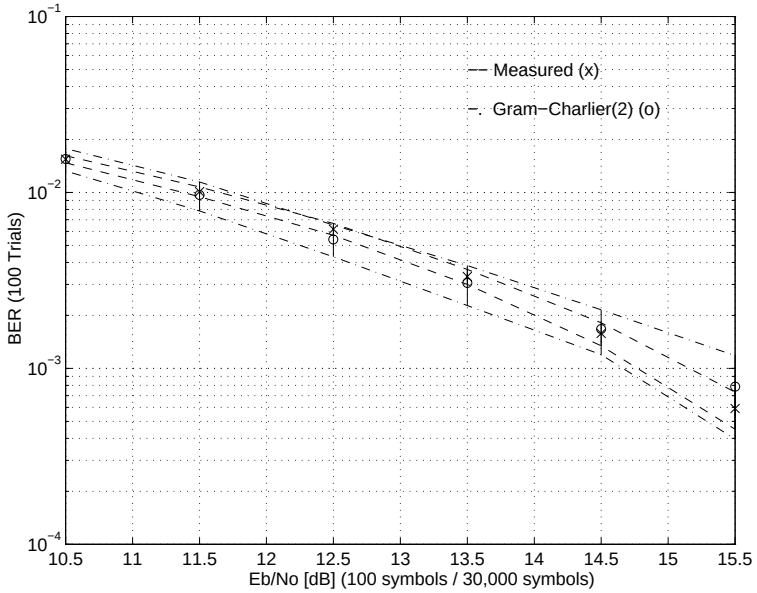

Figure 9.15: DD1 Measured and GC-2 BER (mean ±1 std) in urban multipath and AWGN (using midshort and h_s)

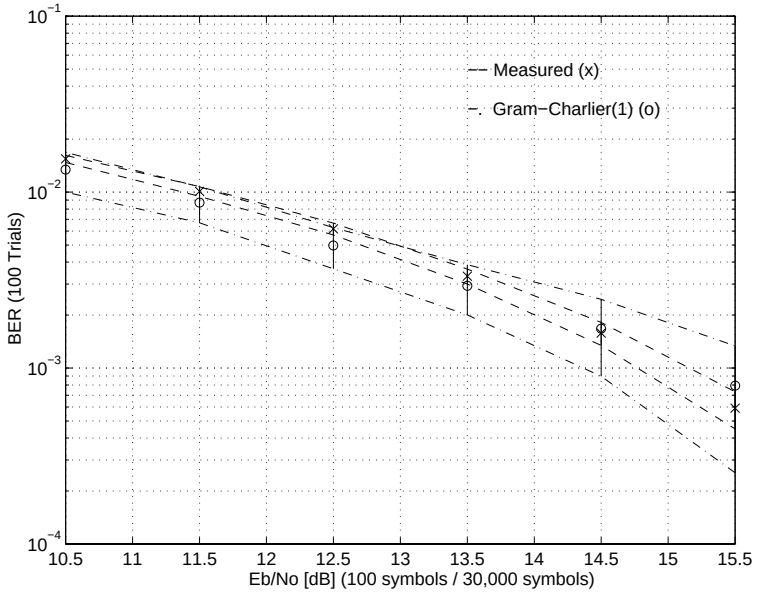

Figure 9.16: DD1 Measured and GC-1 BER (mean ±1 std) in urban multipath and AWGN (using midshort and MAD)

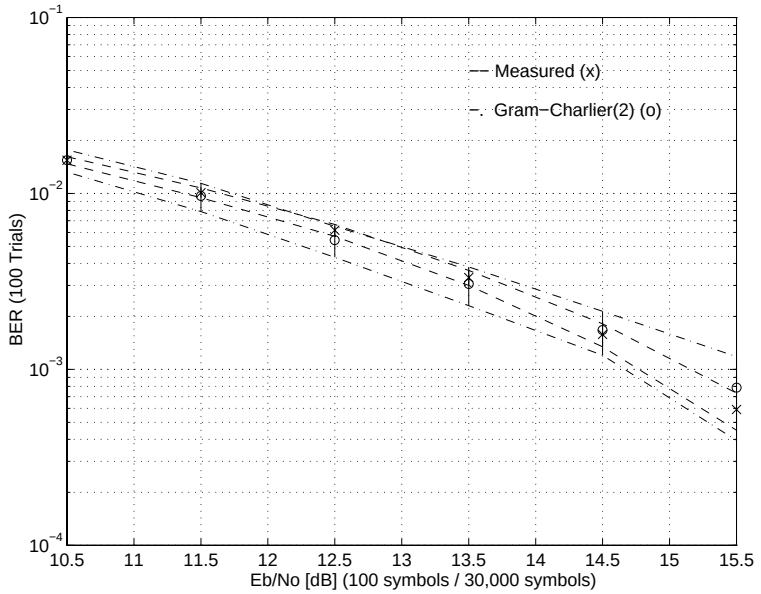

Figure 9.17: DD1 Measured and GC-2 BER (mean ±1 std) in urban multipath and AWGN (using shorth and h_s)

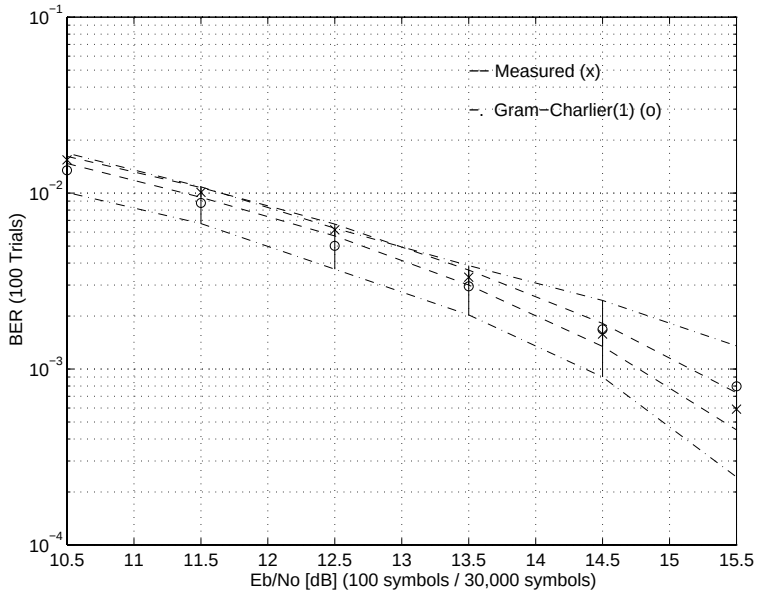

Figure 9.18: DD1 Measured and GC-1 BER (mean ±1 std) in urban multipath and AWGN (using shorth and MAD)

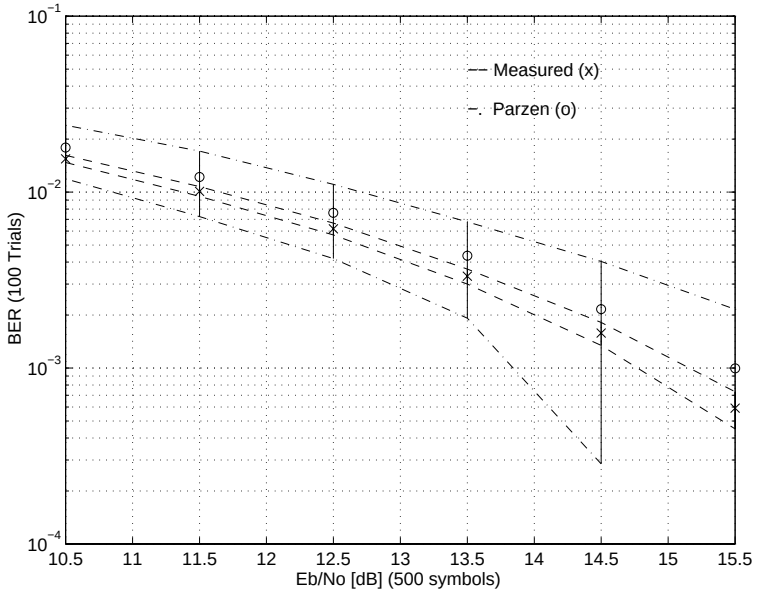

Figure 9.19: DD1 Measured and Parzen BER (mean ±1 std) in urban multipath and AWGN (500 symbols)

9.3.2 Non-Blind Parzen in Urban Multipath and AWGN

In this section, a one-bit differential demodulator (DD1) is again used to compare measured BER to BER estimated with the Parzen pdf estimator. We examine performance in urban multipath (generated by SMRCIM [241]) with AWGN. More training bits are required by Parzen pdf estimation, than by Gram-Charlier pdf estimation. Parzen's estimator is asymptotically unbiased with reference to the number of symbols (i.e., the estimate improves with increased sample size).

Fig. 9.19 shows that 500 training bits are required to achieve a approximate BER estimate in urban multipath and AWGN. As illustrated by Fig. 9.20, the estimate improves when the observation interval is increased to 1000 bits. In GSM data rates, as an example, 500 bits corresponds to about 1.8 msec.

Because Parzen's estimator requires more training bits than Gram-Charlier (about 5-10 times as much), it is of interest to examine the convergence of the Parzen-based BER estimator as a function of sample size (i.e., number of training bits). In urban multipath and AWGN, Fig. 9.21 illustrates the convergence of Parzen-based BER estimator at a BER of approximately 10^{-2} (which, for DD1, corresponds to a $E_b/N_o = 11.5$ dB). Fig. 9.22 illustrates the convergence of Parzen-based BER estimator at a BER of approximately 10^{-3} (which, for DD1, corresponds to a $E_b/N_o = 14.5$ dB). The variance of Parzen's estimator increases as the number of bit errors decreases.

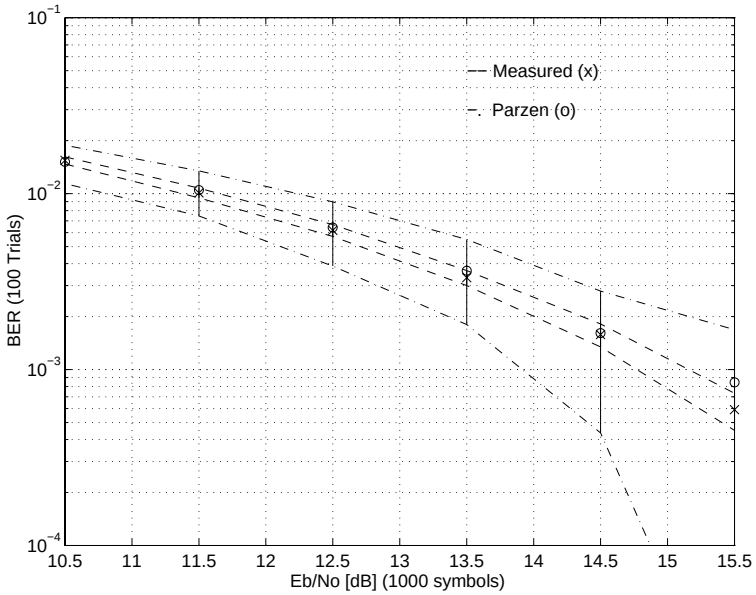

Figure 9.20: DD1 Measured and Parzen BER (mean ±1 std) in urban multipath and AWGN (1000 symbols)

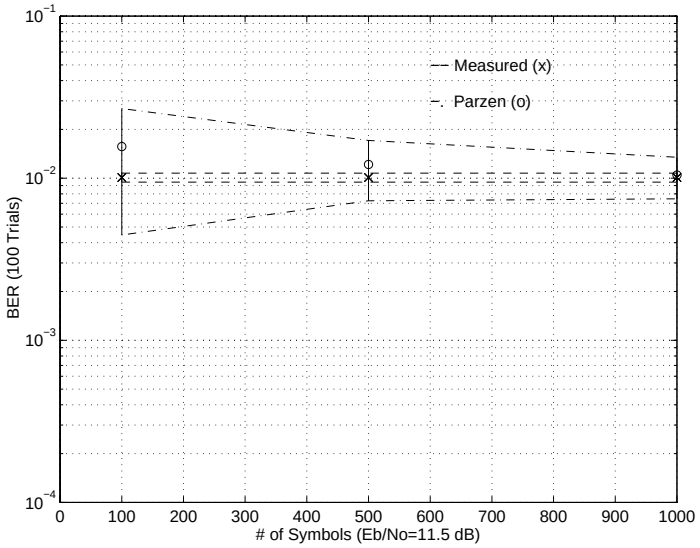

Figure 9.21: DD1 Measured and Parzen BER (mean ±1 std) vs. # of Symbols in urban multipath and AWGN ($E_b/N_o = 11.5$ dB)

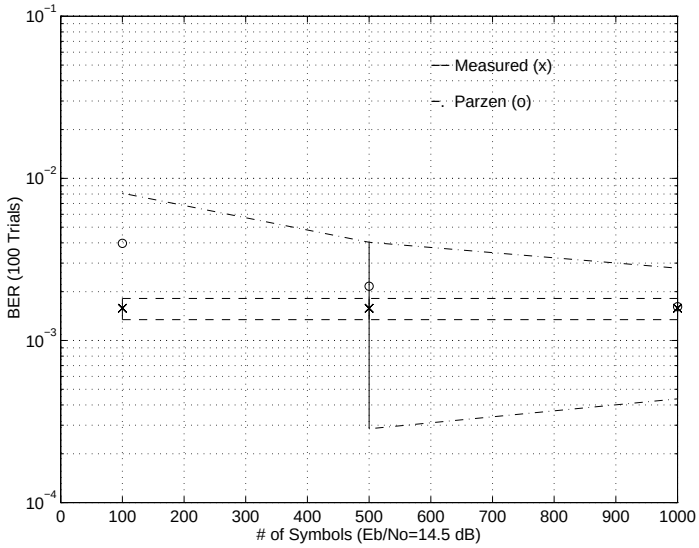

Figure 9.22: DD1 Measured and Parzen BER (mean ±1 std) vs. # of Symbols in urban multipath and AWGN ($E_b/N_o = 14.5$ dB)

9.3.3 Non-Blind Gram-Charlier in Urban Multipath and CCI

Unfortunately, Gram-Charlier estimation generally performs poorly in CCI. This is because the pdfs in CCI tend to look like Gaussian mixtures (as illustrated by Fig. 9.13), and Gram-Charlier only performs well when the pdfs are nearly Gaussian. Much higher orders of Gram-Charlier are required to approximate the measured pdfs. Fig. 9.23 shows the best performance found in simulations, which was 10th order Gram-Charlier with location of scale estimator h_s used in place of the standard deviation. 100 training bits were required.

9.3.4 Non-Blind Parzen in Urban Multipath and CCI

Fig. 9.24 shows that 500 training bits are required to achieve an approximate Parzen BER estimate in urban multipath and CCI. As illustrated by Fig. 9.25, the Parzen estimate improves when the observation interval is increased to 1000 bits.

Because Parzen's estimator requires more training bits (than Gram-Charlier), it is of interest to examine the convergence of the Parzen-based BER estimator as a function of sample size (i.e., number of training bits). In urban multipath and CCI, Fig. 9.26 illustrates the convergence of Parzen-based BER estimator at a BER of approximately 10^{-2} (which, for DD1, corresponds to a $C/I = 9$ dB). Fig. 9.27 illustrates the convergence of Parzen-based BER estimator at a BER of approximately 10^{-3} (which, for DD1, corresponds to a $C/I = 12$ dB).

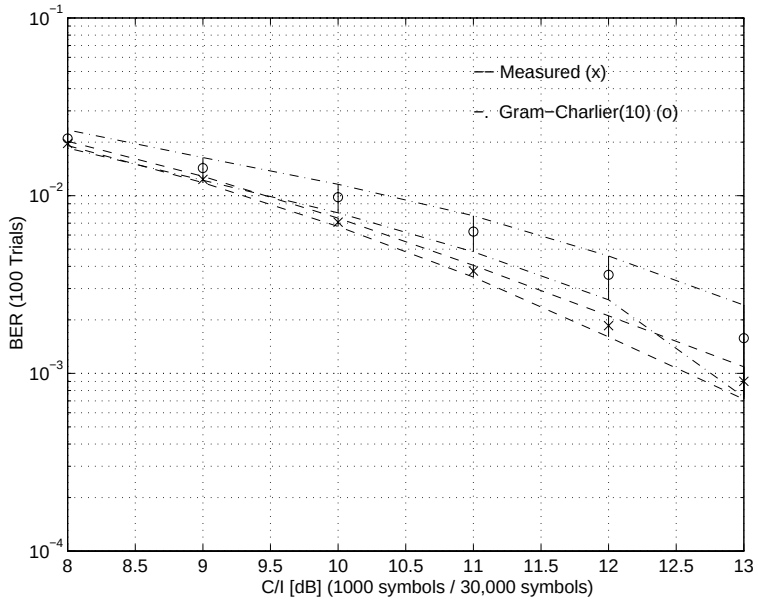

Figure 9.23: DD1 Measured and GC-10 BER (mean ±1 std) in urban multipath and CCI (using mean and h_s)

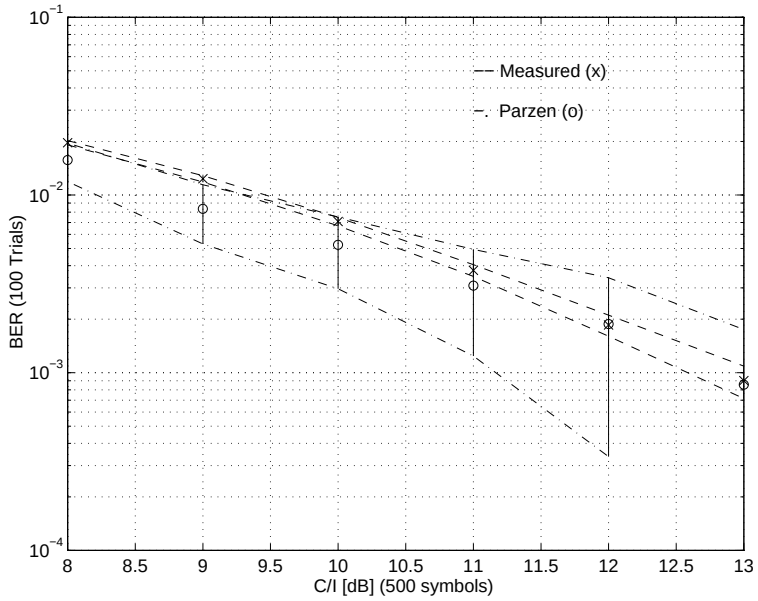

Figure 9.24: DD1 Measured and Parzen BER (mean ±1 std) in urban multipath and CCI (500 symbols)

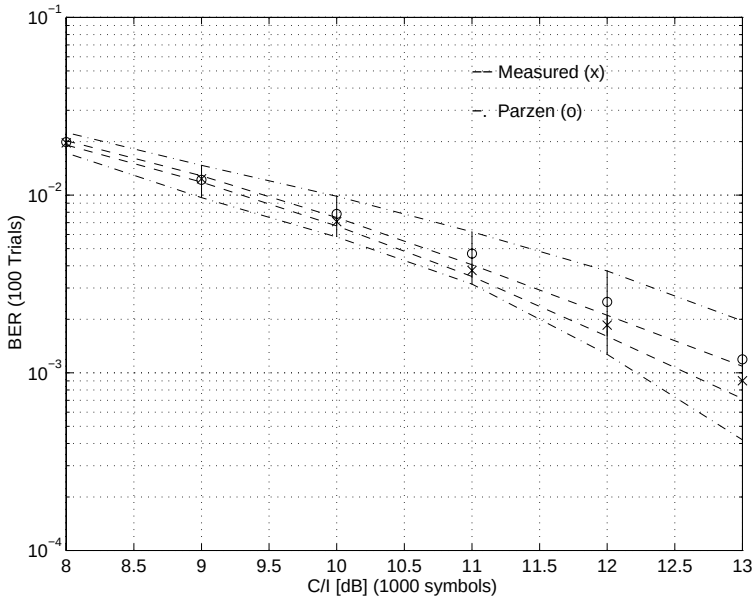

Figure 9.25: DD1 Measured and Parzen BER (mean ±1 std) in urban multipath and CCI (1000 symbols)

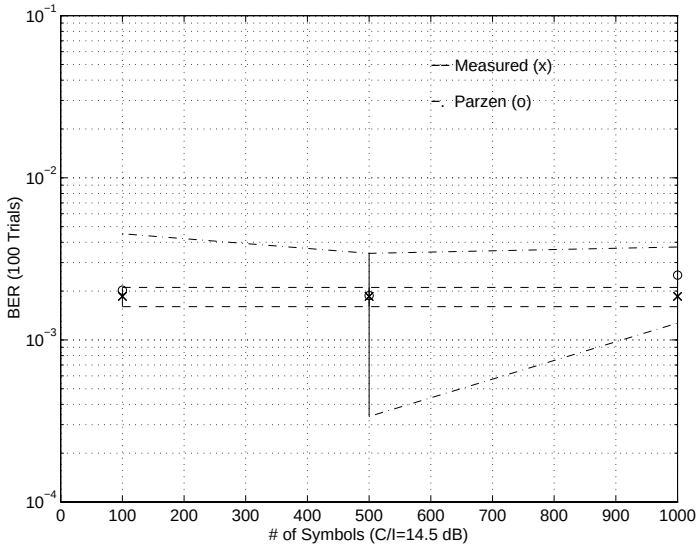

Figure 9.26: DD1 Measured and Parzen BER (mean ±1 std) vs. # of Symbols in urban multipath and CCI ($C/I = 12$ dB)

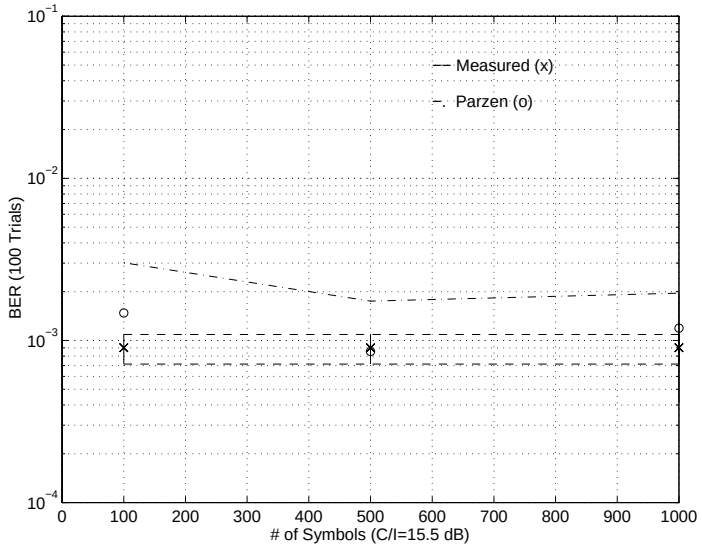

Figure 9.27: DD1 Measured and Parzen BER (mean ±1 std) vs. # of Symbols in urban multipath and CCI ($C/I = 9$ dB)

9.4 Blind BER Estimation in Urban Multipath

This section illustrates via simulation the performance of blind BER estimation, discussed in Section 7.6. Blind estimation means that a training sequence is not required. Instead of multiplying the data by a training sequence (to form a one-sided +1 pdf), a straight-forward blind technique simply takes the absolute value of all the data. Those bits in error (which have crossed the decision threshold) will cause the estimate to degrade, but, as we shall see in some cases, the degradation is often minor. The results of Section 7.6 provide analytical justification for the use of blind Gaussian-based pdf estimation techniques, such as the Gram-Charlier series approximation for pdfs.

For nearly Gaussian distributions, taking the absolute value of the random variable transforms the pdf such that methods like Gram-Charlier can still yield good pdf estimates, provided that the standard deviation of the original data σ_x is less than the mean of the data μ_x (see Section 7.6). This is an important result because a training sequence is not needed. Training bits (normally transmitted) can be replaced by information bits, thereby increasing capacity and improving system flexibility. We apply the technique of Section 7.6 to the Gram-Charlier series approximation for pdfs and to Parzen's pdf estimator. A one-bit differential demodulator (DD1) is used to illustrate the performance of blind Gram-Charlier and Parzen estimation.

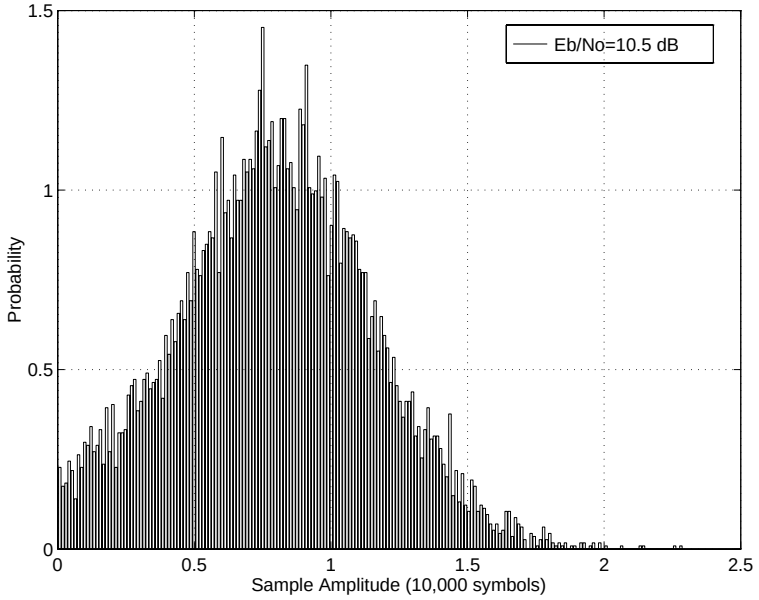

Figure 9.28: Histogram of the absolute value of a DD1 decision statistic $|x|$ in AWGN ($E_b/N_o = 10.5$ dB)

9.4.1 Histograms of x and $|x|$ in Urban Multipath and AWGN

First of all, we consider sample histograms of DD1 decision statistic x and the absolute value of the decision statistic $|x|$ in urban multipath and AWGN. A typical histogram of the DD1 decision statistic in AWGN is given in Fig. 9.12. Fig. 9.28 shows the transformed histogram of the absolute value of the same DD1 decision statistic.

9.4.2 Blind Gram-Charlier in Urban Multipath and AWGN

In this section, we investigate the use of blind Gram-Charlier-based BER estimation in urban multipath with AWGN. Because Gram-Charlier just depends on the general moments of the data, it is reasonable to postulate that it might yield acceptable BER estimates without a training sequence, if one transforms the decision statistic x pdf by taking the absolute value of the data $|x|$.

Fig. 9.29 shows the performance of Gram-Charlier estimation in urban multipath and AWGN. A conventional (using mean and std) 0th order Gram-Charlier (i.e., a Gaussian) estimate gives good BER estimates in urban multipath and AWGN without a training sequence. The variance of the Gram-Charlier estimate is somewhat greater than that obtained with a training sequence, but the performance is still good. Remarkably, as few as 10 symbols are needed to provide good BER estimates.

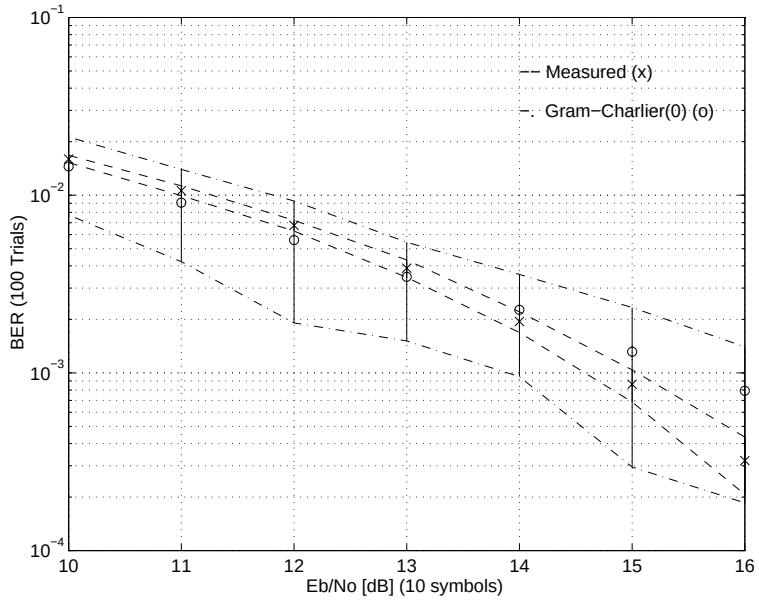

Figure 9.29: DD1 Measured vs. GC-0 BER (mean ± 1 std) in urban multipath and AWGN - no training sequence

9.4.3 Blind Parzen in Urban Multipath and AWGN

In this section, we investigate the use of blind Parzen-based BER estimation in urban multipath and AWGN. Parzen estimation depends upon the actual data symbols (not the general moments), so if the data symbols are transformed (e.g., $|x|$), one might expect Parzen-based BER estimation to experience degradation.

Fig. 9.30 shows the performance of Parzen estimation in urban multipath and AWGN. Parzen's estimator is degraded by the transformation of the decision statistic, but it still yields a rough estimate in urban multipath and AWGN with as few as 100 symbols. Increasing the number of symbols used to calculate the Parzen-based BER does not improve the estimate. However, because Parzen's estimator depends on each data sample (rather than statistical moments), Parzen-based BER estimation will most often require a training sequence. The degradation apparent in these simulation results confirm need for a training sequence. Consequently, taking the absolute value of the data (i.e., losing the error information) degrades the Parzen estimator, making it not very useful for blind BER estimation in urban multipath and AWGN.

9.4.4 Histograms of x and $|x|$ in Urban Multipath and CCI

First of all, we provide sample histograms of DD1 decision statistic x and the absolute value of the decision statistic $|x|$ in urban multipath and CCI. A typical histogram of the DD1 decision statistic in urban multipath and CCI is given in Fig. 9.13. Fig. 9.31 shows

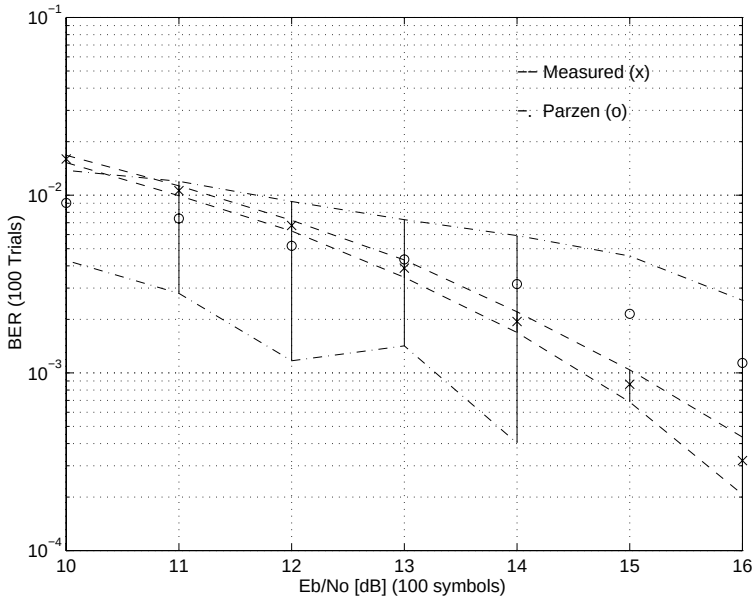

Figure 9.30: DD1 Measured vs. Parzen BER (mean ±1 std) in urban multipath and AWGN - no training sequence

the transformed histogram of the absolute value of the same DD1 decision statistic.

9.4.5 Blind Gram-Charlier in Urban Multipath and CCI

In this section, we investigate the use of blind Gram-Charlier-based BER estimation estimation in urban multipath and CCI. Again, because Gram-Charlier just depends on the general moments of the data, it is reasonable to postulate that it might yield acceptable BER estimates without a training sequence.

Fig. 9.32 shows the performance of Gram-Charlier estimation in urban multipath and CCI. A conventional (using mean and std) 4th order Gram-Charlier is one of the better estimators, yet it only provides a rough estimate of BER in urban multipath and CCI without a training sequence. The variance of the Gram-Charlier estimate is much greater than that obtained with a training sequence, but the mean is approximately the same. At least 100 symbols are needed to get this rough estimate. The poorer performance is likely due to the structure of the non-Gaussian pdf due to the CCI.

9.4.6 Blind Parzen in Urban Multipath and CCI

In this section, we investigate the use of blind Parzen-based BER estimation estimation in urban multipath and CCI. Parzen estimation depends upon the actual data symbols (not the general moments), so if the data symbols are transformed (e.g., $|x|$), one might

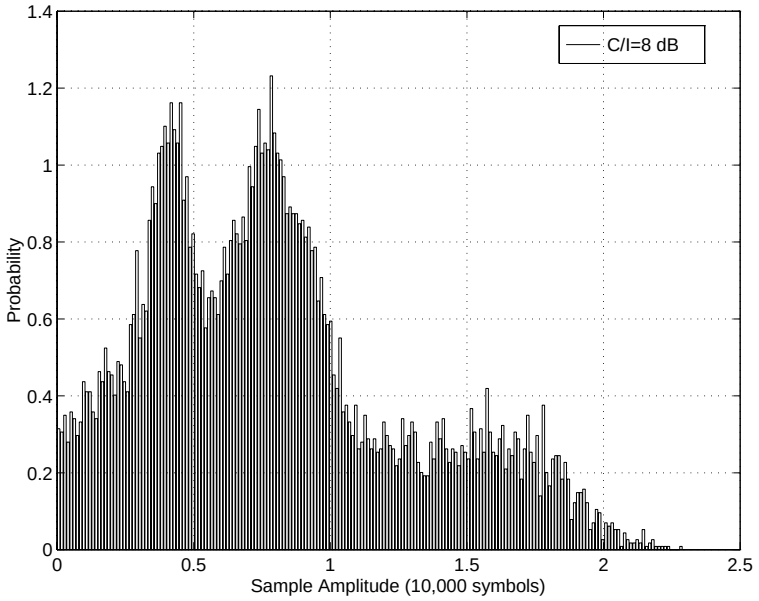

Figure 9.31: Histogram of the absolute value of a DD1 decision statistic $|x|$ in urban multipath and CCI ($C/I = 8$ dB)

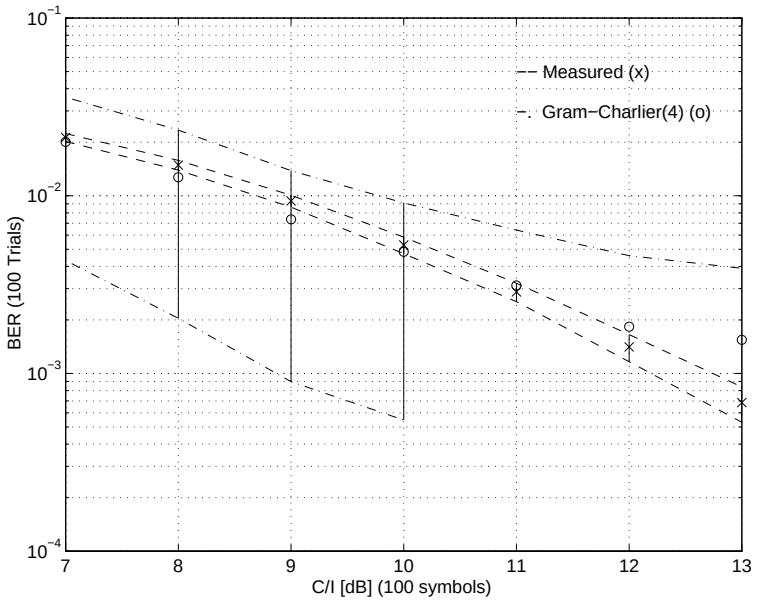

Figure 9.32: DD1 Measured vs. GC-4 BER (mean ± 1 std) in urban multipath and CCI - no training sequence

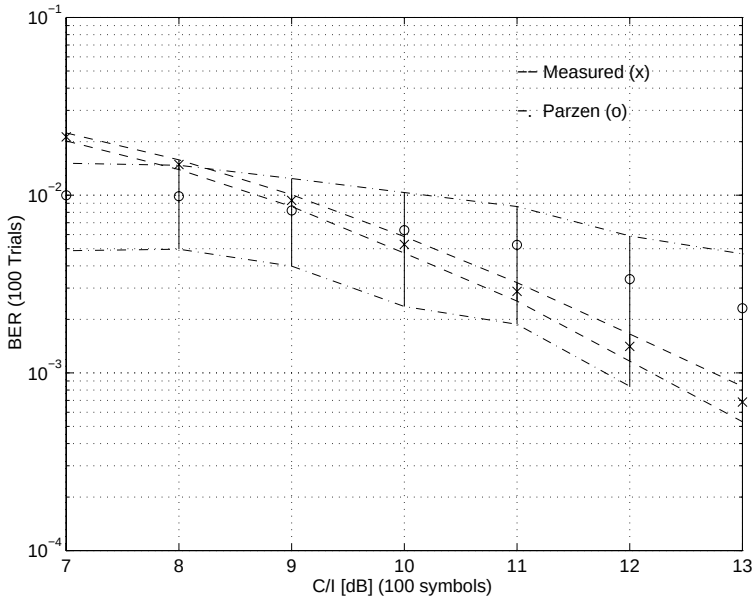

Figure 9.33: DD1 Measured vs. Parzen BER (mean ±1 std) in urban multipath and CCI - no training sequence

expect Parzen-based BER estimation to experience degradation.

Fig. 9.33 shows the performance of Parzen estimation in urban multipath and CCI. Parzen's estimator is again degraded by the transformation of the decision statistic, and it only yields a rough estimate in urban multipath and CCI with 100 symbols. Increasing the number of symbols used to calculate the Parzen-based BER does not improve the estimate. These simulation results confirm need for a training sequence. Taking the absolute value of the data (i.e., losing the error information) degrades the Parzen estimator, making it not very useful for blind BER estimation in urban multipath and CCI.

9.5 Summary

This chapter provides validation of BER estimation by simulations. A simple one-bit differential demodulator (DD1) is used throughout the simulations, where Gram-Charlier and Parzen BER estimation are compared to measured DD1 results (based on 30,000 bits). Comparisons are made for non-blind BER estimation in AWGN and CCI channels and in urban multipath (generated by SMRCIM [241]) with AWGN and CCI. The chapter also provides results for blind BER estimation in SMRCIM urban multipath with AWGN and CCI.

Gram-Charlier performs well in AWGN and requires a very short training sequence

(less than 100 symbols). In other words, only 100 bits are needed with Gram-Charlier BER estimation to obtain the equivalent BER of 30,000 measured bits. Parzen estimation performs well also in AWGN (for E_b/N_o of 11-16 dB), but requires a longer training sequence (about 500 symbols). Gram-Charlier estimation Gram-Charlier estimation does not perform well in CCI (for C/I of 7-14 dB with $E_b/N_o = 20$ dB), whereas Parzen esti mation yields good results (with 500 symbols). Blind simulation results indicate that blind Parzen estimation performs poorly (i.e., Parzen estimation requires a training sequence), whereas blind Gram-Charlier estimation yields reliable estimates in AWGN (with as few as 10 symbols). Blind Gram-Charlier and blind Parzen estimation both performs poorly in CCI.

Chapter 10

BER-based Demodulator Diversity Simulations

10.1 Motivation

This chapter provides measurement support and justification via simulations for the concept of demodulator diversity, an adaptive signal processing scheme where the outputs of a bank of demodulators are combined in some way so as to take advantage of their diverse merits in a changing channel. Demodulator diversity using real-time BER estimation is a new concept which has been investigated very little in the literature. This approach promises to be a major contribution to the field of communications.

With demodulator diversity, we would like to combine the redundant, but different signals, so as to obtain, at the very least, a combined demodulator with a BER which tracks the BER of the best demodulator for given channel impairment. Indeed, the simulations in this chapter show that a demodulator diversity scheme can at least track the BER of the best demodulator, and, in many instances, provide better overall performance than that attainable by any individual demodulator. These techniques are simple and easily implemented, even for a mobile handset. diagram of a demodulator diversity scheme is given in Figure 10.1. As shown in the figure, a demodulator diversity scheme can often be implemented with a common RF front end.

In the first part of the chapter, we examine a demodulator diversity scheme using the three best noncoherent demodulators (from Chapter 5) where a MSE-based criterion is used to adaptively select the best demodulator based on a given observation interval (or training sequence). The second part of the chapter examines a demodulator diversity scheme using a combination of a coherent demodulator with a noncoherent demodulator, where an MSE-based criterion is compared to Gram-Charlier BER-based criterion and Parzen BER-based criterion. In this second scheme, the demodulator outputs are adaptively selected and then adaptively weighted and combined. For both schemes, we include, for comparison, demodulator diversity performance based on MSE because MSE is a commonly used metric in adaptive signal processing (this provides a baseline comparison for the BER-based adaptive techniques).

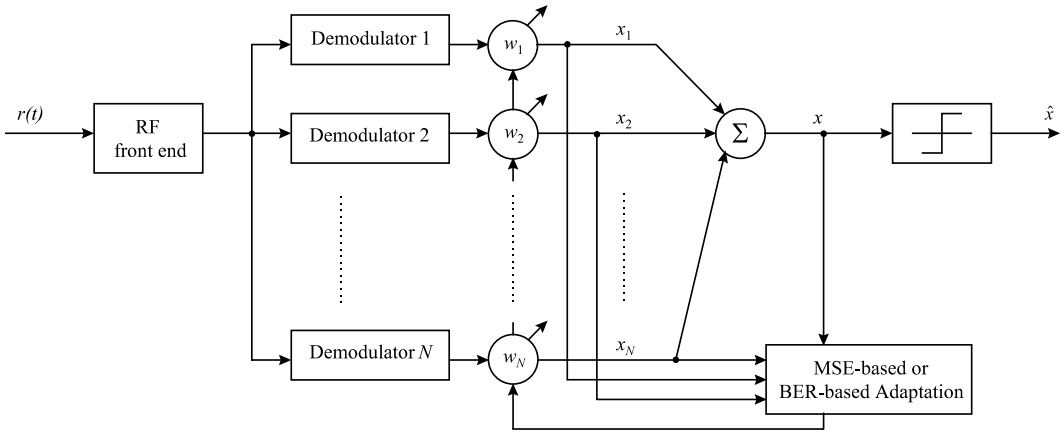

Figure 10.1: Generalized block diagram of a demodulator diversity scheme.

The results for a one-bit differential demodulator (DD1) are also plotted for the second scheme to provide a baseline for comparision of demodulators. In the first demodulator diversity example, results for a limiter discriminator provide a baseline for comparison. The limiter discriminator and one-bit differential demodulator have comparable performance within 1 dB.

Any combination and number of demodulators can be used in a demodulator diversity scheme. A bank of three better performing noncoherent demodulators was examined because noncoherent demodulators tend to be less expensive and avoid the problems associated with coherent demodulation in fast fading (e.g., the coherent demodulator losing phase lock). The second scheme above was chosen to show how a noncoherent demodulator could compensate for the deficiencies of the coherent demodulator in typical wireless environments.

Section 10.4.1 provides surface plots of the Parzen-based BER cost function vs. weights for two cases of urban multipath with AWGN and CCI - (1) when the BERs of the demodulators are nearly the same and (2) when the BERs of the demodulators are different by about an order of magnitude. The plots show that many weight combinations can yield overall BERs *less* than the BER of the best individual demodulator. Section 10.4.3 demonstrates performance of improvements possible with a demodulator diversity scheme using Parzen-based BER estimation, by considering the cases where errors tend to occur in bursts and where errors tend to be randomly dispersed (gains are evident in both cases).

10.2 Demodulator Diversity with Noncoherent Combination by Simple Selection

This section outlines the preliminary results, where a bank of noncoherent demodulators is examined using a simple selection rule based on minimizing MSE. As discussed in Chapters 2 and 4, noncoherent receivers are usually less expensive than coherent receivers, but they tend to have inferior performance to coherent receivers, except in channel conditions such as severe multipath where the coherent has difficulty tracking the rapid phase changes. Noncoherent receivers are popular for use with GMSK in applications such as DECT (Digital European Cordless Telephone), DECT-based wireless LANs, and high data-rate applications.

10.2.1 MMSE Selection of the Demodulator Outputs

As discussed in Section 5.3, the three best noncoherent demodulators were chosen, with each of the three chosen demodulators showing superior performance for particular channel impairments. With demodulator diversity, the outputs of a bank of demodulators are combined in some way to take advantage of their diverse merits in a changing channel. At the very least, we would like a combined demodulator to have a BER which tracks the BER of the best demodulator for given channel impairment. As the channel changes, the BER of the combination would be improved over that of any one demodulator. We first consider a simple selection of demodulator outputs based on a Minimum Mean Square Error (MMSE) criterion. Selection of demodulator outputs for a combination of a coherent and noncoherent demodulators is investigated in Section 10.

The best three demodulators chosen are

- 2-bit differential demodulator with decision feedback
- 1-bit DF, 2-bit DF, & 3-bit DF differential demodulators with combined outputs
- limiter discriminator demodulator

The limiter discriminator and the one-bit differential demodulator (DD1) have comparable performance within 1 dB.

The following simulations involve a burst-by-burst selection among the three demodulator outputs, accomplished by using a training sequence (e.g., as found in the middle of a GSM normal burst as shown in Figure 10.2). One of the three demodulator outputs is chosen for each burst (with one burst per frame in a TDMA format) based on the MMSE criterion as illustrated in Figure 10.3. It was found that the demodulators usually make errors on different bits, so that there is a potential gain of 2-4 dB if appropriate bit-by-bit selection (rather than burst-by-burst selection) is done. This potential gain is included on the plots of the simulations results, examples of which are given in Figures 10.4 - 10.8.

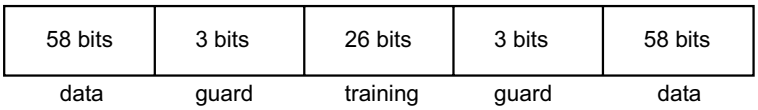

Figure 10.2: GSM normal burst structure.

10.2.2 A Data Fusion Problem

Because the outputs of the demodulators have different probability density functions (pdfs), a data fusion problem exists. The pdfs are indicated by the histograms of the demodulator outputs as given in Figures 5.1 - 5.3. The (200 bin) histograms are based on the transmitted +1 and -1 bits, where the signal is corrupted by rural Rayleigh fading and CCI with $C/I = 8$ dB. Figure 5.1 is the histogram for the 2-bit DF DD, Figure 5.2 is the histogram for the 1-bit DF, 2-bit DF, 3-bit DF DD with combined outputs,[1] and Figure 5.3 is the histogram for the limiter discriminator.

The output pdfs (which indicate the bit error rates, BERs) can be normalized by subtracting the respective means (which are zero in these cases) and by then dividing by their respective standard deviations, with the goal of selection output generally choosing the demodulator with the lowest BER for a given burst. By normalizing the data, we allow the selection BER to follow that of the best demodulator (with lowest BER).

As discussed in Section 6.2, an analogy can be drawn between demodulator diversity and spatial diversity. Though there are differences between array analysis and the present research, an analogy can be drawn to gain insight. Coherent combination techniques (such as maximal ratio combining) used with adaptive arrays could be applied to demodulation diversity. The principles of smart antenna spatial diversity (antenna arrays) are well known. For example, signal 1 and antenna (or sensor) 1 is related to signal 2 at antenna 2 by a complex constant, allowing a steering constant to be set up. With demodulator diversity, the individual statistics of a bank of demodulator outputs often differ from each other.

10.2.3 Results for MMSE Selection of the Demodulator Outputs

The three best noncoherent demodulators show superior performance in particular channel impairments. Using this diversity, we combine the outputs of the demodulators in some way to take advantage of their diverse merits in a changing channel. The first step involves a burst-by-burst selection among the three demodulator outputs, accomplished by using a training sequence. One of the three demodulator outputs is chosen for each burst (with one burst per frame in a TDMA format) based on a Minimum Mean Square

[1] 1-bit DF, 2-bit DF, 3-bit DF differential demodulator with combined outputs is a new demodulator structure described in Section 4.2 and 5.3

Error (MMSE) criterion as illustrated in Figure 10.3.

The results are plotted for all the channel impairments [34]. Only the results of five channel impairments are included here. In Figures 10.4 - 10.8, the BER of the three demodulators are plotted for AWGN, AWGN and urban Rayleigh fading, CCI, CCI urban Rayleigh fading, and AWGN, CCI, and urban Rayleigh fading. In this first demodulator diversity scheme, multipath fading is generated with COST 207 models [70] (detailed in Appendix C). The BER for the MMSE selection of the demodulator outputs is included in each plot. Note that the BER for MMSE selection generally follows the lower BER of the three demodulators. It does not track the lowest BER exactly, because of the data fusion problem mentioned earlier. The normalization of the different demodulator outputs needs to be improved on. This is one inadequacy of MSE-based adaptive selection. BER-based adaptive selection (and weighting) avoids the data fusion problem, precisely because adaptation is based on BER, not MSE.

Also included in each plot of Figures 10.4 - 10.8 is the potential BER, usually 2-4 dB less than the MMSE selection in terms of E_b/N_o . The potential BER is a statistical curve for the case when all three of the demodulators are in error. Between the potential BER and the other curves is a BER region where at least one of the demodulators is yielding the correct bit. If bit-by-bit selection can be made, then the overall BER of the three demodulators can approach this potential BER. In other words, this graphed line represents a possible limit to improvement in the selection diversity scheme.

The coherent demodulator is simulated for comparison (particularly since GSM utilizes mostly coherent demodulation) and is plotted alongside of the noncoherent demodulators in Figures 10.4 - 10.8. Coherent demodulation does not systems such as GSM specify that an equalizer be used to mitigate delay spreads due to channel and filter ISI (discussed in Section 11.4). A coherent demodulator with a Viterbi detector is often used to implement equalization.

This section seeks to provide an introduction to the concept of demodulator diversity. Further theoretical justification for receiver diversity is given in Chapter 6. One reason that this particular demodulator diversity scheme does not provide the gains in performance that are desirable is because the noncoherent demodulators used in this diversity scheme have performances that are close to each other across channel impairments. The next section (Section 10.3) demonstrates significant gains achievable with a diversity scheme of a noncoherent and coherent demodulator, which have very different performances, respectively, in different channel impairments.

10.3 Demodulator Diversity with Coherent and Noncoherent Combination by Simple Selection

In this section, a demodulator diversity scheme (with a coherent demodulator combined with a 123DF differential demodulator) is investigated where simple selection of demodulator outputs is performed. Figures 8.1 and 10.1 provide a general block diagram of the receiver diversity scheme. As discussed in Chapters 2 and 4, noncoherent receivers

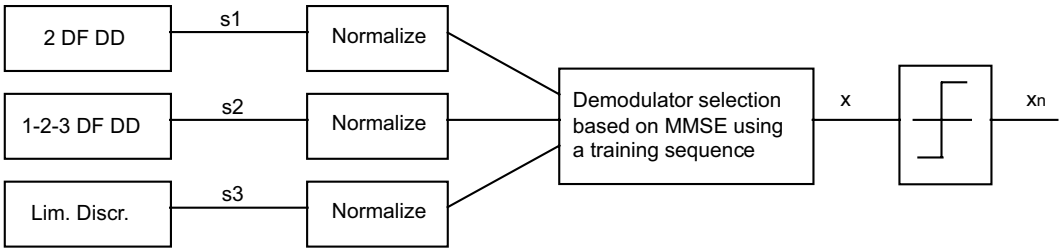

Figure 10.3: Block diagram of selection of three demodulator outputs based on MMSE.

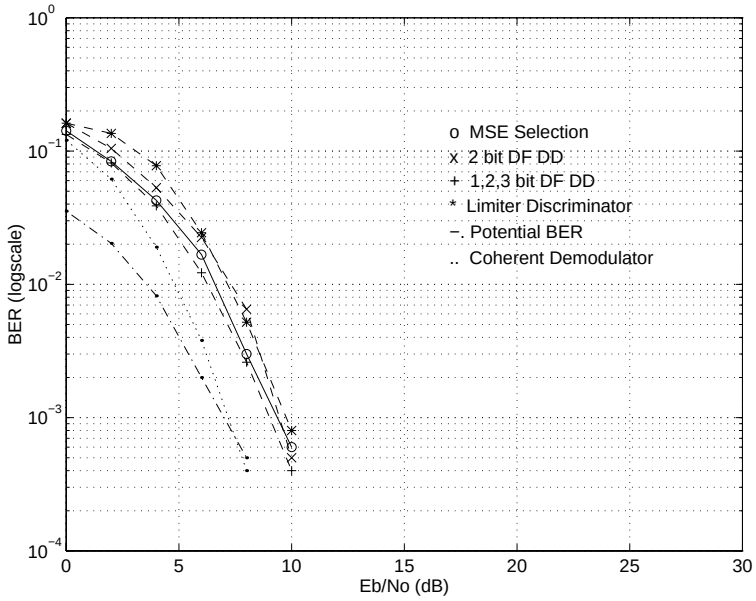

Figure 10.4: In AWGN, BER vs. E_b/N_o of three demodulators and the burst-by-burst MSE selection.

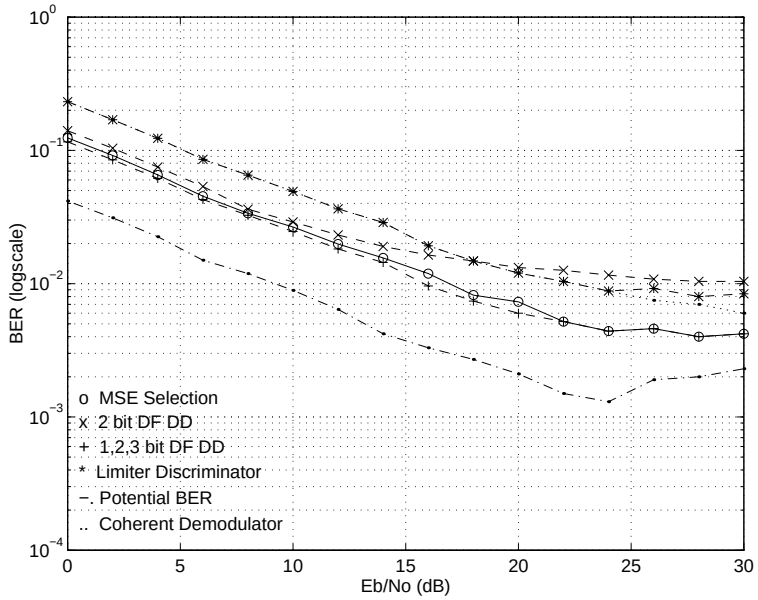

Figure 10.5: In AWGN and urban multipath fading, BER vs. E_b/N_o of three demodulators and the burst-by-burst MSE selection.

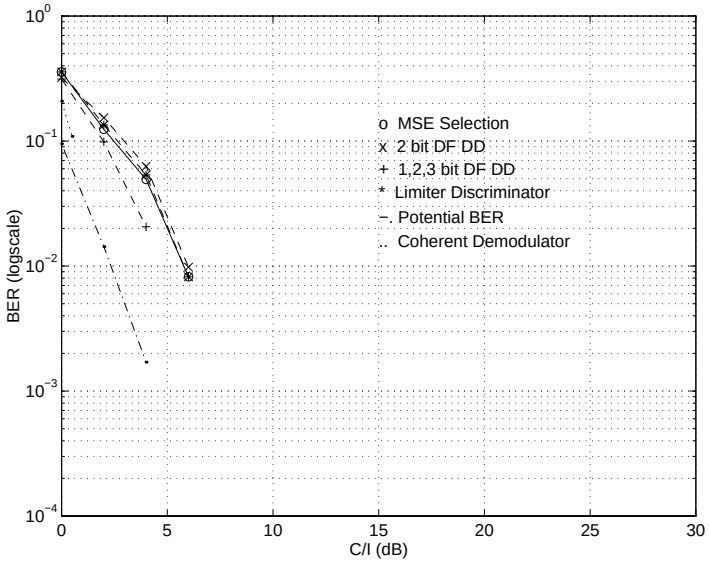

Figure 10.6: In CCI, BER vs. C/I of three demodulators and the burst-by-burst MSE selection.

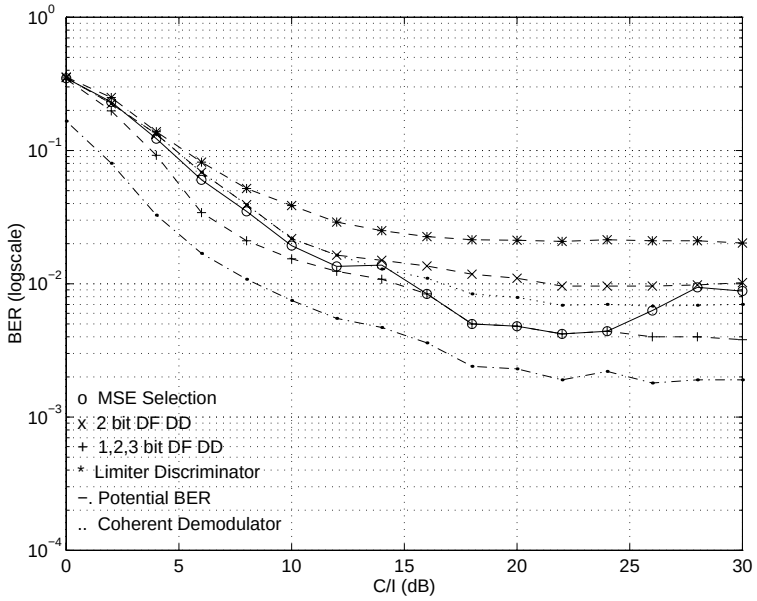

Figure 10.7: In CCI (one interferer) and urban multipath fading, BER vs. C/I of three demodulators and the burst-by-burst MSE selection.

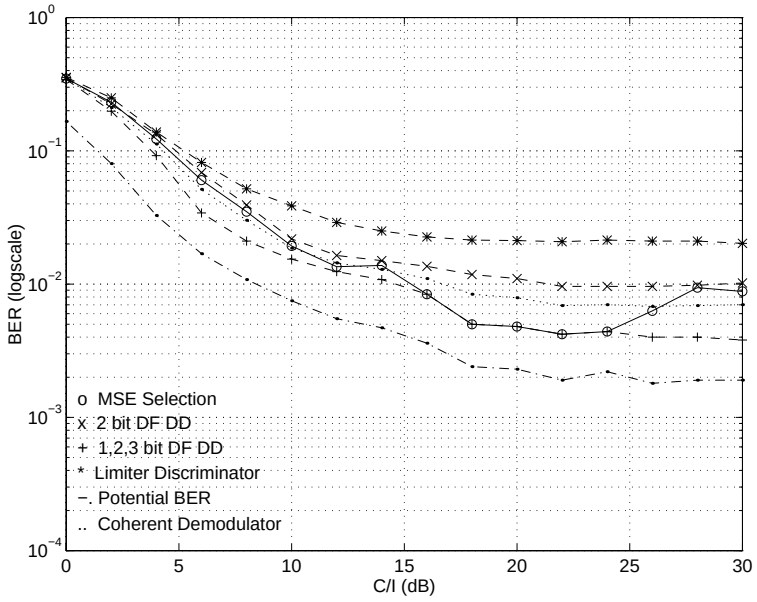

Figure 10.8: In AWGN, CCI (one interferer) and urban multipath fading, BER vs. C/I of three demodulators and the burst-by-burst MSE selection.

are usually less expensive than coherent receivers, but they tend to have inferior performance to coherent receivers, except in channel conditions such as severe multipath where the coherent has difficulty tracking the rapid phase changes. Coherent demodulators are widely used in GSM systems in combination with Viterbi detectors.

Three cases are examined, where selection is based on the criterion of (1) Mean Squared Error (MSE) and where it based on the criterion of lowest BER as estimated by the (2) Gram-Charlier method and by (3) Parzen's method. In all cases, a training sequence (i.e., an observation interval) is used with the criterion upon which selection is based. The wireless channel modeled consists of urban multipath (generated by SMRCIM [203, 241])[2] in AWGN and also in CCI. The CCI case also includes AWGN with an $E_b/N_o = 20$ dB.

In the following examples, we consider the case of bursty errors. The bursty error case is modeled by the coherent demodulator losing phase lock for 1% for the time, where the phase lock loss occurs in bursts so that the majority of errors occur closely together in time. A phase lock loss of 1% of the time is chosen because it is reasonable figure for wireless environments and it results in a coherent demodulator BER performance between 10^{-3} and 10^{-2} (the BER range of interest throughout these simulations, consistent with the GSM specifications as found in Tables 11.1 and 11.2). This case corresponds to a phase lock loss for an interval of time greater than the duration of the signaling frame (e.g., as shown in Figure 10.2 for GSM). The differential demodulator, by contrast, does not require phase lock. In conditions where errors occur in bursts, the results indicate that selection can yield significantly lower BERs compared to the BERs of the individual demodulators.

The case of errors dispersed in time is also of interest. Here, the errors do not occur in bursts, but are randomly dispersed in time (for the case of bursty errors, the majority of errors occur closely together in time). The case where the errors are dispersed is modeled also by the coherent demodulator losing phase lock for 1% for the time, but where the phase lock loss occurs randomly so that errors are dispersed in time (not all occurring closely together in bursts). This case corresponds to a phase lock loss for an interval of time comparable to or less than the duration of the signaling frame (e.g., as shown in Figure 10.2 for GSM). When errors occur randomly (i.e., dispersed in time), simple selection can only approach the lower BER of the individual demodulators. In other words, for random errors, the results indicate that selection of demodulator outputs can never do better than the BER performance of the best demodulator.

For selection, real decisions are sufficient. In addition, for convenience, the outputs of the demodulators should be consistent, that is, they ought to have the same bit stream information (e.g., the output of one demodulator should not be differentially encoded and the output of another demodulator be differentially decoded).[3] For straight selection,

[2]In these simulations, the urban multipath was generated with the software SMRCIM. Refer to Appendix B for details on SMRCIM modeling

[3]Variations of the differential demodulator (DD) result in the demodulator output being differentially encoded in various ways. For example, one-bit DD performs no encoding, whereas two-bit DD performs two-bit encoding; three-bit DD performs three-bit encoding, etc. If a bank of various differential

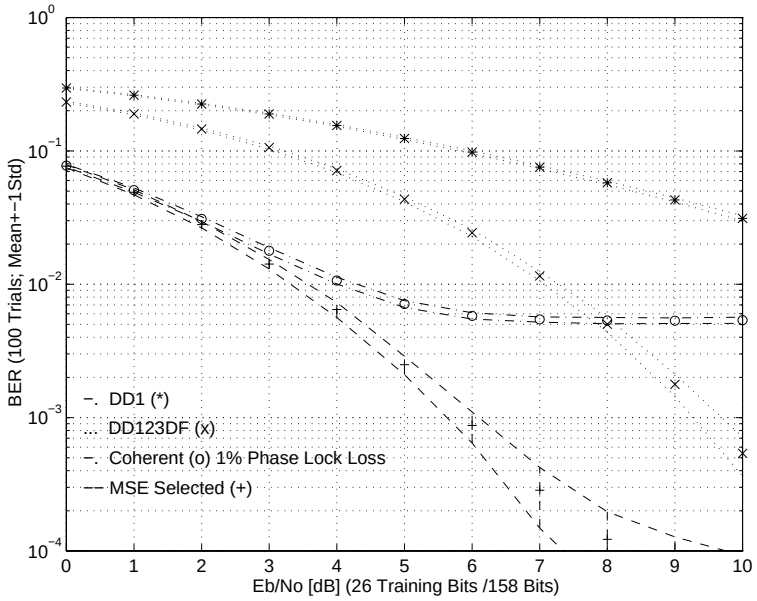

Figure 10.9: Coherent & DD123DF measured and MSE-based Selection BER vs. AWGN in urban multipath

however, this requirement can be circumvented if different training sequences used and matched to the different outputs.

10.3.1 Selection Based on MSE

In this section, selection of the individual demodulators is based on Mean Squared Error (MSE), where a training sequence is used so that the corrupted decision statistic is compared to an expected reference value. The individual demodulator output with the lowest MSE (over the observation interval, or training sequence) is selected. The case of urban multipath and AWGN is illustrated by Fig. 10.9, where the individual BERs of the demodulators are plotted along with the BER attained with selection. Fig. 10.10 shows MSE performance in urban multipath and CCI. In this second demodulator diversity scheme, multipath fading is generated with SMRCIM software [241] (detailed in Appendix B).

10.3.2 Selection Based on Gram-Charlier PDF Estimation

Here, selection of the individual demodulators is based on Gram-Charlier series approximation for pdfs, where a training sequence is used to isolate the decision statistic samples associated with the +1 bits (and consequently the -1 bits also), as explained in Section

demodulators are used, then outputs must have the same coding.

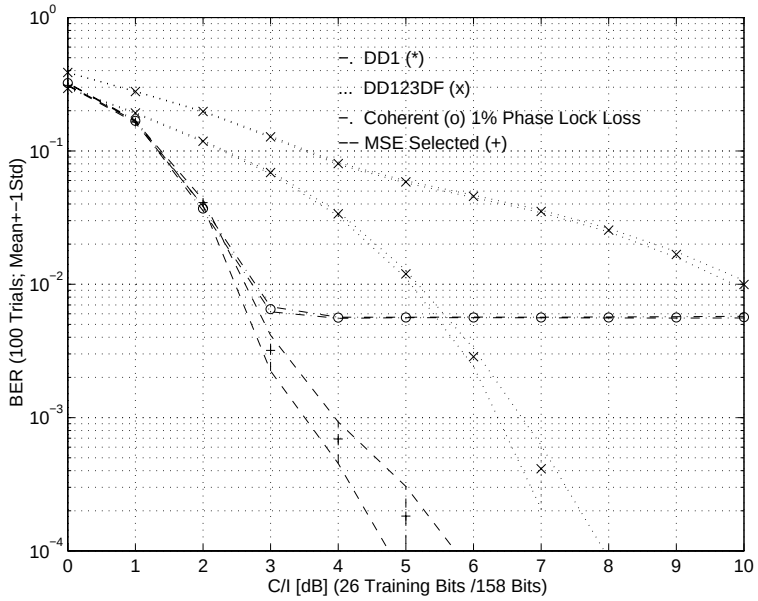

Figure 10.10: Coherent & DD123DF measured and MSE-based selection BER vs. CCI in urban multipath

7.3. The BER of each demodulator is estimated by calculating the area under the pdf to the left of the decision threshold (i.e., the area corresponding to those bits in error). The individual demodulator output with the lowest BER (over the observation interval, or training sequence) is selected. The case of urban multipath and AWGN is illustrated by Fig. 10.11, where the individual BERs of the demodulators are plotted along with the BER attained with selection. Fig. 10.12 shows Gram-Charlier performance in urban multipath and CCI. For the case of bursty errors, BER based on Gram-Charlier selection also outperforms the BER achievable by the individual demodulators by about 3-4 dB.

10.3.3 Selection Based on Parzen PDF Estimation

Here, selection of the individual demodulators is based on Parzen estimate for pdfs, where a training sequence is used to isolate the decision statistic samples associated with the +1 bits (and consequently the -1 bits also). The BER of each demodulator is estimated by calculating the area under the pdf to left of the decision threshold (i.e., the area corresponding to those bits in error). The individual demodulator output with the lowest BER (over the observation interval, or training sequence) is selected. The case of urban multipath and AWGN is illustrated by Fig. 10.13, where the individual BERs of the demodulators are plotted along with the BER attained with selection. Fig. 10.14 shows Parzen performance in urban multipath and CCI. For the case of bursty errors, BER based on Parzen selection also outperforms the BER achievable by the individual demodulators.

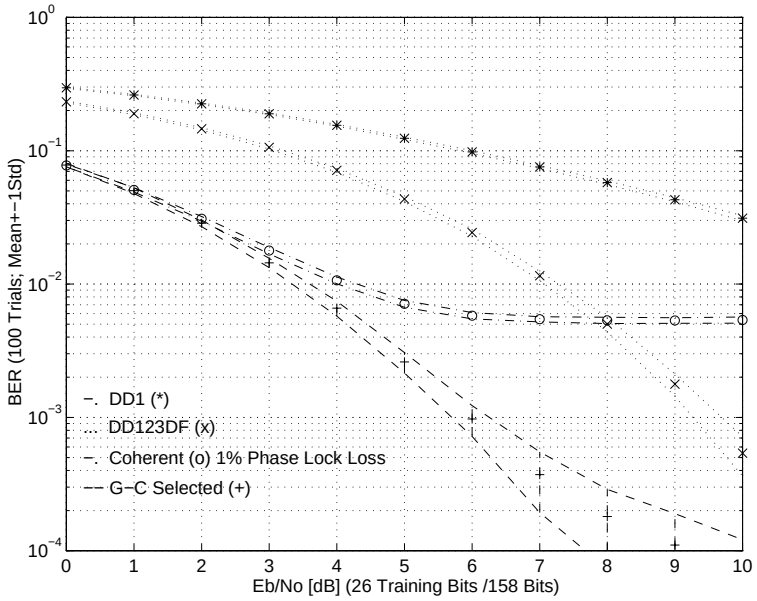

Figure 10.11: Coherent & DD123DF measured and Gram-Charlier-based selection BER vs. AWGN in urban multipath

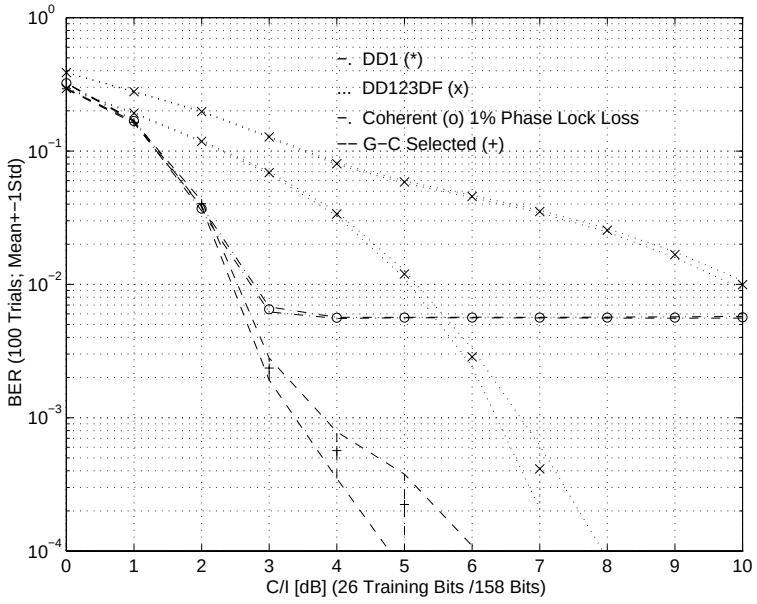

Figure 10.12: Coherent & DD123DF measured and Gram-Charlier-based selection BER vs. CCI in urban multipath

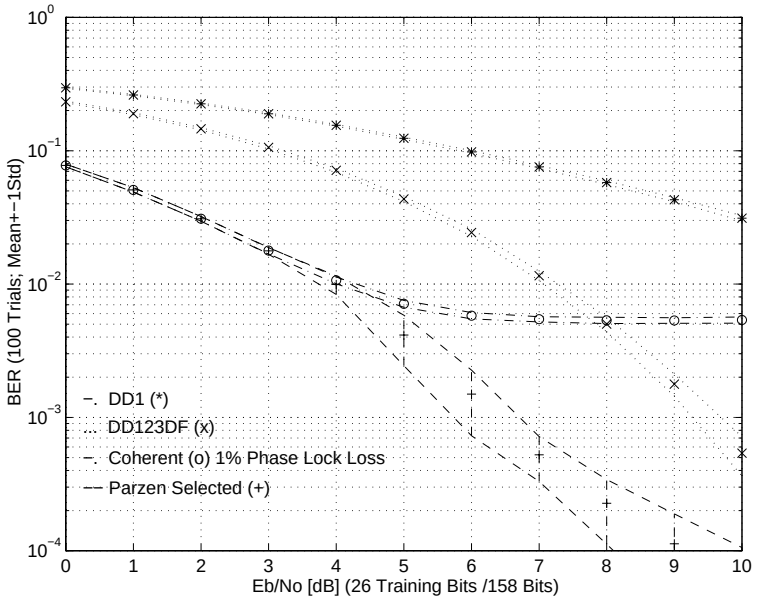

Figure 10.13: Coherent & DD123DF measured and Parzen BER-based selection vs. AWGN in urban multipath

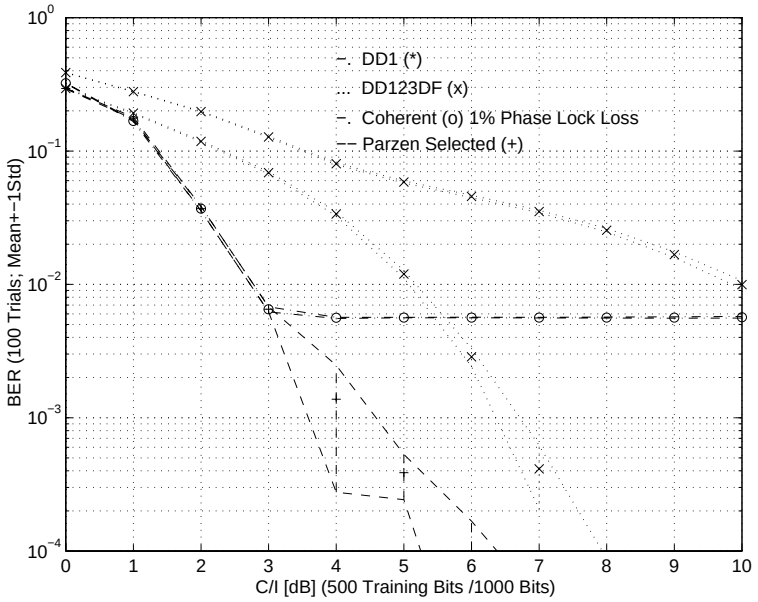

Figure 10.14: Coherent & DD123DF measured and Parzen BER-based selection vs. CCI in urban multipath

10.4 Demodulator Diversity with Coherent and Non-coherent Combination by Adaptive Weighting

Adaptive combining of the demodulator outputs to reduce interference is the next task in the dissertation research. The demodulator outputs are multiplied by some weight vector which will be adapted using the training sequence for each burst or over several bursts. Figures 8.1 and 10.1 provide a general block diagram of the receiver diversity scheme. By adaptive combining, a structure is created that is optimum for most channel impairments and achieves a lower BER than any of the individual demodulators could provide. An adaptive filter is a mechanism for optimal combining.

In this section, we first examine the BER surfaces produced by adaptive weighting. Secondly, adaptive weighting of demodulator outputs is compared to simple selection of the outputs, using a training sequence. Combining based on minimizing the Parzen-based BER estimator is used as an example to illustrate the improvements possible. Since MSE is commonly used as an adaptation criterion, we include MSE results here as a comparison. The following results again are based on simulations where a coherent demodulator is combined with a 123DF differential demodulator in a demodulator diversity scheme. The outputs of the demodulators are weighted. A phase lock loss of 1% of the time is chosen because it is reasonable figure for wireless environments and it results in a coherent demodulator BER performance between 10^{-3} and 10^{-2} (the BER range of interest throughout these simulations, consistent with the GSM specifications as found in Tables 11.1 and 11.2). The wireless channel modeled consists of urban multipath (generated by SMRCIM) in AWGN and also in CCI. The CCI case also includes AWGN with an $E_b/N_o = 20$ dB.

For adaptive weighting, real decisions are be used with real weights (complex decision statistics could also be used with complex weights). In addition, the outputs of the demodulators should be consistent, that is, they ought to have the same bit stream information (e.g., if the output of one demodulator is be differentially encoded, then the output the other demodulator should be differentially decoded).

10.4.1 Parzen BER Surfaces by Adaptive Weighting

In this section, we show that adaptive weighting of demodulator outputs can yield a *lower* BER than the BER attainable by any individual demodulator. BER surface plots are generated to illustrate the improvement possible with adaptive combining of demodulators in a demodulator diversity scheme. The second receiver diversity scheme is used which includes a coherent demodulator in combination with a DD123DF. Fixing E_b/N_o or C/I at some value (and using the fixed demodulator outputs), the two real weights are varied so as to form a two-dimensional grid. Surface plots are generated to illustrate typical bit error performance surfaces encountered with a demodulator diversity scheme using Parzen-based BER estimation. Real weights are used to facilitate visualization of the surfaces. Two cases are considered in urban multipath with AWGN and CCI - (1) when the BERs of the demodulators are nearly the same and (2) when the BERs of the

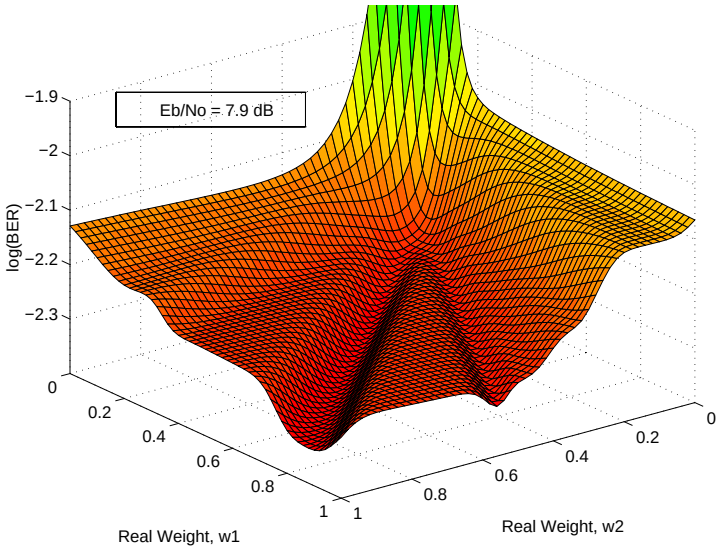

Figure 10.15: Parzen BER vs. Weights for Coherent & DD123DF Combo in SMRCIM urban multipath with AWGN (same BER)

demodulators are different by about an order of magnitude.

BERs Nearly the Same

Here are examples of surface plots in SMRCIM [241] urban multipath with AWGN and CCI where the BERs of the demodulator are virtually the same. The SMRCIM parameters are documented in Appendix B. In urban multipath with AWGN as shown in Fig. 10.15, the BERs of both the coherent demodulator (with weight w_1) and the DD123DF (with weight w_2) are 0.008 at an $E_b/N_o = 7.9$ dB. The combination yields a minimum BER of 0.004 where the weight vector $[w_1\ w_2]$ is [0.84 0.96]. In urban multipath with CCI as shown in Fig. 10.16, the BERs of both the coherent demodulator and the DD123DF are 0.006 at an $C/I = 5.8$ dB. The combination also yields a minimum BER of 0.004 where the weight vector is [0.44 0.40]. This minimum BER is lower than could be achieved by either of the demodulators by themselves in both AWGN and CCI, showing that receiver diversity improves performance (here, for example, by a factor of about two).

In Fig. 10.17, the BER surface for the urban multipath with AWGN case ($E_b/N_o =$ 7.9 dB) is plotted along with a plane denoting the lowest BER achieved by an individual demodulator (in this case, 0.008 or -2.1 dB). In this example, about 87% of the weight combinations yield BERs that are better (i.e., lower) than that of the best individual demodulator. The same is true for urban multipath with CCI ($C/I = 5.8$ dB), as shown in Fig. 10.18, where about 76% of the weight combinations yield BERs that are

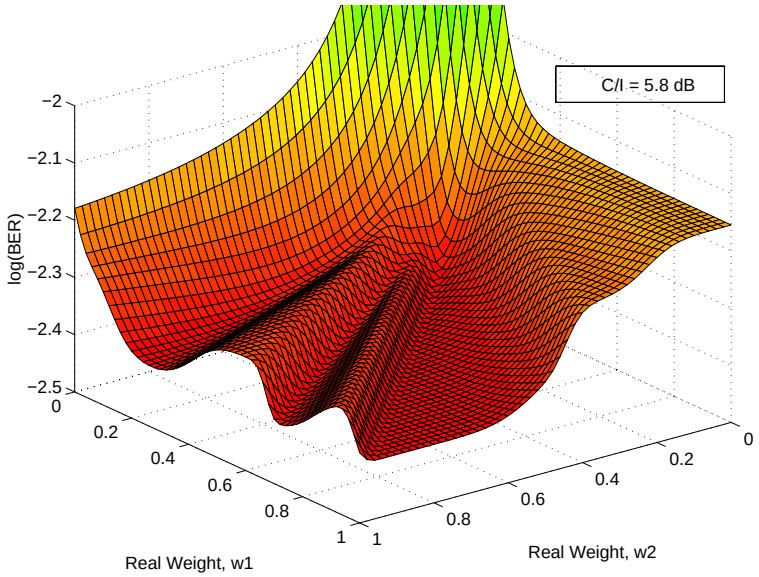

Figure 10.16: Parzen BER vs. Weights for Coherent & DD123DF Combo in urban multipath with CCI (same BER)

better than that of the best individual demodulator. Both of these cases emphasize the improved performance made possible by demodulator diversity.

BERs Different by an Order of Magnitude

Here are examples of surface plots in urban multipath with AWGN and CCI where the BERs of the demodulators are very different (e.g., by an order of magnitude). In urban multipath with AWGN as shown in Fig. 10.19, the BER of the coherent demodulator is about 0.006 and the BER of DD123DF is about 0.078 at $E_b/N_o = 4$ dB. In case, the best performance is achieved by a selection of the best demodulator where the weight vector $[w_1\ w_2]$ is [1 0], with a BER of about 0.006. In urban multipath with CCI as shown in Fig. 10.20, the BER of the coherent demodulator is about 0.028 and the BER of DD123DF is about 0.155 at $C/I = 2$ dB. In case also, the best performance is achieved by a selection of the best demodulator where the weight vector $[w_1\ w_2]$ is [1 0], with a BER of about 0.028.

10.4.2 Weighting Based on MSE

The weighted outputs of the coherent demodulator and differential demodulator are adapted (over the observation interval) to attain a lower BER by using the Method of Steepest Descent with the Parzen-based BER gradient derived in Section 8.3.4. For comparison, selection of the individual demodulators is also performed based on Mean

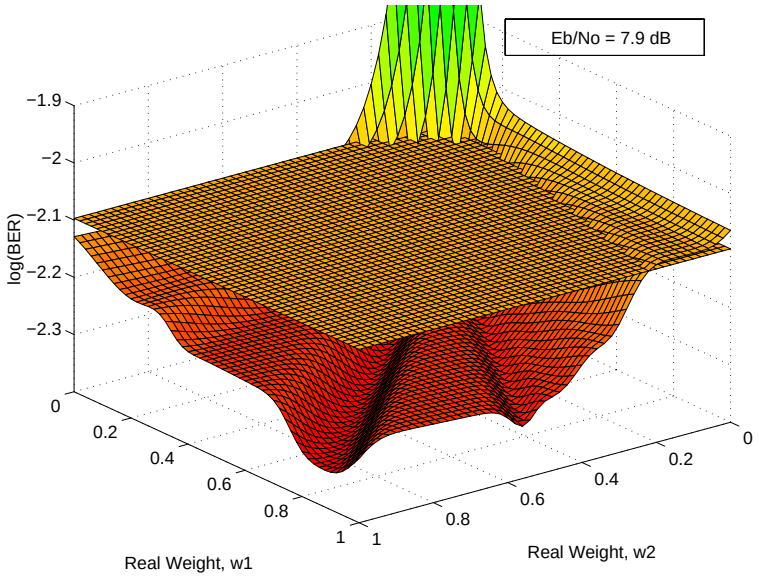

Figure 10.17: Parzen Combo BER and Best Individual BER vs. Weights in urban multipath with AWGN

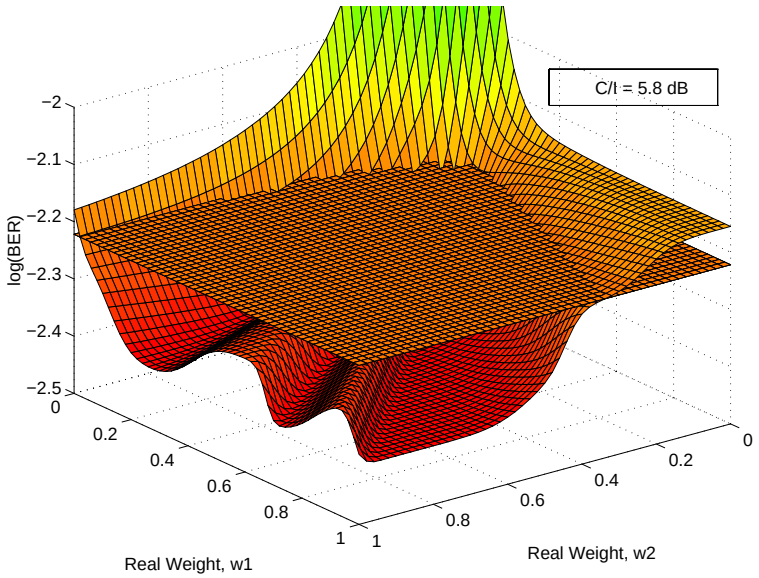

Figure 10.18: Parzen Combo BER and Best Individual BER vs. Weights in urban multipath with CCI

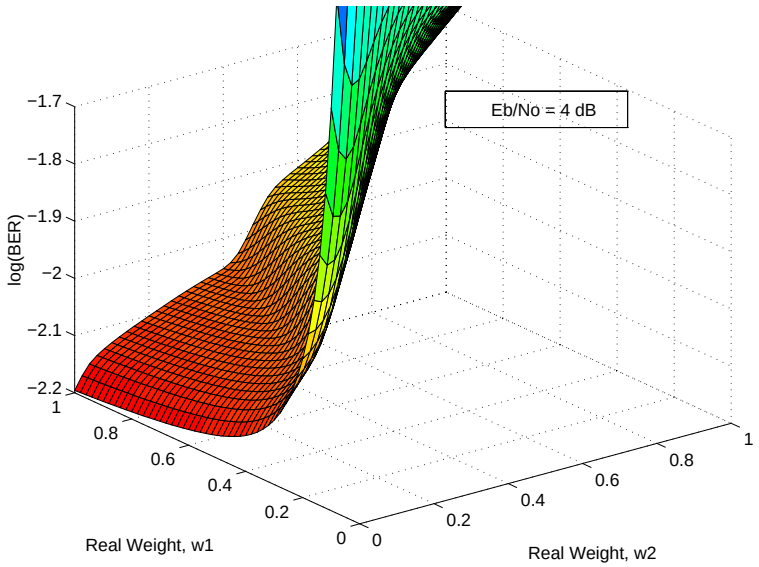

Figure 10.19: Parzen BER vs. Weights for Coherent & DD123DF Combo in urban multipath with AWGN (different BER)

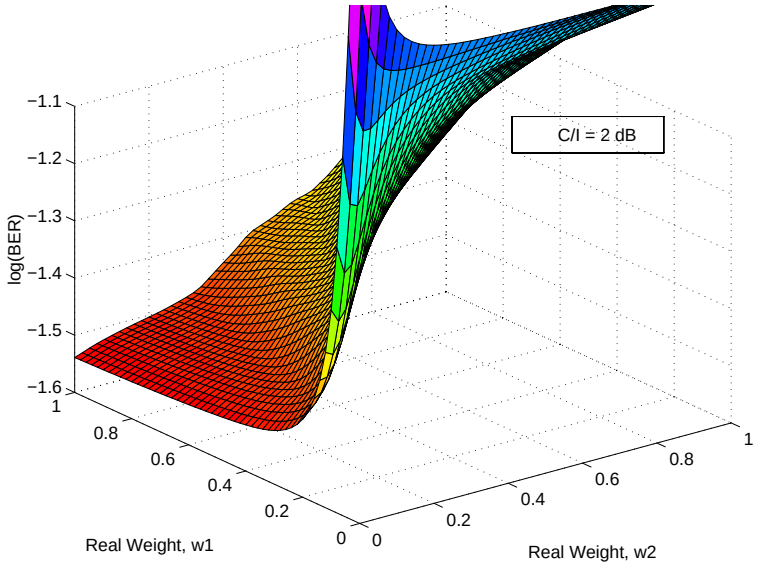

Figure 10.20: Parzen BER vs. Weights for Coherent & DD123DF Combo in urban multipath with CCI (different BER)

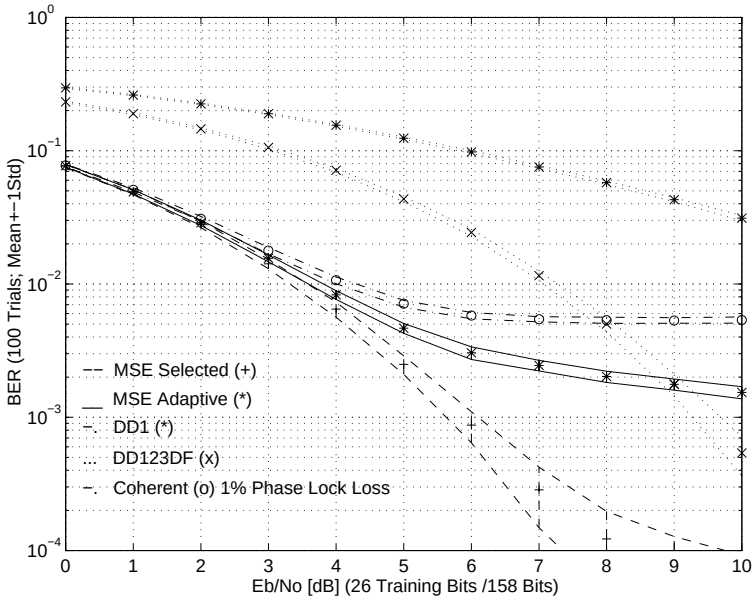

Figure 10.21: Coherent & DD123DF measured and MSE BER vs. AWGN in urban multipath

Squared Error (MSE), where a training sequence is used so that the corrupted data is compared to an expected reference value. The individual demodulator output with the lowest MSE (over the observation interval, or training sequence, indicated by the abscissa label) is selected.

The case of SMRCIM urban multipath and AWGN is illustrated by Fig. 10.21, where the individual BERs of the demodulators are plotted along with the BER attained with selection and also with adaptation based on MSE. Adaptation is performed by a normalized-LMS algorithm, and start-up transients are included in the length of the training sequence. Fig. 10.22 shows MSE performance in SMRCIM urban multipath and CCI. Here, MSE selection and adapation is performed using a GSM-type signaling format (refer to Figure 10.2), where 26-bit midamble of training bits is used to make decisions for the surrounding 158 bits. For the case of bursty errors, MSE selection outperforms MSE adaptation. This is because weight adaptation based on MSE cannot track the channel fast enough. For errors dispersed in time, the MSE will approaches the minimum individual demodulator BER, as shown in Section 10.2.1. These figures also illustrate how the lowest MSE (based on adaptation) does not always correspond to lowest BER.

10.4.3 Weighting Based on Parzen PDF Estimation

Using the gradient of the BER estimator (as given in Eqn. 8.11), the weights of the outputs of the coherent demodulator and differential demodulator are adapted (over

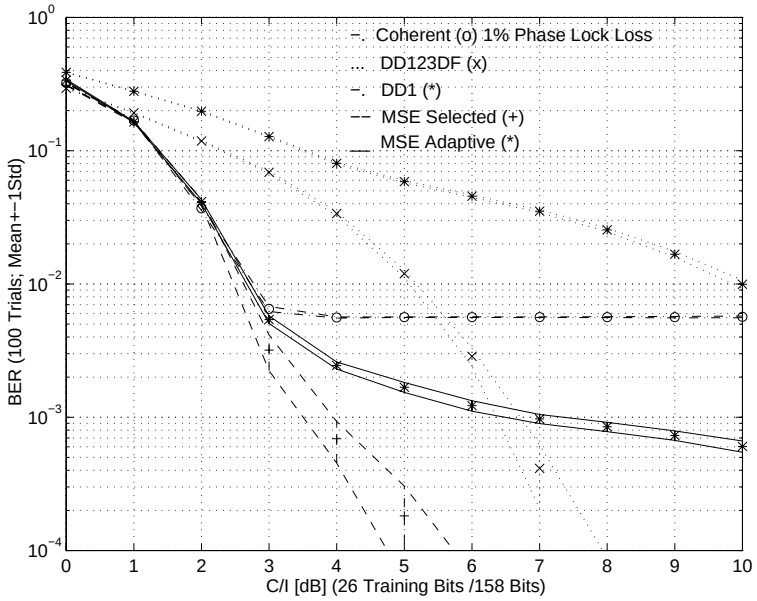

Figure 10.22: Coherent & DD123DF measured and MSE BER vs. CCI in urban multipath

the observation interval) to attain to the lowest BER. This is compared to using BER estimation based on Parzen's pdf estimator, where the individual demodulator output with the lowest estimated BER (over the observation interval) is selected. Parzen's estimator used as an example, instead of Gram-Charlier, because Parzen is more versatile and performs much better in interference environments than Gram-Charlier (even though Parzen's requires a longer training sequence).

In Figures 10.23 through 10.28, the individual BERs of the demodulators are plotted along with the BER attained with selection and also with adaptation based on Parzen's pdf estimator. Adaptation of Parzen-based BER estimation is performed using the gradient derived in Eqn. 8.11 along with the method of steepest descent. LMS-type adaptation algorithms cannot be used because of the nonlinear operation performed with Parzen estimation. The weights are allowed to converge (experience shows that the weights general converge rapidly for the training sequences used in these simulations). Gram-Charlier could be used for BER estimation in a receiver diversity scheme, but that is left as an area for further research.

In the following examples, we consider the case of bursty errors and also the case of errors dispersed in time, in an urban multipath channel with AWGN and CCI. Because Parzen's requires a longer training sequence, a 500 training bits are used to make decisions for the surrounding 15,000 bits. The bursty error case is modeled by the coherent demodulator losing phase lock for 1% for the time, where the phase lock loss occurs in bursts so that the majority of errors occur closely together in time. case where the errors

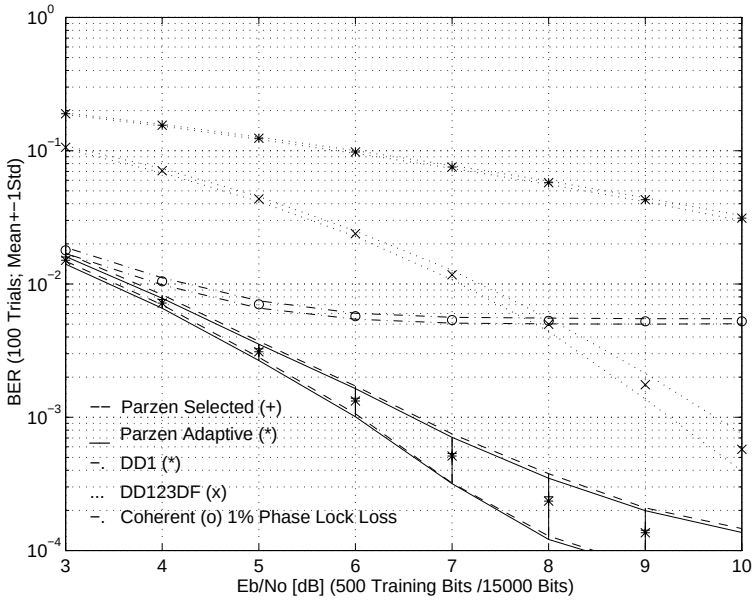

Figure 10.23: Coherent & DD123DF measured and Parzen BER vs. AWGN in urban multipath with error bursts

are dispersed in time is modeled for the time, but where the phase lock loss of errors do occur closely together in time).

Error Bursts

In the case of bursty errors (i.e., the majority of errors occurring together) in urban multipath and AWGN, Fig. 10.23 shows that selection performs as well as adaptation. In other words, for this demodulator diversity scheme in a channel with bursty errors, adapting the weighted demodulator outputs produces negligible improvement over that of simple selection of the individual outputs. The same is true for urban multipath in CCI, as shown in Fig. 10.24.

Fig. 10.23 and 10.24 also show that, in a wireless channel with urban multipath dominated by either AWGN or CCI, only about 500 training bits are needed to obtain good BER estimates.

Error Dispersed

In the case of dispersed errors (i.e., the errors occur randomly, dispersed in time) in urban multipath and AWGN, Fig. 10.25 shows that selection performs as well as adaptation (for certain levels of noise), *except* where the demodulators have comparable BER (e.g., $E_b/N_o \approx 7.9$ dB). In other words, for this demodulator diversity scheme in a channel with dispersed errors, adapting the weighted demodulator outputs *improves* performance

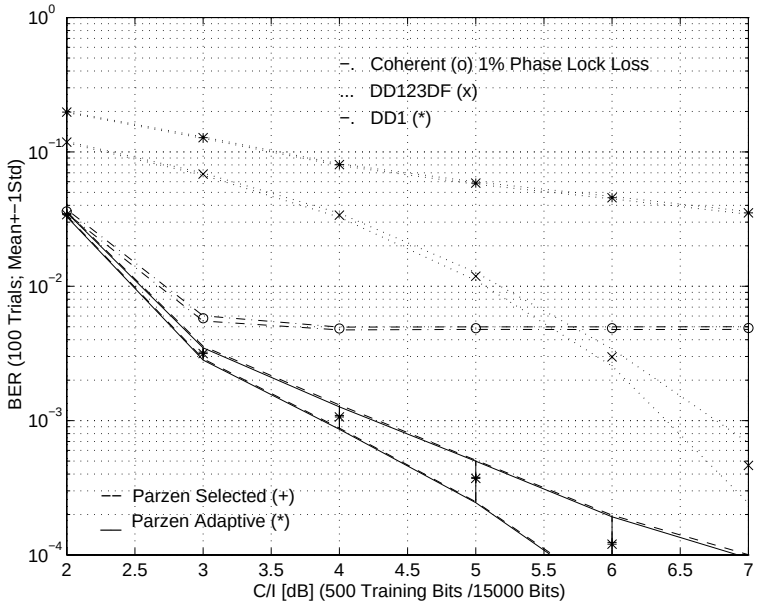

Figure 10.24: Coherent & DD123DF measured and Parzen BER vs. CCI in urban multipath with error bursts

when individual BERs are about the same, over that of simple selection of the individual outputs. The same is true for urban multipath in CCI where the demodulators have comparable BER (e.g., $C/I \approx 5.8$ dB), as shown in Fig. 10.26.

This is an important result because it illustrates that a combination of weighted outputs in a demodulator diversity scheme can yield superior performance to that of any of the individual demodulators used in the diversity scheme. The performance gain is about 1 dB, which is small, but the point here is to provide proof-of-concept that gains are achievable with receiver diversity schemes. One might expect that the best a receiver diversity scheme could do is provide the performance of the best demodulator in a given channel environment, but this gain demonstrates that receiver diversity can yield superior performance. Fig. 10.25 and 10.26 also show that, in a wireless channel with urban multipath dominated by either AWGN or CCI, only about 500 training bits are needed to obtain good BER estimates. In Fig. the use of a training sequence of 1000 bits (instead of 500) yields slight improvement.

10.5 Summary

In this chapter, the concept of demodulator diversity is validated by simulations. Demodulator diversity using real-time BER estimation is a new concept which has been investigated very little in the literature. This approach constitutes a major contribution to the field of communications. First of all, a demodulator diversity scheme using the

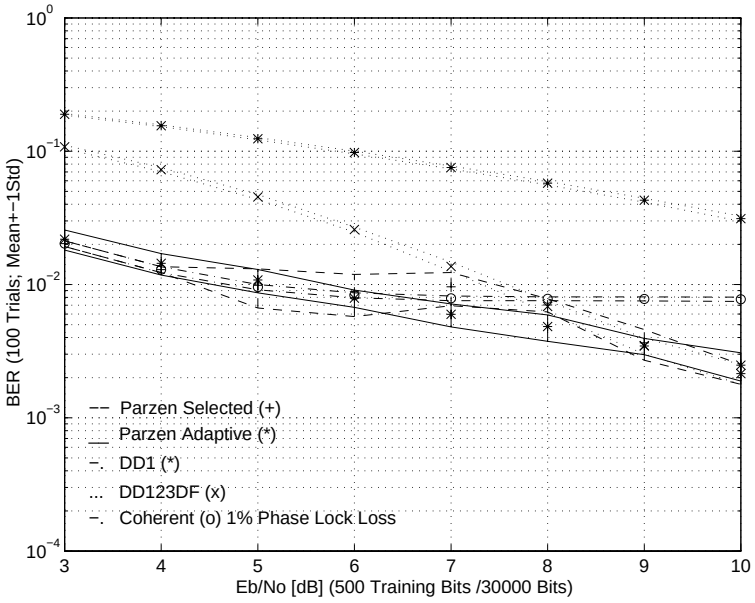

Figure 10.25: Coherent & DD123DF measured and Parzen BER vs. AWGN in urban multipath with error dispersed

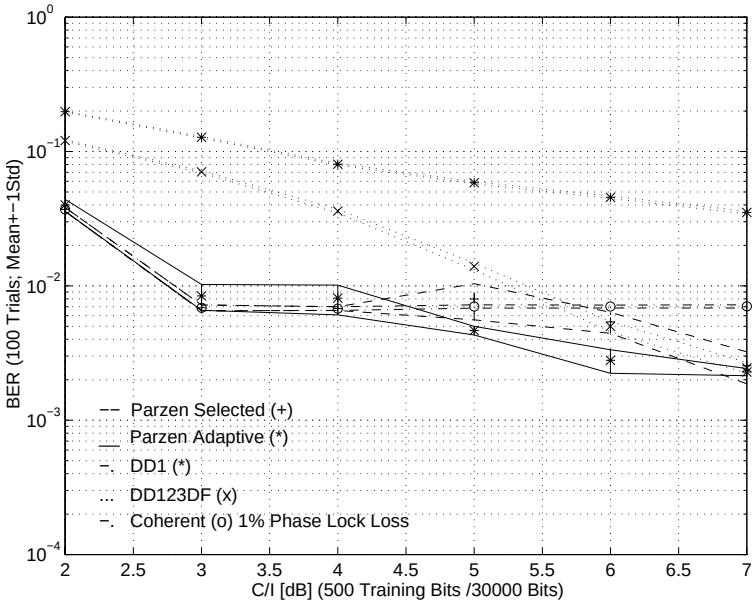

Figure 10.26: Coherent & DD123DF measured and Parzen BER vs. CCI in urban multipath with error dispersed

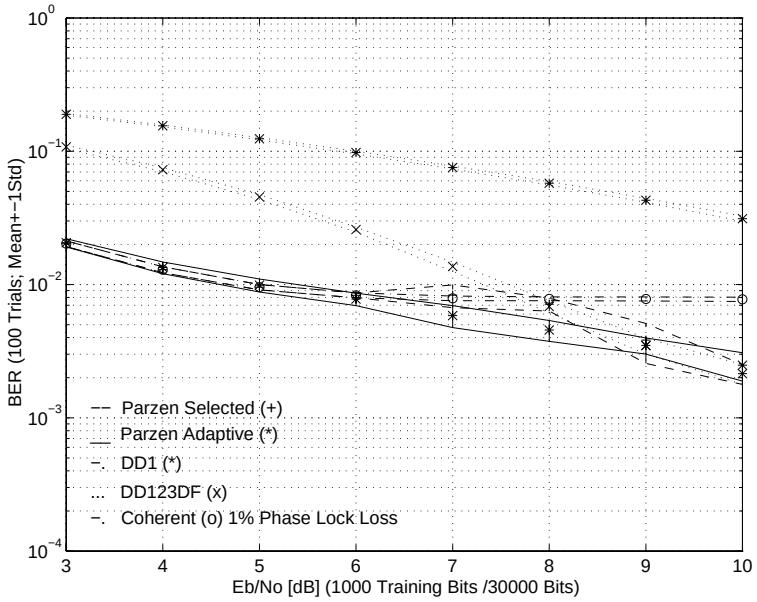

Figure 10.27: Coherent & DD123DF measured and Parzen BER vs. AWGN in urban multipath with error dispersed (1000 bit training sequence)

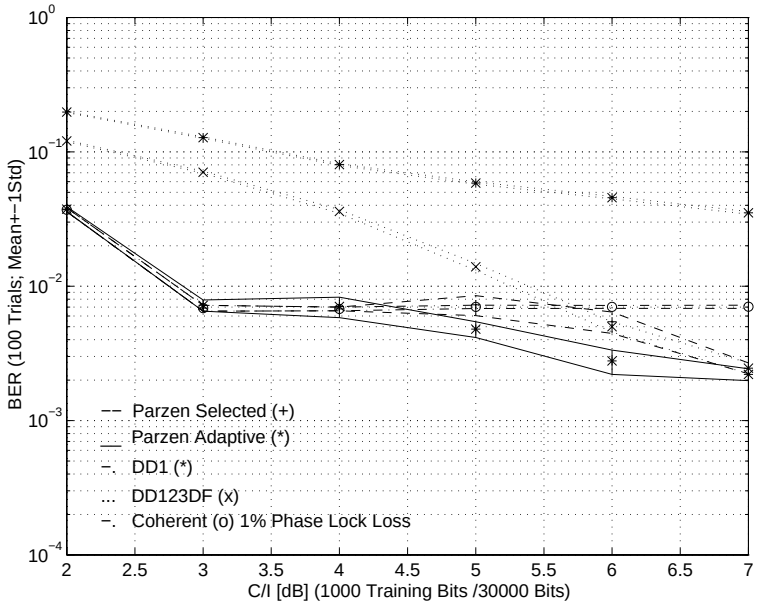

Figure 10.28: Coherent & DD123DF measured and Parzen BER vs. CCI in urban multipath with error dispersed (1000 bit training sequence)

three best noncoherent demodulators (from Chapter 5) is considered where a MSE-based criterion is used to adaptively select the best demodulator based on a given observation interval (or training sequence). Secondly, a demodulator diversity scheme using a coherent demodulator and a noncoherent demodulator is considered, where an MSE-based criterion is compared to Gram-Charlier BER-based criterion and Parzen BER-based criterion. In this second scheme, the demodulator outputs are adaptively selected and then adaptively weighted and combined by Parzen BER-based criterion. the best performance of the individual demodulators for a given channel environment.

In the first demodulator diversity scheme, a limiter discriminator (which has performance comparable within 1 dB to a one-bit differential demodulator) is used as a baseline for comparison of demodulators. The one-bit DF, two-bit DF, three-bit differential demodulator with DF and combined outputs (DD123DF) is a form of demodulator diversity and outperforms the limiter discriminator in AWGN, in CCI, and in various multipath environments. In the second demodulator diversity scheme, a one-bit differential demodulator is used as a baseline for comparison of demodulators. The DD123DF is shown to outperform the one-bit differential demodulator in urban multipath with AWGN and CCI.

Section 10.4.1 of Chapter 10 provides surface plots of the Parzen-based BER cost function vs. weights for two cases of urban multipath with AWGN and CCI - (1) when the BERs of the demodulators are nearly the same and (2) when the BERs of the demodulators are different by about an order of magnitude. The plots show that many weight combinations can yield overall BERs *less* than the BER of the best individual demodulator. Section 10.4.3 of Chapter 10 demonstrates performance improvements possible with a demodulator diversity scheme using Parzen-based BER estimation, by considering the cases where errors tend to occur in bursts (with gains of 3-4 dB) and where errors tend to be randomly dispersed (with gains of 1 dB). MSE-based and BER-based selection and weighting produce results superior to that of the individual demodulators (up to 3-4 dB greater). These techniques are inexpensive and can be easily implemented at the mobile with the use of a Q-function look-up table. The chapter justifies the concept of demodulator diversity by demonstrating that a demodulator diversity schemes can yield substantial gains in performance over individual receivers in typical wireless channels.

Chapter 11

System Performance in GSM

11.1 Motivation

This chapter examines the issues relating to system performance needed to evaluate the impact of interference rejection techniques utilizing BER-based demodulator diversity. Little research has been published on the impact of interference rejection techniques on actual system performance, in general. An understanding of issues which influence system performance will lead to performance measures and criteria which can facilitate the comparison of newer demodulation techniques to conventional demodulators. Such measures allow an evaluation of the impact of receiver diversity and real-time BER estimation on overall system performance.

This chapter demonstrates that BER-based demodulator diversity can increase the probability of coverage and decrease the impact of co-channel interference. Section 11.5.2 illustrates how a BER-based demodulator diversity scheme can potentially allow a frequency reuse factor of $N = 4$ to be employed, instead of $N = 7$ with no degradation in performance. Consequently, BER-based demodulator diversity can significantly increase overall capacity by combatting the effects of interference (accommodating more subscribers in the limited spectral resources) in a cellular system. In addition, the techniques may be used to provide better quality in the mobile phone (though minimum acceptable quality is usually the goal of the service provider). The signal format for GSM will be used as a basis for comparison. The investigation of the impact of BER-based demodulator diversity techniques on GMSK and GSM is a new area of research.

To satisfy the demand arising with the dramatic growth of present communication systems and to minimize channel interference, frequency reuse techniques are applied. However, it is impossible to provide an interference-free system. Radio-frequency (RF) interference is an important performance consideration in the design, operation, and maintenance of mobile communication systems. Several types of interference can be identified in mobile radio systems - adjacent-channel interference (ACI), co-channel interference (CCI), intermodulation interference, and intersymbol interference.

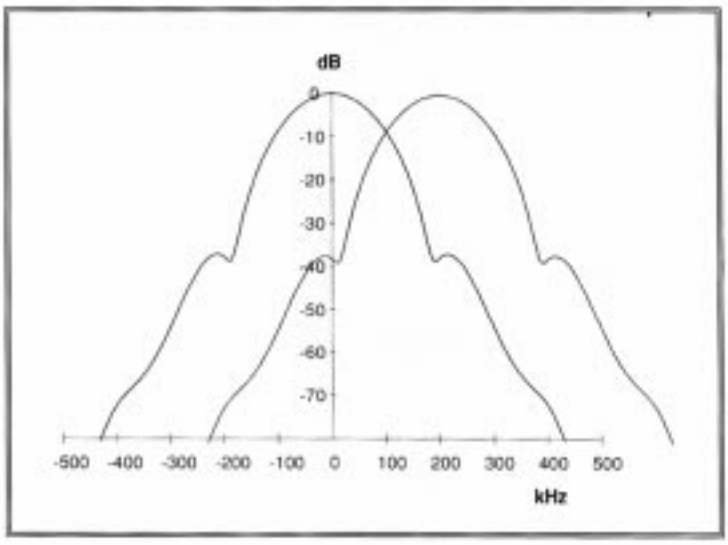

Figure 11.1: GMSK modulation spectrum in GSM for two adjacent central frequencies separated by 200 kHz.

11.2 Types of Interference

ACI is generated by neighbors cells which operate at different carrier frequencies. ACI can be significant in GSM because of spectral overlap between adjacent channels, as illustrated in Figure 11.1. Figure 11.1 shows the theoretical GMSK modulation spectrum (calculated by assuming an infinite random sequence of modulating bits) in GSM, where two adjacent channel frequencies are separated by 200 kHz. The significant overlap is not negligible, but this source of interference can be limited by careful frequency planning, which aims at separating geographically the usage of adjacent frequencies [169].

Intermodulation interference is generated in a nonlinear circuit, where the product of two or more signals results in signals with frequencies which interfere with frequency of the desired signal. The power amplifier of the transmitter and the first frequency converter of the receiver typically produce this kind of interference. Usually, this type of interference can be filtered out, but sometimes nonlinear characteristics can result in non-negligible intermodulation interference [96].

Intersymbol interference is intrinsic to digital networks and is a direct consequence of the limited bandwidth of the transmission medium and/or multipath. As ideal square pulses (with infinite bandwidth) are filtered to meet bandwidth specifications, the pulses (or symbols) are spread in time, interfering with one another. Intersymbol interference (ISI) results from the premodulation Gaussian filtering characteristic of GMSK. ISI also results from channel impairments such as multipath propagation which also causes a spreading of the symbols. In addition, at the receiver, ISI results from bandpass filtering

at RF and IF. GSM requires that demodulation algorithms must be able to cope with two multipaths of equal power received at an interval (or delay spread) of up to 16 μs (i.e., about four bit periods at GSM data rates). In such as situation, the amount of ISI is dramatically increased compared to what is introduced by the modulation itself.

Equalization is required to cope with ISI. An equalizer seeks to equalize the pulse distortion by undoing the ISI. Filter ISI is somewhat fixed, but channel ISI is dynamic, requiring adaptive equalization (where the GSM training sequences can be used to adapt the equalizer) . Equalization is an active area of research, and many types of equalization can be employed. One popular method in GSM uses the Viterbi algorithm, a maximum likelihood technique which finds the most probable emitted sequence, taking in account some assumptions on the possible signals and on the noise statistics [169].

Co-channel interference is the bottleneck for channel capacity in current mobile phone systems. CCI results from distant cells which utilize the same frequencies. The frequency reuse factor is calculated as a function of acceptable CCI, and the determined geographical separation is assumed to sufficiently mitigate CCI. This is not always the case practically, since cell boundaries tend to be amorphous. As cells become smaller and the frequency reuse factor increases, CCI becomes more significant. GSM states that system performance ought to be acceptable down to a $C/I = 9$ dB, but practically this value is more around $C/I = 12$ dB [56].

11.3 Co-channel Interference

The main focus of this chapter is on the impact of co-channel interference on GSM system performance, because co-channel interference tends to be the bottleneck for channel capacity. In GSM, for example, the primary band includes two subbands of 25 MHz each, 890-915 MHz (on the reverse link) and 935-960 MHz (on the forward link). A 10 MHz extension raises the primary band to 880-915 MHz and 925-960 MHz (i.e., twice 35 MHz). DCS1800 (a PCS extension of GSM) includes two domains at 1710-1785 MHz and 1805-1880 MHz (i.e., twice 75 MHz). The central frequencies of the frequency slots are spread evenly every 200 kHz within these bands, starting 200 kHz away from the band borders. 124 different frequency slots are therefore defined in 25 MHz and 374 in 75 MHz [169]. Because of ACI, the normal practice is not to use the border frequency slots (numbered 0 and 124), limiting the number of frequency slots to 122 in 25 MHz.

Frequency reuse is typically applied to accommodate more users in the same area. For seven-cell frequency reuse, these 122 frequency channels are assigned to seven-cells, yielding about 17 frequency channels per cell. Four-cell reuse yields about 30 frequency channels per cell. The RF channels can be reused in the same region as long as the reuse (or co-channel) cells are separated by enough distance to avoid CCI. If the size of each cell in a cellular system is roughly the same, CCI is independent of the transmitted power and becomes a function of the radius of the cell (R), and the distance to the center of the nearest co-channel cell (D). By increasing the ratio of D/R, the spatial separation between co-channel cells relative to the coverage distance of a cell is increased. Using a

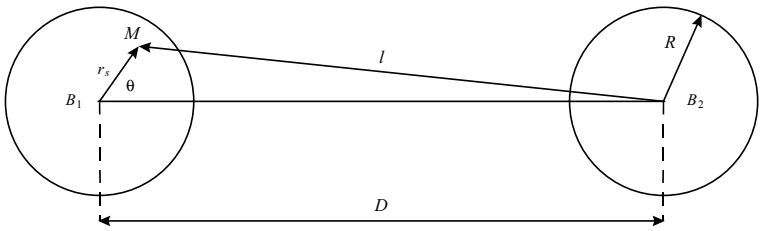

Figure 11.2: Illustration of co-channel interference for a mobile station

cellular hexagonal geography, The co-channel reuse ratio Q is defined as [202]

$$Q = \frac{D}{R} = \sqrt{3N} \tag{11.1}$$

where N is the reuse number satisfying the equation [202]

$$N = i^2 + ij + j^2 \tag{11.2}$$

for positive integers i and j. Clearly, N can be 3, 4, 7, 12, 19, etc. for different combination of i and j.

A smaller value of Q provides larger capacity since the reuse factor N is small, but the transmitting quality is affected. A larger value of Q improves the transmission quality, due to the smaller level of co-channel interference, but the channel capacity becomes limited. A trade off must be made between these two objectives in actual cellular design.

Measurements [202] have shown that at any value of d, the received power $P(d)$ at a particular location is distributed log-normally (normal in dB) about the mean distance value, that is,

$$P(d) = P_o - 10n \log_{10}\left(\frac{d}{d_o}\right) + X_\sigma, \tag{11.3}$$

where X_σ is a zero-mean log-normally distributed random variable with standard deviation σ, P_o is the power received at a close-in reference point in the far field region of the transmitting antenna at a distance of d_o from itself, and n is the path loss exponent. Eqn. 11.3 is used in this chapter to model the carrier and the interference in the C/I ratio [95].

Fig. 11.2 illustrates how co-channel interference is introduced into a mobile station. When the mobile moves in its service cell B_1, it receives the signal from the desired base station B_1, but it also receives an interfering signal from its co-channel cell B_2.

Let $CIR = 10 \log_{10} C/I$, where C is the local mean of the carrier to noise ratio for the desired signal and I is the local mean of the carrier-to-noise ratio for the interfering signal. Since both C and I are zero-mean log-normally distributed, the distribution of the CIR will also be log-normal, with mean μ and standard deviation σ. The probability

of cochannel interference can also be interpreted as an outage probability or blocking rate. In GSM, the tolerable blocking probability is approximately 2%.

Let the mobile be located at (r_s, θ). Assuming uniform usage in a cell, the pdfs of r_s and θ are independent of each other. The average CIR coverage over the desired cell (base station B_1) for the mobile station, $p(CIR > CIR_o)_{MS}$, is then [95]

$$p(CIR > CIR_o)_{MS} = \frac{1}{\pi R^2} \int_0^{2\pi} \int_0^R Q\left(\frac{CIR_o - \left(K - 10n \log_{10} \frac{r_s}{\sqrt{3NR^2 + r_s^2 - 2\sqrt{3N} R r_s \cos\theta}} \right)}{\sigma} \right) r_s \, dr_s \, d\theta \tag{11.4}$$

where $K = -10 \log_{10} n_c$ is a constant related to the number of interfering sources, r_s and l are the distance between the mobile unit to the desired base station and to the interfering base station, respectively, n_c is the number of active cochannel cells, and Q represents the Q-function. The same path loss exponent n is assumed for the desired signal and the interference, and all the interfering sources are assumed to have the same power.

Eqn. 11.4 has been numerically computed for different cell reuse patterns, $N = 7$ and $N = 3$ with $K = 0$ dB, and the resulting graphs are provided as a function of the threshold CIR_o in [95] (where the path loss exponent n is 3.6 and log-normal shadowing power deviation σ is 8 dB – values corresponding to a suburban area). The figures found in [95] also include the worst case CIR coverage, where it is assumed $r_s = R$ and $l = D - R$. It is shown in [95] that the seven-cell reuse pattern provides a mobile station higher CIR coverage than the three-cell reuse pattern. For example, when $CIR_o = 18$ dB, the average CIR coverage drops from 91% for the seven-cell reuse pattern to 72% for the three-cell reuse pattern. It is also noted that the CIR coverage for a three-cell reuse pattern decreases faster for increasing CIR_o than that of the seven-cell reuse pattern.

The co-channel interference introduced at a base station is defined differently than that of the mobile station. As shown in Fig. 11.3, base station B_1 not only receives signals from its desired mobile M_1, but also from M_2 which is in a co-channel cell B_2. The distance from B_1 to M_1 is r_s and from B_1 to M_2 is l. The location of the interfering

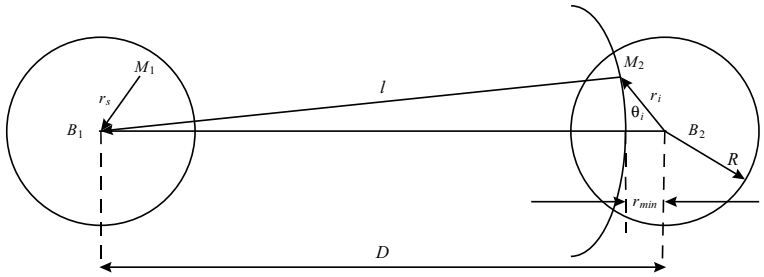

Figure 11.3: Illustration of co-channel interference for a base station

signal (r_i, θ_i) is statistically independent from the location of the desired mobile. The value of r_i varies from r_{min} to R, where $r_{min} = |D - l|$.

Now, the percentage of average CIR coverage over the cell for basestation B_1, $p(CIR > CIR_o)_{BS}$, is

$$p(CIR > CIR_o)_{BS} = \int_0^R \int_{D-R}^{D+R} \frac{2r_s}{\pi R^4} Q\left(\frac{CIR_o - K + 10n\log_{10}(r_s/l)}{\sigma}\right) \left(\int_{r_{min}}^{R} \left|\frac{l}{\pm Dr_i\sqrt{1-\left(\frac{D^2+r_i^2-l^2}{2Dr_i}\right)^2}}\right| dr_i\right) dr_s\, dl \qquad (11.5)$$

Eqn. 11.5 is numerically computed for different cell reuse patterns $N = 7$ and $N = 3$ with $K = 0$ dB in [95]. The worst case CIR coverage where $r_s = R$ and $l = D - R$ is also computed and plotted in the corresponding figures in [95]. The seven-cell reuse pattern provides a base station higher CIR coverage than the three-cell reuse pattern. For example, when $CIR_o = 18$ dB, the average CIR coverage drops from 89% for the seven-cell reuse pattern to 70% for the three-cell reuse pattern. In addition, the CIR coverage for three-cell reuse pattern decreases faster when CIR_o increases than in the case of the seven-cell reuse pattern. This result is the same as for the mobile station case.

To compare the percentage of CIR coverage for a base station and for a mobile station, both cases are plotted in [95] for $N = 7$ and $N = 3$. The CIR coverage for a base station is slightly lower than that for a mobile station. The comparison is based on the assumption that both the base station and the mobile station receive single co-channel interference in addition to the desired signal. The average signal strength of the interfering signal only depends on the location of the desired mobile for a mobile station case, while the signal strength of the interfering signal is independent of the desired mobile location for the base station case. For the base station case, the interfering mobile has random locations when compared to the desired mobile, thus it introduces more interference on average. Consequently, the percentage of average CIR coverage for a base station is generally slightly lower than that for a mobile station.

11.4 GSM Receiver Specifications

Radio propagation in the mobile radio environment is described by highly dispersive mulitpath caused by reflection and scattering. The paths between base station and mobile station (MS) may be considered to consist of large reflections and/or scatterers some distance to the MS, giving rise to a number of waves that arrive in the vicinity of the MS with random amplitudes and delays. Close to the MS, these paths are further randomized by local reflections or diffractions. Since the MS will be moving, the angle of arrival must also be taken into account, since it affects the doppler shift associated

with a wave arriving from a particular direction. Echos of identical delays can be viewed as arising from reflectors located on an ellipse.

11.4.1 GSM Propagation Models

An introduction to the COST 207 models used to model multipath in previous simulations is given in Appendix C. Various multipath environments have been simulated, including urban, hilly urban, hilly, and rural environments. For noise-dominated channels, AWGN has been added with E_b/N_o varied. For interference-dominated channels, CCI has been added with C/I varied.

This section aims at specifying the receiver performance based on GSM specifications [72], assuming that transmitter errors do not occur or are taken into account separately. In the case of the base transceiver stations (BTS), the values apply for measurement at the connection with the antenna of the BTS, including any external multicoupler. All the values given are valid whether or not any of the features, such as discontinuous transmission (DTx), discontinuous reception (DRx), or slow frequency hopping (FH) are used. The received power levels under multipath fading conditions given are the mean powers of the sum of the individual paths.

11.4.2 Nominal Bit Error Rates

GSM specifications require nominal bit error rates, which are error rates in nominal conditions (i.e., without interference and with an input level of 20 dB above the reference sensitivity level [72]). For example, under the following propagation conditions, the chip error rate - equivalent to the bit error rate of the non-protected bits (on TCH/F, class II, where TCH stands for traffic channel, F is full rate, and class II is a classification of priority for bits) - shall have the following limits:

static channel:	BER 10^{-4}
EQ50:	BER 3%

where EQ50 denotes the equalization test for a mobile velocity of 50 km/hr. This performance shall be maintained up to -40 dBm input level for static and multipath conditions. Furthermore, for static conditions, a bit error rate of 10-3 shall be maintained up to -15 dBm for GSM900 (-23 dBm for DCS1800).

The receiver sensitivity performance is specified in Table 11.1 in terms of frame erasure, bit error, or residual bit error rates, according to the type of channel and the propagation condition. The actual sensitivity level is defined as the input level for which this performance is met. The actual sensitivity level shall be less than a specified limit called the reference sensitivity level. The reference sensitivity level shall be:

for GSM 900 small MS:	-100 dBm
for other GSM 900 MS and normal BTS:	-102 dBm
for DCS 1800 MS:	-104 dBm

The specifications above for BTS shall be met when the two timeslots adjacent to the timeslot of interest are detecting valid GSM signals at 50 dB above the power on the timeslot of interest. For the MS, the specifications shall be met with the two adjacent timeslots are 20 dB above the timeslot of interest and the static channel.

In Table 11.1, FACCH is the Fast Associated Control Channel, H stands for half rate transmission, F stands for full rate transmission, SDCCH is the Standalone Dedicated Control Channel, and RACH is the Random Access Channel. Traffic channels (TCH) carry 9.6, 4.8, 2.4 kbps data rates. Traffic channel data is divided into classes of priority (i.e., class Ib and II). TU50 denotes a typical urban environment with mobile velocity at 50 km/hr. TH50 stands for typical hilly environment. RA stands for rural area, and HT denotes hilly terrain.

The reference interference performance (for CCI or ACI) is specified in Table 11.2. The actual interference ratio is defined as the interference ratio for which this performance is met. The actual interference ratio shall be less than a specified limit called the reference interference ratio. The reference interference ratio, for base stations (BTS) and all types of mobile stations (MS), shall be:

for CCI	9 dB
for ACI (200 kHz offset)	-9 dB
for ACI (400 kHz offset)	-41 dB
for ACI (600 kHz offset)	-49 dB

These specifications apply for a wanted signal level of 20 dB above the reference sensitivity level, and for a random, continuous, GSM-modulated interfering signal.

11.4.3 Minimum C/I Ratio

This section summarizes a discussion of carrier-to-interference ratios (C/I) in GSM [169]. C/I ratios follow some statistics, which are best visualized by showing their cumulative distributions, as illustrated in Figure 11.4 [169]. The C/I cumulative distribution in a given cell depends on the locations of the mobile stations in communication with base station, and on the locations of the interfering sources; hence it depends on cellular planning and on frequency reuse. Some objective must be put on the minimum C/I in order to ensure an acceptable quality of service to subscribers. This objective can be expressed as forbidden areas in the cumulative distribution graph.

For example, a criterion can be that at least 90% of the communications have a quality above some given threshold C/I_{90}, as represented in Figure 11.4, where the threshold value is chosen to be 7 dB. The criterion "90% of the calls must experience a C/I better than C/I_{90}" is a "worst case" constraint represented by the forbidden gray area. $C/I = 7$ dB is often quoted as minimum C/I for GMSK [264]. As shown later, GSM recommends a $C/I = 9$ dB [72]. Practically, the minimum value is around $C/I =$ 12 dB for acceptable performance [56].

Other criteria can be used (e.g., C/I_{50}), but usually a "worst case" criterion is the only one taken into account. In fact, there is no real incentive to provided a better

Table 11.1: Reference sensitivity performance.

GSM 900					
Type of Channel	static	TU50 (no FH)	TH50 (ideal FH)	RA130 (no FH)	HT100 (no FH)
FACCH/H (FER)	0.1 %	6.9 %	6.9 %	5.7 %	10 %
FACCH/F (FER)	0.1 %	8.0 %	3.8 %	3.4 %	6.3 %
SDCCH (FER)	0.1 %	13 %	8 %	8 %	12 %
RACH (FER)	0.5 %	13 %	13 %	12 %	13 %
SCH (FER)	1 %	16 %	16 %	15 %	16 %
TCH/F9.6 (BER)	10^{-5}	0.5 %	0.4 %	0.1 %	0.7 %
TCH/F4.8 (BER)	-	10^{-4}	10^{-4}	10^{-4}	10^{-4}
TCH/F2.4 (BER)	-	2×10^{-4}	10^{-5}	10^{-5}	10^{-5}
TCH/H2.4 (BER)	-	2×10^{-4}	10^{-4}	10^{-4}	10^{-4}
TCH/FS (FER)	0.1α %	6α %	3α %	2α %	7α %
class Ib (RBER)	$0.4/\alpha$ %	$0.4/\alpha$ %	$0.3/\alpha$ %	$0.2/\alpha$ %	$0.5/\alpha$ %
class II (RBER)	2 %	8 %	8 %	7 %	9 %

NOTE 1:	The specification for SDCCH applies also for other control channels.
NOTE 2:	FER: Frame erasure rate BER: Bit error rate RBER: Residual bit error rate (defined as the ratio of the number of errors detected over the frames defined as "good" to the number of transmitted bits in the "good" frames).
NOTE 3:	$1 \leq \alpha \leq 1.6$. The value of α can be different for each channel condition but must remain the same for FER and class Ib RBER measurements for the same channel condition.
NOTE 4:	FER for control channels (CCHs) takes into account frames which are signaled as being erroneous (by FIRE code, parity bits, or other means) or where the stealing flags are wrongly interpreted.
NOTE 5:	Ideal FH case assumes perfect decorrelation between bursts.

Table 11.2: Reference interference performance.

GSM 900					
Type of Channel	TU3 (no FH)	TU3 (ideal FH)	TH50 (no FH)	RA50 (ideal FH)	RA250 (no FH)
FACCH/H (FER)	22 %	6.7 %	6.7 %	6.7 %	5.7 %
FACCH/F (FER)	22 %	3.4 %	9.5 %	3.4 %	3.5 %
SDCCH (FER)	22 %	9 %	13 %	9 %	8 %
RACH (FER)	15 %	15 %	16 %	16 %	13 %
SCH (FER)	17 %	17 %	17 %	17 %	18 %
TCH/F9.6 (BER)	8 %	0.3 %	0.8 %	0.3 %	0.2 %
TCH/F4.8 (BER)	3 %	10^{-4}	10^{-4}	10^{-4}	10^{-4}
TCH/F2.4 (BER)	3 %	10^{-5}	3×10^{-5}	10^{-5}	10^{-5}
TCH/H2.4 (BER)	4 %	10^{-4}	2×10^{-4}	10^{-4}	10^{-4}
TCH/FS (FER)	21α %	3α %	6α %	3α %	3α %
class Ib (RBER)	$2/\alpha$ %	$0.2/\alpha$ %	$0.4/\alpha$ %	$0.2/\alpha$ %	$0.2/\alpha$ %
class II (RBER)	4 %	8 %	8 %	8 %	8 %

NOTE 1:	The specification for SDCCH applies also for other control channels.
NOTE 2:	FER: Frame erasure rate BER: Bit error rate RBER: Residual bit error rate (defined as the ratio of the number of errors detected over the frames defined as "good" to the number of transmitted bits in the "good" frames).
NOTE 3:	$1 \leq \alpha \leq 1.6$. The value of α can be different for each channel condition but must remain the same for FER and class Ib RBER measurements for the same channel condition.
NOTE 4:	FER for control channels (CCHs) takes into account frames which are signaled as being erroneous (by FIRE code, parity bits, or other means) or where the stealing flags are wrongly interpreted.
NOTE 5:	Ideal FH case assumes perfect decorrelation between bursts.

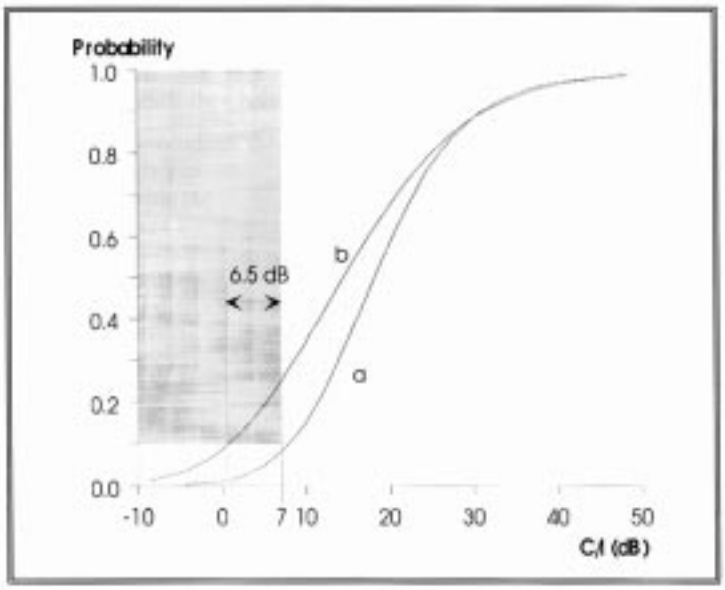

Figure 11.4: Carrier-to-interference (C/I) cumulative distribution. (a) The C/I distribution is outside the forbidden gray area and respects the constraint, whereas, (b) the C/I distribution is not compatible with the quality of service criterion. In order to achieve the required quality, the reuse distance must be increased to shift the distribution (e.g., 6.5 dB must be gained for the 10% worst cases) [169].

quality than the minimum acceptable, because of the associated costs. The actual goal of a telecommunications network is not maximize quality, but to minimize cost, while keeping quality above some threshold.

The quality criterion provides the ability to translate a C/I distribution into a minimum reuse factor. The propagation model of Eqn. 11.3 has the property that a modification of emitter positions (where d is the distance from the transmitting antenna in Eqn. 11.3) of ratio r relative to the reception point changes the reception levels by a simple multiplication factor of r^{α} (in Eqn. 11.3, α is the value with which the power level decrease with distance). We can assume that the cumulative distribution of I (the interference) in dB is simply shifted along the I axis when the reuse distance varies. The minimum reuse distance can then be derived from the I distribution determined for another reuse distance. For instance, for the C/I cumulative distribution shown in Figure 11.4 (case b), the reuse distance is too small and must be increased to compensate 6.5 dB, i.e., by a factor of 1.5 if propagation varies with $d^{-3.5}$ (this corresponds to an increase of the reuse factor by 2.3).

The statistical distribution of C/I could be derived from the statistics of carrier power (C) and from the statistics of interference power (I), if these two distribution are independent. They are on the uplink, but not on the downlink. The lack of equivalence comes from the fact that the mobile station receives interference from a small number of fixed sites (the base stations), whereas a base station is being interfered with by a potentially great number of mobile stations moving around inside the interfering cells. As a first approximation, however, we can ignore these difference and focus on how the features of the system influence the C and I distributions. Primarily, C varies with propagation fluctuations and with the distance between mobile stations and base station, while I depends in particular on the distance between interfering cells, and thus on the reuse factor.

11.4.4 Other Factors Influencing C/I in GSM

In addition to propagation fluctuations and the frequency reuse factor, other features impact the statistics of C/I. Handover strategies, which includes mobile station assisted handover (supported by GSM) influence the statistics of C and can influence the statistics of I when power control is combined with mobile station assisted handover. Power control also influences the C distribution due to the reduction of transmitted power in some cases. With power control, a large number of potential interferers transmit with a power level below maximum, lowering interference levels and shifting the I cumulative distribution. Discontinuous transmission (DTx) and frequency hopping (which provides interference diversity) also influence the C/I statistics. The value of $C/I = 9$ dB (quoted above for GSM) does not take into account power control, mobile station assisted handover, discontinuous transmission, or frequency hopping.

Table 11.3: Capacity (in Erlang) of full rate traffic channels (Erlang B formula, 2% blocking).

TRX in cell	1	2	3	4	5	6	7
Channels	7	14	22	30	37	45	53
Capacity	2.9	8.2	15	22	28	35.5	43
Ratio	0.41	0.57	0.68	0.73	0.76	0.79	0.81

11.4.5 Traffic Intensity

One Erlang represents the amount of traffic intensity carried by a channel that is completely occupied (i.e., 1 call-hour per hour or 1 call-minute per minute). For example, a radio channel that is occupied for thirty minutes during an hour carries 0.5 Erlangs of traffic [202]. GSM uses two values to estimate the communication traffic. The first is the traffic per subscriber, defined as the average probability that a given user is engaged in a conversation at a given moment during the peak hour (measured in Erlangs). The value used in GSM studies is taken to be about 0.05 Erlangs [169]. The second value is the mean duration of an effective communication, usually taken to be 120 seconds (2 minutes).

The capacity (in Erlangs) of a set of full rate traffic channels is given in Table 11.3 for GSM, using the Erlang B formula and assuming 2% blocking. Each transceiver (TRX) in a cell can accommodate around 7 subscribers.

11.5 System Capacity Improvement

This section follows the system capacity discussion found in [95]. System capacity has become the largest obstacle to the growth of the cellular industry. Different techniques are used to expand the capacity of cellular systems, including cell splitting, sectoring, and coverage zone approaches.

11.5.1 Conventional Capacity Improvement Techniques

Cell splitting is the process of subdividing a congested cell into smaller cells, where each subdivided cell has a new base station and reduced transmit power. Generally, there are two kinds of splitting techniques: permanent splitting and dynamic splitting. Permanent splitting is easy to realize as long as the transition from large cells to small cells takes place for low traffic areas. Frequency reassignment should follow the rule based on the frequency-reuse distance ratio with the power adjusted [140]. On the other hand, the dynamic splitting technique determines the orientation of the new set of seven-cells, split dynamically according to the traffic demand. Idle small cell sites

may be activated in order to increase the cell's traffic capacity. Cell splitting, however, can affect the neighboring cells and cause an imbalance in the distribution of power and frequency-reuse distance, and in addition, it tends to be costly.

The sectoring approach replaces a single omni-directional antenna at the base station with several directional antennas, with each antenna radiating within a specified sector. By using this arrangement of antennas, a given cell will interfere only with a fraction of the co-channel cells. The factor by which the co-channel interference is reduced depends on the amount of sectoring used. The penalty paid for improved C/I (or in other words, for increased capacity) is an increase in the number of antennas at each base station and a decrease in trunking efficiency due to the channel sectoring at the base station [202].

In the coverage zone approach, the concept of the microcell zone is introduced to avoid the increased number of hand-offs required in sectoring [202]. In this model, a cell is divided into three or more zones, and each of these zones is connected to a single base station and shares the same radio equipment. As a mobile moves within the cell, it is served by the strongest signal. Any channel can be assigned to any zone by the base station. In addition, the mobile will remain on the same channel when it travels from one zone to another within the cell. The base station simply switches the channel to a different antenna or zone site. This technique is particularly useful along highways or along urban traffic corridors.

11.5.2 Capacity Improvement by BER-based Demodulator Diversity

Besides these system layout improvements for increasing capacity, new digital signal processing techniques, like real-time BER estimation used in demodulator diversity, can be applied at the receiver. These techniques provide an inexpensive and effective method of suppressing the co-channel interference and accommodating more users in the same region.

As mentioned earlier, the commonly employed frequency reuse patterns are three-cell, four-cell and seven-cell reuse. GSM is technically a four-cell reuse system, but is often implemented with seven-cell reuse. The number of available channels is inversely related to the frequency reuse factor. For a path loss exponent of $n = 4$, the mean CIR for four-cell reuse is around 14 dB [95], which is approaching the threshold for acceptable toll quality. For the same n, the mean CIR level for a seven-cell reuse pattern is approximately 18 dB. Thus, from the CIR point of view, a seven-cell reuse pattern is superior to the four-cell reuse pattern. Receiver diversity can improve the CIR of the four-cell reuse system.

In the following figures, we first show the capacity increases possible for demodulator diversity gains relative to the performance of the best individual demodulator in the diversity scheme. Secondly, we show the capacity improvements relative to the performance of the coherent demodulator which has lost phase lock for 1% of the time.

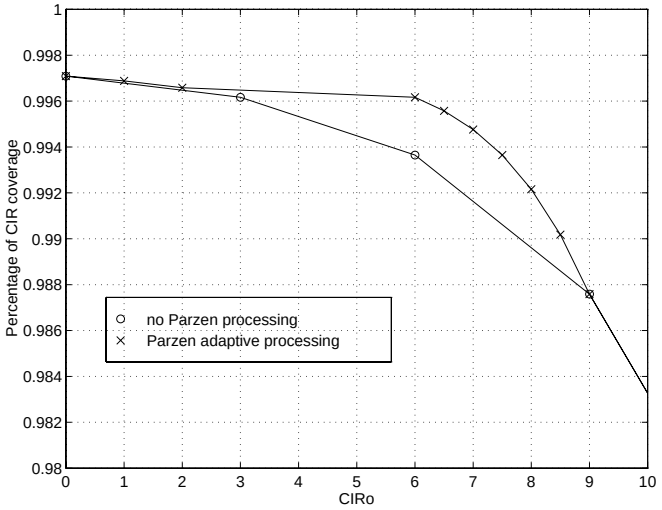

Figure 11.5: Analytical CIR coverage at a mobile station with and without Parzen-based demodulator diversity (gain over best individual demodulator) for $N = 7$ (urban multipath)

Gain Relative to Best Individual Demodulator

From the theoretical results in Chapter 10, CIR improvement of 4 dB over the best individual demodulator is feasible, depending on the channel conditions and the demodulator diversity scheme employed. We now compare the probability of CIR coverage before and after applying the Parzen-based demodulator diversity.

The analytical probability $p(CIR > CIR_o)_{MS}$ of Eqn. 11.4 is plotted as a function of CIR_o for a seven-cell reuse pattern in Fig. 11.5 and for a four-cell reuse pattern in Fig. 11.6 (urban multipath is assumed with a path loss $n = 3.6$). One interferer and a log-normal standard deviation $\sigma = 8$ are assumed. Assuming the CIR gains provided by the Parzen-based demodulator diversity as demonstrated in Section 10.4, the probabilities of average CIR coverage for $N = 7$ and $N = 4$ are also plotted in Fig. 11.5 and Fig. 11.6, respectively. These figures show that the probability of the average CIR coverage is increased for the mobile station by utilizing Parzen-based demodulator diversity. For example, the probability of average CIR coverage for $N = 4$ is 98.1% before applying the Parzen-based demodulator diversity and is increased to 99.1% after applying Parzen-based demodulator diversity for a threshold $CIR_o = 6$ dB.

To compare the probability of the average CIR coverage at a base station before and after applying Parzen-based receiver diversity, the analytical probability of the average CIR coverage $p(CIR > CIR_o)_{BS}$ based on Eqn. 11.5 is plotted in Fig. 11.7 and 11.8 for $N = 4$ and $N = 7$, respectively. One interferer and a log-normal standard deviation $\sigma = 8$ are assumed. The probability of the average CIR coverage with Parzen-based signal processing, again assuming CIR improvements provided in Section 10.4,

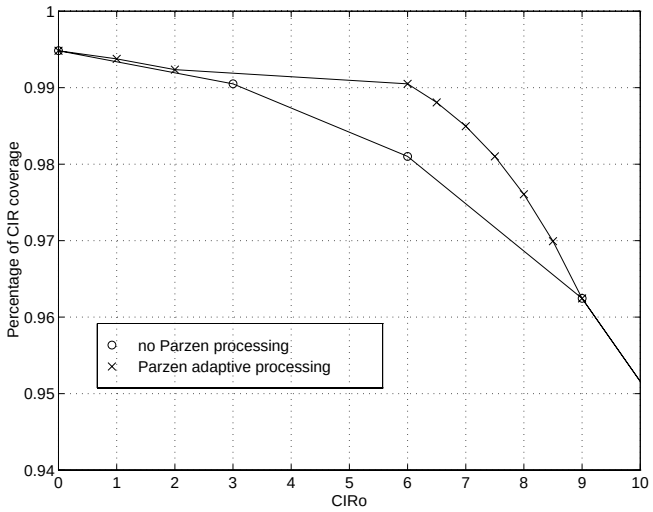

Figure 11.6: Analytical CIR coverage at a mobile station with and without Parzen-based demodulator diversity (gain over best individual demodulator) for $N = 4$ (urban multipath)

is also plotted in the corresponding figures (for urban multipath fading channels with a path loss $n = 3.6$). These figures show that the probability of the average CIR coverage is increased for the base station by utilizing Parzen-based receiver diversity. For example, the probability of average CIR coverage for $N = 4$ is 98.3% before applying the Parzen-based demodulator diversity and is increased to 99.5% after applying Parzen-based demodulator diversity for a threshold $CIR_o = 6$ dB.

Gain Relative to the Coherent Demodulator

From the theoretical results in Chapter 10, the coherent demodulator experiences an error floor under the condition of 1% phase lock loss, as shown in Figure 10.24. The demodulator diversity scheme continues to perform well, however, because the differential demodulator does not experience comparable degradation in the multipath channel. The gain in CIR provided by the diversity scheme relative to the coherent demodulator is consequently very large. To illustrate the potential capacity improvements, we conservatively assume a reasonable gain of 10 dB, though a higher gain could be chosen (refer to Figure 10.24).

To compare the probability of CIR coverage before and after applying the Parzen-based demodulator diversity, the analytical probability $p(CIR > CIR_o)_{MS}$ of Eqn. 11.4 is plotted as a function of CIR_o for a seven-cell reuse pattern in Fig. 11.9 and for a four-cell reuse pattern in Fig. 11.10 (urban multipath is assumed with a path loss $n = 3.6$). One interferer and a log-normal standard deviation $\sigma = 8$ are assumed. Assuming the CIR gains provided by the Parzen-based demodulator diversity as demonstrated in

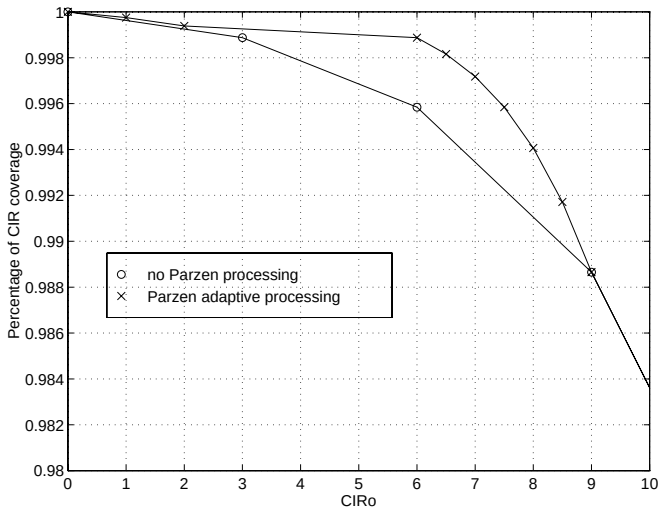

Figure 11.7: Analytical CIR coverage at a base station with and without Parzen-based demodulator diversity (gain over best individual demodulator) for $N = 7$ (urban multipath)

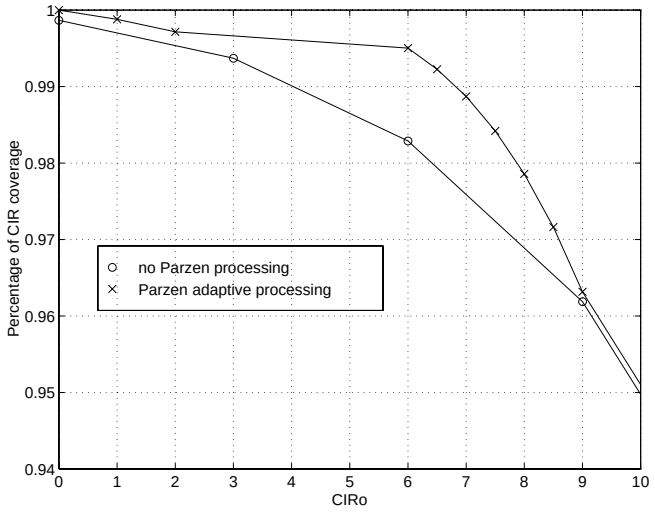

Figure 11.8: Analytical CIR coverage at a base station with and without Parzen-based demodulator diversity (gain over best individual demodulator) for $N = 4$ (urban multipath)

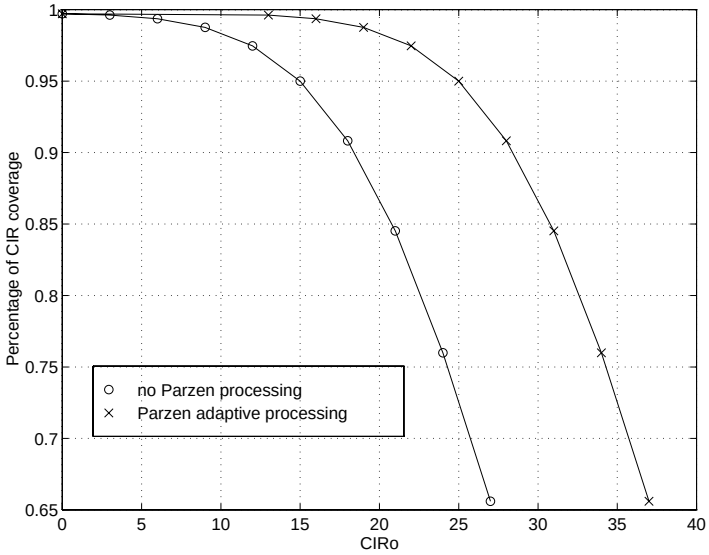

Figure 11.9: Analytical CIR coverage at a mobile station with and without Parzen-based demodulator diversity (gain over the coherent demodulator) for $N = 7$ (urban multipath)

Section 10.4, the probabilities of average CIR coverage for $N = 7$ and $N = 4$ are also plotted in Fig. 11.9 and Fig. 11.10, respectively. These figures show that the probability of the average CIR coverage is increased for the mobile station by utilizing Parzen-based demodulator diversity. For example, the probability of average CIR coverage for $N = 4$ is 88% before applying the Parzen-based demodulator diversity and is increased to 99% after applying Parzen-based demodulator diversity for a threshold $CIR_o = 15$ dB.

To compare the probability of the average CIR coverage at a base station before and after applying Parzen-based receiver diversity, the analytical probability of the average CIR coverage $p(CIR > CIR_o)_{BS}$ based on Eqn. 11.5 is plotted in Fig. 11.11 and 11.12 for $N = 4$ and $N = 7$, respectively. The probability of the average CIR coverage with Parzen-based signal processing, again assuming CIR improvements provided in Section 10.4, is also plotted in the corresponding figures (for urban multipath fading channels with a path loss $n = 3.6$). One interferer and a log-normal standard deviation $\sigma = 8$ are assumed. These figures show that the probability of the average CIR coverage is increased for the base station by utilizing Parzen-based receiver diversity. For example, the probability of average CIR coverage for $N = 4$ is 87% before applying the Parzen-based demodulator diversity and is increased to 99% after applying Parzen-based demodulator diversity for a threshold $CIR_o = 15$ dB.

Figures 11.9 to 11.12 show that a BER-based demodulator diversity scheme can potentially allow a frequency reuse factor of $N = 4$ to be employed, instead of $N = 7$ with no degradation in performance. For the mobile case, from Figure 11.10, a threshold

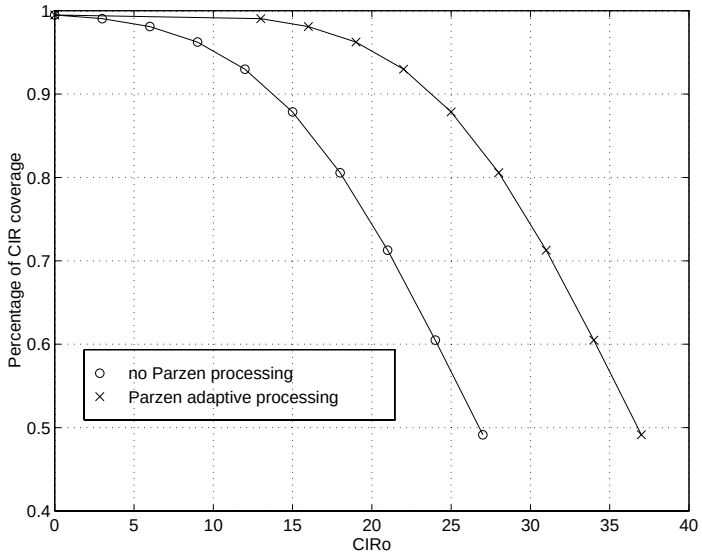

Figure 11.10: Analytical CIR coverage at a mobile station with and without Parzen-based demodulator diversity (gain over the coherent demodulator) for $N = 4$ (urban multipath)

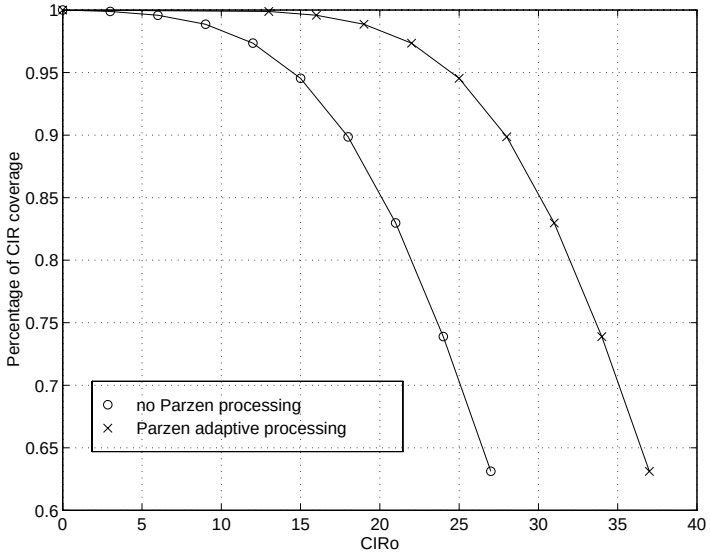

Figure 11.11: Analytical CIR coverage at a base station with and without Parzen-based demodulator diversity (gain over the coherent demodulator) for $N = 7$ (urban multipath)

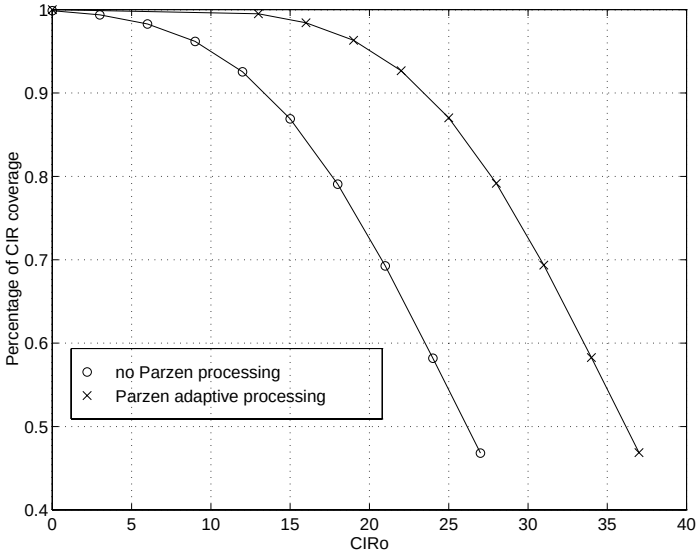

Figure 11.12: Analytical CIR coverage at a base station with and without Parzen-based demodulator diversity (gain over the coherent demodulator) for $N = 4$ (urban multipath)

of $CIR_o = 12$ dB (the specification for GSM) facilitates 93% coverage for a reuse factor of $N = 4$, while from Figure 11.9, only a threshold of $CIR_o = 17$ dB is required to facilitate 93% coverage for a reuse factor of $N = 7$. This means that a 5 dB (17 dB - 12 dB) improvement in CIR in an $N = 4$ system can allow that system to function as if it had a frequency reuse of $N = 7$. In Figure 10.24, demodulator diversity gains relative to the coherent demodulator reasonably exceed 5 dB (we assumed 10 dB in the present simulations). Thus, demodulator diversity can significantly increase capacity by combatting the effects of interference.

11.6 Summary

This chapter investigates the impact of demodulator diversity using BER estimation on overall system performance, where GSM is used as an example. Little research has been published on the impact of interference rejection techniques on actual system performance, in general. System performance is evaluated by considering such performance measures as the impact on frequency reuse and the potential for increased capacity. Section 11.5 demonstrates that the gains provided by a demodulator diversity scheme allow for increased capacity. Some of these techniques can serve as means of increased revenues, and thus lower system costs. The techniques may also be used to provide better quality of service in the mobile phone.

Section 11.5.2 illustrates how a BER-based demodulator diversity scheme can potentially allow a frequency reuse factor of $N = 4$ to be employed, instead of $N = 7$ with no degradation in performance. Gains are taken relative to the performance of the coherent demodulator (which is demodulator predominantly used in GSM). Only a gain of 5 dB in CIR is needed to provided $N = 4$ systems with performance comparable to $N = 7$ systems. Consequently, BER-based demodulator diversity can significantly increase overall capacity by combatting the effects of interference (accommodating more subscribers in the limited spectral resources) in a cellular system). The increase in complexity is small for implementing BER-based signal processing, and the cost of the implementation will be reasonable. BER-based demodulator diversity allows a lower frequency reuse factor, a lower probability of co-channel interference, and a higher probability of average CIR coverage.

Chapter 12

Conclusion

This dissertation makes a significant contribution to the field of communications by providing better ways to demodulate GMSK in the mobile radio environment. To combat interference inherent in cellular wireless systems, the research demonstrates that demodulator diversity and real-time BER estimation provide important improvements, not only in GMSK demodulation, but also for communications in general.

Section 12.1 provides a summary of results, including the most important contributions and other original results of interest. Section 12.2 concludes with a list of future research opportunities which spring from this research.

12.1 Summary of Results

This research justifies the concept of demodulator diversity by demonstrating that a demodulator diversity scheme can yield substantial gains in performance over individual receivers in typical wireless channels (e.g., 3-10 dB in E_b/N_o or C/I, as shown in Chapter 10). Practical real-time BER estimation techniques have tremendous ramifications for communications in general, and for wireless communications in particular. The results show that BER can often be estimated by use of a relatively short observation interval (10 to 500 training symbols) and, in some cases, without any training sequence at all.

The rejection of interference provided by these approach also facilitates increased capacity in cellular systems, which means increased revenues for wireless communications providers. This research demonstrates that BER estimates can serve as the criteria for adaptive signal processing. Section 11.5.2 illustrates how a BER-based demodulator diversity scheme can potentially allow a frequency reuse factor of $N = 4$ to be employed, instead of $N = 7$, with no degradation in performance (i.e., a lower reuse factor means more channels are available in a cell, thus significantly increasing overall capacity). BER estimation techniques can also be used in equalization allowing equalization to be based on the most important criterion BER (not MSE). BER estimation techniques can be used to perform dynamic allocation of resources. Dynamic allocation of resources includes variable coding, variable data rates, variable of allocation of spectrum or time slots, etc.

12.1.1 Most Important Contributions

This section outlines the most significant contributions of this dissertation, which are as follows:

- Formally introducing and validating the theoretical concept of demodulator diversity.
- Introducing and demonstrating the application of Parzen and Gram-Charlier pdf estimators to real-time BER estimation.
- Formulating methods of real-time BER-based adaptive signal processing, opening the door for application to equalization and dynamic allocation of resources, as well as to demodulator diversity.
- Proposing and demonstrating the use of real-time BER estimation with demodulator diversity by adaptive selection and weighting.
- Validating demodulator diversity schemes by simulation.
- Validating real-time Parzen-based and Gram-Charlier-based BER estimation by simulation.
- Extensively documenting an overview of single-channel interference rejection techniques in digital wireless communications, showing the applicability of signal processing solutions to wireless communications problems.

12.1.2 Other Significant Contributions

Included in this section are some other significant contributions of this research which, while not most important, are still original in this disseration. Other contributions are as follows:

- Proposing ten new noncoherent GMSK demodulators, one of which (the one-bit DF, two-bit DF, three-bit DF differential demodulators with combined outputs, DD123DF) performs better than other noncoherent demodulators examined from the literature.
- Documenting an extensive literature review of GMSK demodulation techniques (coherent and noncoherent).
- Proposing and demonstrating the use of robust estimators of scale and location in the Gram-Charlier series approximation for pdfs.
- Providing analytical justification for the use of blind Gaussian-based pdf estimation techniques for blind BER estimation, allowing bit normally reserved for training to be used to increase quality of service or capacity.

- Validating blind BER estimation by simulation.
- Uniquely investigating the performance of several GMSK demodulator structures (twenty-three) in impairments other than AWGN, such as CCI, multipath (generated according to the COST 207 models for urban, bad urban, hilly, and rural environments), and various combinations.
- Uniquely investigating the performance of coherent and noncoherent GMSK demodulator structures using SMRCIM [241] generated multipath with AWGN and CCI.
- Demonstrating the thesis that no one GMSK demodulator is superior in all channel impairments, but particular demodulators improve GMSK reception, depending on the dominant channel impairment (out of twenty-five channel environments simulated).
- Analytically deriving the gradient of Parzen's estimator.
- Applying the gradient of Parzen's estimator to BER estimation and demodulator diversity.
- Analyzing the impact on system performance of demodulator diversity and BER estimation on the GSM system, relating carrier-to-interference ratio (C/I) gains to system capacity improvements.
- Analytically showing the difficulty of determining *a priori* expressions for the pdf of a differential demodulator in typical wireless environments.
- Comparing demodulator diversity to antenna diversity (i.e., spatial diversity).
- Analytically deriving the theoretical minimum mean squared error (MMSE) of demodulator diversity in AWGN.

12.2 Future Work

This dissertation lays the groundwork for new areas of research in wireless communications. Suggestions for future work springing from this research follows:

- Apply BER estimation to dynamic allocation of resources.
- Demonstrate BER estimation for BER-based equalization.
- Apply the BER estimation and demodulator diversity ideas to a host of receiver structures and signaling formats.
- Investigate the use of complex weights with and without complex demodulator outputs.

- Investigate performance of Gram-Charlier and Parzen at BER lower than 10^{-3}, as would be required for high data rate, fixed communications applications.
- Investigate other methods of blind pdf (or BER) estimation.
- Derive cost function and gradient for adaptive weighting with Gram-Charlier estimation. Problem: it is a series approximation, not guaranteed to converge (so it can be biased).
- Extend this BER estimation work to symbol error rate (SER), where more than two states are used to represent a symbol.
- Investigate phase-lock-loop (PLL) performance using the pdf estimators. Most PLL research relies on MSE criterion for gauging performance. Determine if analytic expressions used in PLL analysis can be tied to BER.
- The capacity analysis of Section 11.3 makes *a priori* assumptions about the channel environments (i.e., Rayleigh and/or log-normal fading) and their effects on the probability of bit error. Further research could investigate the application of *a posteriori* pdf estimation techniques (like Parzen and Gram-Charlier) to capacity analysis.
- Investigate improving demodulator diversity weighting and equalization using Parzen estimation by better adaptation algorithms (alternatives to Method of Steepest Descent). Look at other more robust gradient-based methods to perform minimization of BER. Quantify the convergence performances of the different algorithms.
- For CCI, order the data and try to estimate the tail of the first Gaussian in the Gaussian mixture (using robust estimators of location to estimate the mode).
- Investigate using estimators of scale and location to calculate the moments of the Gram-Charlier approximation.
- Conduct a thorough literature review of estimators for probability density functions and cumulative distribution functions.
- Investigate using estimators of cumulative distribution functions (cdfs) for BER estimation.
- Investigate the use of cumulants to derive analytical expressions for decision statistics and consequently for BER.
- Investigate techniques for choosing the order of a Gram-Charlier estimate (perhaps take the MSE between the histogram of the measured data and each G-C order function). One could also examine the moments (e.g., Gaussian only first two moments are non-negligible) as a way to estimate order.

Appendix A

DD123DF and Coherent BER Estimation in AWGN

A.1 DD123DF BER Estimation in AWGN

A one-bit, two-bit, three-bit differential demodulator with decision feedback (DD123DF) is used in the demodulator diversity simulations of Chapter 10. This appendix illustrates the performance of the DD123DF receiver in AWGN using the Gram-Charlier series approximation for pdfs. Histograms of the demodulator outputs in COST 207 rural multipath and AWGN channels are also given to illustrate the decision statistic pdfs on which BER estimation is based.

A.1.1 1-bit, 2-bit, 3-bit DF Differential Demodulator (DD123DF)

In subsequent simulations, a 123DF differential demodulator (a combination of one-bit, two-bit, and three-bit differential demodulators with DF) is used (denoted DD123DF). Simulations in this research have shown that this noncoherent demodulator yields superior performance over that of conventional noncoherent demodulators (one-bit differential demodulation and limiter discriminator demodulation). We examine the performance of the differential demodulator in urban multipath and AWGN and CCI. Fig. A.1 contains a histogram of the decision statistic at the output of the differential demodulator in AWGN ($E_b/N_o = 6$ dB). Differential demodulation is a nonlinear operation and produces a decision statistic with a density other than Gaussian.

A.1.2 DD123DF in AWGN

In the AWGN case, the output pdf is nearly Gaussian, though, and justifies the use of Gram-Charlier to approximate it. Fig. A.2 plots measured BER and Gram-Charlier-based BER vs. E_b/N_o for the differential demodulator in AWGN. The Gram-Charlier series approximation for pdfs yields a good estimate of BER in this example at low

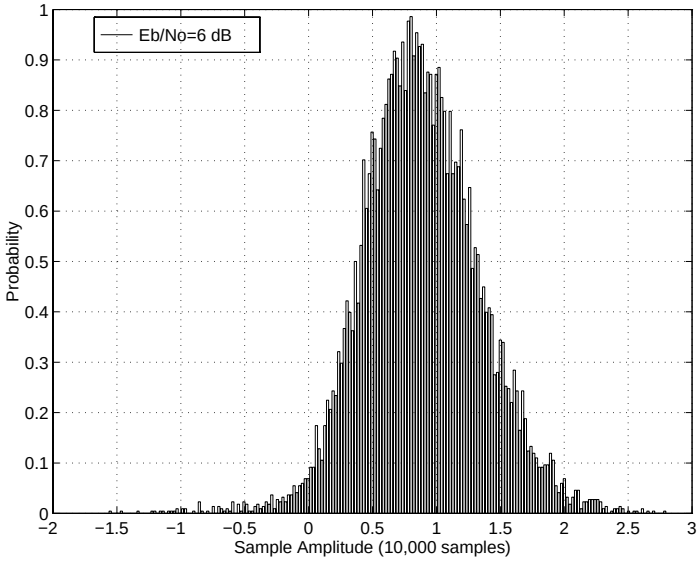

Figure A.1: Histogram of DD123DF output in AWGN

E_b/N_o, with the variance becoming greater at higher E_b/N_o. In this case, good estimates can be achieved with as few as 26 training bits, using robust estimators of scale.

Here, to achieve good BER estimation with few training bits, robust estimators of location and scale (discussed in Section 7.5) are substituted for the mean and standard deviation used in the Gram-Charlier series approximation for pdfs (as defined in Section refG-Cdefined). In Fig. A.2, the midshort is used in place of the sample mean, and the scale estimator h_s is used in place of the sample standard deviation. In this case, Gram-Charlier estimation using robust estimators outperforms normal Gram-Charlier estimation for a small number of samples. As shown in Fig. A.3, conventional Gram-Charlier estimation performs well also, but for a much larger number of training bits (1000 bits).

A.1.3 DD123DF in COST207 Rural Multipath and AWGN

Fig. A.4 shows a typical histogram of DD123DF output in rural multipath (generated using COST 207 models, as discussed in Appendix C). The multi-modal distribution (i.e., the output appears to consist of multiple Gaussian distributions) causes Gram-Charlier estimation to be inadequate for estimating the pdf (and thus, the BER). This distribution is similar to that obtained with coherent demodulation in COST 207 rural multipath (shown in Appendix A.2, Fig. A.7. Parzen's estimator can handle this type of distribution. The trade-off between Gram-Charlier estimation and Parzen estimation is that Parzen estimation generally requires more training bits.

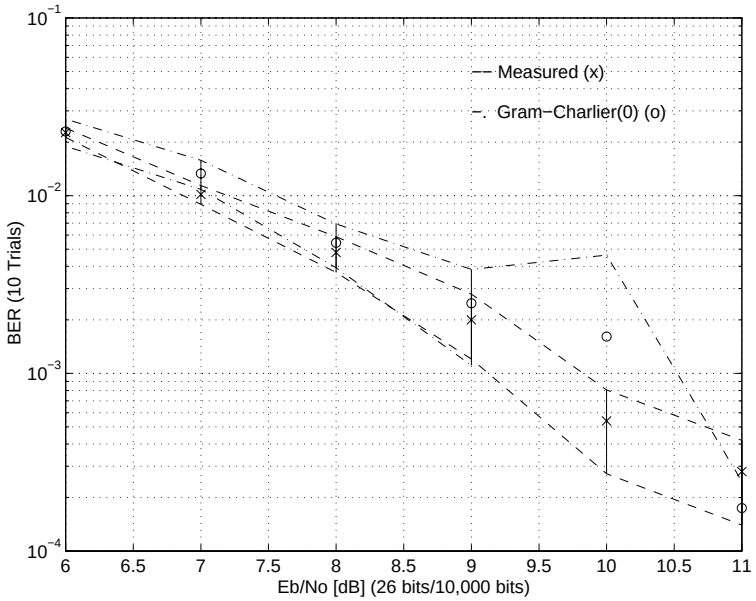

Figure A.2: DD123DF measured & Gram-Charlier (0th order) BER using midshort and h_s in AWGN (mean ± 1 std) with 26-bit training sequence

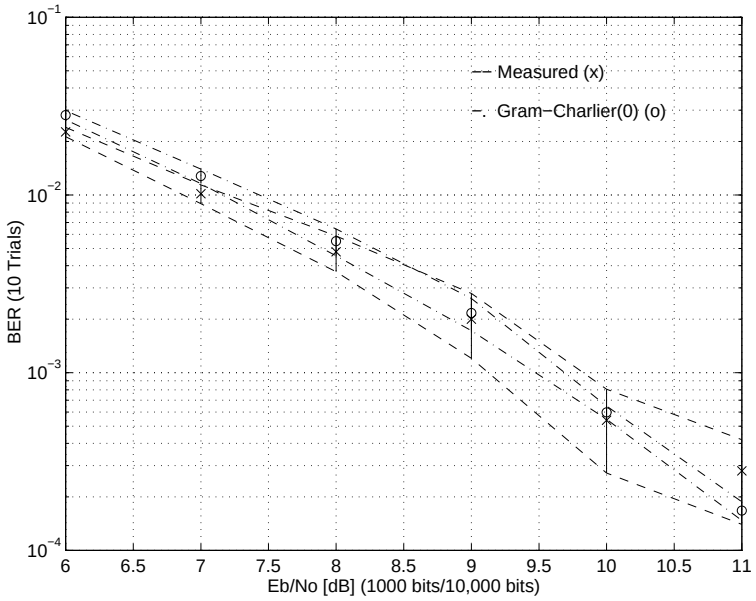

Figure A.3: DD123DF measured & Gram-Charlier (0th order) BER in AWGN (mean ± 1 std) with 1000-bit training sequence

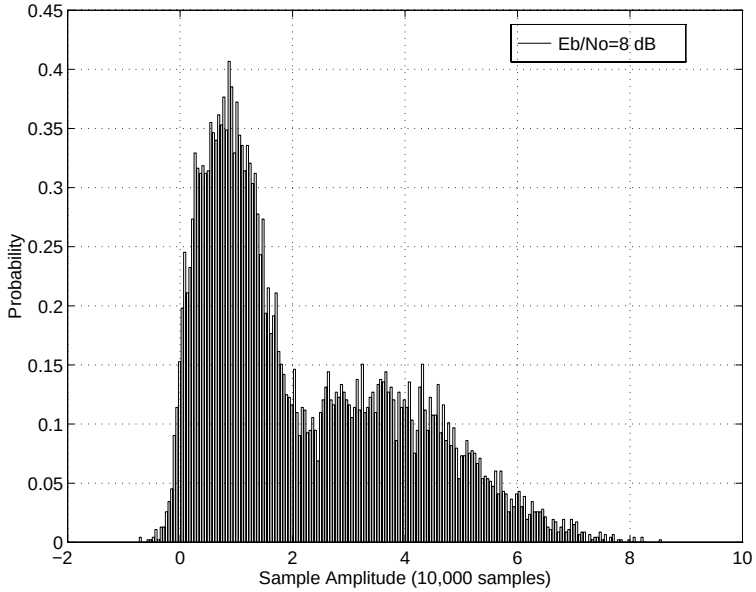

Figure A.4: Histogram of DD123DF output in rural multipath (COST 207) and AWGN

A.2 Coherent Demodulator BER Estimation in AWGN

A coherent demodulator is used in the demodulator diversity simulations of Chapter 10. This appendix illustrates the performance of the coherent receiver in AWGN using the Gram-Charlier series approximation for pdfs. Histograms of the demodulator output in COST 207 rural multipath and AWGN channels are also included to illustrate the decision statistic pdfs on which BER estimation is based.

A.2.1 Coherent Demodulator

In subsequent simulations, a coherent demodulator is used since it is commonly employed in wireless systems (such as GSM). The coherent demodulator has an integrate and dump filter on the in-phase and quadrature portions of the signal to approximate matched filtering. We examine the performance of the coherent demodulator in multipath and AWGN and CCI. Fig. A.5 contains a histogram of the decision statistic at the output of the coherent demodulator in AWGN ($E_b/N_o = 5$ dB). As expected, because coherent demodulation is a linear operation, the noise at the output is Gaussian.

A.2.2 Coherent Demodulator in AWGN

Fig. A.6 plots measured BER and Gram-Charlier-based BER vs. E_b/N_o for the coherent demodulator in AWGN. The Gram-Charlier series approximation for pdfs yields a good estimate of BER in this example, with the variance being slightly greater than that of

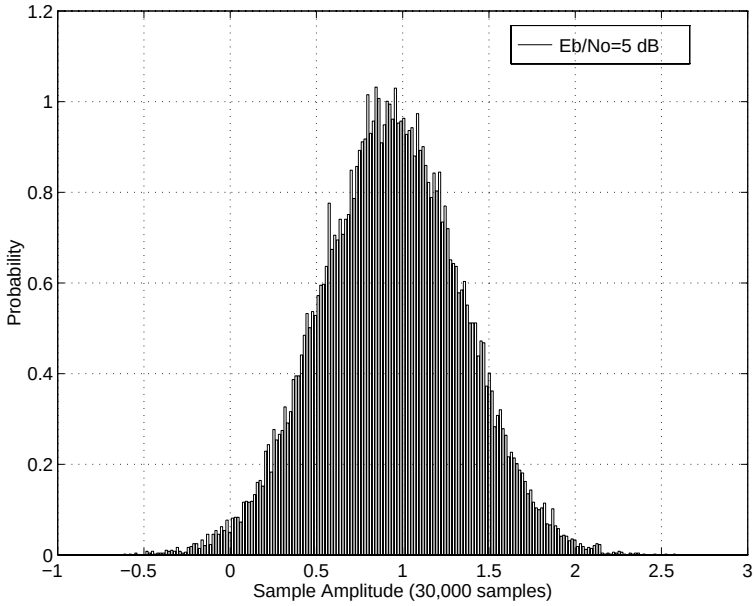

Figure A.5: Histogram of coherent output in AWGN

the measured BER. In this case, very good estimates can be achieved with as few as 26 training bits.

A.2.3 Coherent Demodulator in COST207 Rural Multipath and AWGN

Fig. A.7 shows a typical histogram of coherent output in rural multipath (generated using COST 207 models, as discussed in Appendix C). The coherent demodulator is assumed to track the multipath phase drift by updating the phase over an observation interval (e.g., with a training sequence). A GSM burst structure is assumed with a 26-bit midamble in the middle of 158 information bits. The multi-modal distribution (i.e., the output appears to consist of multiple Gaussian distributions) prohibits Gram-Charlier from estimating the pdf (and thus, the BER). Parzen's estimator can handle this type of distribution. The trade-off between Gram-Charlier estimation and Parzen estimation is that Parzen estimation generally requires more training bits.

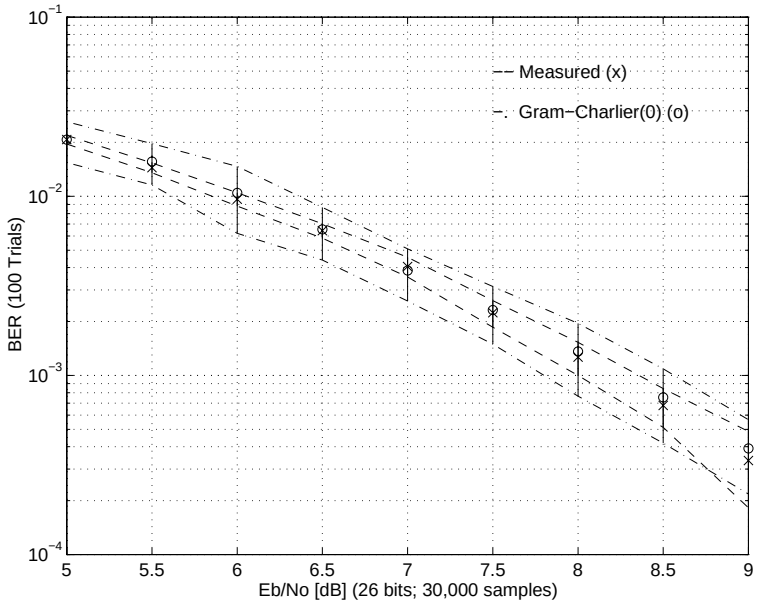

Figure A.6: Coherent measured & Gram-Charlier (0th order) BER in AWGN (mean ± 1 std)

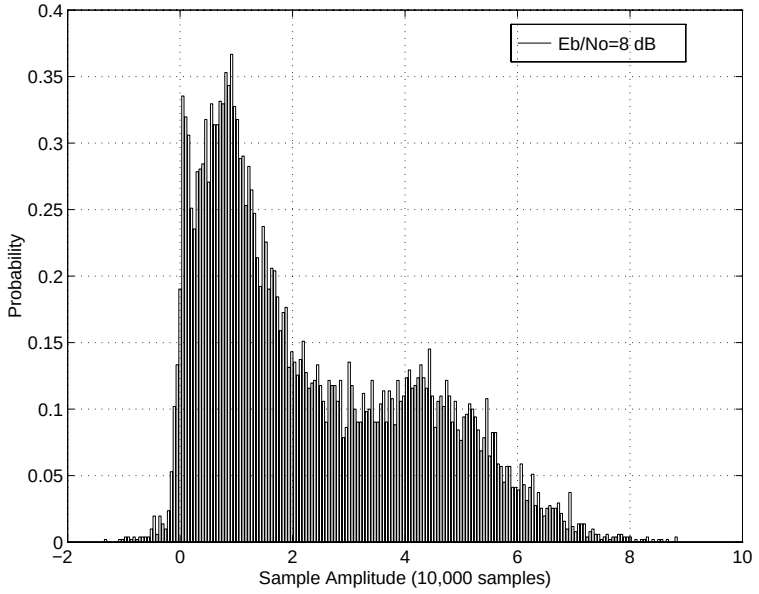

Figure A.7: Histogram of coherent output in rural multipath (COST 207) and AWGN

Appendix B

SMRCIM Model

The Mobile & Portable Radio Research Group (MPRG) at Virginia Tech has developed a software package called Simulated Mobile Radio Channel Impulse Model (SMRCIM) [241]. The first section of this appendix comes from promotional material on SMRCIM. The second section outlines how SMRCIM was used in the present research.

B.1 SMRCIM: A Mobile Radio Channel Simulator

SMRCIM simulates the wide band impulse responses and/or narrow band (flat fading) signal strengths of 600 MHz to 5 GHz mobile radio channels. SMRCIM can simulate urban, suburban, and microcellular mobile radio channels. Simulation is based on statistical models of individual multipath components developed from measurements in many different mobile environments. SMRCIM provides an inexpensive way to study or create channel responses, and can be used as a channel model to study bit error rates in frequency-flat and frequency-selective fading environments. SMRCIM can also be used to study the performance of channel access, equalization, diversity and modulation, as well as handoff and co-channel interference. SMRCIM could be used to drive hardware simulators, as well.

SMRCIM recreates multipath power delay profiles (squared magnitude impulse responses) with 625 ns temporal resolution of multipath signals (62.5 ns in microcellular environments). Excess delay spreads of up to 40 μs (4 μs for microcellular) are simulated. SMRCIM first generates power delay profiles at equally spaced locations as a mobile receiver moves along a track that is an integer multiple of 4.5 λ up to 20 meters long. Then, the user may specify a high resolution factor that synthesizes the amplitudes and phases of closely spaced impulse responses which yield strikingly accurate impulse responses and CW fading for outdoor communication channels. Rician CW fading between stationary radio terminals is also simulated with user-selected 'K' factors.

Menu driven commands make SMRCIM user-friendly. User specified transmitter-receiver (T-R) separation distance and mobile speed and heading make simulating mobile radio channels very flexible. SMRCIM accommodates T-R separations which range from 100 meters to 20 km, which makes it a powerful research or design tool for path

loss analysis, co-channel interference studies, or capacity analysis for future microcellular systems. Simulation results such as complex impulse responses and CW fading, and important parameters such as topography, rms delay spread, path loss, and T-R separation are automatically stored on disk for further analysis.

B.2 Application of SMRCIM in this Research

In the simulations of this research, we choose urban multipath, a vehicle speed of $v = 50$ km/hr (about 31 mph) moving away from the basestation, and a carrier frequency of $f_c = 900$ MHz. An impulse response was generated in SMRCIM and interpolated to make it consistent with data rate R represented in the simulations ($R = 270.833$ kbps). The samples of the impulse response are space 0.625 ns apart. The impulse response changes as the mobile travels $\lambda/4$ m (83.333 msec at $v = 50$ km/hr). The T-R (Transmitter-Receiver) separation is assumed to be 1 km. The path loss reference is 10 m with a path loss exponent of 2.6. A street width of 48 m is assumed.

A typical impulse response (magnitude and phase) used in simulations is given in Fig. B.1. Fig. B.2 was generated by SMRCIM software and shows the power loss vs. excess delay as the mobile moves 1.5 m on the upper left. Fig. B.2 also includes the RMS delay spread (in μs) on the bottom right, the signal level (in dB about the median) vs. distance (in meters) on the bottom left, and the percent probability that the signal level is less than abscissa on the upper right.

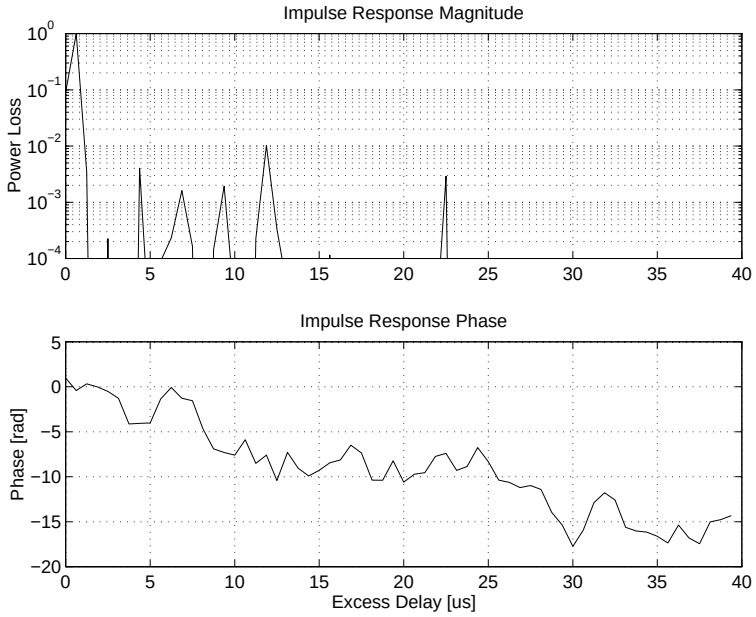

Figure B.1: Impulse Response of SMRCIM urban multipath ($v = 50$ km/hr; $f_c = 900$ MHz)

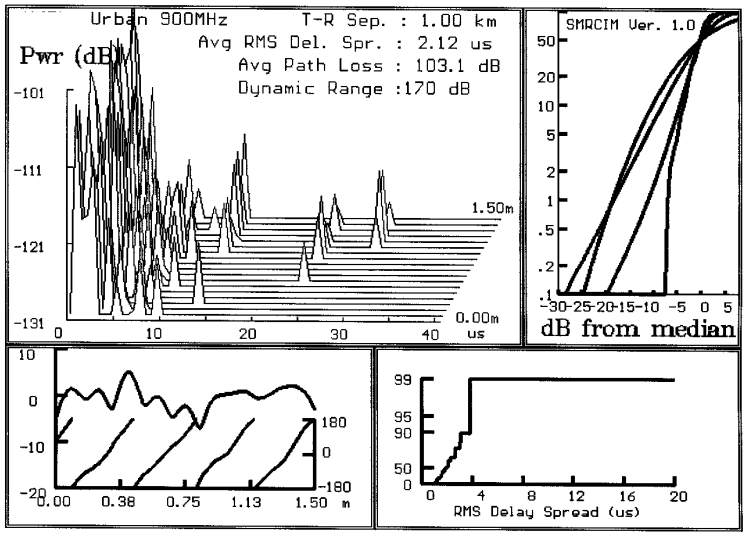

Figure B.2: Power vs. excess delay (upper left), percent probability that the signal level is less than abscissa (upper right), the signal level (in dB about the median) vs. distance (bottom left), and RMS delay spread (bottom right)

Appendix C

COST 207 Model

This appendix introduces and describes the COST 207 propagation models [70] which are used to evaluate systems such as GSM. These models have been used throughout this research to simulate multipath in urban, hilly urban, hilly, and rural environments.

It has been shown that the criterion for wide sense stationarity is satisfied for distances of about 10 meters. Based on the wide sense stationary uncorrelated scattering (WSSUS) model, the average delay profiles and the Doppler spectra are necessary to simulate the radio channel. In order to allow practical simulation, the different propagation models are presented in the following terms:

1. A discrete number of taps, each determined by their time delay and their average power;

2. The Rayleigh distributed amplitude of each tap, varying according to a Doppler spectrum.

Propagation conditions are categorized into several classes, each modeled by a six tap setting - a typical case for rural areas (RAx), a typical case for hilly terrain (HTx), a typical case for urban areas (TUx), and a profile for an equalization test (EQx) - where x is the vehicle speed (in km/h). These models are defined by six tap settings, illustrated in Table C.1 for RAx. where CLASS is the classical Doppler spectrum and RICE is the sum of a classical Doppler spectrum and one direct path such that the total multipath propagation is equal to that of the direct path. These channels have been implemented in MATLAB [256].

Table C.1: Typical case for rural area, RAx (6 tap setting).

Tap number	Relative time (μs)		Average relative power (dB)		Doppler spectrum
	(1)	(2)	(1)	(2)	
1	0.0	0.0	0.0	0.0	RICE
2	0.1	0.2	-4.0	-2.0	CLASS
3	0.2	0.4	-8.0	-10.0	CLASS
4	0.3	0.6	-12.0	-20.0	CLASS
5	0.4	-	-16.0	-	CLASS
6	0.5	-	-20.0	-	CLASS

Bibliography

[1] B. Aazhang, B.-P. Paris, and G. C. Orsak. Neural networks for multi-user detection in code-division multiple-access communications. *IEEE Transactions on Communications*, 40(7):1212–1222, July 1992.

[2] M. Abdulrahman, D. D. Falconer, and A. U. H. Sheikh. Equalization for interference cancellation in spread spectrum multiple access systems. In *VTC*, pages 71–74, May 1992.

[3] M. Abdulrahman, D. D. Falconer, and A. U. H Sheikh. DFE convergence for interference cancellation in SS MA systems. In *VTC*, pages 807–810, 1993.

[4] M. Abdulrahman, D. D. Falconer, and A. U. H Sheikh. Decision feedback equalization for CDMA in indoor wireless communications. *IEEE Journal on Selected Areas in Communications*, 12(4):698–706, May 1994.

[5] A. Abrardo, G. Benelli, A. Bini, and A. Garzelli. New diversity receiver for mobile communications. *Electronics Letters*, 29(25):2168–9, December 1993.

[6] A. Abrardo, G. Benelli, and G. Cau. Multiple symbols differential detection of GMSK. *Electronics Letters*, 29(25):2167–8, December 1993.

[7] A. Abrardo, G. Benelli, and G. Cau. Multiple symbol differential detection of GMSK for mobile communications. *IEEE Transactions on Vehicular Technology*, 44(3):379–389, August 1995.

[8] B. G. Agee. Solving the near-far problem: Exploitation of spatial and spectral diversity in wireless personal communication networks. In *Virginia Tech's Third Symposium on Wireless Personal Communications*, pages 15–1, June 1993.

[9] Yoshihiko Akaiwa. Digital modulations/demodulation techniques for mobile radio communications in japan. *IEICE Transactions*, E74(6):1503–11, June 1991.

[10] M. G. Amin, G. Venkatesan, and S. Tyler. A new approach for interference excision in spread spectrum using time-frequency distributions. In *SPIE*, volume 2563, pages 59–68, July 1995.

[11] F. Amoroso. Adaptive A/D converter to suppress CW interference in DSPN spread spectrum communications. *IEEE Trans. Commun.*, COM-31:1117–1123, October 1983.

[12] F. Amoroso. Performance of the adaptive A/D converter in combined CW and gaussian interference. *IEEE MILCOM*, 1984.

[13] F. Amoroso. Adaptive A/D converter to suppress co-channel constant envelope interference in a mobile digital link. *Telecommunication Systems - Modeling, Analysis, Design and Management*, 2(1):109–19, 1993.

[14] F. Amoroso and J. L. Bricker. Performance of the adaptive A/D converter in combined CW and gaussian interference. *IEEE Trans. Commun.*, COM-34:209–213, March 1986.

[15] F. Amoroso and J. L. Bricker. Increasing the up-link CW interference immunity of non-coherent direct sequence pseudonoise (DSPN) reception with on-board processing. *International Journal of Satellite Communications*, 11(3):107–18, May-June 1993.

[16] D. F. Andrews and et al. *Robust Estimates of Location: Survey and Advances.* Princeton University Press, Princeton, NJ, 1972.

[17] Sirikiat Ariyavisitakul, Susumu Yoshida, Fumio Ikegami, and Tsutomu Takeuchi. Fractional-bit differential detection of MSK: A scheme to avoid outages due to frequency-selective fading. *IEEE Transactions On Vehicular Technology*, VT-36(1), February 1987.

[18] D. K. Asano and S. Pasupathy. Improved post-detection processing for limiter-discriminator detection of cpm in a rayleigh, fast fading channel. *IEEE Transactions on Vehicular Technology*, 44(4):729–733, November 1995.

[19] V. Aue and J.H. Reed. CDMA demodulation and interference rejection using an optimal time-dependent filter. Master's thesis, Mobile & Portable Radio Research Group, Virginia Tech, February 1994.

[20] V. Aue and J.H. Reed. An interference robust CDMA demodulator that uses spectral correlation properties. In *IEEE Vehicular Technology Conference*, pages 563–567, 1994.

[21] Y. Bar-Ness and B. H. Bunin. Adaptive co-channel interference cancellation and signal separation method. In *IEEE International Conference on Communications - ICC'89*, pages 825–830, June 1989.

[22] Y. Bar-Ness, Z. Siveski, and D. W. Chen. Bootstrapped decorrelating algorithm for adaptive interference cancellation in synchronous CDMA communications systems. In *IEEE Third International Symposium on Spread Spectrum Techniques & Applications*, pages 162–166, July 1994.

[23] N. J. Bershad. Error probabilities for DS spread-spectrum systems using an ALE for narrow-band interference rejection. *IEEE Transactions on Communications*, 36(5):588–95, May 1988.

[24] Tom Biedka. personal conversation, January 1996.

[25] R. Bijjani and P. K. Das. Rejection of narrowband interference in PN spread-spectrum systems using neural networks. In *GLOBECOM '90: IEEE Global Telecommunications Conference and Exhibition. 'Communications: Connecting the Future'*, volume 2, pages 1037–41, December 1990.

[26] F. A. Bishop and R. S. Leahy. Enhancement of frequency hopped signals by convergence bandwidth discrimination. In *1985 IEEE Military Communications Conference: MILCOM '85. Conference Record*, volume 2, pages 334–8, October 1985.

[27] J. L. Bricker. Mathematical methodology for analysis fo the adaptive A/D converter in combined CW and gaussian interference. In *MILCOM*, pages 545–551, 1984.

[28] M. Buehrer and B. D. Woerner. A survey of multiuser receivers for cellular CDMA. Technical report, Mobile & Portable Radio Research Group, Virginia Tech, March 1996.

[29] K. V. Cai. Optimization of 2-bit A/D adaptive converter performance in CW interference. In *MILCOM*, pages 552–558, 1984.

[30] Scott N. Carney and Donald W. Dennis. Data transmission performance of 18 kbps non-coherent GMSK in the land mobile environment. In *36th IEEE Vehicular Technology Conference*, pages 121–6, May 1986.

[31] I. Cha and S. A. Kassam. Interference cancellation using radial basis function networks. In *IEEE Sixth SP Workshop on Statistical Signal and Array Processing Conference*, pages 221–4, October 1992.

[32] I. Cha and S. A. Kassam. Interference cancellation using radial basis function networks. *Signal Processing*, 47(3):247–68, December 1995.

[33] Chihkang Chen. *Spectral correlation characterization of modulated signals with application to signal detection and source location.* PhD thesis, Department of Electrical and Computer Engineering, University of California at Davis, 1988.

[34] M. P. Chen. Detection improvement methods for a GMSK signal. Technical report, Mobile & Portable Radio Research Group, Virginia Tech, 1996.

[35] S. Chen, S. McLaughlin, and B. Mulgrew. Complex-valued radial basis function network, part ii: Application to digital communications channel equalisation. *Signal Processing - An International Journal*, 36(2):175–188, March 1994.

[36] S. Chen, S. McLaughlin, B. Mulgrew, and P. M. Grant. Adaptive bayesian decision feedback equalizer incorporating co-channel interference compensation. In *ICC '94*, pages 530–533, 1994.

[37] S. Chen and B. Mulgrew. Overcoming co-channel interference using an adaptive radial basis function equalizer. *Signal Processing*, 28:91–107, 1992.

[38] S. Chen, B. Mulgrew, and S. McLaughlin. Adaptive bayesian decision feedback equalizer based on a radial basis function network. In *SUPERCOMM /ICC '92*, page 343.3, 1992.

[39] Woochul Chung, Youngyearl Han, and Pyeongjung Song. Performance evaluation of differential GMSK using k-th order detectors. In *Proceedings Of The 43rd IEEE Vehicular Technology Conference*, pages 17–20, 1993.

[40] Leon W. Couch. *Digital And Analog Communication Systems*. Macmillian Publishing Company, New York, 4 edition, 1993.

[41] S. Crozier, B. Mazur, and R. Matyas. Performance evaluation of differential detection of MSK. In *IEEE MILCOM '82*, pages 131–135, 1982.

[42] Kazuhiro Daikoku, Kazuaki Murata, and Kohji Momma. High-speed digital transmission experiments in 920 MHz urban and suburban mobile radio channels. *IEEE Transactions On Vehicular Technology*, VT-31(2):70–5, May 1982.

[43] Giovanna D'Aria, Flavio Muratore, and Valerio Palestini. Simulation and performance of the pan-european land mobile radio system. *IEEE Trans. on Vehicular Technology*, 41(2), May 1992.

[44] M. E. Davis and L. B. Milstein. Anti-jamming properties of a DS-CDMA equalization filter. In *12th Annual IEEE Military Communications Conference*, volume 3, pages 1008–1012, 1993.

[45] G. Dimos and T. Upadhyay. Low-cost solution to narrowband GPS interference problem. In *National Aerospace and Electronics Conference*, pages 145–153, 1995.

[46] Wing Shing Djen, Nam Dang, and Kamilo Feher. Performance improvement methods for DECT and other non-coherent GMSK systems. In *Vehicular Technology Society 42nd VTS Conference. Frontiers Of Technology. From Pioneers To The 21st Century*, volume 1, pages 97–100, 1992.

[47] Z. S. Dobrosavljevic and M. L. Dukic. On narrowband interference suppression using dfb filter in DSSS systems under impulsive channel conditions. In *IEEE Third International Symposium on Spread Spectrum Techniques & Applications*, pages 530–535, July 1994.

[48] J. F. Doherty. An adaptive technique for improving spread spectrum interference rejection. In *RF Expo EAST*, pages 385–7, October 1991.

[49] J. F. Doherty. A constrained LMS algorithm for interference rejection. In *MILCOM '92 - 'Communications - Fusing Command, Control and Intelligence' Conference*, volume 2, pages 696–700, October 1992.

[50] J. F. Doherty. Linearly constrained interference rejection for improved spread spectrum performance. In *SUPERCOMM/ICC '92. Discovering a New World of Communications*, volume 3, pages 1257–61, June 1992.

[51] J. F. Doherty. Direct sequence spread spectrum interference rejecton using vector space projection techniques. In *Virginia Tech's Third Symposium on Wireless Personal Communications*, pages 9/1–9, June 1993.

[52] J. H. Doherty. Linearly constrained direct-sequence spread-spectrum interference rejection. *IEEE Transactions on Communications*, 2/3/4:865–872, Feb/Mar/Apr 1994.

[53] F. Dominique and P. Petrus. Spectral redundancy exploitation in narrow band interference rejection for a PN-BPSK system. In *MILCOM '94*, volume 2, pages 405–409, 1994.

[54] F. Dominique and T. P. Subramanian. Combined self-organising feature map - LMS adaptive filter for digital co-channel interference suppression. *Electronics Letters*, 23(3):168–9, February 1996.

[55] Francis Dominque. personal conversation, January 1996.

[56] Anil Doradla. personal conversation, January 1996.

[57] A. Dual-Hallen. Decorrelating decision-feedback multiuser detector for synchronous code-division multiple-access channel. *IEEE Transactions on Communications*, 41(2):285–290, February 1993.

[58] A. Duel-Hallen, J. Holtzman, and Z. Zvonar. Multiuser detection for CDMA systems. *IEEE Personal Communications*, pages 46–58, April 1995.

[59] M. L. Dukic, D. O. Cuberovic, Z. D. Stojanovic, and I. S. Stojanovic. Performance analysis of DS spread-spectrum receiver using decision feedback and transversal interference suppression filters under multiple narrow-band interference. In *Communication Systems: Towards Global Integration. Singapore ICCS '90*, volume 2, pages 25–2/1–5, November 1990.

[60] M. L. Dukic, Z. S. Dobrosavljevic, Z. K. Stojanovic, and I. S. Stojanovic. Rejection of narrowband interference in DSSS systems using two-stage decision feedback filters. In *IEEE Third International Symposium on Spread Spectrum Techniques & Applications*, pages 526–529, July 1994.

[61] M. L. Dukic, Z. D. Stojanovic, and I. S. Stojanovic. A new direct sequence spread spectrum receiver using decision feedback and transversal filters for rejection of the narrow-band interference and errors caused by signal distortion. In *MELECON '89: Mediterranean Electrotechnical Conference. Integrating Research, Industry and Education in Energy and Communication Engineering*, pages 395–8, April 1989.

[62] M. L. Dukic, Z. D. Stojanovic, and I. S. Stojanovic. Performance of direct-sequence spread-spectrum receiver using decision feedback and transversal filters for combating narrowband interference. *IEEE Journal on Selected Areas in Communications*, 8(5):907–14, June 1990.

[63] Jr. E. R. Ferrara. A method for canceling interference from a constant envelope signal. *IEEE Transactions on Acoustics, Speech and Signal Processing*, ASSP-33(1):316–19, February 1985.

[64] M. S. El-Tanany, H. P. Stern, and S. A. Mahmoud. Data detection and timing recovery for a noncoherent discriminator-based GMSK receiver. *IEEE*, pages 243–48, 1989.

[65] Said M. Elnoubi. Analysis of GMSK with differential detection in land mobile radio channels. *IEEE Transactions On Vehicular Technology*, VT-35(4), November 1986.

[66] Said M. Elnoubi. Analysis of GMSK with discriminator detection in mobile radio channels. *IEEE Trans. Veh. Technology*, VT-35:71–76, May 1986.

[67] Said M. Elnoubi. Analysis of GMSK with two-bit differential detection in land mobile radio channels. *IEEE Transactions On Communications*, COM-35(2):237–40, February 1987.

[68] Said M. Elnoubi. Predetection filtering effect on the probability of error of GMSK with discriminator detection in mobile radio channels. *IEEE Transactions On Vehicular Technology*, 37(2):104–7, May 1988.

[69] Said M. Elnoubi. Comments on GMSK with differential phase detection in the satellite mobile channel. *IEEE Transactions On Communications*, 40(4):666–9, April 1992.

[70] ETSI. Digital land mobile radio communications. cost 207. final report (14 march, 1984 - 13 september, 1988). Technical report, Commission of the European Communities, Brussels, Luxembourgh, 1989.

[71] ETSI. GSM recommendation 05.04, modulation. Technical report, European Telecommunications Standards Institute, October 1993.

[72] ETSI. GSM recommendation 05.05, radio transmission and reception. Technical report, European Telecommunications Standards Institute, January 1994.

[73] Kamilo Feher. A comparison between coherent and noncoherent mobile systems in large doppler shift, delay spread and C/I environment. In *3rd International Mobile Satellite Conference*, June 1993.

[74] K. Fukawa and H. Suzuki. Blind interference cancelling equalizer for mobile radio communications. *IEICE Transactions on Communications*, E77-B(5):580–588, May 1994.

[75] W. A. Gardner and W. A. Brown. Frequency-shift filtering theory for adaptive cochannel interference removal. In *Twenty-Third Asilomar Conference on Signals, Systems and Computers*, volume 2, pages 562–7, November 1989.

[76] W.A. Gardner. Cyclic wiener filtering: Theory and method. *IEEE Transactions on Communications*, 41(1):151–163, January 1993.

[77] W.A. Gardner and S. Venkataraman. Performance of optimum and adaptive frequency-shift filters for cochannel interference and fading. In *Twenty-Fourth Asilomar Conference on Signals, Systems and Computers*, volume 1, pages 242–7, Nov 1990.

[78] L. Garth, R. Vijayan, and H. V. Poor. A new approach to interference suppression in spread-spectrum systems. In *Military Communications in a Changing World MILCOM, 91*, volume 1, pages 375–9, November 1991.

[79] L. M. Garth and H. V. Poor. Narrowband interference suppression in impulsive channels. *IEEE Transactions on Aerospace and Electronic Systems*, 28(1):15–34, January 1992.

[80] J. Gevargiz, P. K. Das, and L. B. Milstein. Adaptive narrow-band interference rejection in a DS spread-spectrum intercept receiver using transform domain signal processing techniques. *IEEE Transactions on Communications*, 37(12):1359–66, December 1989.

[81] G. B. Giannakis and A. V. Dandawate. Linear and non-linear adaptive noise cancelers. In *ICASSP: 1990 International Conference on Acoustics, Speech and Signal Processing*, volume 3, pages 1373–6, April 1990.

[82] S. Glisic. Ber and interference suppression filter misadjustment analysis for DS/CDMA receiver operating in the presence of FH interference. In *MILCOM '93*, page 15M.2, 1993.

[83] S. G. Glisic and M. D. Pajkovic. Rejection of FH signal in DS spread spectrum system using complex adaptive filtering. In *A New Era: 1990 IEEE Military Communications Conference*, volume 1, pages 349–53, October 1990.

[84] S. G. Glisic and M. D. Pajkovic. Rejection of FHMA signal in DS spread spectrum system using complex adaptive filtering. In *Military Communications in a Changing World MILCOM, 91*, volume 1, pages 365–9, November 1991.

[85] A. M. J. Goiser and M. K. Sust. Adaptive interference rejection in a digital direct sequence spread spectrum receiver. In *IEEE Military Communications Conference - MILCOM '89*, pages 514–520, 1989.

[86] A. M. J. Goiser and M. K. Sust. Adaptive interference rejection for non-coherent digital direct sequence spread spectrum receivers. In *GLOBECOM '90: Communications: Connecting the Future*, volume 1, pages 285–90, December 1990.

[87] R. P. Gooch and B. Daellenbach. Prevention of interference capture in a blind (CMA-based) adaptive receive filter. In *Twenty-Third Asilomar Conference on Signals, Systems ands Computers*, volume 2, pages 898–902, November 1989.

[88] P. M. Grant, S. Mowbray, and R. D. Pringle. Multipath and co-channel CDMA interference cancellation. *IEEE Second International Symposium on Spread Spectrum Techniques & Applications*, page 5.1, November 1992.

[89] C. D. Greene, J. H. Reed, and T. C Hsia. An optimal receiver using a time -dependent adaptive filter. In *MILCOM*, 1989.

[90] R. F. Guertin. Narrowband interference suppression in a spread-spectrum system using vector space methods. In *MILCOM '89*, pages 508–513, 1989.

[91] T .A. Gulliver. Order statistics diversity combining in worst case noise and multitone jamming. In *MILCOM 91*, volume 1, pages 385–389, November 1991.

[92] A. Haimovich and A. Vadhri. Rejection of narrow-band interferences in PN spread spectrum systems using an eigenvanalysis approach. In *MILCOM '94*, volume 3, pages 1007–1011, 1994.

[93] Simon Haykin. *Adaptive Filter Theory*. Prentice-Hall, Englewood Cliffs, NJ, second edition, 1991.

[94] Simon Haykin. Neural networks expand SP's horizons. *IEEE Signal Processing Magazine*, pages 24–49, March 1996.

[95] Rong He. *AMPS Co-channel interference rejection techniques and Their Impact on System Capacity*. PhD thesis, Virginia Tech, 1995.

[96] Rong He. Co-channel interference rejection techniques for AMPS signals using spectral correlation characteristics. preliminary review of dissertation research, Virginia Tech, July 1995.

[97] Y. He, S.-F. Lei, P. Das, and G. J. Saulnier. Suppression of narrowband jammers in a DS spread spectrum receiver using modified adaptive filtering technique. In *GLOBECOM '88. Communications for the Information Age. Conference Record*, volume 1, pages 540–5, December 1988.

[98] F. Hendessi, H. M. Hafez, and A. U. H. Sheikh. Structure and performance of FRESH-decision feedback equalizer in the presence of adjacent channel interference. In *43rd IEEE Vehicular Technology Conference*, pages 641–644, 1993.

[99] J. H. Higbie. Adaptive nonlinear suppression of interference. In *MILCOM 88: 21st Century Military Communications - What's Possible?*, pages 381–389, 1988.

[100] Kenkichi Hirade, Mitsuru Ishizuka, Fumiyuki Adachi, and Koichi Ohtani. Error-rate performance of digital FM with differential detection in land mobile radio channels. *IEEE Transaction On Vehicular Technology*, VT-28(3), August 1979.

[101] Masahiko Hirono, Toshio Miki, and Kazuaki Murota. Multilevel decision method for band-limited digital FM with limiter-discriminator detection. *IEEE Transactions On Vehicular Technology*, VT-33(3):114–122, August 1984.

[102] R. D. Holley and J. H. Reed. Time dependent adaptive filters for interference cancellation in CDMA systems. Master's thesis, Mobile & Portable Radio Research Group, Virginia Tech, October 1993.

[103] M. L. Honig. Orthogonally anchored blind interference suppression using the sato cost criterion. In *1995 IEEE Int'l Symposium on Information Theory*, page 314, 1995.

[104] M. L. Honig, U. Madhow, and S. Verdu. Blind adaptive interference suppression for near-far resistant CDMA. In *GLOBECOM '94*, pages 379–38, 1994.

[105] M. L. Honig, U. Madhow, and S. Verdu. Blind adaptive multiuser detection. *IEEE Trans. on Information Theory*, 41(4):944–960, July 1995.

[106] Jun Horikoshi and Shigeo Shimura. Multipath distortion of differentially encoded GMSK with 2-bit differentially detection in bandlimited frequency selective mobile radio channel. *IEEE Transaction On Vehicular Technology*, 39(4), November 1990.

[107] I. Howitt. *Radial Basis Function Methodology for Use in Digital Communications*. PhD thesis, University of California, Davis, 1995.

[108] I. Howitt, J. H. Reed, R. Vemuri, and T. C. Hsia. Rbf growing algorithm applied to the equalization and co-channel interference rejection problem. In *IEEE World Congress on Computational Intelligence /International Conference on Neural Networks*, June 1994.

[109] I. Howitt, J. H. Reed, V. Vemuri, and T. C. Hsia. Recent developments in applying neural nets to equalization and interference rejection. In *Virginia Tech's Third Symposium on Wireless Personal Communications. Proceedings*, June 1993.

[110] Ivan Howitt. personal conversation, March 1996.

[111] R. Iltis, J. Ritcey, and L. B. Milstein. Interference rejection in FFH systems using least-squares estimation techniques. *IEEE Transactions on Communications*, 38(12):2174–83, December 1990.

[112] R. A. Iltis. Interference cancellation for enhanced detection of frequency-hopped signals. In *ICASSP '86*, volume 2, pages 973–976, April 1986.

[113] R. A. Iltis. A glrt-based SS receiver for joint channel estimation and interference suppression. *IEEE Transactions on Communications*, 37(3):277–288, March 1989.

[114] Mitsuru Ishizuka and Yasuhiko Yasuda. Improved coherent detection of GMSK. *IEEE Transactions On Communications*, COM-32(3), March 1984.

[115] W. Jacklin, J. Grimm, and D. Ucci. The simulation of a two-dimensional SS system with locally optimal processing. In *MILCOM '93*, page 9.6, 1993.

[116] D. H. Johnson and D. E. Dudgeon. *Array Signal Processing: Concepts and Techniques*. Prentice-Hall, Englewood Cliffs, NJ, 1993.

[117] E. G. Kanterakis. A novel technique for narrowband /broadband interference excision in DS-SS communications. In *MILCOM '94*, volume 2, pages 628–632, 1994.

[118] T. Kasparis, M. Georgiopoulos, and E. Payne. Non-linear filtering techniques for narrow-band interference rejection in DSSS systems. In *MILCOM '91*, page 17.1, 1991.

[119] D. J. Kennedy and E. K. Koh. Frequency-reuse interference in TDMA/QPSK satellite systems. In *Fifth International Conference on Digital Satellite Communications*, pages 99–107, March 1981.

[120] Koto Kinoshita, Masaharu Hata, and Hiromi Nagabuchi. Evaluation of 16 kbit/s digital voice transmission for mobile radio. *IEEE Transactions On Vehicular Technology*, VT-33(4):321–7, November 1984.

[121] Takao Kishi, Iwao Sasase, and Shinsaku Mori. Optimum bandwidth of predetection gaussian bandpass filter for differentially encoded GMSK. In *IEEE GLOBECOM '84*, pages 22.4.1–22.4.4, 1984.

[122] R. Kohno. Pseudo-noise sequences and interference cancellation techniques for spread spectrum systems-spread spectrum theory and techniques in japan. *IEICE Transactions*, E74(5):1083–92, May 1991.

[123] Israel Korn. GMSK with differential phase detection in the satellite mobile channel. *IEEE Transactions On Communications*, 38(11):1980–6, November 1990.

[124] Israel Korn. GMSK with limiter discriminator detection in satellite mobile channel. *IEEE Transactions On Communications*, 39(1):94–101, January 1991.

[125] Israel Korn. GMSK with frequency-selective rayleigh fading and co-channel interference. *IEEE Journal On Selected Areas In Communications*, 10(3):506–515, April 1992.

[126] Fred Kostedt and James C. Kemerling. Practical GMSK data transmission. *Wireless Design & Development*, pages 21–4, 1995.

[127] A. Krieger. An adaptive algorithm for interference suppression in SS communications systems. In *1990 24th Asilomar Conference on Signals, Systems and Computers*, volume 1, pages 373–378, 1990.

[128] D. M. Krinsky, A. H. Haddad, and C. C. Lee. An adaptive DSSS receiver for burst type interference. *IEEE JSAC*, 13(1):59–70, January 1995.

[129] N. Kurita, I. Sasame, and S. Mori. Suppression of narrowband interference in FFH systems by hardlimited combining receiver using transversal filters. *1992 IEEE Int'l Conf. on Selected Topics in Wireless Communications*, pages 445–48, June 1992.

[130] Hyuck M. Kwon, Leonard E. Miller, and Jhong S. Lee. Limiter-differential detection of a frequency-hopped CPFSK diversity system in partial-band jamming. *IEEE Journal On Selected Areas in Communications*, 10(4), May 1992.

[131] O. W. Kwon, C. K. Un, and J. C. Lee. Performance of constant modulus adaptive digital filters for interference cancellation. *Signal Processing*, 26(2):185–96, February 1992.

[132] J. D. Laster. Advances in single-channel adaptive interference rejection for digital wireless communications. Signal Processing Magazine, 1996. accepted for publication.

[133] J. D. Laster. Improved GMSK demodulation emphasizing single-channel interference rejection techniques. preliminary review of dissertation research, Virginia Tech, January 1996.

[134] J. D. Laster and J. H. Reed. A tutorial on single-channel interference rejection techniques. In *Virginia Tech's Fourth Symposium on Wireless Personal Communications*, pages 2.1–2.25, June 1994.

[135] J. D. Laster and J. H. Reed. *Wireless Personal Communications: Research Developments*, chapter A survey of adaptive single-channel interference rejection techniques for wireless communications. Kluwer, 1995.

[136] B. Lee and J. Essman. On a new scheme of reference signal generating method for interference suppression in DSSS systems. In *MILCOM '90*, page 36.6, 1986.

[137] E. K. B. Lee. Rapid converging adaptive interference suppression for DS CDMA systems. In *GLOBECOM '93*, pages 1683–1687, 1993.

[138] J. H. Lee and C .W. Lee. Adaptive filters for suppressing irregular hostile jamming in direct sequence spread-spectrum system. In *1987 IEEE Military Communications Conference. 'Crisis Communications: The Promise and Reality'*, volume 1, pages 118–22, October 1987.

[139] Sang U. Lee, Young M. Chung, and Jae M. Kim. On the bit error probabilities of GMSK in the rayleigh fading channels. In *38th IEEE Vehicular Technology Conference: 'Telecommunications Freedom - Technology On The Move'*, pages 249–54, June 1988.

[140] W. C. Y. Lee. *Mobile Communications Design Fundamentals*. John Wiley & Sons, Inc., New York, 1993.

[141] S. K. Leung and Kamilo Feher. A novel scheme to aid coherent detection of GMSK signals in fast rayleigh fading channels. In *Second International Mobile Satellite Conference IMSC '90*, pages 605–11, June 1990.

[142] S. K. Leung and Kamilo Feher. Differential detection of GMSK signals in a frequency selective, fast rayleigh fading mobile radio channel with co-channel interference. In *IREECON '91, Australia's Electronics Convention Proceedings*, volume 1, pages 53–6, 1992.

[143] W. Libing, B. Guangguo, and W. Boxiu. Suppression of FM interference in QAM systems using adaptive decision-feedback filters. In *1991 International Conference on Circuits and Systems*, volume 1, pages 161–3, June 1991.

[144] N. W. K. Lo, D. D. Falconer, and A. U. H.Sheikh. Adaptive equalization for a multipath fading environment with interference and noise. In *VTC*, pages 252–256, 1994.

[145] N. W. K. Lo, D. D. Falconer, and A. U. H. Sheikh. Adaptive equalization techniques for multipath fading and co-channel interference. In *VTC*, pages 653–656, 1993.

[146] R. Lupas and S. Verdu. Linear multiuser detectors for synchronous code-division multiple-access channel. *IEEE Trans. Commun.*, IT-32(1):85–96, January 1989.

[147] U. Madhow and M. L. Honig. Error probability and near-far resistance of minimum mean squared error interference suppression schemes for CDMA. In *GLOBECOM '92. Communication for Global Users. IEEE Global Telecommunications Conference*, volume 3, pages 1339–43, December 1992.

[148] U. Madhow and M. L. Honig. Minimum mean squared error interference suppression for direct-sequence spread-spectrum code-division multiple-access. In *ICUPC '92*, pages 10.04/1–5, September 1992.

[149] U. Madhow and M. L. Honig. MMSE interference suppression for DSSS CDMA. *IEEE Transactions on Communications*, 42(12):3178–3188, December 1994.

[150] M. Majmundar. Adaptive single-user receivers for DS CDMA systems. Master's thesis, Mobile & Portable Radio Research Group, Virginia Tech, March 1996.

[151] A. Mammela. The performance of adaptive interference suppression filters used in PN spread-spectrum systems. In *EUROCON 88: 8th European Conference on Electrotechnics*, pages 126–9, June 1988.

[152] N. B. Mandayam and B. Aazhang. Adaptive multiuser interference rejection algorithm for DS-CDMA. In *1994 IEEE Int'l Symposium on Information Theory*, 1994.

[153] Tatsuro Masamura. Intersymbol interference reduction for differential MSK by nonredundant error correction. *IEEE Transaction on Vehicular Technology*, 39(1), February 1990.

[154] Tatsuro Masamura, Shuichi Samejima, Yoshiteru Morihiro, and Hiroaki Fuketa. Differential detection of MSK with nonredundant error correction. *IEEE Transactions on Communications*, 27(6):912–918, June 1979.

[155] Lloyd J. Mason. Error probability evaluation for systems employing differential detection in a rician fast fading environment and gaussian noise. *IEEE Transactions on Communications*, COM-35(1):39–46, January 1987.

[156] M. Maulhardt, A. M. Davis, and J. May. Numerical design of nonlinear adaptive filters. In *ICASSP 86. IEEE-IECEJ-ASJ International Conference on Acoustics, Speech and Signal Processing*, volume 3, pages 2131–4, April 1986.

[157] M. Medley, G. Saulnier, and P. Das. Applications of the wavelet transform in SS communications systems. In *SPIE - The Int'l Society for Optical Engineering*, volume 2242, pages 54–68, 1994.

[158] R. Mendoza, J. H. Reed, T. C. Hsia, and B. G. Agee. Interference rejection using the time-dependent constant modulus algorithm (CMA) and the hybrid CMA/spectral correlation discriminator. *IEEE Transactions on Signal Processing*, 39(9), September 1991.

[159] Lamine Mili. personal conversation, August 1996. Virginia Tech.

[160] S. L. Miller. An adaptive direct-sequence code-division multiple-access receiver for multiuser interference rejection. *IEEE Trans. on Comm.*, 43(2/3/4), February/March/April 1995.

[161] L. B. Milstein. Interference rejection techniques in spread spectrum communications. *Proceedings of the IEEE*, 76(6), June 1988.

[162] L. B. Milstein and J. Wang. Interference suppression for CDMA overlays of narrowband waveforms. In *IEEE Third International Symposium on Spread Spectrum Techniques & Applications*, pages 61–68, July 4-6 1994.

[163] U. Mitra and H. V. Poor. Neural network techniques for adaptive multiuser demodulation. *IEEE JSAC*, 12(9):1460–1470, December 1994.

[164] M. Miyagi, T. Ogawa, I. Sasase, and S. Mori. Suppression of CW interference and filtered noise in QPRS systems using decision-feedback filters. In *ICASSP 1990*, volume 3, pages 1703–6, April 1990.

[165] P. E. Mogenson, F. Frederiksen, P. K. Thomsen, S. Safavi, and L. B. Lopes. Evaluation of an advanced receiver concept for DECT. In *VTC '95*, pages 1–6, 1995.

[166] A. M. Monk, M. Davis, L. B. Milstein, and C.W. Helstrom. A noiseless-whitening approach to multiple access noise rejection -part i: Theory and background. *IEEE Journal on Selected Areas of Communications*, 12(5):817–827, June 1994.

[167] P. N. Monogioudis, R. Tafazolli, and B. G. Evans. Linear adaptive fractionally spaced equalization of CDMA multiple-access interference. *Electronics Letters*, 29(21):1823–5, October 1993.

[168] P. N. Monogioudis, R. Tafazolli, and B. G. Evans. Lfse interference cancellation in CDMA systems. In *ICC '94*, pages 1160–1163, 1994.

[169] Michel Mouly and Marie-Bernadette Pautet. *The GSM System for Mobile Communications*. 49, rue Lousie Bruneau, F-91120 Palaiseau, France, 1992.

[170] R. S. Mowbray, R. D. Pringle, and P. M. Grant. Adaptive CDMA cochannel interference cancellation. In *Signal Processing VI - Theories and Applications. EUSIPCO-92, Sixth European Signal Processing Conference*, volume 3, pages 1591–4, August 1992.

[171] R. S. Mowbray, R. D. Pringle, and P. M. Grant. Increased CDMA system capacity through adaptive cochannel interference regeneration and cancellation. *IEE I (Communications, Speech and Vision)*, 139(5):515–24, October 1992.

[172] B. Mulgrew. Applying radial basis functions. *IEEE Signal Processing Magazine*, pages 50–62, March 1996.

[173] Kazuaki Murota and Kenkichi Hirade. GMSK modulation for digital mobile radio telephony. *IEEE Transactions On Communications*, COM-29(7), July 1981.

[174] T. Nagayasu and S. Sampei. Elimination of adjacent channel interference via nonlinear filters. *Electronics and Communications in Japan, Part 1: Communications*, 77(5):23–32, 1994.

[175] R. S. Nelson and T. Kasparis. Digital processing for non-stationary narrow-band interference suppression in fading channels. In *SOUTHEASTCON '94*, pages 408–12, 1994.

[176] J. J. Nicolas and J. S. Lim. Equalization and interference rejection for the terrestrial broadcast of digital hdtv. Technical report, Research Laboratory of Electronics, MIT, 1993.

[177] P. Niger and P. Vandamme. Performance of equalization techniques in a radio interference environment. In *SUPERCOMM /ICC '90*, page 307.6, 1990.

[178] R. C. North, R. A. Axford, and J. R. Zeidler. The performance of adaptive equalization for digital communication systems corrupted by interference. In *Asilomar*, volume 2, pages 15488–1554, 1993.

[179] T. Ogawa, I. Sasase, and S. Mori. Suppression of CW interference and colored noise in qpsk system using decision-feedback filters. *Transactions of the Institute of Electronics, Information and Communication Engineers E*, E72(7):804–10, July 1989.

[180] T. Ogawa, I. Sasase, and S. Mori. Suppression of narrow-band interference and multipath by spread-spectrum receiver using decision-feedback filters. In *IEEE Pacific Rim Conference on Communications, Computers and Signal Processing*, volume 2, pages 673–6, May 1991.

[181] Shigeaki Ogose. Optimum gaussian filter for MSK with 2-bit differential detection. *The Transactions of the IECE of Japan*, E. 66(7):459–62, July 1983.

[182] K. Ohno and F. Adachi. Application of MLSE to GMSK signal reception using frequency demodulator. *Electronic Letters*, 23:1311–12, November 1987.

[183] K. Ohno and F. Adachi. Half-bit offset decision frequency detection of differentially encoded GMSK signals. *Electronics Letters*, 23(24):1311–12, November 1987.

[184] K. Ohno and F. Adachi. Performance evaluation of various decision schemes for frequency demodulation of narrow band digital fm signals in land mobile radio. *IEEE Transactions On Vehicular Technology*, 39(2 P. 109-16), May 1990.

[185] Athanasios Papoulis. *Probability, Random Variables, and Stochastic Processes*. McGraw-Hill, Inc, New York, third edition, 1991.

[186] E. Parzen. Estimation of a probability density function and its mode. *Annals of Mathematical Statistics*, 33:1065–1076, 1962.

[187] S. Pasupathy. MSK: A spectrally efficient modulation. *IEEE Communications Magazine*, 1979.

[188] P. Patel and J. Holtzman. Analysis of a simple successive interference cancellation scheme in a DS/CDMA system. *IEEE Journal on Selected Areas of Communications*, 12(5):796–807, June 1994.

[189] C. N. Pateros and G. J. Saulnier. Adaptive correlator receiver performance in direct sequence spread spectrum communication. In *MILCOM '92 - 'Communications - Fusing Command, Control and Intelligence'*, volume 2, pages 427–31, October 1992.

[190] C. N. Pateros and G. J. Saulnier. Interference suppression and multipath mitigation using an adaptive correlator direct sequence spread spectrum receiver. In *SUPERCOMM/ICC '92. Discovering a New World of Communications*, volume 2, pages 662–6, June 1992.

[191] M. Peng, C. L. Nikias, and J. G. Proakis. Adaptive equalization for PAM and QAM signals with neural networks. In *Twenty-Fifth Asilomar Conference on Signals, Systems and Computers*, pages 496–500, 1991.

[192] F. J. Pergal. Adaptive threshold A/D conversion techniques for interference rejection in DSPN receiver applications. In *IEEE Military Communications Conf.*, pages 4.7.1–4.7.7, October 1987.

[193] B. R. Petersen and D. D. Falconer. Suppression of adjacent-channel, cochannel, and intersymbol interference by equalizers and linear combiners. *IEEE Transactions on Communications*, 42(12):3109–3118, December 1994.

[194] H. V. Poor. Adaptivity in multiple-access communications. In *34th IEEE Conf. on Decision and Control*, volume 1, pages 835–40, December 1995.

[195] H. V. Poor and L. A. Rusch. Narrowband interference suppression in spread spectrum CDMA. *IEEE Personal Communications Magazine*, pages 14–27, 1994. third quarter.

[196] J. G. Proakis. *Digital Communications*. McGraw-Hill, Inc., New York, third edition, 1995.

[197] M. B. Pursley. The role of spread-spectrum in packet radio networks. *Proceedings of the IEEE*, 75(1):116–134, January 1987.

[198] K. Raivio, O. Simula, and J. Henriksson. Improving design feedback equaliser performance using neural networks. *Electronic Letters*, 27(23):2151–2153, November 1991.

[199] P. B. Rapajic and B. S. Vucetic. Adaptive receiver structures for asynchronous CDMA systems. *IEEE Journal on Selected Areas of Communications*, 12(4):685–697, May 1994.

[200] P. B. Rapajic and B. S. Vucetic. Linear adaptive transmitter-receiver structures for asynchronous CDMA systems. *European Transactions on Telecommunications*, 6(1):21–27, January-February 1995.

[201] P.B. Rapajic and B. S. Vucetic. Linear adaptive fractionally spaced single user receiver for asynchronous CDMA systems. In *1993 IEEE International Symposium on Information Theory*, page 45, 1993.

[202] T. S. Rappaport. *Wireless Communications: Principles and Practices*. Prentice Hall PTR, Upper Saddle River, New Jersey, 1996.

[203] T. S. Rappaport, W. Huang, and M. J. Feuerstein. Performance of decision feedback equalizers in simulated urban and indoor radio channels. *IEICE Transactions on Communications*, E76-B(2), February 1993.

[204] Siegmund M. Redl, Matthias K. Weber, and Malcolm W. Oliphant. *An Introduction to GSM*. Artech House, 1995.

[205] J. H. Reed and B. Agee. A technique for instantaneous tracking of frrequency agile signals in the presence of spectrally correlated interference. In *1992 Asilomar Conference on Signals, Systems and Computers*, 1992.

[206] J. H. Reed and T. C. Hsia. The performance of time-dependent adaptive filters for interference rejection. *IEEE Transactions on Acoustics, Speech and Signal Processing*, 38(8), August 1990.

[207] J. H. Reed, N. M. Yuen, and T. C Hsia. An optimal receiver using a time-dependent adaptive filter. *IEEE Transactions on Communications*, 43(2/3/4):187–190, February/March/April 1995.

[208] Peter J. Rousseeuw. *Robust Regression and Outlier Detection*. John Wiley & Sons, New York, 1987.

[209] Peter J. Rousseeuw and Christophe Croux. Alternatives to the median absolute deviation. *Journal of the American Statistical Association*, 88(424):1273–1283, December 1993.

[210] M. J. Rude and L. J. Griffiths. An untrained, fractionally-spaced equalizer for co-channel interference environments. In *Twenty-Fourth Asilomar Conference on Signals, Systems and Computers*, volume 1, pages 468–72, November 1990.

[211] L. A. Rusch and H. V. Poor. Narrowband interference suppression in CDMA SS communications. *IEEE Trans. on Comm.*, 42(2):1969–1979, April 1994.

[212] D. Ruth and M. Wickert. A time varying transform domain excision filter for interference rejection in DSSS. In *MILCOM '92*, page 38.3, 1992.

[213] Shuichi Samejima, Kyoshi Enomoto, and Yoshio Watanabe. Differential psk system with nonredundant error correction. *IEEE Journal on Selected Areas of Communications*, 1(1):74–81, January 1983.

[214] E. H. Satorius, S. Krishnan, X. Yu, L. J. Griffiths, I. S. Reed, and T. Truong. Suppression of narrowband interference via single channel adaptive preprocessing. In *Twenty-Second Asilomar Conference on Signals, Systems and Computers*, volume 1, pages 270–3, November 1988.

[215] Gary J. Saulnier, Charles M. Puckette, Jr. Richard C. Gaus, Robert J. Dunki-Jacobs, and Timothy E. Thiel. A VLSI demodulator for digital rf network applications: Theory and results. *IEEE Journal on Selected Areas in Communications*, 8(8), October 1990.

[216] D. L. Schilling, G. R. Lomp, and J. Garodnick. Broadband-CDMA overlay. In *43rd IEEE Vehicular Technology Conference*, pages 452–455, 1993.

[217] Gerhard Schultes, Arpad L. Scholtz, Ernst Bonek, and Peter Beith. A new incoherent direct conversion receiver. In *40th IEEE Vehicular Technology Conference. on the Move in the 90's*, pages 668–74,6–9 May, 1990.

[218] B. Shah and G.J. Saulnier. Adaptive jammer suppression using decision feedback in a spread-spectrum receiver. In *MILCOM 88. 21st Century Military Communications -What's Possible?*, volume 3, pages 989–95, October 1988.

[219] K. Sam Shanmugan and Arthur M. Breipohl. *Random Signals: Detection, Estimation, and Data Analysis*. John Wiley & Sons, New York, 1988.

[220] D. C. Shin and C. L. Nikias. Adaptive noise canceler for narrowband/wideband interferences using higher-order statistics. In *1993 IEEE International Conference on Acoustics, Speech and Signal Processing*, volume 3, pages 111.364–366, 1993.

[221] D. C. Shin and C. L. Nikias. Adaptive interference canceler for narrowband and wideband interferences using higher-order statistics. *IEEE Transactions on Signal Processing*, 42(10):2715–2728, October 1994.

[222] Soon S. Shin and P. Takis Mathiopoulos. Differentially detected GMSK signals in CCI channels for mobile cellular telecommunications systems. *IEEE Transactions On Vehicular Technology*, 42(3), August 1993.

[223] Marvin K. Simon and Charles C. Wang. Differential versus limiter-discriminator detection of narrow-band FM. *IEEE Transactions On Communications*, COM-31(11), November 1983.

[224] Marvin K. Simon and Charles C. Wang. Differential detection of gaussian MSK in a mobile radio environment. *IEEE Transactions on Vehicular Technology*, VT-33(4), November 1984.

[225] Z. Siveski, Y. Bar-Ness, and D. W. Chen. Error performance of synchronous multiuser CDMA detector with multidimensional adaptive canceler. *European Transactions on Telecommunications*, 5(6):73/719–78/724, November-December 1994.

[226] S. Smith and P. H. Wittke. Differential detection of GMSK in rician fading. *IEEE Transactions On Communications*, 42(2-4):l 216–20, February-April 1994.

[227] Z. D. Stojanovic, M. L. Dukic, and I. S. Stojanovic. A new method for the narrowband interference rejection in the direct sequence spread-spectrum systems using transversal filters. In *MELECON '87: Mediterranean Electrotechnical Conference and 34th Congress on Electronics Joint Conference*, pages 149–52, March 1987.

[228] F. G. Stremler. *Introduction to Communication Systems*. Addison-Wesley Publishing Company, Inc., New York, third edition, 1990.

[229] E. G. Strom and S. L. Miller. Optimum complexity reduction of minimum mean square error DS-CDMA receivers. In *IEEE VTC*, volume 1, pages 568–72, 1994.

[230] Carl Erik Sundberg. Continuous phase modulation. *IEEE Communication Magazine*, 24, April 1986.

[231] Hiroshi Suzuki. Optimum gaussian filter for differential detection of MSK. *IEEE Transaction on Communications*, COM-29(6):916–8, June 1981.

[232] M. Tahernezhad and L. Zhu. Performance evaluation of LMS-based adaptive suppression schemes in asynchronous CDMA. *Int. J. Electronics*, 79(5):541–550, 1995.

[233] F. Takawira and L.B. Milstein. Narrowband interference rejection in PN spread spectrum communications systems using decision feedback filters. In *MILCOM '86*, volume 2, pages 20.4/1–5, October 1986.

[234] M. V. Tazebay and A. N. Akansu. A smart time-frequency exciser for SS communications. In *ICASSP '95*, volume 2, page 1209, 1995.

[235] S. Theodoridis, N. Kalouptsidis, J. Proakis, and G. Koyas. Interference rejection in PN SS systems with LS linear phase FIR filters. *IEEE Transactions on Communications*, 37(9):991–994, September 1989.

[236] G. W. Travis and H. F. Lenzing. Shipboard HF interference: problems and mitigation. In *MILCOM '89: Bridging the Gap. Interoperability, Survivability, Security. Conference Record*, volume 1, pages 106–10, October 1989.

[237] J. Treichler and M. G. Larimore. Constant modulus algorithm based techniques for adaptive interference rejection. In *MILCOM '86*, page 47.3, 1986.

[238] J. R. Treichler and B. G. Agee. A new approach to multipath correction of constant modulus signals. In *IEEE Trans. on Acoustics, Speech and Signal Processing*, volume ASSP-31, pages 459–472, April 1983.

[239] J. R. Treichler and M. G. Larimore. New processing techniques based on the constant modulus adaptive algorithm. *T-ASSP*, 33(2):420–431, April 1985.

[240] A. M.D. Turkmani and P. P. S. Carter. Software investigation of co-channel interference in a digital cellular radio system. Technical report, The University of Liverpool, UK, 1990.

[241] Virginia Polytechnic Institute & State University. Simulated mobile radio channel impulse model (smrcim). software available for licensing, 1996. developed by the Mobile & Portable Radio Research Group.

[242] V. G. Valeev and A. A. Yazovskii. Adaptive nonlinear converters for suppression of non-gaussian interference. *Radioelectronics and Communication Systems*, 30(8):60–3, 1987.

[243] Prabodh Varshney and Surinder Kumar. Performance of GMSK in a land mobile radio channel. *IEEE Transaction On Vehicular Technology*, 40(3), August 1991.

[244] Prabodh Varshney and J. Eric Salt. Ber analysis of GMSK with differential detection in a land mobile channel. *IEEE Transactions On Vehicular Technology*, 42(4):683–9, November 1993.

[245] S. Verdu. Minimum probability of error for asynchronous multiple-access channel. *IEEE Trans. on Info. Theory*, IT-32(5):642–651, September 1986.

[246] S. Verdu. Adaptive multiuser detection. In *Proceedings of the 1994 International Symposium on Spread Spectrum Technology and Applications*, pages 43–50, July 1994.

[247] R. Vijayan and H. V. Poor. Nonlinear techniques for interference suppression in spread-spectrum systems. *IEEE Transactions on Communications*, 38(7):1060–5, July 1990.

[248] A.J. Viterbi. Very low rate convolutional codes for maximum theoretical performance of spread-spectrum multiple access channels. *IEEE Journal on Selected Areas of Communications*, 8(4):641–649, May 1990.

[249] A.J. Viterbi. The orthogonal-random waveform dichotomy for digital mobile personal communications. *IEEE Personal Comm*, pages 18–24, 1994. 1st Quarter.

[250] J. Wang and L. Milstein. Applications of suppression filters for CDMA overlay situations. In *SUPERCOMM /ICC '92*, page 310.3, 1992.

[251] J. Wang and L. B. Milstein. CDMA overlay situations for microcellular mobile communications. *IEEE Transactions on Communications*, 43(2/3/4):603–614, February/March/April 1995.

[252] Noah Webster. *Webster's II: New Riverside University Dictionary*. The Riverside Publishing Company, Boston, 1984.

[253] P. Wei, J. R. Zeidler, and W. H. Ku. Adaptive interference suppression for CDMA overlay systems. *IEEE Journal on Selected Areas in Communications*, 12(9):1510–1523, December 1994.

[254] L.B. White. Blind equalization of constant modulus signals using an adaptive observer approach. *IEEE Transactions on Communications*, 44(2):134–136, February 1996.

[255] B. Widrow and Jr. M. E. Hoff. Adaptive switching circuits. *IRE WESCON Conv. Rec. pt. 4*, pages 96–104, 1960.

[256] The Math Works. *Matlab version 4.2*. The Math Works, Inc., 1984-1994.

[257] The Math Works. *Matlab v. 4.2 - Optimization Toolbox*. The Math Works, Inc., 1994.

[258] Bo Wu, Jing Wang, and Yan Yao. A direct conversion receiver for GMSK in digital mobile communications. In *43rd IEEE Vehicular Technology Conference*, pages 404–7, 1993.

[259] Zengjun Xiang and Guangguo Bi. Complex neuron model with its applications to M-QAM data communications in the presence of co-channel interferences. In *ICASSP: 1992 IEEE International Conference on Acoustics, Speech and Signal Processing*, volume 2, pages 305–8, March 1992.

[260] Zengjun Xiang and Guangguo Bi. Fractionally spaced decision feedback multilayer perceptron for adaptive MQAM digital mobile radio reception. In *SUPERCOMM/ICC '92. Discovering a New World of Communications*, volume 3, pages 1262–6, June 1992.

[261] Zengjun Xiang and Guangguo Bi. Lattice polynomial perceptron based M-QAM digital communication reception systems. In *1992 Int'l Conf. on Communication Technology*, volume 2, pages 27.05/1–5, 1992.

[262] Zengjun Xiang and Guangguo Bi. New fractionally spaced recursive polynomials perceptron model for adaptive M-QAM digital mobile radio reception. *Electronics Letters*, 28(22):2049–51, October 1992.

[263] Zengjun Xiang and Guangguo Bi. Polynomial perceptrons and their applications to fading channel equalization and co-channel interference suppression. *IEEE Transactions on Signal Processing*, 42(9):2470–2479, September 1994.

[264] M. D. Yacoub. *The Mobile Communications Handbook*, chapter Cell Design Principles, pages 319–332. CRC Press & IEEE Press, 1996.

[265] Steve Kau Yao and J. H. Reed. Differential detection of GMSK signals. Technical report, Virginia Tech, October 1994.

[266] Keying Ye. PDF of Z=XY-UV, 1996. Derivation of the pdf of a function of four random variables.

[267] Abbas Yongacoglu, Dimitrios Makrakis, and Kamilo Feher. Differential detection of GMSK using decision feedback. *IEEE Transactions On Communications*, 36(6), June 1988.

[268] S. Yoshida, A. Uhirokawa, S. Yanagi, and Y. Furuya. DS/CDMA adaptive interference canceller on differential detection in fast fading channel. In *VTC*, pages 780–784, 1994.

[269] H. Yoshino, K. Fukawa, and H. Suzuki. Interference canceling equalizer (ice) for mobile radio communications. In *ICC '94*, pages 1427–1432, 1994.

[270] B. Zhu, N. Ansari, and Z. Siveski. Convergence and stability analysis of a synchronous adaptive CDMA receiver. *IEEE Trans. on Comm.*, 43(12):3073–79, December 1995.

[271] Rodger E. Ziemer and Carl R. Ryan. Minimum-shift keyed modem implementations for high data rates. *IEEE Communications Magazine*, pages 28–37, October 1983.

[272] Z. Zvonar and D. Brady. Adaptive multiuser receivers with diversity reception for nonselective rayleigh fading asynchronous CDMA channels. In *MILCOM '94*, volume 3, pages 982–986, 1994.

Jeff D. Laster (born 6/7/62) is a native of Georgia and Virginia. He attended Georgia Tech from 1980-1982. From there, he transferred to obtain a B.A. in the Humanities. He finished a B.S.E.E. in 1991 from Virginia Tech. The recipient of a Bradley Fellowship and a DuPont Fellowship, he obtained a M.S.E.E. from Virginia Tech in 1993 with a thesis under Dr. Warren Stutzman on attenuation scaling by frequency in rain. A member of the Mobile & Portable Radio Research Group (MPRG), he received his Ph.D. in January 1997 from Virginia Tech under Dr. Jeff Reed with a dissertation on robust GMSK demodulation using receiver diversity and real-time BER estimation. He presently is a Research Scientist with the Center for Transportation Research at Virginia Tech.